Investigating the biosynthesis of natural rubber through the characterisation of rubber associated proteins

A thesis submitted to the University of Warwick for the degree of Doctor of Philosophy

Daniel Brown
School of Life Sciences
University of Warwick
September 2016

Contents

List of Figures

List of Abbreviations

3AT	3-Amino-1,2,4-triazole
AD	activation domain
APP	allylic diphosphate
APS	ammonium persulfate
Arabidopsis	*Arabidopsis thaliana*
CBD	chitin-binding domain
CFP	cyan fluorescent protein
CPT	*cis*-prenyltransferase
dH_20	distilled water
DB	DNA binding domain
DMAPP	dimethylallyl pyrophosphate
DTT	Dithiothreitol
E. coli	*Escherichia coli*
ECL	enhanced chemiluminescence

EDTA	ethylenediaminetetraacetic acid
eIF-5A	eukaryotic initiation factor 5A
FPP	farnesyl pyrophoshphate
FPPS	farnesyl diphosphate synthase
GFP	green fluorescent protein
GGPP	geranylgeranyl pyrophosphate
GGPPS	geranylgeranyl diphosphate synthase
HRP	horseradish peroxidase
HRT (1/2)	*Hevea* rubber transferase (1/2)
IPP	isopentenyl pyrophosphate
IPPS	isopentenyl pyrophosphate synthate
KCl	potassium chloride
L. sativa	*Lactuca sativa*
LiAc	Lithium acetate
LDAP	lipid droplet associated protein
M. luteus	*Micrococcus luteus*
MEP	2-C-methyl-D-erythritol 4-phosphate
MES	2-(N-morpholino)ethanesulfonic acid
MESG	2-amino-6-mercapto-7-methylpurine ribonucleoside
$MgSO_4$	magnesium sulfate
MVA	mevalonate
N. benthamiana	*Nicotiana benthamiana*
NaCl	sodium chloride
NP-40	nonyl phenoxypolyethoxylethanol

OE-PCR	overlap extension-PCR
ORF	open reading frame
P. americana	*Persea americana*
P-loop	phosphate binding loop
PCR	polymerase chain reaction
PEG	polyethylene glycol
PM-IRRAS	polarization modulation infrared reflection-absorption spectroscopy
PNP	purine nucleoside phosphorylase
RBSP	rubber biosynthesis stimulator protein
REF	rubber elongation factor
RFP	red fluorescent protein
RPKM	reads per kilobase of transcript per million mapped reads
TBS	tris-buffer saline
T. brevicorniculatum	*Taraxacum brevicorniculatum*
T. koksaghyz	*Taraxacum koksaghyz*
TEMED	tetramethylethylenediamine
TPT	*trans*-prenyltransferase
Tris-HCL	tris(hydroxymethyl)aminomethane hydrochloride
TWEEN	polyoxyethylene (20) sorbitan monolaurate
S. cerevisiae	*Saccharomyces cerevisiae*
SDS	sodium dodecyl sulfate
SDS-PAGE	SDS-polyacrylamide gel electrophoresis
SRPP	small rubber particle protein

YFP	yellow fluorescent protein
YPDA	yeast peptone dextrose adenine

List of amino acids with abbreviations

Amino Acid	**Code**	**Abbreviation**
Alanine	A	Ala
Cysteine	C	Cys
Aspartic acid	D	Asp
Glutamic acid	E	Glu
Phenylalanine	F	Phe
Glycine	G	Gly
Histidine	H	His
Isoleucine	I	Ile
Lysine	K	Lys
Leucine	L	Leu
Methionine	M	Met
Asparagine	N	Asn
Proline	P	Pro
Glutamine	Q	Gln
Arginine	R	Arg
Serine	S	Ser
Threonine	T	Thr
Valine	V	Val
Tryptophan	W	Trp
Tyrosine	Y	Tyr

Acknowledgments

Thank you to my supervisors Professor Lorenzo Frigerio at Warwick, and Dr Alessandra Di Cola at TARRC for their help, guidance and support throughout the project.

Thank you to everybody in C46 past and present including; Dr Emily Breeze, Dr Charlotte Carroll, Rachel Clewes, Dr Amanda Dowson, Natasha Dzimitrowicz and Dr Mistianne Feeney.

Thank you to everybody from the TARRC Biotechnology division past and present including; Dr Maria-Kolesnikova-Allen, Daniel Beckett, Dr Chloe Thompson, Rachel Greenhill, Dr Ishtiaq Khaliq, Ewan Mollinson, Vania Serkiova, Dr Nurul Siddiqui and Cristina Ribeiro. A particular mention for Alessandra and Cristina for their help with protein purification.

Finally, I'd like to thank my family, and most importantly a big thank you to my fiancée Rebekah Darbyshire for her continued love and support throughout.

Declaration

The data presented in this thesis represents original work conducted by myself under the supervision of Professor Lorenzo Frigerio at the University of Warwick and Dr Alessandra Di Cola at the Tun Abdul Razak Research Centre (TARRC). The research was funded by a BBSRC CASE grant and by the Tun Abdul Razak Research Centre. All sources of information have been acknowledged by a reference, and none of this work has been used in any previous application for a degree.

Daniel Brown

September 2016

Summary

Natural rubber from the *para* rubber tree *Hevea brasiliensis* is one of world's most important natural resources. Despite its use in the manufacture of a wide range of essential items the mechanisms by which natural rubber is synthesised is poorly understood.

Natural rubber is a long chain cis-polyisoprene, composed of units of isopentenyl pyrophosphate (IPP) which is contained within rubber particles. Rubber particles consist of a hydrophobic polyisoprene interior surrounded by a monolayer membrane. Due to the insoluble nature of rubber the only place that polymerisation could occur is on this membrane by a hypothetical membrane bound rubber transferase. Whether this is a single enzyme or complex is currently unknown.

Cis-prenyltransferases (CPTs) are a group of enzymes responsible for the polymerisation of cis-polyisoprene. The first plant CPTs were identified in Arabidopsis which paved the way for the identification of two *Hevea* CPTs, HRT1 and HRT2. HRT2 is able catalyse the formation of long chain polyisoprene products in the presence of rubber particles and is the focus of this thesis.

Hevea takes at least 4 years to reach maturity. Its long life cycle coupled with the difficulty of genetic transformation meant that direct study on Hevea was not feasible for this project. Instead transient expression in *N. benthamiana* as well as some preliminary work in *L. sativa* was used to characterise rubber associated proteins.

HRT2 was found to be a cytosolic protein and in theory incapable of polymerising natural rubber on the surface of rubber particles. The scope of the project was therefore widened to include possible interactors that could act to bring it to a membrane. These interactors were identified and cloned based on existing literature and included small rubber particle protein (SRPP), rubber elongation factor (REF), rubber biosynthesis stimulator protein (RBSP) and a newly characterised *cis*-prenyltransferase like (CPTL) protein, HevNogo.

Whilst HRT2 on its own was unable to associate with a membrane, expression with HevNogo induced its subsequent localisation to the plasma membrane. This interaction initially took place on the endoplasmic reticulum. The HRT2/HevNogo complex may

be part of a rubber transferase complex, however it is likely that additional components are required.

Chapter 1: Introduction

1.1 Natural rubber

Derived from the latex of the *para* rubber tree *Hevea brasiliensis*, natural rubber is amongst the most important natural resources, with special properties that cannot adequately be replaced by synthetic alternatives. It is heat proof, shock proof, water resistant, elastic and malleable. Natural rubber is used in the manufacture of a wide range of material including condoms, medical equipment and tyres.

1.1.1 Rubber transferase

The search for rubber transferase, an enzyme or complex that catalyses the formation of natural rubber, has been ongoing since its existence was first hypothesised over 50 years ago. As natural rubber consumption is rapidly outpacing production it is becoming more important than ever to learn just what is involved in the synthesis of rubber. This could provide the first steps to creating improved transgenic lines or even natural rubber production *in vitro*, which could safeguard rubber supply in the years to come.

1.1.2 Latex

Latex is a milky white substance that is the raw ingredient for making natural rubber. Latex is produced by a wide range of plants and also some fungi. The reasons for latex production are still elusive its major component natural rubber, cannot be broken down as a food source or used for any further processes. Currently latex is thought to act as a defence against biting insects (Dussord & Eisner 1987, Farrell *et al* 1991, Zalucki *et al* 2001) and possibly pathogens. A high proportion of stress related and defence genes are upregulated in *Hevea* latex compared to *Hevea* leaf tissue (Ko *et al* 2016)

1.1.3 *Hevea brasiliensis*

Whilst many plant species produce latex, currently the only viable commercial source of natural rubber comes from *Hevea*. This is due to the tree's superior yield of latex compared to other rubber producing species such as dandelions or guayule, the ease of harvest and also the quality of the natural rubber it produces.

Hevea is a tropical plant, originating in the Amazon in South America, seeds were smuggled out and cultivated in parts of the British Empire such as India and South East Asia. This is where rubber is mainly produced today, with Thailand, Indonesia and Malaysia being the top three exporters in the world.

In part thanks to rapidly developing countries such as China and India, there is a rising demand for rubber products due to an increasing number of vehicles and machinery in these countries. Although demand for natural rubber products is increasing, supply is an issue as there is a diminishing amount of land available for cultivation. This is partly due to farmers switching to palm oil plantations which are more profitable and take less time than *Hevea* to produce a harvestable crop. Diminishing supply is also due to the poor quality of farming practises that have remained basically unchanged for more than a hundred years. This, along with the monoclonal nature of *Hevea* trees used to produce natural rubber, means that supply for the future is under threat.

Hevea brasiliensis trees typically take around 7-10 years to reach maturity and then are productive for a further 20 years. The long life cycle of *Hevea* is currently a barrier to transgenic studies in the organism.

Latex is the cytoplasmic content of secretory laticifer cells within the bark of *Hevea*. Laticifers are specialised elongated cells that form a network throughout the tree; they are similar to, and are derived from, phloem tissue. Harvesting latex involves making shallow cuts into the bark of the tree, bisecting the laticifers. This allows the latex to run out (Figure 1.1) and be collected. The process is known as ‘tapping’ and a careful management allows the same section of bark to be tapped for up to 5 years. Latex production is also able to be increased via stimulation by ethylene treatment. This is done by the addition of ethephon, a well-known plant growth regulator which is converted to ethylene by the plant (Abraham *et al* 1968, Zhu *et al* 2009)

Harvested latex is processed into natural rubber via vulcanisation. Natural rubber is a long chain polymer and vulcanisation is a curing process in which sulphur and other curing agents are added along with carbon black. At high temperatures the polymers form disulphide bond cross-links contributing to the unique properties of natural rubber.

1.1.4 Natural rubber is a *cis*-polyisoprene

The main component of natural rubber is *cis*-1, 4-polyisoprene. Polyisoprenes are synthesised by the subsequent condensation and 'head to tail' polymerization of the isoprene precursor IPP, onto a farnesyl pyrophosphate (FPP) or a geranylgeranyl pyrophosphate (GGPP) initiator molecule. This creates a long hydrocarbon tail, with a pyrophosphate head onto which subsequent IPP polymerization occurs. These reactions are catalysed by a group of enzymes known as prenyltransferases and in the case of *cis*-polyisoprenes, *cis*-prenyltransferases (CPTs). (Figure 1.2).

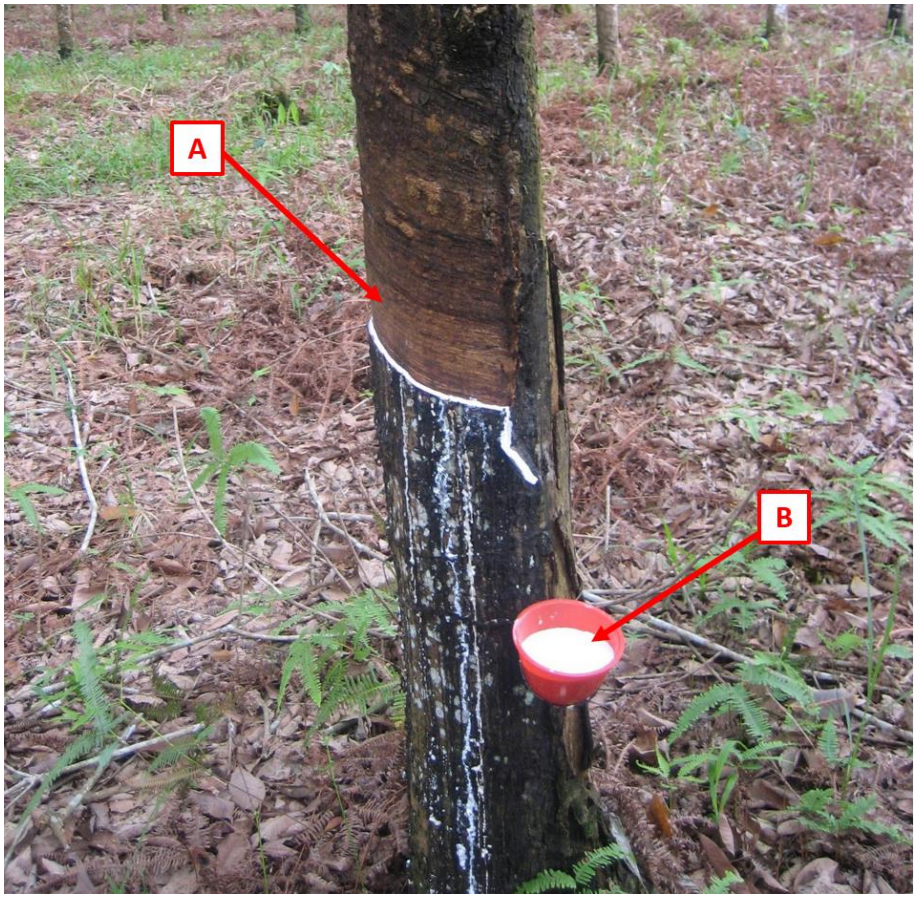

Figure 1.1 ***Hevea brasiliensis***
(A) The bark of *Hevea* is 'tapped' by making a series of cuts through the laticifers then (B) the milky white latex sap runs out and is collected for further processing into natural rubber

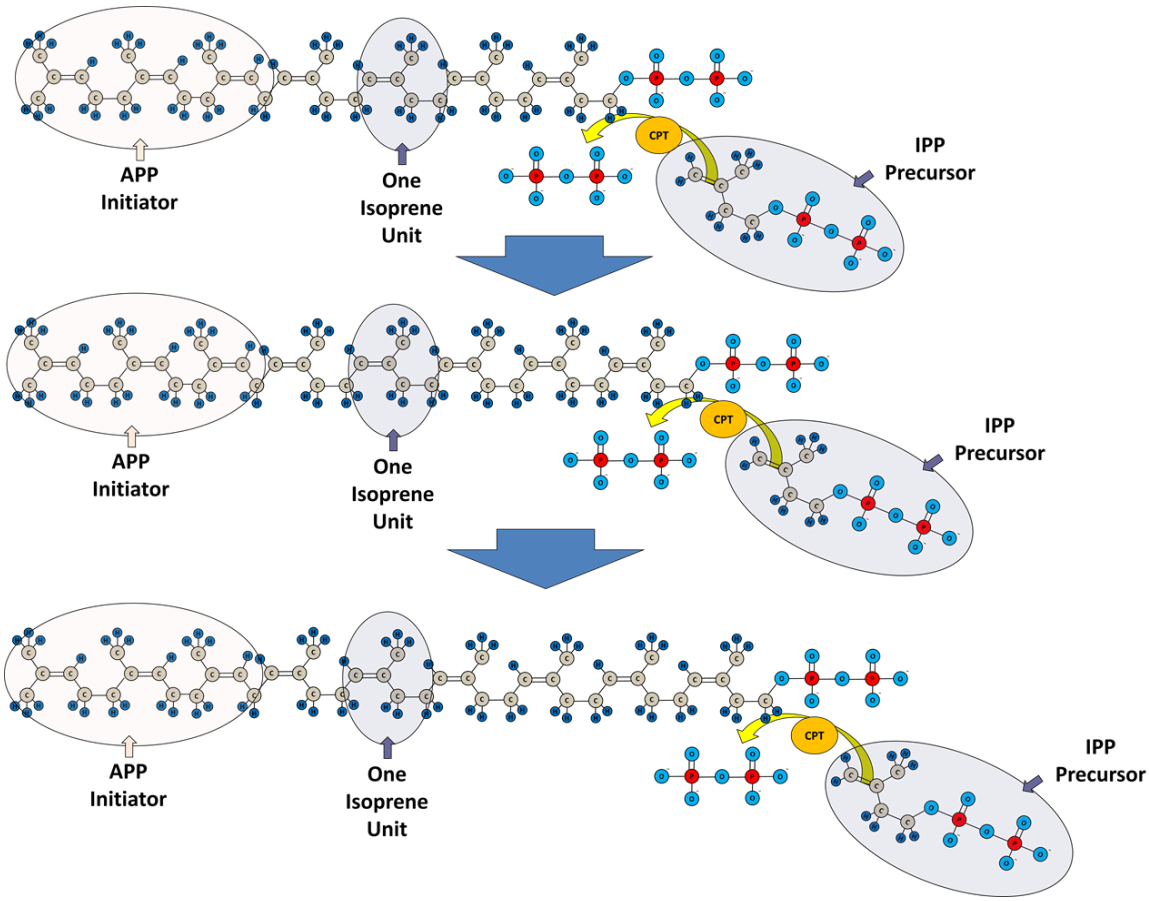

Figure 1.2 Polymerisation of IPP to form *cis*-polyisoprene

Natural rubber is mainly *cis*-1, 4-polyisoprene. Polyisoprene is formed from the sequential condensation of IPP initiators onto an APP initiator molecule. This is catalysed by the action of *cis*-prenyltransferase (CPT) enzymes in a series of condensation reactions. Condensation occurs 'head to tail' IPP joins the chain, with a pyrophosphate group remaining at the 'tail' of the polymer ready to accept subsequent incoming IPP. Pyrophosphate is a by-product of the reaction.

1.2 Prenyltransferase

The synthesis of natural rubber requires 4 main processes; these are the formation of isopentenyl pyrophosphate (IPP) which is the basic unit of natural rubber, the production of initiator molecules such as farnesyl pyrophosphate (FPP) and geranylgeranyl pyrophosphate (GGPP), the subsequent polymerization of IPP onto the initiator molecule and finally the termination of rubber synthesis when the rubber molecule is released from the rubber biosynthetic enzyme or complex. As natural rubber is made from *cis*-(1, 4)-polyisoprene, the polymerization of IPP to make natural rubber is most likely carried out by a prenyltransferase enzyme (Yusof *et al* 2000).

1.2.1 Isoprene synthesis

Polyisoprenes are a wide range of compounds all based upon a skeleton of isoprene C_5H_8 which derives from IPP precursor. IPP itself is synthesised either via the plastidic 2-C-methyl-D-erythritol 4-phosphate (MEP) or cytosolic mevalonate (MVA) pathways. Traditionally IPP for natural rubber synthesis was believed to originate from only the MVA pathway. However a more recent study by Chow *et al* (2012), by stimulating latex production through ethylene treatment, then measuring gene expression by qRT-PCR showed that enzymes from both the MVA and MEP pathways are upregulated and that they both contribute to IPP for natural rubber synthesis.

Whilst this thesis concerns potential rubber biosynthetic enzymes 'post IPP synthesis' the precursor pathways and enzymes is also the subject of intensive research, as it could provide ways to increase natural rubber yield.

1.2.2 Polyisoprene synthesis via prenyltransferases

MEP and MVA pathways synthesise IPP, with the MEP pathway also synthesising the IPP isomer dimethylallyl pyrophosphate (DMAPP). The enzymes farnesyl diphosphate synthase and geranylgeranyl diphosphate synthases convert IPP and DMAPP to FPP and GGPP respectively. FPP or GGPP, which will hereafter be jointly referred to as allylic diphosphates (APP) unless specified, act as an initiator onto which further IPP polymerization occurs. Chow *et al* (2012) demonstrates by qRT-PCR that both FPPS

and GGPPS enzymes are up-regulated during latex production which was stimulated by ethylene treatment.

The polymerization of IPP is carried out by a group of enzymes known as prenyltransferases. Prenyltransferases are classified into three major, non-orthologous, categories: (1) IPPSs, (2) protein prenyltransferases and (3) terpenoid cyclases. IPPSs are further divided into two types, (a) TPT and (b) CPT, and whilst both types catalyse sequential IPP polymerization, the two classes of enzyme are not related, and have completely different nucleotide sequences and conserved regions. TPTs, which include FPPS and GGPPS, catalyse the condensation of IPP to form isoprene chains in *trans*-configuration. More recently discovered are CPTs (Fujihashi *et al* 2001), which catalyse the condensation of IPP to form isoprene chains in *cis*-configuration (Figure 1.2). As natural rubber is mainly *cis*-1,4-polyisoprene, the search for a rubber biosynthetic enzyme predominantly focuses on CPTs.

1.2.3 *Cis*-prenyltransferase

1.2.3.1 APP and IPP binding

The catalytic domain of CPTs are thought to have an IPP binding site, an APP binding site and a hydrophobic cleft which functions to accommodate the elongating hydrophobic hydrocarbon chain (Figure 1.3).

The first crystal structure of a CPT, determined by Fujihashi *et al* (2001) was that of an undecaprenyl diphosphate synthase protein, responsible for the synthesis of UPP in *M. luteus*. UPP contains 11 units of isoprene and is involved in the construction of bacterial cell walls. The enzyme purified from *M. luteus* was found to have an elongated tunnel containing largely hydrophobic amino acid residues. At the entrance to this tunnel there is a structural P-loop, which is a conserved motif responsible for binding phosphates such as the phosphates of APP (Figure 1.3)

Comparison of known CPTs revealed 5 conserved regions, I-V (Figure 1.4), later found to be common to all conventional CPTs. Further studies into *M. luteus* undecaprenyl diphosphate by Kharel *et al* (2001) show that of particular importance are regions III and V. These are involved in the binding incoming IPP molecules. Region V contains

a ‘positively charged triangle’ of arginine and glutamic acid residues at R197, R203 and E216. By replacing these residues with non-polar ones at R197S, R203S and E216Q, then measuring the incorporation of radioactive ^{14}C-IPP, Kharel showed that the affinity of the mutated enzyme for IPP is significantly reduced. According to the crystal structure, conserved region III lies adjacent to region V, and contains a Phe-Ser motif that may be involved in binding the diphosphate groups of IPP. Replacement of these residues at F73A and S74A also results in a significant decrease in IPP activity. All of these mutations show only a reduction in IPP affinity but no change for APP, indicating regions III and V are exclusively involved in IPP binding but not in binding APP.

1.2.3.2 The hydrophobic cleft as a chain length limiting factor

The crystal structure and conserved regions of the *E. coli* CPT undecaprenyl pyrophosphate synthase were determined by Ko *et al* (2001) and corresponds to that of *M. luteus*. The major domain contains parallel β-strands which form a funnel shape with hydrophobic residues lining the interior surface of the funnel. This is known as the hydrophobic cleft.

Sequential addition of IPP creates a product with a hydrophobic carbon chain, which must leave the active site (Ko *et al* 2001). This is thought to be solved by the presence of the large hydrophobic cleft in the CPT enzyme, which may accommodate the elongating polymer chain keeping it in place for subsequent additions of IPP. The size and relative space inside the cleft could be important in determining overall product size.

Ko *et al* (2001) showed that larger amino acid residues may act to limit the space available in the hydrophobic cleft and thus limit the size of the polyisoprene that may be formed. *E. coli* undecaprenyl pyrophosphate synthase produces the 11 isoprene unit UPP and has a large leucine residue (L137) located in the cleft. However the *S. cerevisiae* CPT, RER2, which produces longer 16 isoprene unit products, has a smaller alanine residue in the corresponding position.

By using site-directed mutagenesis to switch the larger leucine-137 to alanine and then determining the product size by TLC analysis, Ko *et al* was able to increase the polyisoprene product of *E. coli* undecaprenyl pyrophosphate to 15 units of isoprene comraped to 11 in wild type. This demonstrates that the hydrophobic cleft is an important limiting factor in the size of polyisoprene products, as the elongating

hydrophobic polyisoprene chain needs somewhere to go, in order for it to remain attached to the CPT enzyme itself. The presence of a smaller residue at corresponding positions within the cleft seems to be a hallmark of long chain CPTs.

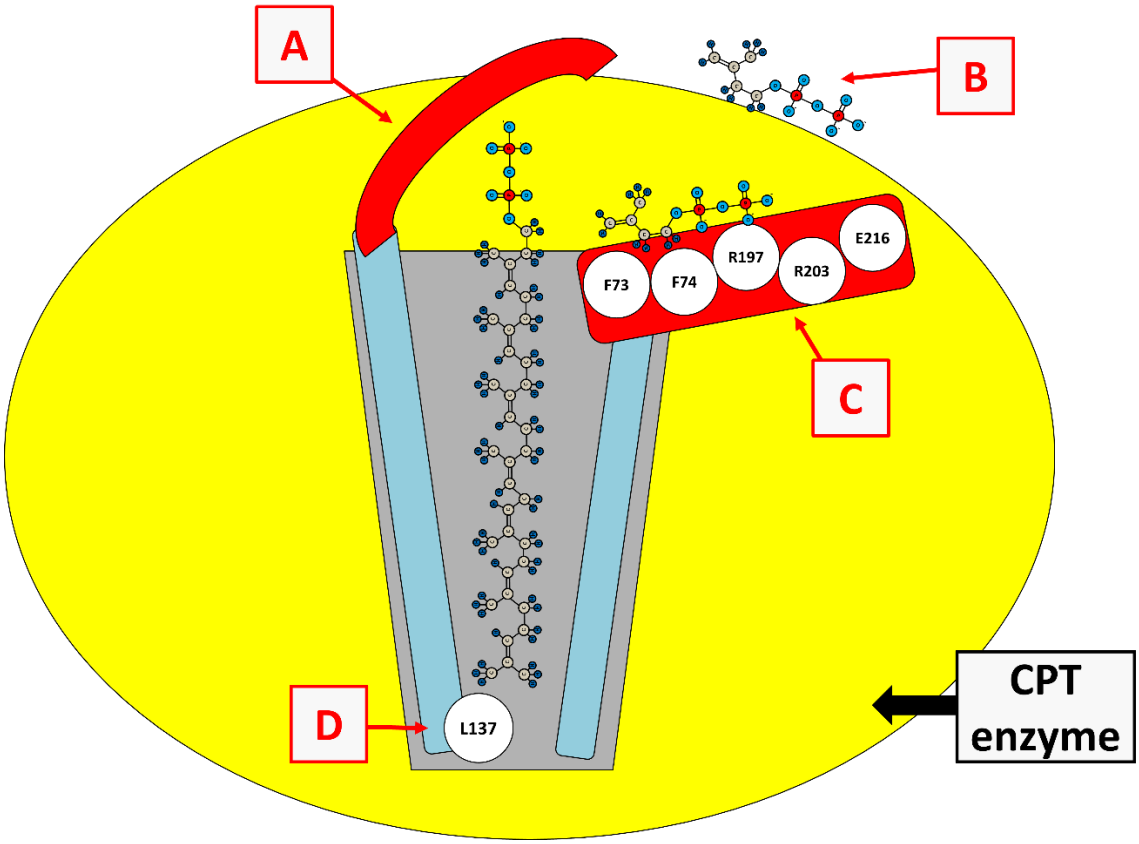

Figure 1.3 Model of a 'conventional' CPT enzyme, based upon crystal structure from *M. luteus* undecaprenyl pyrophosphate synthase and point mutation experiments by Kharel (2004) and Ko (2001)

APP initiator molecule is held in the active site by a structural p-loop (A) which binds pyrophosphate groups of APP and any subsequent pyrophosphate groups of the active end. Incoming IPP monomers (B) are thought to be held in place by positively charged residues within conserved regions III and V (C) which according to crystal structure lie adjacent to one another. The elongating polyisoprene extends into the hydrophobic cleft (D) which consists of hydrophobic residues. The size of the cleft is said to limit the length of any potential polyisoprene product.

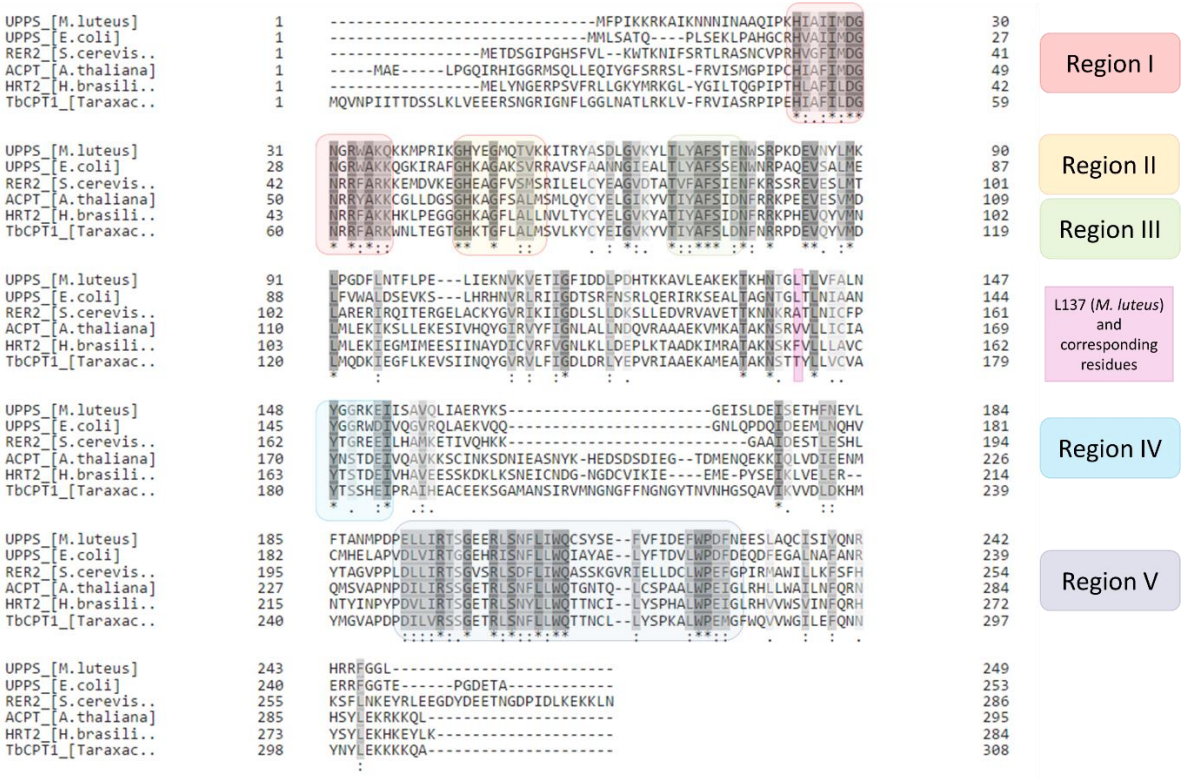

Figure 1.4 Amino acid sequence alignment of a selection of CPT from different organisms
Conserved residues are highlighted in red (region I), orange (region II), green (region III), cyan (region IV) and dark blue (region V). Also highlighted is the L137 (pink) and corresponding residues in other CPT proteins

1.2.3.3 Nogo receptor-like proteins may act as a subunit of CPT enzyme

Dolichols are necessary in N-linked glycosylation, functioning as a glycosyl carrier lipid (Harrison *et al* 2011). Like natural rubber, dolichols are long chain polyisoprenes and are synthesised by CPT enzymes. The CPT enzyme that is responsible for dolichol synthesis in humans is known as hCIT (Adair *et al* 1984).

In a study on reticulon binding partners in humans, a Nogo-B receptor protein, NgBR was isolated and characterised (Miao *et al* 2006). The study by Miao *et al* was completely unrelated to glycosylation or dolichol synthesis in humans. However it was later shown that NgBR shared sequence homology and also interacted with, the human dolichol CPT hCIT (Harrison *et al* 2011).

Harrison *et al* (2011) determined via the use of co-immunoprecipitation that NgBR interacts with hCIT. In addition by measuring the activity of hCIT via ^{14}C-IPP incorporation in HeLa cells, Harrison *et al* showed that overexpression of NgBR resulted in increased hCIT activity. Whilst suppression of NgBR led to a loss of hCIT activity and subsequent loss of dolichol synthesis.

This new class of 'Nogo-B Receptor related' CPTs are known as CPTL and have now been discovered in plants including the *Arabidopsis* gene LEW1 (Zhang *et al* 2008) which is involved in dolichol synthesis, and was identified by screening the *Arabidopsis* mutant *lew1* which lacks the ability to synthesise dolichol. This raises the question; does a Nogo-B receptor like protein aid the *Hevea* CPT in the process of rubber biosynthesis?

1.2.3.4 Length of natural rubber polyisoprene

Isoprenoids are categorised according to the number of isoprene units they contain. Most contain between 2 units and 8 units of isoprene, polyisoprenes are isoprenoids larger than 8 units including dolichols. CPTs have been shown to produce polyisoprene up to 20 units, with the hydrophobic cleft of the enzyme acting to limit the size of the polyisoprene product (Kharel *et al* 2001). Natural rubber however, is unusual in that it contains thousands of isoprene units; it is very unlikely that the hydrophobic cleft of a rubber CPT could ever be large enough to accommodate the extremely long and increasingly hydrophobic chains of natural rubber polyisoprene found in *Hevea*. This problem may be solved by rubber particles present in the latex of *Hevea*, which could act to accept the long polymer chains within their hydrophobic interior.

1.3 Rubber particles

The polyisoprene natural rubber component of latex is contained within organelles known as rubber particles. Rubber particles exist as a colloidal suspension in the latex and consist of a hydrophobic core of *cis*-1, 4-polyisoprene molecules surrounded by a phospholipid monolayer membrane (Dai *et al* 2013) which contains various proteins. The 'active' end of natural rubber polyisoprene chain has a pyrophosphate group due to it being present on the IPP precursor and this end is able to mix with the phospholipid head groups of the monolayer membrane due to their hydrophilic nature. Rubber biosynthesis is hypothesized to take place on the surface of these particles (Archer & Audley 1963).

Rubber particles are present in many rubber producing species with *Hevea* possessing the most complex particles, with the highest number of membrane proteins (Cornish 2000). Rubber particles can range from 0.2μm to 10μm in diameter and segregate in two distinct sizes, termed small and large rubber particles, which are present in different layers of *Hevea* laticifers. Looking at sections of *Hevea* laticifer tissue, Sando *et al* (2009) determined that large rubber particles were present in all layers, whereas small rubber particles are present only in the inner conducting phloem of the laticifers.

1.3.1 Rubber biosynthesis is thought to occur within the outer membrane of rubber particles

The polyisoprene product size of 'conventional' CPTs is hypothesized to be limited by the size of the enzymes' hydrophobic clefts. This in theory would inhibit the formation of very high polymer chains. However, the presence of rubber particles within laticifers may allow for the synthesis of the very high chain lengths seen in polyisoprene rubber: IPP polymerization may take place at the surface of rubber particles with the elongating polyisoprene rubber extending into the hydrophobic interior of the particle. In this model the rubber biosynthetic enzyme or complex would be bound to the membrane and may even traverse it into the interior (Figure. 1.5).

Cornish (2000) demonstrates that APP is able to cross the membrane of rubber particles, with the hydrophilic pyrophosphate head of the APP initiator, lining up with the hydrophilic phosphate head of the phospholipid membrane, and the hydrophobic carbon tail mingling with the hydrophobic fatty acid polyisoprene interior. Thus the 'active' end of the rubber molecule is always located at the surface of the rubber particle, available for further IPP addition via the action of rubber biosynthetic enzyme, which is most likely a CPT. The elongating rubber polymer is therefore able to extend and is compartmentalised in the interior of the rubber particle (Figure 1.5). This model, relies on a membrane-bound rubber transferase.

1.3.2 Chain linkage and other components in natural rubber

There is some evidence that within rubber particles, the individual *cis*-polyisoprene chains themselves are linked via phospholipids at the terminating end of the chain. Tarachiwin *et al* (2005a) measured the length of natural rubber before and after treatment with phospholipases. Treatment of natural rubber with phospholipases causes a decrease in its molecular weight; this may be a result of eliminating the phospholipids that link chains together, thus breaking a larger multi-chain molecule into a smaller one (Tarachiwin *et al* 2005b). The presence of phosphates and phospholipids at the terminating end of the rubber chain is also supported by data from NMR analysis (Tarachiwin *et al* 2005a)

The most common phospholipids in rubber particles are α-lecithins (Sansatsadeekul *et al* 2011), phosphatidylcholine and phosphatidylethanolamine. It is possible that they enhance the stability and contribute to the formation of rubber particles. It could also be possible that the presence of very high molecular weight natural rubber in *Hevea* is due to chain linkage and not purely a consequence of the synthesis of longer polyisoprene chains.

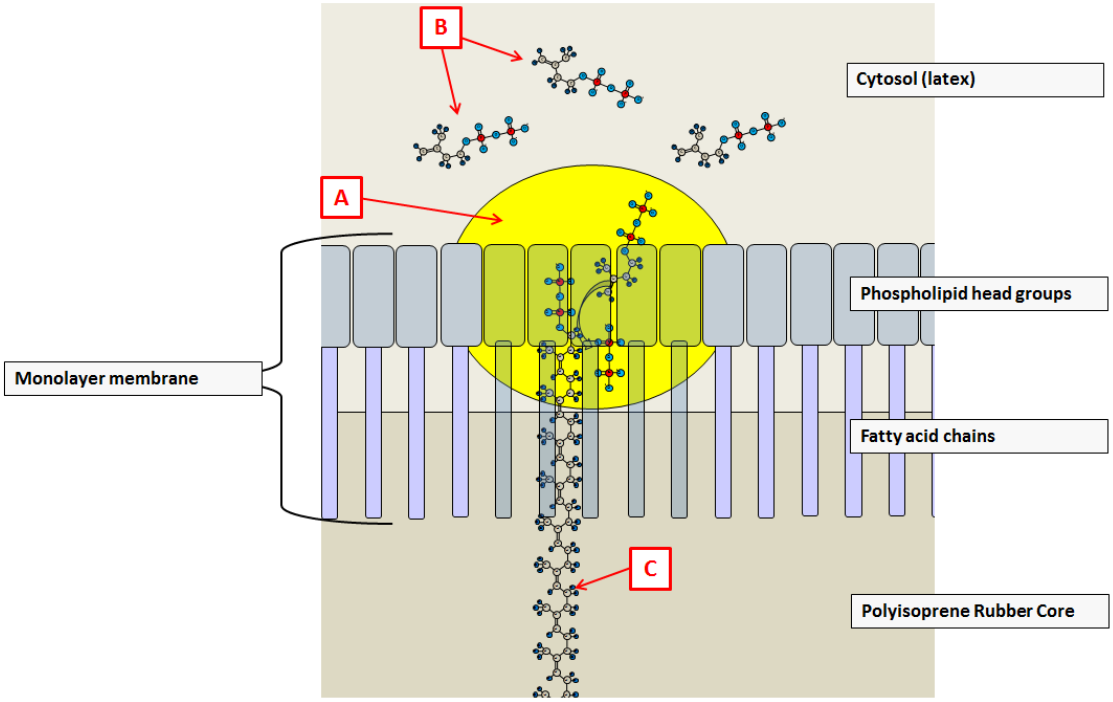

Figure 1.5 Model of a potential rubber biosynthetic enzyme or complex located on a rubber particle membrane

The rubber biosynthetic complex (A) is bound within the monolayer membrane of the rubber particle. Incoming IPP molecules (B) can be polymerised onto the ever elongating rubber chain. Unlike 'conventional' CPTs (Figure 1.4) where the hydrophobic cleft is a limiting factor, here the increasingly hydrophobic, elongating rubber polymer (C) extends into the polyisoprene core whilst the hydrophilic 'active end' remains at the surface to allow for further IPP incorporation.

1.3.3 Rubber particles and lipid bodies

Rubber particles are thought to be topologically similar to lipid bodies, which have a structure consisting of a hydrophobic core of either isoprenoids or storage lipids such as triglycerides surrounded by a monolayer membrane (Herman *et al* 2008). By raising antibodies against well-known isoprene pathway enzymes and carrying out immunofluorescence on liverwort samples containing lipid bodies, Suire (2000) was able to show that many enzymes involved in IPP and APP synthesis are found on the surface of lipid bodies. We hypothesise they are also found on rubber particles.

There is still much debate about lipid body formation, but one model is that they develop and 'bud' from the endoplasmic reticulum (Duckett and Lingrone 1995) with the help of oleosin proteins (Napier 1996). Oleosin protein are located on lipid bodies and act to stabilise the formation of these vesicles and prevent fusion of them (Shimada & Hara-Nishimura 2010). Perhaps fulfilling a similar role, the two most common proteins found on rubber particles are the closely related small rubber particle protein (SRPP) and rubber elongation factor (REF), both members of the SRPP protein family. In other species, members of this family are located on lipid bodies, a further argument to the similarities and possible shared origins of rubber particles and lipid bodies, more on this in **section 1.5.5**.

1.4 Potential CPT proteins involved in rubber biosynthesis

Published research about possible rubber enzymes is limited. However a rubber biosynthetic enzyme or complex would need to meet a number of requirements. First it is required that it would be or contain, a type of CPT in order to polymerize *cis*-1, 4-polyisoprene. Second, it is required that it would have to be a membrane - associated complex located on rubber particles, in order to facilitate the elongation of polyisoprene within rubber particles themselves. Thirdly, as rubber particles are theorized to originate from the endoplasmic reticulum, it is also probable that any potential protein or complex would be associated with this organelle. Aside from conventional CPT enzymes as described in **section 1.2.3** other candidate proteins include the Nogo-receptor-like CPTLs, the SRPP protein family which are highly abundant in latex and rubber

biosynthesis stimulator protein (RBSP) which has been shown to boost IPP polymerization (Chow *et al* 2006). In the next sections I will go into more detail about candidate proteins which could form a complex to catalyse the formation of natural rubber, and which are the focus of this thesis.

1.4.1 Plant CPTs

The first CPTs successfully identified were undecaprenyl diphosphate synthase in *Micrococcus luteus*, *E. coli* and yeast. In *Micrococcus luteus*, Shimizu *et al* (1998) first identified the primary protein structure of and cDNA sequence of the undecaprenyl diphosphate synthase gene. Shimizu *et al* created an expression DNA library in *E. coli* and screened colonies for uptake of radioactive ^{14}C-IPP on substrate containing *cis*-APP. Only a CPT enzyme would be able to process *cis*-APP, this would distinguish CPTs from the better known *trans*-prenyltransferases. Working with positive colonies the study subsequently narrowed down and isolated both the protein and the cognate cDNA coding region. Shimizu *et al* found that CPTs were completely different in sequence, conserved regions, and structure to TPTs and represented a completely new class of enzyme. The undecaprenyl diphosphate synthase structure and catalytic domains were later determined as detailed in **section 1.2.3**. This was the basis for all subsequent work on CPTs including the identification of dolichol synthases in *S. cerevisiae* (Sato *et al* 1999, Kato *et al* 1999), and paved the way for the identification of the first plant CPTs in *Arabidopsis*.

Using conserved regions of the *Micrococcus luteus* CPT sequences as determined by Shimizu *et al* (1998) as a starting point, the first *Arabidopsis* CPT gene (ACPT) was identified by Oh *et al* (2000) and named ACPT. Like undecaprenyl diphosphate synthase ACPT contains the 5 conserved regions I-V previously described (Figure 1.4). Oh *et al* managed to isolate and purify the ACPT protein and include it in a rubber biosynthesis assays. Using thin layer chromatography (TLC) to determine the size of the polyisoprene reaction products, Oh *et al* found that ACPT could synthesise the formation of long chain polyisoprene products approximately 24 isoprene units in length, however it could not synthesise the formation of products approaching anything like the length of natural rubber. *Arabidopsis* CPTs however provided the basis for

further cloning and identification of other plant CPTs, both in non-latex producing species such as tomatoes (Akhtar *et al* 2013), and latex producing species such as dandelions (Schmidt *et al* 2010), lettuce (Qu *et al* 2015) and most importantly *Hevea* itself (Asawatreretanakul *et al* 2003).

1.4.2 Plant CPTs in *Hevea*

In 2003, two plant CPTs that were specifically expressed in the latex of *Hevea* were identified and cloned in a study by Asawatreretanakul *et al* (2003). Using degenerate primers based on the conserved CPT sequences of ACPT, the authors managed to extract the two CPTs from cDNA of *Hevea* latex and called them HRT1 and HRT2.

1.4.2.1 A possible role for HRT2 in rubber biosynthesis

HRT1 and HRT2 proteins were purified and examined using *in-vitro* rubber transferase assays to measure IPP incorporation. Product polymer length was determined by gel permeation chromatography analysis in order to determine the activity of the two proteins (Asawatreretanakul *et al* 2003). Only HRT2 was found to display any activity and even this was quite limited, producing products of around 16 isoprene units, nothing like natural rubber which is thousands of isoprene units long, and less even than the products of ACPT. However this did show that HRT2 was indeed a functioning CPT enzyme even if it was not capable of producing long chain rubber polyisoprene by itself.

Next Asawatreretanakul *et al* added purified rubber particles to the assays containing HRT1 or HRT2. Rubber particle addition dramatically increased IPP incorporation, and led to the detection of large amounts of long chain products comparable to the length of natural rubber itself. Rubber particle addition to HRT1 had no additional affect, and rubber particles alone produced a small amount of long chain rubber-like products, though significantly less than with the addition of HRT2 to the mix. The findings show that, although HRT2 is capable of producing long chain rubber products, it can only do so in the presence of rubber particles. The rubber particles may contain additional co-factors. A potential co-factor could be from the SRPP protein family, or a CPTL, Nogo-receptor like protein, or a hitherto unknown protein.

Considering the importance of large/small residues in the hydrophobic cleft of CPTs, (**section 1.2.3.2**), it should be noted that HRT2 has a large residue at the corresponding position, despite its ability to synthesise long chain polymers in the presence of rubber particles. This may further support the hypothesis that in rubber synthesis the hydrophobic cleft common to 'conventional' CPTs may be bypassed in some way, and the hydrophobic rubber particle interior instead accepts the long polymer chains.

1.4.3 Plant CPTs from other latex producing species

Dandelions produce latex, in particular the species *Taraxacum kok-saghyz* and *Taraxacum brevicorniculatum* produce high quality natural rubber and are touted as a potential alternative source of natural rubber. However there are a number of barriers to overcome, including latex yield and the ease of extraction, areas in which *Hevea* holds a significant advantage. However due to the relative ease of genetic manipulation compared to *Hevea*, much of the research into rubber biosynthesis takes places in *Taraxacum* species.

In addition to dandelion, rubber producing plants include the lettuce species *Lactuca sativa* which produces latex with high polymer weight comparable to dandelion although not quite as high as *Hevea*. *L. sativa* however along with dandelion, and as opposed to *Hevea* is ideal for investigating rubber biosynthesis due to its short life cycle and relative ease of transformation.

CPT enzymes have been identified in *Taraxacum* and also *Lactuca sativa*. In addition CPTL proteins have been shown to interact with CPTs in these species (Epping *et al* 2015, Qu *et al* 2015). The roles of CPT and CPTL proteins in other rubber producing species could shed light on rubber biosynthesis in *Hevea* itself.

1.4.3.1 The role of *Taraxacum* CPT in polyisoprene synthesis

Three CPTs were identified in *T. brevicorniculatum*, initially thought to be *T. kok-saghyz* but later retconned, by Schmidt (2010a) from *T. brevicorniculatum* roots, using the conserved CPT regions as the basis for RT-PCR. The three CPTs TbCPT1-3 were shown to contain the 5 conserved regions common to known CPTs.

TbCPT 1-3 were found to be most strongly expressed in *T. brevicorniculatum* latex and a parallel study (Schmidt *et al* 2010b) used western blot analysis on *T. brevicorniculatum* rubber particles, with antigens designed against TbCPT 1-3, to demonstrate that TbCPTs are associated with rubber particles. This was the first study to show that CPTs are present are associated with these structures.

In the same study TbCPTs 1-3 were expressed in yeast strain SNH23-7D which contains a supressed mutant yeast CPT gene *rer2* which synthesises dolichol (Sato *et al* 1999). Each of the three TbCPTs were able to compensate for the suppression of the yeast *rer2* gene showing that each TbCPT were able to synthesise the formation of CPT products in a similar manner to ACPT or HRT2 without rubber particles.

Further evidence for the role of TbCPTs in polyisoprene and rubber biosynthesis was shown by Post *et al* (2010). She showed that that RNAi silencing of TbCPT leads to a knockout of rubber polyisoprene synthesis in *T. brevicorniculatum*, by comparing the latex extracts of TbCPT-RNAi lines to wild type, with partial silencing resulting in partially reduced synthesis and complete silencing resulting in total elimination of rubber synthesis. TbCPT-RNAi lines of *T. brevicorniculatum* also contain much smaller and fewer rubber particles than wild type. These results show the importance of CPTs in rubber synthesis in *T. brevicorniculatum* and further hints at probable role for CPTs in a rubber biosynthetic complex in *Hevea*.

1.4.3.2 The role of *Taraxacum brevicorniculatu* TbRTA and *Lactuca sativa* CPTL in rubber synthesis

As previously mentioned in **section 1.2.3.3**, Nogo receptor like proteins NgBR, later classed as a CPTL, may interact with CPT and be required for dolichol biosynthesis (Harrison *et al* 2011). A plant CPTL LEW1 was later identified in *Arabidopsis* (Zhang *et al* 2008) , and very recently a CPTL protein was identified first in *T. brevicorniculatum* (Epping *et al* 2015) that shared homology to LEW1 and NgBR.

Epping *et al* (2015) reported that the *T. brevicorniculatum* CPTL, TbRTA was able to interact with TbCPTs bringing TbCPT to the endoplasmic reticulum. In addition knock-down of TbRTA by RNAi resulted in a knockout of rubber biosynthesis. TbRTA was shown to be expressed highly in *T. brevicorniculatum* latex and immunoblotting of TbRTA revealed that it was associated with rubber particles. Knock-down of TbRTA

also resulted in an inhibition of TbCPT. This was hypothesised to be an elimination of the rubber transferase complex assembly.

Following this work by Epping *et al* a further CPTL protein has been found in *L. sativa* (Qu *et al* 2015). Qu *et al* showed that the *L. sativa* CPTL was able to interact with *L. sativa* CPT and demonstrated via transient expression in *Nicotiana benthamiana* leaves, that co-infiltration with CPTL alters the localisation of CPT was from cytosolic to the endoplasmic reticulum, showing that CPTL could act to tether a 'conventional' CPT to the ER. As rubber particles are hypothesised to originate from the endoplasmic reticulum it is possible that a CPTL in *Hevea* could act to tether CPTs to rubber particles as well, although this has yet to be determined.

1.5 The SRPP protein family

First identified as agents responsible for latex allergy, the highly homologous REF and SRPP proteins are the most abundant proteins found on rubber particles. They are both part of, and the original members of, what is now known as the SRPP protein family. REF and SRPP are significantly more highly expressed in *Hevea* latex compared with other tissues (Tang *et al* 2016). SRPP protein homologs have now started to be found throughout the plant kingdom (Schmidt *et al* 2010a, Horn *et al* 2013, but are so far thought to be plant specific, with no relatives discovered in bacteria, yeast or animal species.

1.5.1 *Hevea* SRPP

Originally known as Hevb3 and first identified as one of the agents responsible for latex allergy, SRPP was first cloned and characterised by Oh *et al* (1999). Although SRPP was originally not thought to be upregulated in response to latex stimulation by ethylene treatment, this was disproven by a later study (Chow *et al* 2012). Oh *et al* did however show that SRPP has a role to play in rubber biosynthesis, with recombinant SRPP increasing IPP incorporation in rubber biosynthesis assays.

1.5.2 *Hevea* REF

The most abundant protein found in latex and originally known as Hevb1, rubber elongation factor (REF) is a candidate component of the rubber biosynthetic complex. Like SRPP is it one of the proteins responsible for latex allergy. REF was given its name after it was demonstrated by Dennis & Light (1989) to affect IPP incorporation on rubber particles themselves, although its precise functions or mechanisms was not known at the time or indeed even now. Disruption of the REF protein resulted in IPP polymerization being brought to a halt (Dennis & Light 1989).

Priya *et al* (2007) compared the transcription levels of REF mRNA from different *Hevea* clones which had varying latex yields. Priya *et al* showed a positive correlation between REF expression and the latex yield, with REF expressed up to 5 times as much in the high yielding clones such as RRII105 compared to low yielding clones such as KRS163. REF was also upregulated in response to ethylene treatment that stimulated latex synthesis.

1.5.3 Differences between SRPP and REF

SRPP and REF share a high degree of homology, however SRPP is a 24kDa protein whereas REF at 14kDa exists almost as a truncated version of SRPP with its C terminus missing (Figure 1.6). However experiments where the 'elongated' C- terminus of SRPP is deleted and brought in line with REF reveal no change in SRPP properties (Berthelot *et al* 2014b).

Whereas homologs of SRPP have now been discovered in many other plant species (Kim *et al* 2016), so far the truncated REF version has only been identified in *Hevea*. It may be that whilst REF could be important in rubber biosynthesis, it is not essential. However it could be an essential factor for the particularly high molecular weight rubber found in *Hevea*. SRPP has also been shown to not be present in some rubber-producing species (Singh *et al* 2003) though its hypothesised role in stabilising rubber particles may be taken up by another unrelated protein.

Bahri and Hamzah (1996) investigated the localisations of SRPP and REF in *Hevea*, and raised primary antibodies against both proteins. They showed that SRPP was located on

small rubber particles, hence its name, whereas REF was located on large rubber particles. As small rubber particles are the primary site for rubber biosynthesis it was concluded that SRPP had the greater importance. Later it was demonstrated by Bahri & Hamzah, that REF is also located on small rubber particles (Xiang *et al* 2012). This, coupled with Priya *et al*'s (2007) findings, indicates that both proteins could have a role to play in rubber biosynthesis.

While both REF and SRPP associate with rubber particles, they are predicted to do so in different ways. Using model membranes with polarization modulation infrared reflection-absorption spectroscopy (PM-IRRAS) analysis, Berthelot (2014a) showed that recombinant SRPP acts to coat model monolayer membranes, whereas REF inserts into the membrane. The validates Dennis and Light's (1989) observations when they found that REF was difficult to wash off from rubber particles whereas SRPP could be more easily removed, perhaps indicating REF is more tightly embedded into the membrane. In addition Berthelot (2014a) demonstrates that REF protein may form micelles and break off from the membrane. This micellization may even be related to the 'budding process,' from which rubber particles are thought to originate from the endoplasmic reticulum.

Figure 1.6 Amino acid sequence alignment of *Hevea* SRPP and REF
The two proteins are very homologous sharing many conserved regions. However REF has a 'truncated' C terminus compared to SRPP

1.5.4 The role of the SRPP family in dandelion latex

SRPP proteins have been identified in many rubber-producing plant species, including dandelion (*T. brevicorniculatum).* Five of these proteins, TbSRPP1-5, were discovered (Schmidt *et al* 2010a) which were homologous to SRPP in *Hevea,* although no REF homolog has been identified.

Hillebrand *et al* (2012) showed by immunogold labelling of purified rubber particles of *T. brevicorniculatum*, that TbSRPP are located on the rubber particles themselves, much like the *Hevea* SRPP. Hillebrand *et al* created transgenic SRPP-RNAi to downregulate TbSRPP, RNAi lines containing only around 30% rubber content compared to wild type, a significant decrease in the amount of rubber synthesised. C^{14}-IPP incorporation was also measured, again showing a significant decrease in RNAi lines compared to wild type. Hillebrand *et al* reported that the molecular weight of the rubber produced was not affected. However, research carried out around the same time by Collins-Silva *et al* (2012), on closely related *T. koksaghyz* SRPP proteins showed that RNAi lines do decrease the molecular weight of rubber produced, as well as severely reducing rubber content. So, whilst it can be concluded that SRPPs are involved in polyisoprene rubber synthesis and certainly enhance it, whether they are essential for synthesis, particularly in *Hevea*, is debatable. The importance of SRPP proteins may differ from organism to organism and even from SRPP to SRPP isoform.

Rubber particles extracted from SRPP RNAi lines of *T. brevicorniculatum* show a greater aggregation and discrepancy in size (Hillebrand *et al* 2012), indicating that SRPP is important for the stability of rubber particles. TbSRPPs, as *Hevea* SRPP is predicted to do by PM-IRRAS analysis, may coat the monolayer membrane, presenting an outward facing negative charge to the cytosol of the latex. This could act to stabilise rubber particles in the colloidal suspension and provide a stable surface and maintain a high surface area to volume ratio of rubber particles for optimum synthesis of high molecular mass rubber. The fact that *Hevea* SRPP is predominantly found on small rubber particles where high molecular mass rubber is synthesised may support this hypothesis.

1.5.5 The SRPP protein family, their role in non-latex producing species

The evolutionary reasons for latex production are poorly understood. The function of the SRPP protein family in non-latex producing species may provide an answer to the reason behind later production. *Arabidopsis* contains a number of SRPP proteins. Kim *et al* (2016) used transient expression in *N. benthamiana* leaves to show that *Arabidopsis* SRPP proteins associate with lipid bodies. Whilst *N. benthamiana* leaves do not usually contain lipid bodies Kim co-infiltrated with the transcription factor LEC2 in order to induce lipid body formation, and establish that SRPP subsequently localises to them. Whilst lipid bodies may have a variety of roles, one such possibility, is their involvement in plant stress responses (van der Schoot *et al* 2011).

BAR's *Arabidopsis* eFP browser (Winter *et al* 2007) shows that *Arabidopsis* SRPP protein At3g05500, is upregulated in response to leaf wound stress (Figure 1.7.). As previously mentioned, one potential function of natural rubber is as a defence against biting insects or pathogens. At3g05500 is also upregulated in response to *Pseudomonas syringae* infection, perhaps highlighting a role for the SRPP protein family as anti-microbial or as general stress related proteins. It is possible that latex has this role in plants, as SRPP and REF are the most abundant proteins located in latex and on rubber particles.

The SRPP protein family has been identified in other non-latex producing species. This includes LDAP1 and LDAP2 in the avocado, *Persea americana*. Horn *et al* (2013) identified LDAP1-2 and found the proteins were located on lipid bodies in both *P. americana*, and in a similar manner to *Arabidopsis* SRPPs, *N. benthamiana* cells. Whilst Kim *et al* (2016) used transient expression with LEC2, Horn *et al* transformed BY2 cells which were induced to form lipid bodies. *P. americana* SRPPs may play a role in lipid body stabilisation, and also in compartmentalizing triacylglycerols and other hydrophobic compounds (Horn *et al* 2013). SRPPs may have a similar role in compartmentalising and stabilising polyisoprene latex in *Hevea*.

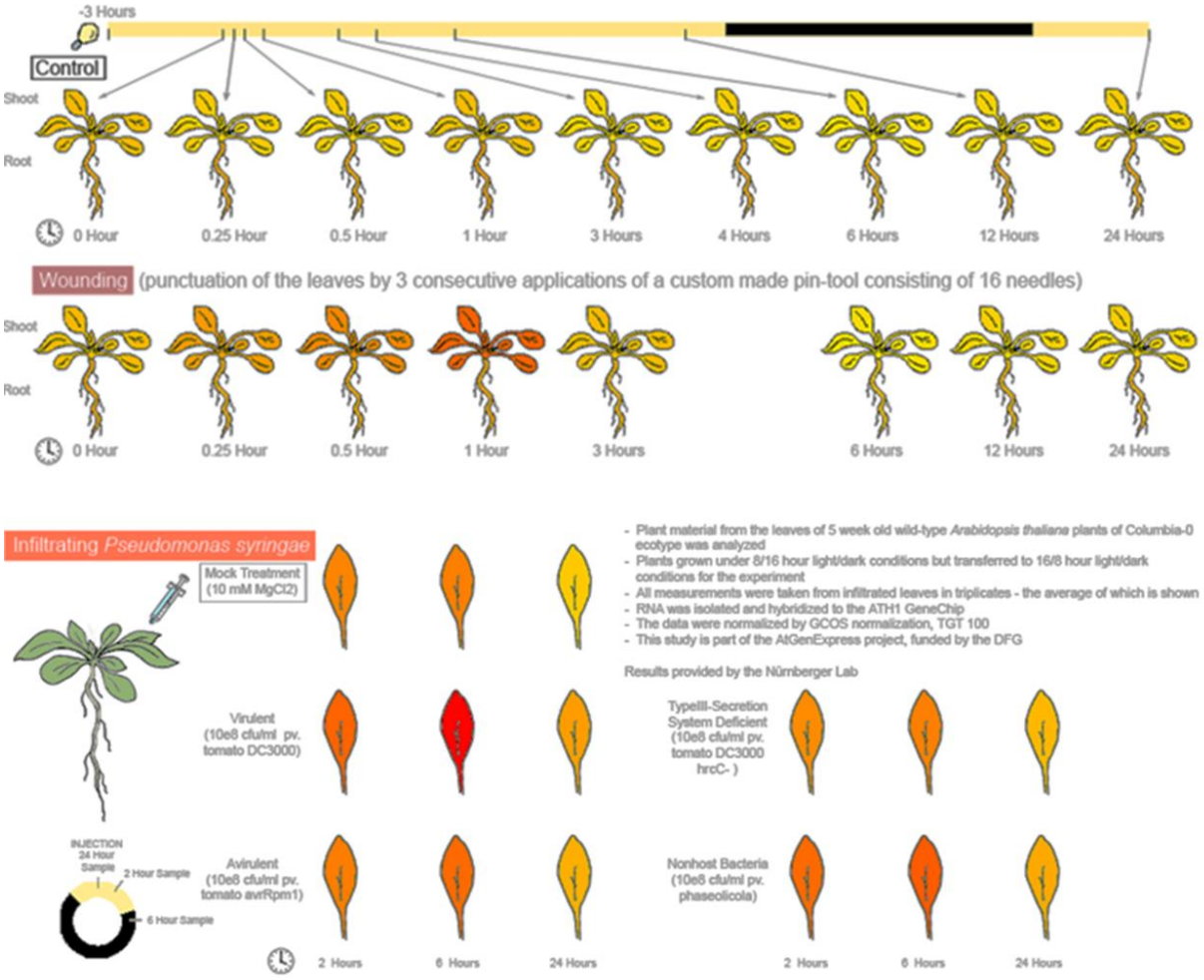

Figure 1.7 Expression profile of *Arabidopsis* SRPP At3g05500 from *Arabidopsis* eFP browser (Winter *et al* 2007)

Compared to the control (top row) At3g05500 is strongly expressed in response to both leaf wounding with the highest levels of expression occurring 1 hour after puncture. At3g05500 is also highly expressed in response to infection with virulent *Pseudomonas syringae*. Yellow indicates basal level of expression with darker red indicating higher levels of expression.

1.6 Other potential rubber synthetic proteins – Rubber biosynthesis stimulator protein

Although CPT and SRPP/REF are currently the most promising targets for a potential rubber biosynthetic complex, there are likely to be many other genes involved. One such protein could be *Hevea* eIF-5A, also known as RBSP. Yusof *et al* (2000) first isolated RBSP from *Hevea* latex fractions with the fractions being included in rubber biosynthesis assays measuring the uptake of radiolabelled ^{14}C-IPP. The study found that RBSP fractions dramatically increased the rate of ^{14}C-IPP incorporation by up to 240% compared to controls. A subsequent study by Chow *et al* (2006) this time using recombinant RBSP also showed a significant increase in ^{14}C-IPP incorporation when RBSP was added to rubber biosynthesis assays. Although since this finding research into RBSP has been limited, it has been shown to upregulated in response to ethylene treatment in a similar manner to HRT2 (Chow *et al* 2012) and will be included in my search for a rubber biosynthetic complex.

1.7 Project aims

Little is known about the cell biology of natural rubber biosynthesis within *Hevea brasiliensis* despite the importance of natural rubber as a resource. The nature of *Hevea*, including its long life span and its resistance to any form of transient genetic transformation, mean very little is known about the genes/proteins involved in producing natural rubber although some work has been conducted in other species such as dandelion.

So far, whilst individual proteins such as HRT2, REF, SRPP and RBSP have been shown to have an effect on IPP incorporation *in vitro*, there has been no research investigating potential interactions between these different proteins as part of a larger protein complex.

Whilst HRT2 is a CPT expressed in latex, and can under certain conditions form long chain polyisoprene, little is known about how and if it can interact with rubber particles. As HRT2 alone cannot synthesise natural rubber and can only do so in the presence of rubber particles, it is likely that it interacts with other proteins on the rubber particle

surface; again, there has been limited research investigating this mechanism. Some CPTs are now known to require the action of Nogo-receptor like CPTL proteins in order to function. The key question of this thesis is that if there is such a CPTL homolog in *Hevea* does it interact with rubber particles or HRT2 itself?

1.7.1 Aims and experimental approach

The lack of basic information on the enzymes and processes involved in rubber biosynthesis make the generation of high yielding transgenic lines of *Hevea* impossible at the current time. Therefore the initial aim of this thesis was to clone and characterise more of the cell biology of rubber biosynthetic proteins starting with HRT2. Whilst HRT2 was a convenient starting point, the scope of the project was widened to include other potential rubber associated proteins SRPP, REF, RBSP and if found, a *Hevea* CPTL. Using transient expression in *N. benthamiana*, confocal microscopy was used to determine their subcellular localisation, their possible membrane or rubber particle association and their topology. Whilst much of the work was conducted in *N. benthamiana*, attempts were also made to conduct experiments in the latex producing species *Lactuca sativa*, as the correct system could be crucial for proper localisation and functioning of these proteins.

Based on the TbRTA protein characterised by Epping *et al* (2015) the *Hevea* genome was searched for a CPTL protein in *Hevea*. The *Hevea* CPTL named HevNogo was then cloned and characterised in order to determine its cell localisation and if it could interact with HRT2.

Molecular biology techniques such as Yeast-2-Hybrid and co-immunoprecipitation, were used to investigate potential interactions between the candidate proteins HRT2, SRPP, REF, RBSP and HevNogo.

To investigate the capacity for any group of these enzymes to enhance IPP incorporation in rubber biosynthesis assays, attempts were made to produce recombinant HRT2, SRPP, REF and HevNogo proteins, although protein production was met with limited success.

Chapter 2: Material and Methods

2.1 Suppliers of chemicals and reagents

Reagents were obtained from the following suppliers and were of analytical grade if possible.

Supplier	**Country**	**Reagent or Material**
Amersham	UK	ECL Prime Western Bloting Detection Reagant
B&Q	UK	Compost
Bioline	UK	Accuzyme™ DNA polymerase
Chromotek	Germany	Anti GFP and RFP
		Anti myc
		GFP and RFP Trap™ Beads
Invitrogen	UK	1kb plus DNA Ladder
		BP Clonase™ II
		LR Clonase™ II
		Restriction endonucleases and buffers
		Shrimp alkaline phosphotase
		T4 DNA Ligase and Ligase buffer
Miltenyi Biotech	Germany	Anti-GFP-HRP
MP Biomedical SAS	UK	Agarose
National Diagnostics	USA	Protogel 30
New England Biolabs	UK	Chitin Resin
		Color Prestained Protein Standard, Broad Range (11-245 kDa)
		ER 2566 *E. coli* expression cells
		KLD enzyme mix and buffer
		Restriction endonucleases and buffers
		T4 DNA Ligase and Ligase buffer
Promega	USA	Anti mouse IgG HRP conjugate
QIAGEN	Germany	Qiaprep Maxi® Plasmid Kit
		Qiaprep® Spin Plasmid Kit
		Qiaquick® Gel Extraction Kit

		Qiaquick® PCR purification Kit
Roche	Germany	cOmplete™ protease inhibitor tablets
Sigma-Aldritch	UK	Acetosyringone
		Anti Rabbit IgG HRP conjugate
		Antibiotics
		Antibiotics
		β-mercaptoethanol
		Brefeldin A
		Coomassie R-250
		DTT
		DMSO
		EDTA
		Formaldehyde
		FPP
		Gluthathione (oxidised and reduced)
		Guanadine hydrochloride
		IPP
		Magnesium sulfate
		Murashige and Skoog basal medium
		Nile Red
		NP40
		Oligonucleotides
		Silver Nitrate
		Sodium thiosulfate
		TEMED
		Triton X
		TWEEN-20
		Urea
Sinclair	UK	Vermiculite
Tesco	UK	Marvel dried milk powder
Thermo-Fisher	USA	Acetic acid (glacial)
		Acetone

		GeneJET Plasmid Miniprep Kit
		Glucose
		Hydrochloric acid
		Sodium chloride
		Sodium dodecyl suplhate
		Sucrose
VWR International	UK	GelRed^{TM} nucleic acid stain
		IPTG

2.2 List of buffers and media

Name	**Components**
Breaking buffer	0.5 M NaCl, 20 mM Tris-HCl (pH 8.5), 7 M Guanidine-HCl
Column buffer	0.5 M NaCl, 20 mM Tris-HCl (pH 8.5)
DNA leaf extraction buffer	200 mM Tris (pH7.5), 250 mM NaCl, 250 mM EDTA, 0.5% SDS
E. coli cell lysis buffer	0.5 M NaCl, 20 mM Tris-HCl (pH 8.5), 0.1% NP-40
Infiltration medium	(To make 50 ml) 5 ml of 1 M MES solution, 5ml of 1 M sodium triphosphate solution, 250 mg glucose, 10 ul of 1 M acetosyringone, made up to 50 ml with dH_2O.
Laemmli buffer 2X	4% SDS, 20% glycerol, 120 mM Tris-HCl (pH 6.8), 0.02% bromophenol blue, 4% β-mercaptoethanol
LB Medium	10 g/l tryptone, 5 g/l yeast extract, 10 g/l NaCl
Low salt	10 g/l tryptone, 5 g/l yeast extract, 0.085 M NaCl
LBA	10 g/l tryptone, 5 g/l yeast extract, 170 mM NaCl, 15 g/l agar

Plant cell lysis buffer	10 mM Tris-HCl (pH 7.5), 150 mM NaCl, 0.5 mM EDTA, 0.5% NP-40, 1 protease inhibitor tablet per 50 ml (fresh each time)
Plant cell wash buffer	10 mM Tris-HCl (pH 7.5), 150 mM NaCl, 0.5 mM EDTA
Renaturation buffer A	0.5 M NaCl, 20 mM Tris-HCl, 8 M Urea
Renaturation buffer B	0.5 M NaCl, 20 mM Tris-HCl, 6 M Urea
Renaturation buffer C	0.5 M NaCl, 20 mM Tris-HCl, 4 M Urea
Renaturation buffer D	0.5 M NaCl, 20 mM Tris-HCl, 2 M Urea, 0.1 mM oxidised glutathione, 1 mM reduced glutathione
Renaturation buffer E	0.5 M NaCl, 20 mM Tris-HCl, 0.1 mM oxidised glutathione, 1 mM reduced glutathione
SOC media	20 g/l tryptone, 5 g/l yeast extract, 10 mM NaCl, 2.5 mM KCL, 20 mM $MgSO_4$, 20 mM glucose
Stacking gel buffer	0.5 M Tris-HCl (pH 6.8), 0.4% SDS
Resolving gel buffer	1.5 M Tris-HCl (pH 8.8), 0.4% SDS
TAE buffer	40 mM Tris, 20 mM Acetate, 1mM EDTA, pH 8.3
Transfer buffer	1X Tris/Glycine, 20% methanol, 70% dH_2O
YPDA	20 g/l Bacto yeast extract, 40 g/L Bacto peptone, 40 g/L glucose monohydrate, 80 mg/l adenine hemisulfate, up to 1 l with dH_2O
YPDA (plates)	addition of 17 g/l agar
Silver Stain solutions (single use recipes)	
(1) Fixer solution	60 ml 50% acetone, 1.5 ml 50% TCA, 25 µl formaldehyde

(2) Wash solution	50% acetone
(3) Enhancer solution	10 mg Na-thiosulfate, made up to 60 ml in dH_2O
(4) Staining solution	135 mg silver nitrate, 500 µl formaldehyde, made up to 50 ml in dH_2O
(5) Developing solution	1.2 g Na_2CO_3, 25 µl formaldehyde, 2.5 mg Na-thiosulfate, made up to 60 ml in dH_2O
(6) Stopping solution	1% Acetic Acid

2.3 Preparation, maintenance and transformation of competent cells

2.3.1 Preparation of chemically competent *E. coli* DH5α cells

A starter culture was prepared by inoculating 10 mls of LB with 50 µl of DH5α cells and incubated for 16 hours at, shaking at 220 rpm. 500 µl of this culture was used to inoculate 100 ml of LB in a 1l conical flask. The cells were incubated at 37ºC, shaking for 220 rpm. A measurement of OD_{600} was taken (Biochrom Ultrospec 3300 Pro Spectrophotometer) using LB as a blank. At an OD_{600} reading of ~0.6, cells were harvested by centrifugation at 4ºC for 15 minutes. The supernatant was discarded and the cell pellet was re-suspended in 25 ml ice cold 50 mM $CaCl_2$. The cells were incubated on ice for 10 minutes and then harvested by centrifugation as described previously. The supernatant was discarded and the cells were re-suspended in 3 ml ice cold 50 mM $CaCl_2$. The cells were incubated for 1 hour on ice before being transferred to pre-cooled 1.5 ml Eppendorf tubes in 50 µl aliquots. These were frozen in liquid nitrogen and stored at -80ºC. All media and flask used were pre-sterilized using an autoclave.

2.3.2 Preparation of chemically competent T7 expression host *E. coli* cells

2.3.2.1 ER2566 cells

A sterile loop was used to streak ER2566 cells onto an LBA plate; these were grown overnight at 37ºC, the subsequent colonies viable for a starter culture for up to four weeks at 4ºC. A starter culture was prepared by using a loop to inoculate 10 mls of LB with ER2566 cells which were incubated for 16 hours at, shaking at 220 rpm. 100 µl of this culture was used to inoculate 10 ml of LB in a 50 ml falcon tube. The cells were incubated at 37ºC, shaking at 220 rpm. A measurement of OD_{600} was taken (Biochrom Ultrospec 3300 Pro Spectrophotometer) using LB as a blank. At an OD_{600} of ~0.6 cells were harvested by centrifugation at 4ºC for 10 minutes. The supernatant was discarded and the cells were re-suspended in 10ml ice cold 100mM $MgCl_2$. The cells were incubated for 5 minutes on ice and then harvested by centrifugation as described previously. The supernatant was discarded and the cells were re-suspended in 1 ml ice

cold 100 μM $CaCl_2$. The cells were incubated for 1 hour on ice before being transferred to pre-cooled 1.5 ml Eppendorf tubes in 50 μl aliquots and used immediately for transformation. All media and tubes were pre-sterilized and all procedures carried out in a sterile flow cabinet.

2.3.2.2 C43 (Rosetta™) cells

The protocol is the same as for ER2566 cells except for the addition of 24 μg/ml chloramphenicol to LB media in order to select for the pRARE2 plasmid.

2.3.3 Preparation of chemically competent *Agrobacterium tumefaciens* C58 and GV3101 cells

C58 and GV3101 cells from glycerol stocks (20 mM $CaCl_2$, 20% glycerol) were inoculated in 10 mls of LB and incubated for 16 hours at 28°C shaking at 220 rpm to produce a starter culture. 1 ml of this culture was used to inoculate 100 ml of LB in a 1l conical flask. Cells were grown at 28°C, shaking at 220 rpm. A measurement of OD_{600} was taken (Biochrom Ultrospec 3300 Pro Spectrophotometer) using LB as a blank. At an OD_{600} of ~0.6 cells were harvested by centrifugation at 4°C for 10 minutes. The supernatant was discarded and the cells were re-suspended in 1ml ice cold 20 mM $CaCl_2$. On ice the cells were transferred to pre-cooled 1.5 ml Eppendorf tubes in 50 μl aliquots. These were frozen in liquid Nitrogen and stored at -80°C. All media and flask used were pre-sterilized using an autoclave.

2.3.4 Transformation of *E. coli* DH5α cells

Each tube of cells containing 50 μl aliquots of cells was allowed to thaw on ice for ~5 minutes. 0.1-1 ug of plasmid DNA was added to each tube which was incubated on ice for 30 minutes. Cells were heat shocked at 42°C for 30 seconds then incubated on ice for at least a further 2 minutes. 950 μl of SOC media was added to each tube which was incubated at 37°C shaking at 220 rpm for 1 hour. Cells were harvested by centrifugation at 3000 rpm for 5 minutes. 850 μl of supernatant was discarded and the pellet re-suspended in the remaining 150 μl. This suspension was plated on LBA plates with appropriate antibiotics and incubated at 37°C overnight.

2.3.5 Transformation of E. *coli* cells for protein expression

2.3.5.1 ER2566 cells

Each tube of cells containing 50 µl aliquots of cells was allowed to thaw on ice for ~5 minutes. 0.1-1 ug of plasmid DNA was added to each tube which was incubated on ice for 30 minutes and then at room temperature for 10 minutes. 950 µl of SOC media was added to each tube which was incubated at 37°C, shaking at 220 rpm for 1 hour. Cells were harvested by centrifugation at 3000 rpm for 5 minutes. 850 µl of supernatant was discarded and the pellet re-suspended in the remaining 150 µl. This suspension was plated on LBA plates with appropriate antibiotics and incubated at 37°C overnight. A starter culture containing 10 mls LB with appropriate antibiotics was prepared by picking a colony. This was incubated at 30°C, shaking at 220 rpm for 16 hours and was used as a started culture for subsequent IPTG induction

2.3.5.2 C43 (Rosetta™) cells

The protocol is the same as for ER2566 cells except for the addition of 24 µg/ml chloramphenicol to LB media in order to select for the pRARE2 helper plasmid.

2.3.5.3 Transformation of lethal/unstable constructs into ER2566 and C43 (Rosetta™) cells

When transforming HRT2 and HevNogo constructs, cells were not plated on LBA. Instead after the addition of 950 µl SOC, and incubation at 37°C, shaking at 220 rpm for 1 hour, 100 µl of this cell culture was used to inoculate 10 mls of LB containing 1% glucose and appropriate antibiotics. This was incubated at 30°C, shaking at 220 rpm for 16 hours and was used as a started culture for subsequent IPTG induction.

2.3.6 Transformation of C58 and GV3101 cells

Each tube containing 50 µl aliquots of cells was allowed to thaw on ice. 0.1 to 1 µg of plasmid DNA was added to each tube and incubated for 10 minutes on ice. The cells were then frozen on dry ice for 2 minutes before being allowed to thaw on ice; this was repeated once before the cells were allowed to thaw at room temperature for 10 minutes.

450 µl of SOC was added to each tube and the cells were incubated at 28°C, shaking at 220 rpm for 3 hours. 400 µl of supernatant was discarded and the pellet re-suspended in the remaining 100 µl. This suspension was plated on LBA plates with appropriate antibiotics and incubated at 28°C for 2-4 days.

2.4 Nucleic acid techniques

2.4.1 Preparation of plasmid DNA from *E. coli* DH5α cells

The 'ThermoFisher GeneJET Plamid Miniprep Kit' was used to purify plasmid DNA. A single colony of cells was used to inoculate 10 mls of LB. This was incubated at 37°C for 16 hours, shaking at 220 rpm. Cells were harvested by centrifugation at 3,000 rpm for 10 minutes (Eppendorf 5810-R centrifuge), the supernatant was discarded and plasmid DNA extracted according to the manufacturer's instructions. DNA was eluted in 30 µl of manufacturer's elution buffer and stored at -20°C.

2.4.2 Preparation of genomic DNA from plant leaf tissue

Approximately 1 cm^2 of leaf tissue was transferred to a 1.5 ml Eppendorf tube and homogenised using a sterile pestle in 400 µl of DNA leaf extraction buffer. The mix was incubated at room temperature for 1 hour then centrifuged at 13,000 rpm for 1 minute. 300 µl of supernatant was transferred to a clean 1.5 ml Eppendorf tube then 300 µl of ice cold isopropanol was added. The mixture was vortexed and left to stand for 2 minutes to allow for DNA precipitation, before centrifugation at 13,000 rpm for 10 minutes. The supernatant was discarded and the pellet was re-suspended in 500 µl of ice cold 70% ethanol before centrifugation once more at 13,000 rpm for 5 minutes. The supernatant was discarded and the pellet allowed to completely dry. 100 µl of dH_2O was used to re-suspend the pellet and typically 1-5 µl of the solution was used for PCR.

2.4.3 Amplification of DNA by PCR

DNA fragments were amplified from either *Hevea* plant genomic/ cDNA or from a vector containing the desired sequence. Bioline's 2x 'ACCUZYME^{TM} Mix' containing ACCUZYME DNA Polymerase, $MgCl_2$ and ultra-pure dNTPs, was generally used for PCR and reactions typically carried out in a Biometra T3000 Biocycler. A typical PCR reaction contained 1 µl (10 ng/µl) of template DNA, 1 µl each of 20 µM primer, 22 µl dH2O and 25 µl of ACCUZYME^{tm} Mix. A typically PCR protocol involved an initial denaturation for 3 minutes at 98^{o}C, followed by 25 cycles of denaturation, annealing and extension at 98^{o}C for 15 seconds, 55^{o}C for 15 seconds and 72^{o}C for 90 seconds/kb respectively, followed by a final extension of 2 minutes. PCR conditions varied depending on template length and complexity, and also primer melting temperature, and were optimised for each reaction. Reaction products were analysed by agarose gel electrophoresis and either excised/purified via agarose gel extraction or via PCR purification.

2.4.4 Mutation of plasmid DNA via PCR/KLD reaction

Mutations were carried out via PCR with the use of an NEB 'Q5® Site-Directed Mutagenesis Kit.' An initial PCR reaction was carried out using 'Q5 Hot Start High-Fidelity 2X Master Mix' and back-to-back mutagenic primers. A typical reaction contained 1 µl (10 ng/µl) of template plasmid DNA, 25 µl of 'Q5 Hot Start High-Fidelity 2X Master Mix' with 1 µl each of 10 µM primer, 9 µl of dH_2O and 12.5 µl of 'Q5 Hot Start High-Fidelity 2X Master Mix.' A typically PCR protocol involved an initial denaturation for 20 seconds at 98^{o}C, followed by 25 cycles of denaturation, annealing and extension at 98^{o}C for 10 seconds, 65^{o}C for 20 seconds and 72^{o}C for 20 seconds/kb respectively, followed by a final extension of 2 minutes. PCR conditions varied depending on template concentration, length and complexity, and also primer melting temperature, conditions were optimised for each reaction.

Kinase, Ligase and Dpn1 (KLD) treatment, to phosphorylate and ligate the blunt ended PCR product, and also to remove template DNA, was carried out in a single reaction typically using 1 µl of PCR product, 5 µl of 2X KLD Reaction Buffer, 1 µl of 10X KLD Enzyme Mix and 3 µl of dH_2O with the reaction taking place at room temperature for 5 minutes. 5 µl of KLD reaction was used to transform competent DH5α cells.

Initial PCR product was analysed by agarose gel electrophoresis, in the event of multiple bands the correct band was excised and purified by agarose gel purification before addition to the KLD mix.

2.4.5 Restriction endonuclease digestion of DNA

In order to prepare insert fragments and vector for ligation and to screen potential constructs for correct insertion of vector, restriction digests were performed. Using restriction endonucleases typically provided by NEB, a typical reaction contained 1 µl per restriction enzyme, 2 µl of 2X NEB CutSmart® buffer, 500 ng of DNA and up to 20 µl of dH_2O. Reactions were carried out at 37°C for 1 hour followed by a 65°C heat shock for 15 minutes using a Biometra T3000 Biocycler. Reaction products were analysed using agarose gel electrophoresis and excised/purified if required via agarose gel purification.

2.4.6 Ligation of DNA fragments

DNA ligations were performed using NEB T4 ligase, following restriction digest, insert and vector were ligated at a 3:1 molar ratio for cohesive end ligations and a 5:1 molar ratio for blunt end ligations. A typical reaction consisted of 10-50 ng of vector, an appropriate amount of insert, 2 µl of 10X T4 DNA Ligase buffer, 1 µl of T4 DNA ligase and up to 20 µl volume with dH_2O. Cohesive end ligations were performed at room temperature for 10 minutes and blunt end ligations were carried out at room temperature for 16 hours. Reactions were purified using a QIAGEN 'MiniElute Reaction Cleanup Kit' according to manufactures protocol and eluted in 10 µl of elution buffer, 2.5 µl of this was used to transform competent cells. Subsequent colonies were screen using PCR for insert and subsequent purified plasmid was screen for insert using restriction digest.

2.4.7 Agarose gel electrophoresis of DNA

Agarose gels were typically made with 1% (w/v) agarose dissolved in 1X TAE buffer containing GelRed Nucleic Acid Gel Stain (1 µl per 20 ml volume). DNA to load was mixed with 6X NEB Purple Loading Dye with approximately 10 µl inserted into each lane, 10 µl of Invitrogen '1kb' or '1kb Plus' DNA ladder diluted with dH20 and orange-G loading dye, was used as a marker. DNA was electrophoresed at 100 V until the dye reached the end of the gel and DNA was visualised using a UV trans-illuminator.

2.4.7.1 Agarose gel extraction

Visualised bands were excised from the gel using a sharp razor and transferred to 2 ml Eppendorf tubes. DNA was purified from the gel using a QIAGEN QIAquick® Gel extraction kit according to manufacturer's instructions and eluted in 30µl of elution buffer. Purified DNA was stored at -20^{o}C until further use.

2.4.8 Gateway cloning

Invitrogen Gateway® technology was also used to generate constructs. Primers were designed to amplify DNA fragments and attach *att*b1 and *att*b2 sites to the N' and C' terminals respectively. DNA fragments were purified and used directly for BP clonase reactions. DNA was cloned initially into an entry vector via a BP reaction and then subsequently transferred into the desired destination vector via an LR reaction.

2.4.8.1 BP reaction

A typical BP reaction contained approximately 150 ng of *att*B DNA product, 150 ng of pDonrZeo vector, 0.5 µl of BP Clonase^{TM} II enzyme, then made up to a total volume of 5 µl with dH_20. The reaction was well mixed and then incubated either for 2 hours at 25^{o}C or on lab bench overnight. 1 µl of Proteinase K solution was added to terminate the reaction which was then incubated at 37^{o}C for 15 minutes. 1 µl of this reaction was transformed using DH5α cells which were plated on appropriate antibiotics. Un-recombined gateway vector was eliminated due to the presence of the lethal ccdB gene which could not grow in DH5α. Colonies were screened as described previously to check for positive entry clones.

2.4.8.2 LR reaction

A typical LR reaction contained approximately 150 ng of the desired gene in the entry vector, 150 ng of Destination vector, 0.5 µl of LR Clonase™ II enzyme, then made up to a total volume of 5 µl with dH_20. The reaction was well mixed and then incubated either for 2 hours at 25°C or on lab bench overnight. 1 µl of Proteinase K solution was added to terminate the reaction which was then incubated at 37°C for 15 min. 1 µl of this reaction was transformed using DH5α cells which were plated on appropriate antibiotics. Un-recombined destination vector was eliminated due to the presence of the lethal ccdB gene which could not grow in DH5α. Colonies were screened as described previously to check for positive clones.

2.4.9 DNA Sequencing

Sequencing of genomic, plasmid DNA or PCR products was carried out using GATC Biotech's Sanger Sequencing service with samples prepared according to their instructions.

2.5 Constructs and cloning

All constructs generated in this thesis were synthesised using oligonucleotide primers to amplify DNA fragments which were then cloned into destination vectors, either directly or via sub-cloning. DNA fragments were cloned into these vectors either by restriction digest and ligation or via Gateway™ technology. A complete list of oligonucleotide primers used for cloning and sequencing can be found in appendix table A1, and vector maps can be found in appendix **section A.3**.

2.5.1 List of cell lines used in this project

Line	Helper Plasmid	Application	Selection
E. coli DH5α	n/a	Cloning	n/a
E. coli DB3.1	n/a	Cloning	n/a
A. tumefaciens C58	pSOUP	Plant Transformation	Rifampicin (10 μg/ml) and Tetracycline (50 μg/ml)
A. tumefaciens GV3101	pMP90	Plant Transformation	Rifampicin (10 μg/ml) and Gentamycin (50 μg/nl)
E. coli ER2566	n/a	Protein Expression	n/a
E. coli C43 Rosetta ™	pRARE	Protein Expression for rare codons	Chloroamphenicol (35 μg/ml)
S. cerevisiae Y187	n/a	Yeast 2 Hybrid	n/a
S. cerevisiae AH109	n/a	Yeast 2 Hybrid	n/a

2.5.2 List of vectors used in this project

Vector	Application	Selection	Reference
35S:CamV Cassette	pGreen sub-vector	Ampicillin (50 μg/ml)	Hellens *et al* 2000
pGreenII-0029	Plant Transformation	Kanamycin (50 μg/ml)	Hellens *et al* 2000
pDONRzeo	Gateway Vector	Zeocin (50 μg/ml)	Invitrogen™ 2012

pGWB605/606/654/655	Plant Transformation	Streptomycin (50 µg/ml)	Nakamura *et al* 2010
pDEST22	Yeast 2 Hybrid	- Leucine	Invitrogen™ 2005
pDEST32	Yeast 2 Hybrid	- Tryptophan	Invitrogen™ 2005
PTXB1	Protein Expression	Ampicillin (50 µg/ml)	NEB™ #E6901S

2.5.3 List of constructs generated during this project

Construct	Vector	Description
35S:HRT2-YFP	pGreenII-0029	Full length genomic DNA of HRT2 fused in frame with a YFP tag at the C-terminus
35S:YFP-HRT2	pGreenII-0029	Full length genomic DNA of HRT fused in frame with a YFP tag at the N-terminus
35S:HRT2-mCherry	pGreenII-0029	Full length genomic DNA of HRT2 fused in frame with an mCherry tag at the C-terminus
35S:mCherry-HRT2	pGreenII-0029	Full length genomic DNA of HRT2 fused in frame with an mCherry tag at the N-terminus
35S:SRPP-GFP	pGreenII-0029	Full length cDNA of SRPP fused in frame with an GFP tag at the C-terminus
35S:GFP-SRPP	pGreenII-0029	Full length cDNA of SRPP fused in frame with an GFP tag at the N-terminus
35S:GFP-SRPPΔC	pGreenII-0029	A 35S:GFP-SRPP mutant lacking the C-terminus residues 249-253
35S:REF-mCherry	pGreenII-0029	Full length cDNA of REF fused in frame with an mCherry tag at the C-terminus
35S:mCherry-REF	pGreenII-0029	Full length cDNA of REF fused in frame with an mCherry tag at the N-terminus
35S:HevNogo	pGreenII-0029	Full length cDNA of HevNogo
35S:HevNogo-CFP	pGreenII-0029	Full length cDNA of HevNogo fused in frame with a CFP tag at the C-terminus
35S:CFP-HevNogo	pGreenII-0029	Full length cDNA of HevNogo fused in frame with a CFP tag at the N-terminus

35S:HevNogoΔTM1-CFP	pGreenII-0029	A 35S:HevNogo-CFP mutant lacking residues 32-58
35S:HevNogoΔTM2-CFP	pGreenII-0029	A 35S:HevNogo-CFP mutant lacking residues 87-108
35S:RBSP-GFP	pGWB605	Full length cDNA of RBSP with a GFP tag in frame with the c' terminus
35S:GFP-RBSP	pGWB606	Full length cDNA of RBSP with a GFP tag in frame with the n' terminus
35S:HevNogo-RFP	pGWB654	Full length cDNA of HevNogo with an RFP tag in frame with the c' terminus
T7:HRT2-YFP-intein	pTXB1	Full length DNA of HRT2-YFP fused with a self-cleavable intein-CBD tag at the c' terminus
T7:GFP-SRPP-intein	pTXB1	Full length DNA of GFP-SRPP fused with a self-cleavable intein-CBD tag at the c' terminus
T7:REFmCherry-intein	pTXB1	Full length DNA of REF-mCherry fused with a self-cleavable intein-CBD tag at the c' terminus
T7:HRT2-myc-intein	pTXB1	Full length genomic DNA of HRT2 fused with a c' terminal myc epitope tag and a self-cleavable intein-CBD tag at the c' terminus.
T7:HevNogo-myc-intein	pTXB1	Full length cDNA of HevNogo fused with a c' terminal myc epitope tag and a self-cleavable intein-CBD tag at the c' terminus.
Gal4AD-HRT2	pDEST22	Full length HRT2 DNA fused to GAL4 activation domain at the c'terminus
Gal4AD-SRPP	pDEST22	Full length SRPP DNA fused to GAL4 activation domain at the c'terminus
Gal4AD-REF	pDEST22	Full length REF DNA fused to GAL4 activation domain at the c'terminus

Gal4AD-HevNogo	pDEST22	Full length HevNogo DNA fused to GAL4 activation domain at the c'terminus
Gal4BD-HRT2	pDEST32	Full length HRT2 DNA fused to GAL4 binding domain at the n'terminus
Gal4BD-SRPP	pDEST32	Full length SRPP DNA fused to GAL4 binding domain at the n'terminus
Gal4BD-REF	pDEST32	Full length REF DNA fused to GAL4 binding domain at the n'terminus
Gal4BD-HevNogo	pDEST32	Full length HevNogo DNA fused to GAL4 binding domain at the n'terminus
35S:HevNogo-roGFP	pSSO1	Full length HevNogo DNA fused to roGFP at the c' terminus
35S:roGFP-HevNogo	pCMO1	Full length HevNogo DNA fused to roGFP at the n' terminus
PTXB1 (InteinT3C)	PTXB1	PTXB1 vector with point mutation (T3C) in the intein-CBD domain
35S:LEC2	pGreenII-0029	Full length LEC2 cDNA

2.5.4 List of constructs used in the project that were generated previously

Construct	**Application**	**Reference**
GFP-HDEL	Luminal ER marker	Batoko *et al* 2000
ST-YFP	Golgi marker	Saint-Jore *et al* 2002
SKL-GFP	Peroxisome marker	Monosov *et al* 1996
GFP-Calnexin	ER membrane marker	Irons *et al* 2003
Gal4BD-NFYB2/ Gal4AD-NFYB2	Transcription factor (Y2H positive control)	Calvenzani *et al* 2012
Gal4AD-NFYC2/ Gal4BD-NFYC2	Transcription factor (Y2H positive control)	Calvenzani *et al* 2012

GFP-Rab2b	Pre-vacuolar compartment marker	Kotzer *et al* 2004

2.6 Recombinant protein production and purification

The desired DNA sequences were cloned into PTXB1, which encodes a self-cleavable intein tag and a chitin binding domain, by the methods described in section **2.4**. Constructs were then transformed into competent T7 host cells via the methods described in section **2.3**. Protein expression was induced via IPTG and purified as described below. The methods described are modified from the NEB T7 IMPACT^{TM} kit.

2.6.1 IPTG induction

Following on from section **2.3.5** a starter culture was used to inoculate 1l of sterilised LB media, containing appropriate antibiotics, and 1% glucose. The cells were incubated at 37^{o}C, shaking at 220 rpm. A measurement of OD_{600} was taken (Biochrom Ultrospec 3300 Pro Spectrophotometer) using LB as a blank. At an OD_{600} value of ~0.5, a 1 ml aliquot of the culture was taken as a pre-IPTG sample, the cell were harvested via centrifugation. 0.5 mM of IPTG was added and the culture was incubated at 37^{o}C for a further 3 hours. A 1 ml aliquot of the culture was taken as a post-IPTG sample, the cells were harvested via centrifugation. The culture was spun down at 4000 rpm for 10 minutes with the supernatant discarded. Induction of protein was verified via comparison of the pre and post IPTG samples via SDS-PAGE. IPTG induction conditions varied with each protein with temperature and time optimised with each induction varying from 37^{o}C for 2 hours to 15^{o}C for 24 hours.

2.6.2 Cell lysis and protein extraction

Cells were re-suspended in 20 mls of *E. coli* lysis buffer containing protease inhibitors. Cells were lysed, on ice, via sonication in short bursts of 10 seconds ‘on’ followed by a cooling period of 30 seconds ‘off’, with care being taken not to allow the cells to

overheat and the protein denature. The cells were centrifuged at 11,500 rpm for 30 minutes at 4^{o}C. Both the supernatant and pellet were analysed using SDS-PAGE for presence of the protein. Soluble protein present in the supernatant was ready to load onto a chitin column for purification. In the case of insoluble protein, either induction conditions were optimised or the protein in the pellet was unfolded and refolded to obtain soluble protein.

2.6.2.1 Unfolding and refolding insoluble protein aggregates

The cell pellet containing insoluble aggregates was re-suspended in 50 mls of breaking buffer and stired for 1 hour at 4^{o}C. The solution was then centrifuged at 11,500 rpm, and the supernatant transferred into a 'tubing dialysis 19 mm' dialysis membrane. The supernatant was then dialysed successively against renaturation buffer solution A-E (see **2.2 lists of buffers and media)**. The dialysed solution was centrifuged again at 11,500 rpm to remove any remaining impurities and the supernatant was loaded onto a chitin binding column.

2.6.3 Protein cleavage and purification

A GE Healthcare 'X16 15 ml column' was packed with 10 mls of chitin bead slurry and fitted onto an AKTA AVANT along with the protein extract. The column was washed with 200 mls of column buffer before the protein extract was loaded onto the column. In-column cleavage was induced via the addition of 100 mM DTT with incubation for 2-5 days at 4^{o}C. On column cleavage products were analysed by SDS-PAGE. The purified protein was eluted in column buffer whilst the intein tag remained bound to the beads in the column. Eluted fractions were analysed via SDS-PAGE to check for successful elution of the target protein.

2.7 Protein detection via SDS-PAGE

2.7.1 Preparation of polyacrylamide protein gels

Protein gels consist of a combination of a separating gel and a stacking gel and were poured in a BIORAD PROTEAN^{TM} II xi cell which was assembled according to manufacturer's instructions. To make one separating gel the following components were used; 7.5 ml H^2O, 7.5 ml resolving gel buffer, 15 ml acrylamide, 150 µl of 10% APS, 15 µl TEMED. The gel was left approximately 1 hour to polymerise before the stacking gel was poured directly on top. The stacking gel consisted of 6 ml H^2O, 2.5 ml stacking gel buffer, 1.5 ml acrylamide, 30 µl of 10% APS and 15 µl of TEMED with appropriate sized well combs. The gel was left for 1 hour to polymerise and was either used directly or stored at 4^{o}C for up to two weeks.

2.7.2 Separation of proteins by SDS-PAGE

Protein samples were typically mixed with 2X Laemmli loading dye and denatured by incubating at 98^{o}C for 10 minutes. Protein gels were run under constant voltage of 80 V using a 'BIORAD powerpack 300' until the blue loading dye had run off the edge of the gel.

2.7.3 Detection of protein by Coomassie staining

Protein gels were incubated on a shaking platform, in staining solution for approximately 1-2 hours or until the gel turned entirely blue to match the staining solution. Gels were then transferred to de-staining solution and incubated overnight until blue bands were visible and the remainder of the gel had turned clear, sometimes multiple changes of de-staining solution were used.

2.7.4 Detection of protein by silver staining

Protein gels were incubated in fixer solution for 15 minutes on a shaking platform, the fixer solution was poured off, and the gel washed in dH_2O; 3x quickly, 1x for 5 minutes

then 3x quickly. The gel was transferred to wash solution for 5 minutes shaking, the wash solution was poured away and enhancer solution added for 1 minute before pouring off. The gel was washed 3x in dH_2O before staining solution was added and the gel incubated for 8 minutes, shaking. The gel was transferred to a final wash in dH_2O before developing solution was added. Bands appeared very quickly in about 10-20 seconds after which the gel was transferred into stopping solution. After 2 minutes the gel was again rinsed with H_2O and was left in water until analysis. All solutions were made fresh on the day and components can be found in **section 2.2**.

2.7.5 Detection of protein by Western blot

2.7.5.1 Transfer, blocking and immunodetection

Cut to roughly the size of the protein gel, a 0.45 μm PVDF membrane and 4 sheets of 3 mm Whatman chromatography paper were equilibrated in transfer buffer, with the PVDF membrane pre-wetted in methanol for approximately 30 seconds. The protein gel was also equilibrated in transfer buffer for 10 minutes with gentle shaking. Protein from the protein gel was transferred onto the PVDF membrane using a Sigma-Aldrich techware Semi-dry blot apparatus with a constant current of 300 mA for 60-90 minutes. The membrane was blocked in a 5% (w/v) milk and 1X TBS/0.1% Tween solution for either 1 hour at room temperature or 4^{o}C overnight with gentle shaking.

The membrane was washed 3x 5 minutes in 1X TBS/0.1% Tween solution before the primary antibody was added at an appropriate concentration in 5% (w/v) milk and 1X TBS/0.1% Tween solution. The membrane was incubated with the primary antibody for either 1 hour at room temperature or 4^{o}C overnight with gentle shaking. The membrane was washed 3x 10 minutes in 1X TBS/0.1% Tween before the secondary antibody was added at an appropriate concentration in 5% (w/v) milk and 1X TBS/0.1% Tween solution and incubated for 1 hour at room temperature. The membrane was washed 2x 10 minutes in 1X TBS/0.1% Tween then 1x 10 minutes in TBS. Protein was detected using the Amersham ECL kit according to manufacturer's instructions and imaged using a BioRad ChemiDoc^{TM} system.

2.7.5.2 Antibodies

Antibody	Animal	Antigen	Concentration	Supplier
Anti-CBD	Mouse ,monoclonal	CBD	1:5000	New England Biolabs
Anti-GFP	Mouse, monoclonal	CFP, GFP, YFP	1:1000	Chromotek (Germany)
Anti-GFP-HRP	Mouse, monoclonal	CFP, GFP, YFP	1:5000	Miltenyi Biotech (Germany)
Anti-myc	Rabbit, polyclonal	Myc-epitope tag	1:1000	Sigma-Aldritch
Anti-RFP	Rabbit, polyclonal	RFP, mCherry	1:1000	Chromotek (Germany)
Anti-Mouse (secondary)	Goat	Mouse antibody	1:5000	Promega (Germany)
Anti-Rabbit (secondary)	Goat	Rabbit antibody	1:5000	Sigma-Aldritch

2.8 Growth and maintenance of *Nicotiana benthamiana* and *Lactuca sativa*

N. benthamiana and *L. sativa* leaf epidermal cells were manipulated and used for transient expression during this study.

2.8.1 Germination and growth of *Nicotiana benthamiana*

N. benthamiana seeds were sown in propagation trays containing soaking wet soil mix of 80% compost and 20% vermiculite, which were then covered with clear autoclave bags to retain humidity until germination. Growth conditions were 26^{o}C with a 16 hour light/ 8 hour dark cycle with regular watering. After 10 days seedlings were transferred to individual pots and plants were typically suitable for transformation 4-8 weeks after sowing, until flowering heads appeared.

2.8.2 Germination and growth of *Lactuca sativa*

L. sativa seeds were sown into individual pots containing wet soil mix of 80% compost and 20% vermiculite, which were then covered with clear autoclave bags to retain humidity until germination. Growth conditions were 22ºC with a 16 hour light/ 8 hour dark cycle, with regular watering. The plants were kept covered until 2 weeks after germination at which point they were uncovered and left for a further week until transformation. Plants were typically ready for transformation 4 weeks after sowing but had a narrow transformation window of 1-2 weeks.

2.8.3 Transformation of *Nicotiana benthamiana* and *Lactuca sativa* by *Agrobacterium tumefaciens* infiltration

A colony or glycerol stock of *A. tumefaciens* with the desired construct, see **section 2.3.6** was used to inoculate a 10 ml culture of low salt LB containing appropriate antibiotics. The culture was incubated for 16-20 hours at 28ºC, shaking at 220 rpm until an OD_{600} value between 0.6-1 was reached. The culture was centrifuged at 3000 rpm for 10 minutes and the pellet re-suspended in 10 mls of dH_2O. This was repeated twice to remove residual traces of antibiotics. The cell culture was re-suspended in 1 ml of infiltration media and incubated at room temperature for 1 hour. The cells were diluted using infiltration media to an approximate value of OD^{600} of 0.05-0.2 depending on the construct. Co-infiltrations of multiple constructs were made by mixing the desired cultures at this point. A pipette tip was used to make a small puncture hole on the underside of the leaf in the epidermal cells. The *A. tumefaciens* cell culture was infiltrated into the leaf using a 1 ml disposable syringe with the area infiltrated marked. Before analysis, the plant was incubated in the same conditions as prior to infiltration for 2-4 days in the case of *N. benthamiana* and 3-7 days in the case of *L. sativa*.

2.9 Confocal microscopy

Leaf samples from infiltrated *N. benthamiana* or *L. sativa* were analysed using either an inverted Leica TCS SP5 or a Zeiss LSM 880 confocal microscopy, with images collected using either a 40x or 63 x oil objective lens.

2.9.1 Detection

Leaf samples approximately 0.25 cm^2 were excised from the plant and mounted on a microscope slide in dH_20. Fluorophores were detected with their appropriate excitation and emission spectra with sequential scanning used when multiple fluorophore wavelengths overlapped. Image processing was done via the LAS AF Lite software for SP5 images, and Zeiss Zen (Blue edition) for 880 images.

2.9.1.1 Excitation and emission values of fluorophores in this project

Fluorophore	Peak Excitation (nm)	Peak Emission (nm)	Type	Reference
CFP	405	485	Protein	Clonetech Laboratories, Palo Alto, CA
GFP/ EGFP	488	509	Protein	Clonetech Laboratories, Palo Alto, CA
YFP	514	535	Protein	Clonetech Laboratories, Palo Alto, CA
RFP	561	588	Protein	Clonetech Laboratories, Palo Alto, CA
mRFP1	584	607	Protein	Campbell *et al* 2002
mCherry	587	610	Protein	Clonetech Laboratories, Palo Alto, CA
FM4-64	558	654	Lipophilic dye	Invitrogen
Nile Red	514	636	Lipophilic dye	Thermo Fisher

2.9.2 Staining the plasma membrane with FM4-64

To stain the plasma membrane, infiltrated *N. benthamiana* leaf sections were excised with a scalpel and incubated in a 1.5 ml Eppendorf tube containing 1 µl/ml FM4-64 dye in dH_2O and incubated for 10 minutes in the dark, at room temperature. The leaf tissues were washed for 2x 10 minutes in 1 ml of dH_20 then mounted onto a microscope slide for analysis.

2.9.3 Staining lipid bodies with Nile red

To stain lipid bodies, infiltrated *N. benthamiana* leaf sections were excised with a scalpel and incubated in a 1.5 ml Eppendorf tube containing 2 µl/ml Nile red stain in dH_2O and incubated for 30 minutes in the dark, at room temperature. The leaf tissues were washed for 2x 10 minutes in 1 ml of dH_20 then mounted onto a microscope slide for analysis.

2.9.4 Brefeldin-A treatment

To inhibit the secretory pathway, infiltrated *N. benthamiana* leaf sections were excised with a scalpel and incubated on a microscope slide with 5 µg/ml of Brefeldin A dissolved in dH_2O. With care being taken not to allow the slide to dry out, the leaf tissue was incubated for 1 hour at room temperature before analysis.

2.10 Detection of protein-protein interactions

2.10.1 Yeast-2-Hybrid

Gateway cloning was used to insert constructs into bait and prey destination vectors pDEST32 and pDEST22 which contain the DNA binding domain and the Transcription activation domain of GAL4 protein respectively. pDEST32 was transformed into yeast strain AH109 and pDEST22 transformed into Y187, the two strains were then mating and protein-protein interactions detected by the presence of growth on selective plates.

2.10.1.1 Lithium acetate transformation of *Saccharomyces cerevisiae*

10ml cultures of *S. cerevisiae* strains AH109 and Y187 were inoculated in YPDA media and grown overnight at 30°C, shaking at 220 rpm. 1 ml of culture, enough for 10 transformations, was transferred to a 1.5 ml Eppendorf tubes and the yeast cells centrifuged at 2000 rpm for 5 minutes. The supernatant was discarded and the pellet was re-suspended in 1 mls of 0.1M LiAc, this was repeated twice. The re-suspended cells were incubated in a 30°C water bath for 1 hour.

The desired construct DNA was prepared by mixing approximately 1500 ng of DNA, with 4 µl of denatured salmon sperm DNA, and 290 µl of 50% PEG 3350, made up to 300 µl with dH_2O. The DNA mixture was then preheated to 30°C before the addition of 100 µl of the desired yeast cell suspension.

The cell/DNA mixture was incubated at 30°C for 50 minutes and then heat shocked at 42°C for 15 minutes. The cells were then harvested by centrifugation at 3000 rpm for 5 minutes, the supernatant discarded and the cells re-suspended in 200 µl of dH_2O. The cells were then spread onto selective plates lacking in amino acids specific to the vector

- Leucine for pDEST32 and – Tryptophan for pDEST32. Yeast plates were incubated at 30°C for 2-4 days and resulting colonies screened via colony PCR for presence of the desired insert.

2.10.1.2 Yeast mating

Positive colonies containing the desired construct were inoculated in 10 mls of selective media at 30°C, shaking at 220 rpm for 16 hours, interactions were tested by mating the desired constructs then plating them onto selective media. Using a template 3 µl of each Y187 yeast culture was pipetted as a spot onto a YPDA 'master plate' and allowed to dry. The desired AH109 cell culture was then pipetted onto the first and allowed to dry to prevent smearing. The master plate was then incubated at 30°C for 1-2 days until colony growth occurred.

2.10.1.3 Replica plating and replica cleaning

To test for successful mating and protein-protein interaction the constructs were 'replica plated' onto selective media. This was done by gently pressing the YPDA master plate onto autoclaved velvet in order to transfer the colonies. The appropriate selective plates were then pressed gently against the velvet and incubated for 1-2 days at 30°C. The selection plates were then 'cleaned' by pressing firmly against autoclaved velvet three times to remove all visible cells, the plates were then incubated for a further 1-2 days at 30°C, mating and protein-protein interactions were analysed by studying the resultant growth.

Plate and selection	Purpose
YPDA master plate	Initial growth and basis for replica plating
SD -Leucine/ -Tryptophan	Growth indicates successful mating
SD -Leucine/ -Tryptophan/ - Histidine	Growth indicates protein-protein interaction
SD -Leucine/ - Tryptophan/ - Histidine/ 2 mM 3AT	Growth indicates protein-protein interaction and inhibits HIS3 gene

2.10.2 Co-immunoprecipitation assays

1ml of ice cold plant cell wash buffer was added to 20 µl of GFP or RFP-Trap_A beads. The slurry was centrifuged at 2,000 rpm, the supernatant discarded and the beads re-suspended in 1 ml of ice cold 'plant cell wash buffer'. This was repeated twice and the equilibrated beads kept on ice until use.

N. benthamiana leaf epidermal cells were co-infiltrated with the desired constructs as detailed in **section 2.8.3**. After 3 days infiltrated leaf sections weighing roughly 0.5 g were excised from the plant, transferred to a 1.5 µl Eppendorf tube and flash frozen in liquid nitrogen. The tubes containing leaf tissue were transferred to dry ice in order to remain frozen and two metal beads were added, tissue was then ground using a Retsch MM300 tissue grinder for 4 minutes at 30 l/s. 0.5 ml of ice cold plant tissue lysis buffer was added, the tubes were vortexed for 15 seconds before being tumbled for 1 hour at 4^{o}C. The plant mixture was centrifuged at 14,000 rpm, at 4^{o}C for 10 minutes. The supernatant was transferred to a fresh, pre-chilled, 1.5 ml Eppendorf tube with a sample of supernatant set aside for SDS-PAGE analysis. 1 ml of plant cell wash buffer/ bead slurry was added and the mixture tumbled for 2 hours at 4^{o}C.

The mixture was centrifuged at 2,000 rpm, 2 minutes, 4^{o}C, a sample of supernatant was taken for analysis and the rest discarded. The beads were washed 3x in plant cell wash buffer as described previously. The pellet was resuspended in 25 µl of 2x Laemmli buffer and analysed via SDS-PAGE

2.11 Pyrophosphatase assay

The assay was carried out using EnzChek® Pyrophosphate Assay Kit. A typical reaction composed of 40 µl of 0.25 M HEPES buffer with 50 mM $MgCl_2$ (pH7.6), 2 µl DTT, 5 µl of 2M KCl, 80 µl MESG, 5 µl of 0.16 mg/ml PNP, 2 µl of 0.2 mg/ml of inorganic pyrophosphatase. IPP and FPP was added to the assay according to the amounts specified in (Chiang *et al* 2011) which was 4 µl of 100 mM IPP solution and 6 µl of 1 mM FPP. dH_20 was added to a final volume of 200 µl. The reaction took place in a quartz cuvette.

The assay was carried out at 30ºC with all the components added. After 3-5 minutes 2 µl of 80 µg/ml recombinant protein in TBS buffer, was added to the mix. Absorbance was measured a dual beam Cary 100 Bio UV Visible Spectrophotometer set to 360 nm controlled again a cuvette containing all components except recombinant protein as a control. As a positive control 2 µl of 0.1 M Na-pyrophosphate was added to the mix at the end of the run.

Chapter 3: Cell localisation, characterisation and interactions of Rubber Associated Proteins

3.1 Introduction

There is very little information regarding the cell biology of rubber- associated proteins and the mechanisms of rubber biosynthesis within *Hevea*. Due to the hydrophobic nature of polyisoprene rubber, a soluble enzyme or substrate would have difficulty interacting with such a long and insoluble polymer. It is proposed therefore that the only place rubber biosynthesis could occur is on the surface of rubber particles, via the intermediary action of a hypothetical membrane-bound rubber transferase enzyme or complex. Currently the most promising candidate for a rubber transferase enzyme is HRT2, (Asawatreratanakul *et al* 2003) a CPT enzyme cloned from the latex of *Hevea*. In other latex producing species such as dandelions, CPTs have been shown to be crucial in rubber biosynthesis (Post *et al* 2010) and it is likely they also fulfil this role in *Hevea*. Despite HRT2's potential importance, currently there is no information on whether it does or even can, associate with rubber particles.

As well as HRT2, there is a range of proteins that are thought to be involved in rubber biosynthesis or rubber particle stabilisation. REF and SRPP are the two most abundant proteins in latex. SRPP dandelion homologs have been shown to affect IPP incorporation in dandelion latex. RBSP is up-regulated in response to latex stimulation and has also been shown to increase IPP incorporation (Chow *et al* 2006).

It is not feasible to study *Hevea* proteins in their native species due to the difficulty of genetic manipulation. This makes it difficult to directly determine whether proteins actually localise to rubber particles in *Hevea*. However there are some indirect methods available which I used in this study.

Rubber particles are thought to be structurally similar to lipid bodies, with a number of rubber related family proteins are found on lipid bodies in non-rubber producing species, specifically members of the SRPP protein family. Like rubber particles, lipid bodies consist of a hydrophobic core surrounded by a hydrophilic membrane, though the core consists of triglycerides rather than polyisoprene. Lipid bodies are thought to 'bud' from and originate on the endoplasmic reticulum. While this has never been observed directly, lipid body associated proteins, oleosins, also localise to the endoplasmic reticulum in tissues devoid of lipid bodies (Beaudoin *et al* 2000), and triglyceride synthesis occurs in the lumen of the endoplasmic reticulum (Napier *et al* 1996). The endoplasmic reticulum

membrane protein calnexin has also been shown to be present on the surface of lipid bodies (Brasaemle *et al* 2004) further reinforcing the theory that these organelles originate in this manner.

As oleosins and calnexin are present on lipid bodies and the endoplasmic reticulum, it is likely that any rubber particle associated complex would also be membrane bound to the endoplasmic reticulum in a non-rubber particle or lipid body rich environment such as the leaves of epidermal cells of *N. benthamiana*.

The hypothesis is that if HRT2 is responsible for rubber biosynthesis and is able to bind to rubber particles then it will most likely be associated with the endoplasmic reticulum either by itself or as part of a larger complex. In this chapter the endoplasmic reticulum is used in place of the donor membrane of rubber particles although attempts are also made to express proteins in system more akin a native rubber particle/ lipid body rich environment.

3.1.2 Aims and experimental approach

The aim of this section was to express rubber related proteins transiently in *N. benthamiana* leaf epidermal cells, in order to determine their cell localisations for the first time by confocal microscopy,. The search is for a membrane bound protein, using the endoplasmic reticulum or other membrane as a proxy for rubber particles, due to the limitations of working in a non-native system.

Once initial information on cellular localisation was acquired, then an attempt was made to characterise potential interactions between the five candidate proteins HRT2, SRPP, REF, HevNogo and RBSP using a combination of confocal microscopy, yeast-2-hybrid and co-immunoprecipitation. As there is limited information regarding the cell biology, this chapter represents a first step in the characterisation of these proteins.

In this report I cloned a CPTL protein called ‘HevNogo’. CPTL proteins have been shown to affect latex production in *T. brevicorniculatum* (Epping *et al* 2015) and *L. sativa* (Qu *et al* 2015) and HevNogo may have a similar role in *Hevea*. The cell localisation of HevNogo is covered in this section along with the other rubber associated

proteins. The identification, cloning and characterisation of HevNogo is covered subsequently in **section 3.5**.

3.2 Constructs and cloning

Sequences for rubber related proteins were identified from existing literature and verified by analysing the TARRC *Hevea* genome database. All constructs used for transient expression, were amplified from either cDNA or genomic DNA (see section 2.5.3) and combined with a fluorescent protein tag. The fluorescent tag was appended to either the C or N terminus (Figure 3.1) in order to account for the possible effect of the tag on cellular localisation. This was done using OE-PCR to fuse the fluorescent tag in frame with the rubber gene sequence. An exception to this is RBSP-GFP which was cloned via Gateway cloning using a destination vector containing GFP. All constructs used for transient expression were fused downstream of a 35S promoter, with sequences also modified to contain restriction sites at both ends to allow for restriction/ligation cloning into a 35S:CamV Cassette, the 35S:construct was then amplified and sub-cloned into the final pGreen vector. A list of primers and restriction enzymes used can be found in appendix table A1.

Figure 3.1a (next page) Workflow of cloning

The literature (A) regarding rubber biosynthesis was reviewed to identify target genes for the study. Recently TARRC has published the first genome sequence for *Hevea brasiliensis*, with this the target genes identified in the literature, was searched for and verified, with the use of the TARRC genome browser, to check for sequence identify, and the presence of introns within the coding region. Depending on the presence of introns, the target genes where amplified from either (B) genomic or cDNA taken from the leaves of *Hevea*, with primers (C) designed based on the *Hevea* genome sequence. In order to visualise the target rubber related proteins each gene was fused to a fluorescent tag, primers were designed to amplify fluorescent proteins from previously generated constructs (D) present in our lab. The primers were designed to amplify the target sequence (E) and also to create complimentary overhanging ends which could anneal to the targeted fusion protein in a second round of PCR (F). The primers were also designed to add an appropriate restriction site onto each end of the final fusion product, these were used for restriction digest and ligation of the fusion, into a 35S CamV Cassette vector which had also been digested with the same enzymes to create complimentary ends (G). The ligation put the rubber-protein fusion in frame with a 35S promoter (H), this was then sub cloned into a pGreen transformation plasmid by designing primers to amplify the 35S promoter plus rubber protein fusion, which was then ligated directly into pGreen (I). The pGreen plasmid was transformed into *A. tumefacien* (J), followed by infiltration into *N. benthamiana* leaf cells (K).

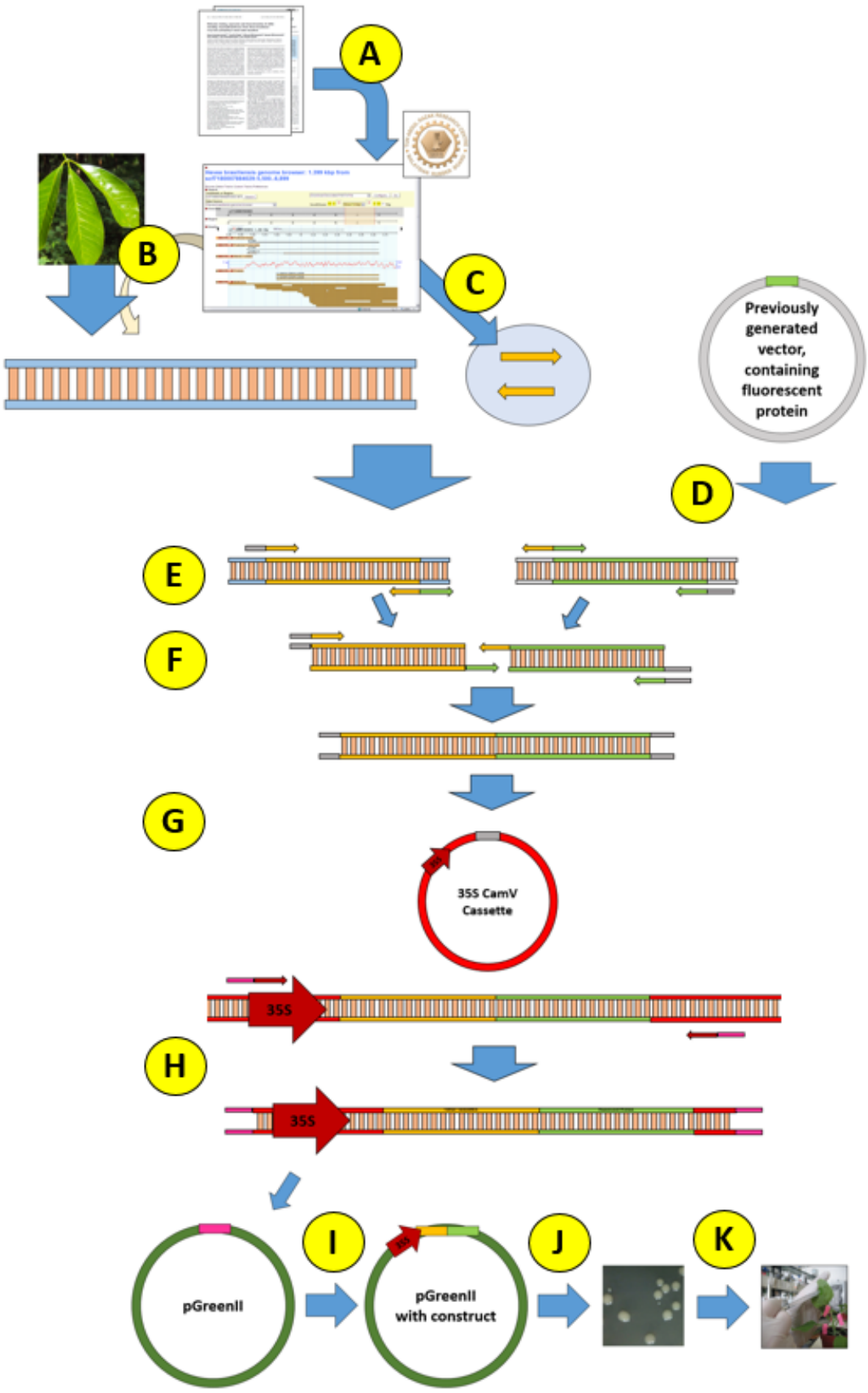
A
B
C
D
Previously generated vector, containing fluorescent protein
E
F
G
35S CamV Cassette
35S
H
35S
pGreenII
I
pGreenII with construct
J
K

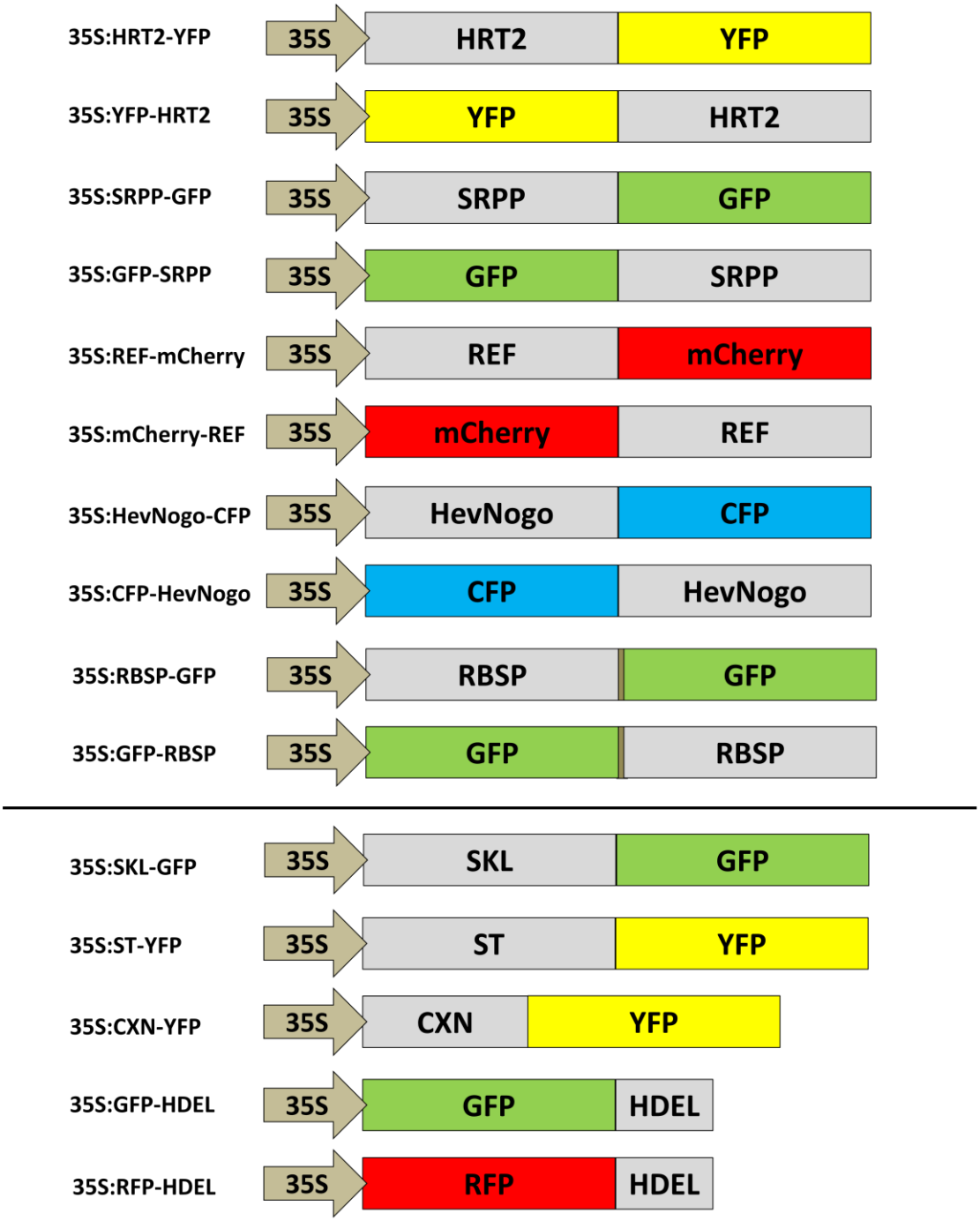

Figure 3.1b Constructs used for the transient expression of rubber associated proteins
Above the line are constructs generated for this project which have, with one exception, a fluorescent tag fused in frame at either the N' or C' terminal. Below the line are various constructs previously generated (see **section 2.5.4** for references), that were used as markers for certain organelles. All constructs are driven by a 35S promoter

3.3 Cellular localisations of rubber related proteins

3.3.1 Expression of HRT2 in *N. benthamiana* results in a cytosolic localisation

In order to analyse its subcellular localisation, HRT2 was tagged with YFP at both the N' and C' terminus. 35S:HRT2-YFP and 35S:YFP-HRT2 were transformed into *A. tumefaciens* C58 and infiltrated in the leaf epidermal cells of *N. benthamiana* and imaged after 3 days (Figure 3.2). HRT2 displayed a cytosolic localisation characterised by a diffuse pattern, and negative staining of organelles such as chloroplasts. The HRT2-YFP fusion protein size is 59kDA which is just under the threshold to freely diffuse into the nucleoplasm. This is demonstrated by strong signal in the nucleus, but not the nuclear membrane or nucleolus, this is typical of a cytosolic enzyme. The orientation of the fluorescent tag has no effect on the cellular localisation of HRT2 with both HRT-YFP and YFP-HRT2 configurations localising to the cytoplasm.

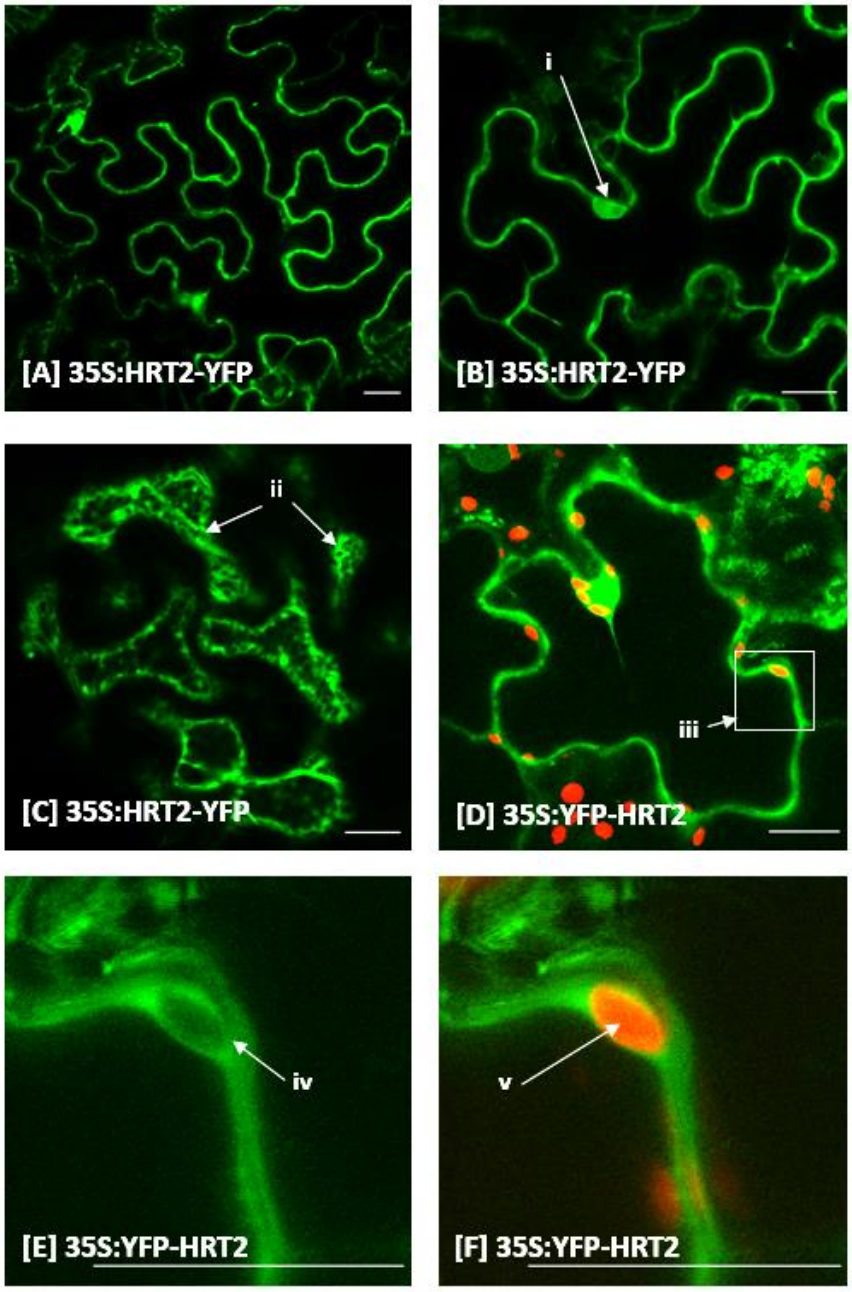

Figure 3.2 HRT2 localises to the cytosol

HRT2 was transiently expressed in *N. benthamiana* leaf cells and imaged after 3 days. (A) Overview of 35S:HRT2-YFP (green) transformed cells. (B) Image of a single cell showing localisation in the nucleoplasm (i) but no nuclear membrane signal, consistent with cytosolic localisation. (C) View of the cell cortex, showing 35S:HRT2-YFP signal (green) with (ii) negative outlines of organelles. (D) 35S:YFP-HRT2 (green) with chloroplasts (red). (E) Magnified image of box (iii) shows the cytoplasm enveloping the space where a chloroplast is present. (F) Same image as E with the chloroplast (red)

Scale bars=20µm

3.3.2 Expression of SRPP in *N. benthamiana* results in large protein aggregates and localisation on the endoplasmic reticulum

SRPP was tagged with a GFP at both the N' and C' terminal. 35S:SRPP-GFP and 35S:GFP-SRPP were transformed into *A. tumefaciens* C58 then infiltrated in the leaf epidermal cells of *N. benthamiana* and imaged after 3 days (Figure 3.3a). The orientation of the fluorescent tag affected the cellular localisation of SRPP. 35S:SRPP-GFP accumulated in large protein aggregates which were extremely bright and could also be visualised through a light microscope. 35S:GFP-SRPP also resulted in the accumulation of large protein aggregates but also localisation on the endoplasmic reticulum, demonstrated by the characteristic network pattern of the endoplasmic reticulum, signal from the nuclear envelope and also co-localisation with RFP-HDEL (Figure 3.3b). The orientation of the GFP tag had a drastic effect on cell localisation with SRPP-GFP displaying no localisation except for the aggregates whereas GFP-SRPP had a clear membrane localisation.

Nile red is a lipophilic dye that is soluble, and will fluoresce strongly, in the presence of lipids, but not fluoresce in a non-polar environment such as water (Greenspan *et al* 1985). It is used extensively as a selective stain of lipid environments such as lipid bodies or rubber particles. The aggregates were stained with Nile red to test for the possibility of in-vivo rubber particle formation but the dye did not stain the aggregates (Figure 3.3b).

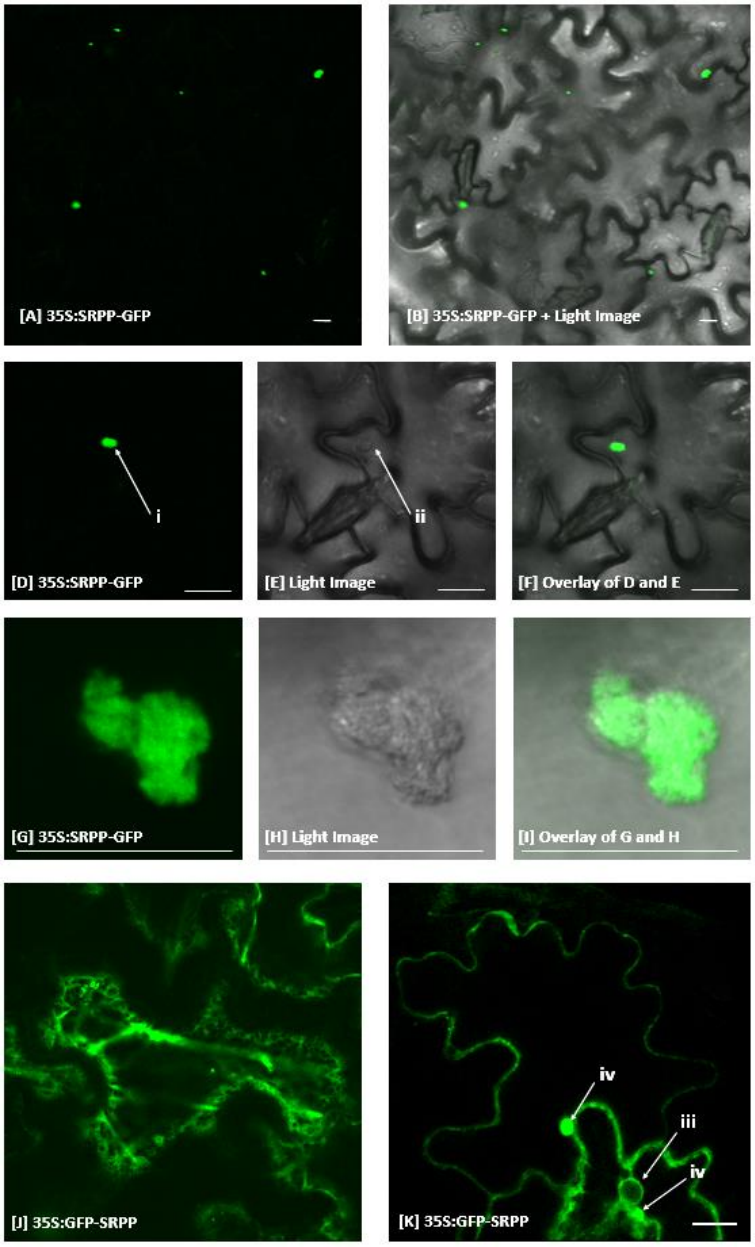

Figure 3.3a SRPP forms large aggregates as well as localising to the endoplasmic reticulum

SRPP was transiently expressed in *N. benthamiana* leaf cells and imaged after 3 days. (A) Overview of 35S:SRPP (green) transformed cells. (B) Light image to give context, also showing 35S:SRPP-GFP aggregates.

(D) Cell transformed with SRPP-GFP (green) with large aggregate (i) but no other localisation. (E) Light image showing protein aggregate visible as a small indentation (ii). Overlay of images D and E showing the aggregate which is visible in both GFP and light channels.

(G) Close up of SRPP aggregate, also displayed in the light channel (H) and overlay image (I).

(J) Overview of 35S:GFP-SRPP transformed cells showing endoplasmic reticulum localisation. (K) Overview of 35S:GFP-SRPP transformed cells showing nuclear membrane (iii) and protein aggregates (iv)

Scale bars=20µm

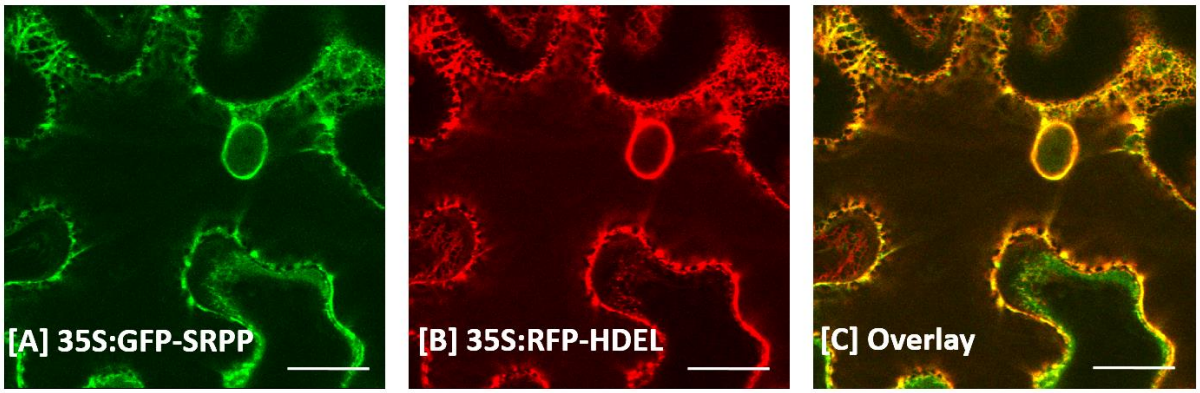

Figure 3.3b Co-localisation with RFP-HDEL confirms SRPP localisation to the endoplasmic reticulum.
GFP-SRPP and RFP-HDEL were transiently expressed in *N. benthamiana* leaf cells and imaged after 3 days.
(A) GFP channel showing cells transformed with 35S:GFP-SRPP (green). (B) RFP channel showing cells transformed with RFP-HDEL (red). (C) Overlay of images A and B showing co-localisation of 35S:GFP-SRPP with 35S:RFP-HDEL on the endoplasmic reticulum and nuclear membrane.
Scale bars=20µm

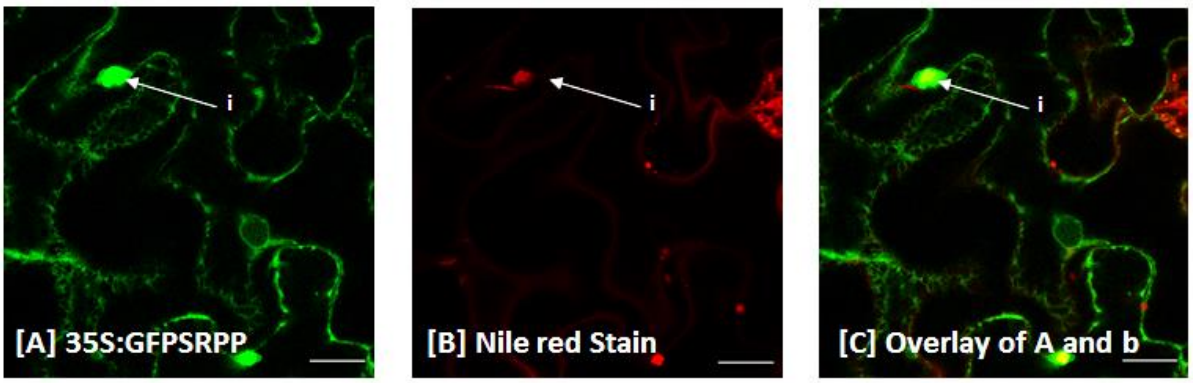

Figure 3.3c Nile red does not stain the SRPP protein aggregates
GFP-SRPP was transiently expressed in in *N. benthamiana* leaf cells and imaged after 3 days. Leaf sections were stained by immersion in Nile red for 1 hour
(A) GFP channel showing cells transformed with 35S:GFP-SRPP (green). (B) Nile red channel showing Nile red stain (red). (C) Overlay of images A and B demonstrating Nile red does not stain the protein aggregates.
Scale bars=20µm

3.3.3 Expression of REF in *N. benthamiana* results in localisation to the endoplasmic reticulum.

REF was tagged with mCherry on both the C' and N' terminus. 35S:REF-mCherry and 35S:mCherry-REF were transformed in *A. tumefaciens* C58 then infiltrated in *N. benthamiana* leaf epidermal cells and imaged after 3 days (Figure 3.4). REF localised to the endoplasmic reticulum displaying the characteristic network pattern as well as localisation to the nuclear membrane. Endoplasmic reticulum localisation was also confirmed by co-localisation with GFP-HDEL (Figure 3.4b). The orientation of the fluorescent tag had no effect on the localisation of REF.

3.3.3.1 REF expression results in punctate structures

As well as localising to the endoplasmic reticulum, REF also display signal from small punctate structure. Co-localisation with the endoplasmic reticulum membrane and luminal markers, calnexin and HDEL, as well as markers for Golgi, peroxisomes and pre-vacuolar compartments reveal these structures are distinct from all of them (Figure 3.4c).

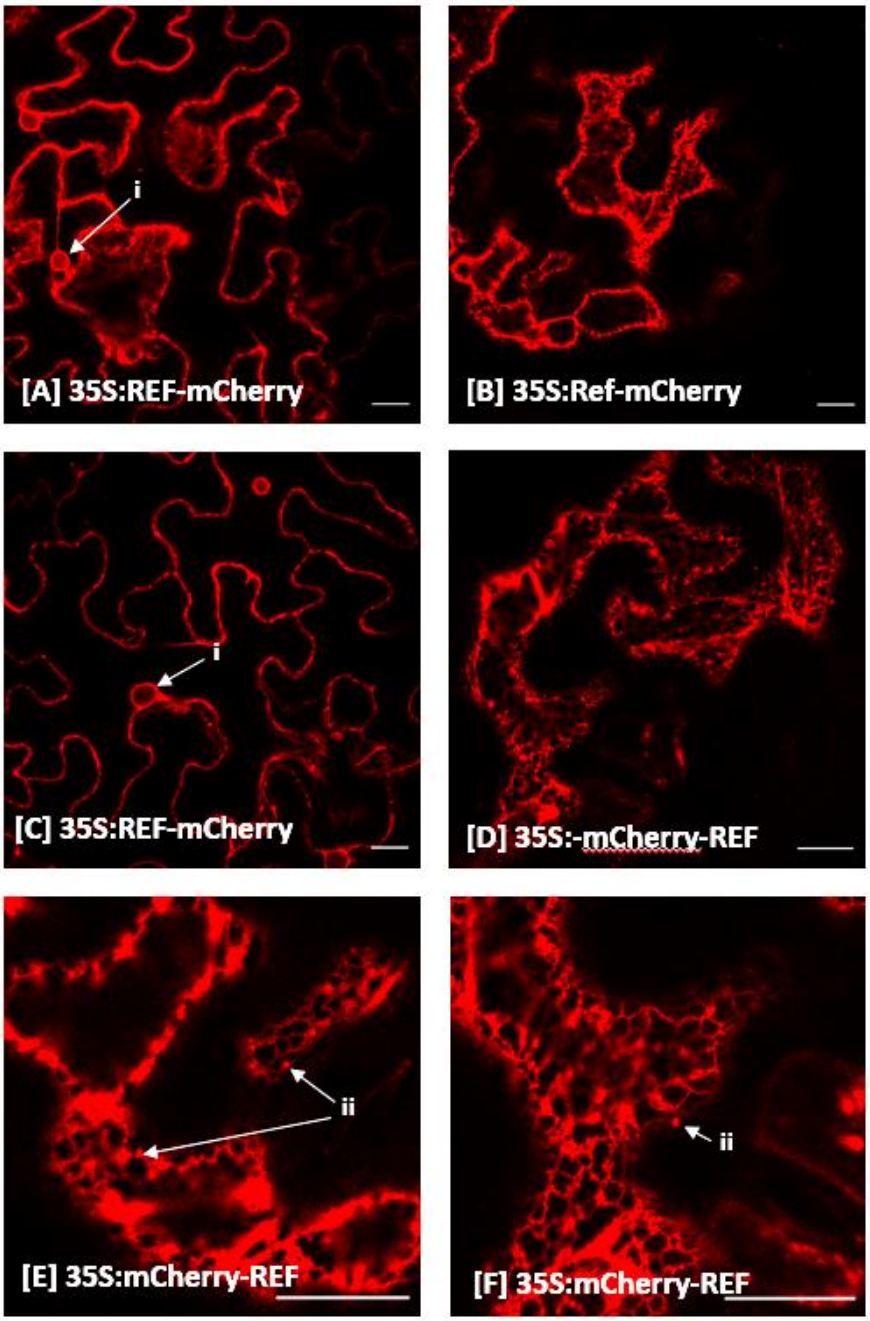

Figure 3.4a REF localises to the endoplasmic reticulum and in punctate structures
REF was transiently expressed in *N. benthamiana* leaf cells and imaged after 3 days.
(A) Overview of 35S:REF-mCherry (red) transformed cells, REF signal is present on the nuclear membrane (i). (B) Cortex of leaf epidermal cell expressing 35S:REF-mCherry (red) showing characteristic endoplasmic reticulum pattern. (C) Close up of epidermal leaf cells showing (ii) punctate structures. (D) Overview of 35S:mCherry-REF (red) transformed cell. (E) Overview of 35S:mCherry-REF (red) transformed cell, Ref signal is present on the nuclear membrane (i). (F) Close up of 35S:mCherry-REF showing (ii) punctate structures. **Scale bars=20µm**

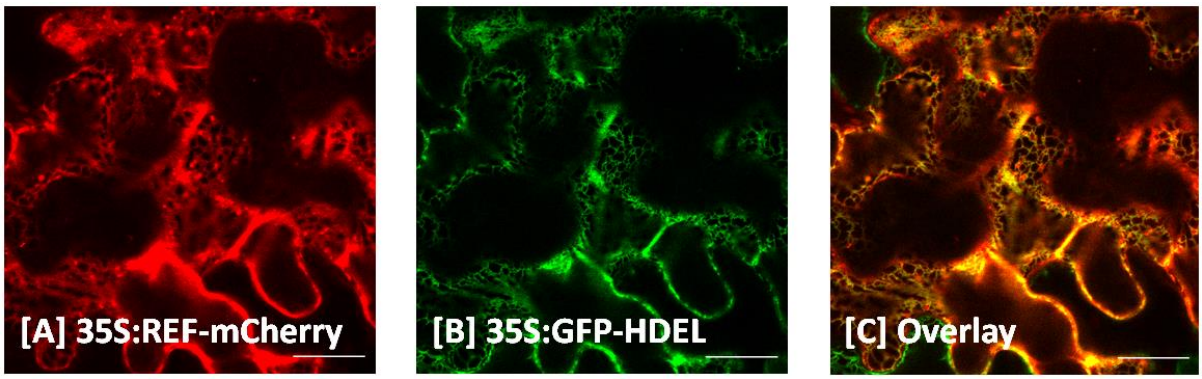

Figure 3.4b Co-localisation with GFP-HDEL confirms REF localisation to the endoplasmic reticulum

REF and GFP-HDEL were transiently expressed in *N. benthamiana* leaf cells and imaged after 3 days.

(A) mCherry channel showing cells transformed with 35S:REFmCherry (red). (B) GFP channel showing cells transformed with GFP-HDEL (green). (C) Overlay of images A and B showing co-localisation of 35S:REF-mCherry with 35S:GFP-HDEL on the endoplasmic reticulum., however the punctate structures of REF remain distinct.

Scale bars=20µm

Figure 3.4c (next page) The identify of REF punctate structures remains unknown

REF and was transiently expressed in *N. benthamiana* leaf cells with a selection of marker protein and imaged after 3 days.

(A, D, G and J) mCherry channel showing cells transformed with 35S:REF-mCherry (red) with punctate structures visible.

(B) YFP channel (green) showing cells expressing ST-YFP, golgi bodies are marked (ii)

(E) GFP channel (green) showing cells expressing GFP-RabF2b, pre-vacuolar compartments are marker (iii)

(H) GFP channel (green) showing cells expressing peroxisomes (iv)

(K) YFP channel (green) showing cells expressing calnexin

(C, F, I and M) Overlay of REF and the corresponding marker showing that the punctate structures (i) are distinct from any of them (ii, iii, iv)

Scale bars=20µm

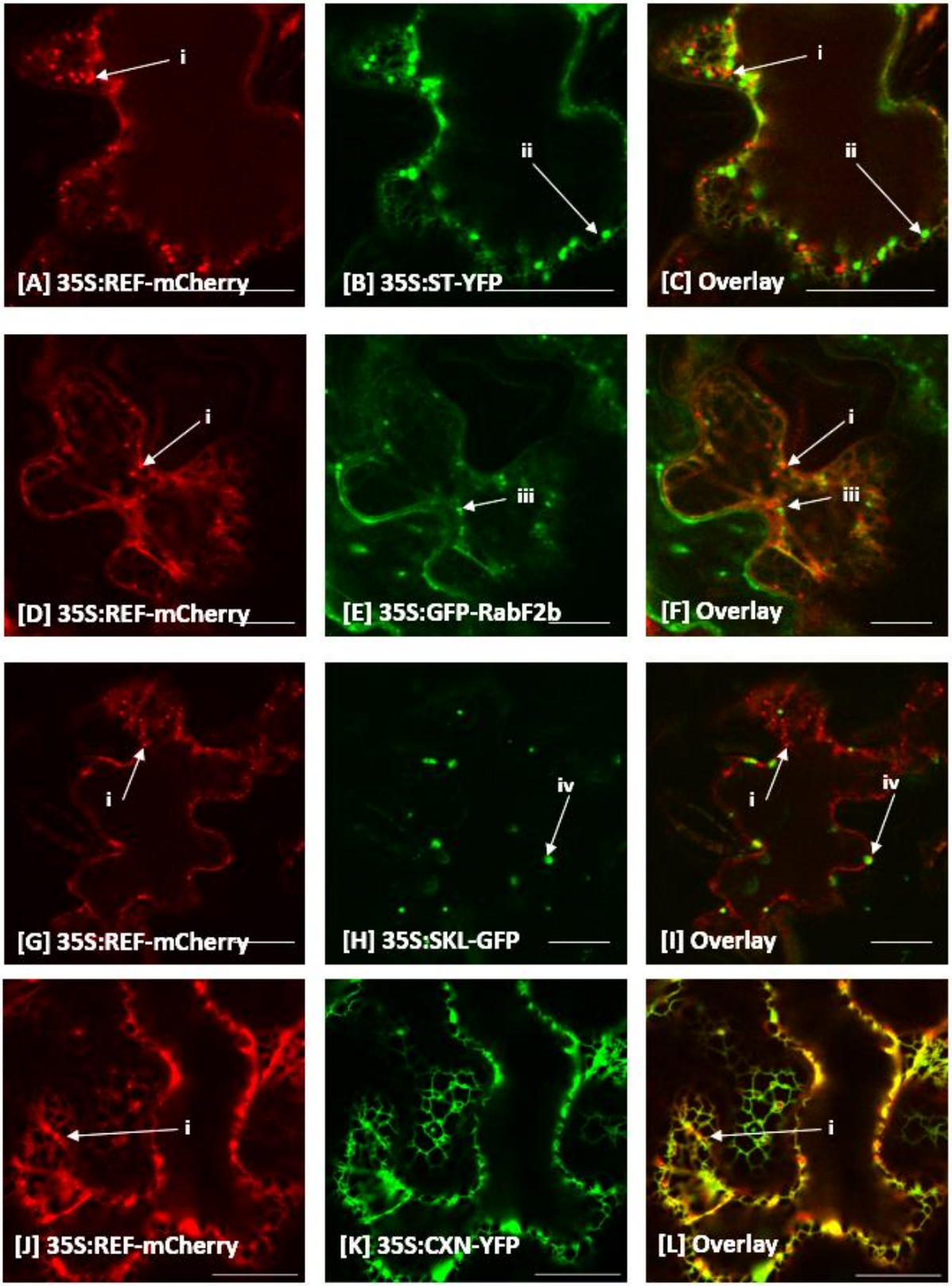
i
[A] 35S:REF-mCherry
ii
[B] 35S:ST-YFP
i
ii
[C] Overlay
i
[D] 35S:REF-mCherry
iii
[E] 35S:GFP-RabF2b
i
iii
[F] Overlay
i
[G] 35S:REF-mCherry
iv
[H] 35S:SKL-GFP
i
iv
[I] Overlay
i
[J] 35S:REF-mCherry
[K] 35S:CXN-YFP
i
[L] Overlay

3.3.4 Expression of HevNogo in *N. benthamiana* results in cellular localisation to the endoplasmic reticulum

A CPTL homolog HevNogo was cloned and characterised. The identification and initial cloning of HevNogo will be covered in more explicit detail later in **section 3.5**. HevNogo was tagged with CFP on both the C' and N' terminus. 35S:HevNogo-CFP and 35S:CFP-HevNogo were transformed in *A. tumefaciens* C58 then infiltrated in *N. benthamiana* leaf epidermal cells and imaged after 3 days (Figure 3.5a). HevNogo localised to the endoplasmic reticulum displaying the characteristic network pattern as well as localisation to the nuclear membrane. Endoplasmic reticulum localisation was also confirmed by co-localisation with RFP-HDEL (Figure 3.5b)

3.3.5 Expression of RBSP in *N. benthamiana* results in a cytosolic cellular localisation

RBSP was amplified by PCR from RRIM2025 cDNA and cloned into gateway destination vectors pGWB605 and pGWB606 which resulted in GFP fusion at the N' and C' terminus respectively. These were transformed into *A. tumefaciens* GV3101 then infiltrated in *N. benthamiana* leaf epidermal cells and imaged after 3 days (Figure 3.6). RBSP displayed a cytosolic localisation characterised by a diffuse pattern and localisation in the nucleoplasm of the leaf cells. The orientation of the fluorescent tag had no effect on the localisation of RBSP.

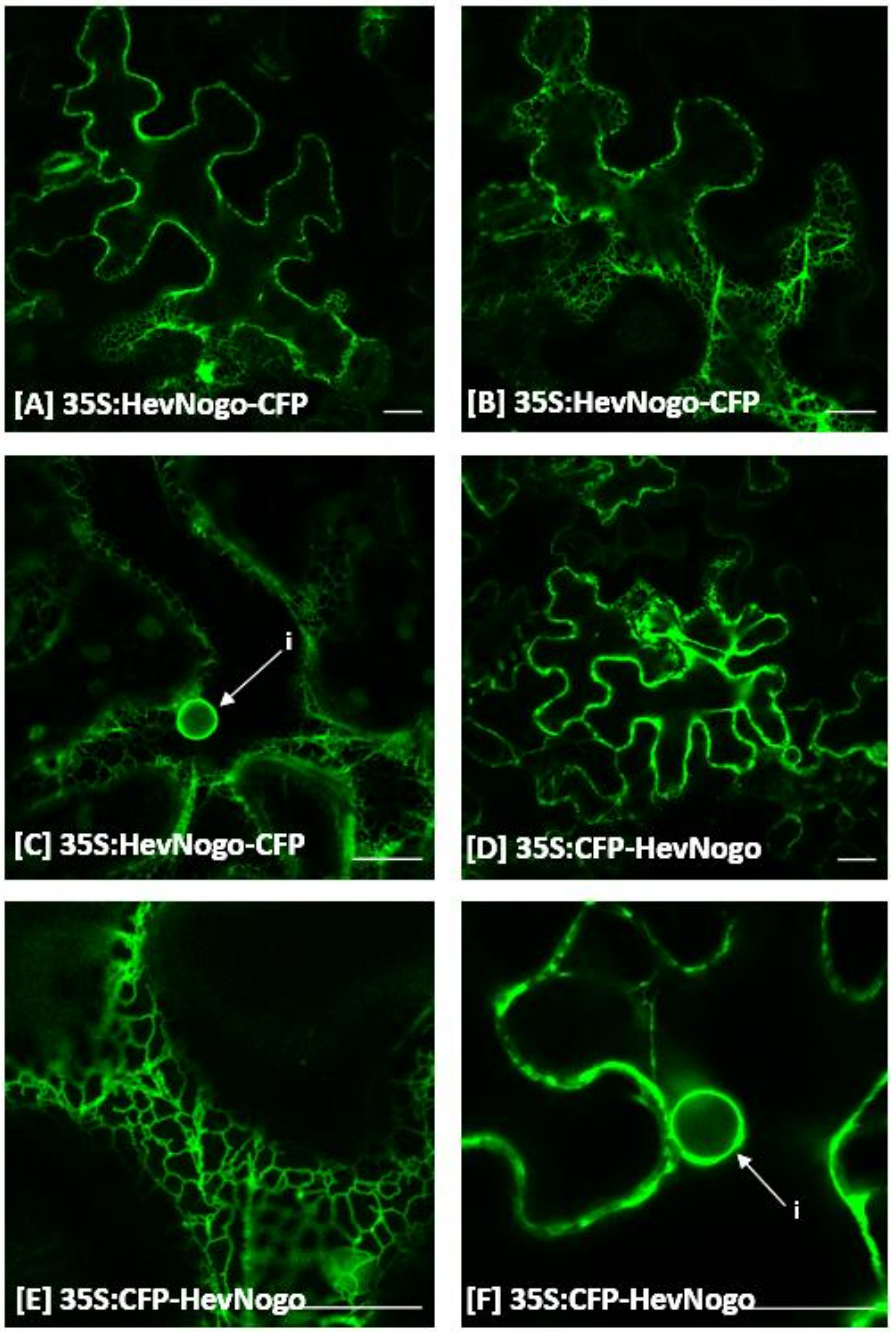

Figure 3.5a HevNogo localises to the endoplasmic reticulum
HevNogo was transiently expressed in *N. benthamiana* leaf cells and imaged after 3 days. (A) Overview of a 35S:HevNogo-CFP (green) –expressing cell. (B) 35S:HevNogo-CFP transformed cell cortex with characteristic endoplasmic reticulum network pattern. (C) 35S:HevNogo-CFP signal is present on the nuclear membrane (i) which is contiguous with the endoplasmic reticulum. (D) Overview of 35S:CFP-HevNogo (green). (E) Cell cortex of epidermal cell expressing 35S:CFP-HevNogo (green) displaying characteristic endoplasmic reticulum pattern. (F) 35S:CFP-HevNogo signal is present on the nuclear membrane (i)
Scale bars=20µm

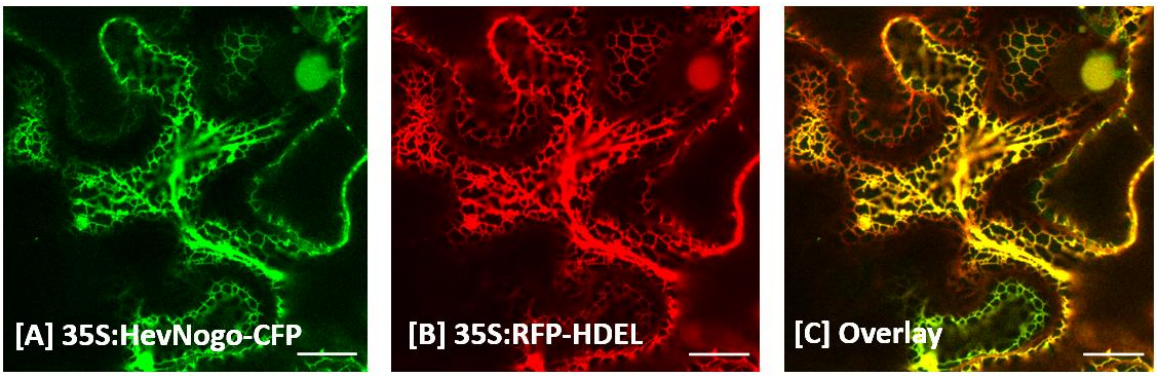

Figure 3.5b Co-localisation with RFP-HDEL confirms HevNogo localisation to the endoplasmic reticulum

HevNogo and RFP-HDEL were transiently expressed in *N. benthamiana* leaf cells and imaged after 3 days.

(A) CFP channel showing cells transformed with 35S:HevNogo-CFP (green). (B) RFP channel showing cells transformed with RFP-HDEL (red). (C) Overlay of images A and B showing co-localisation of 35S:HevNogo-CFP with 35S:RFP-HDEL on the endoplasmic reticulum.

Scale bars=20µm

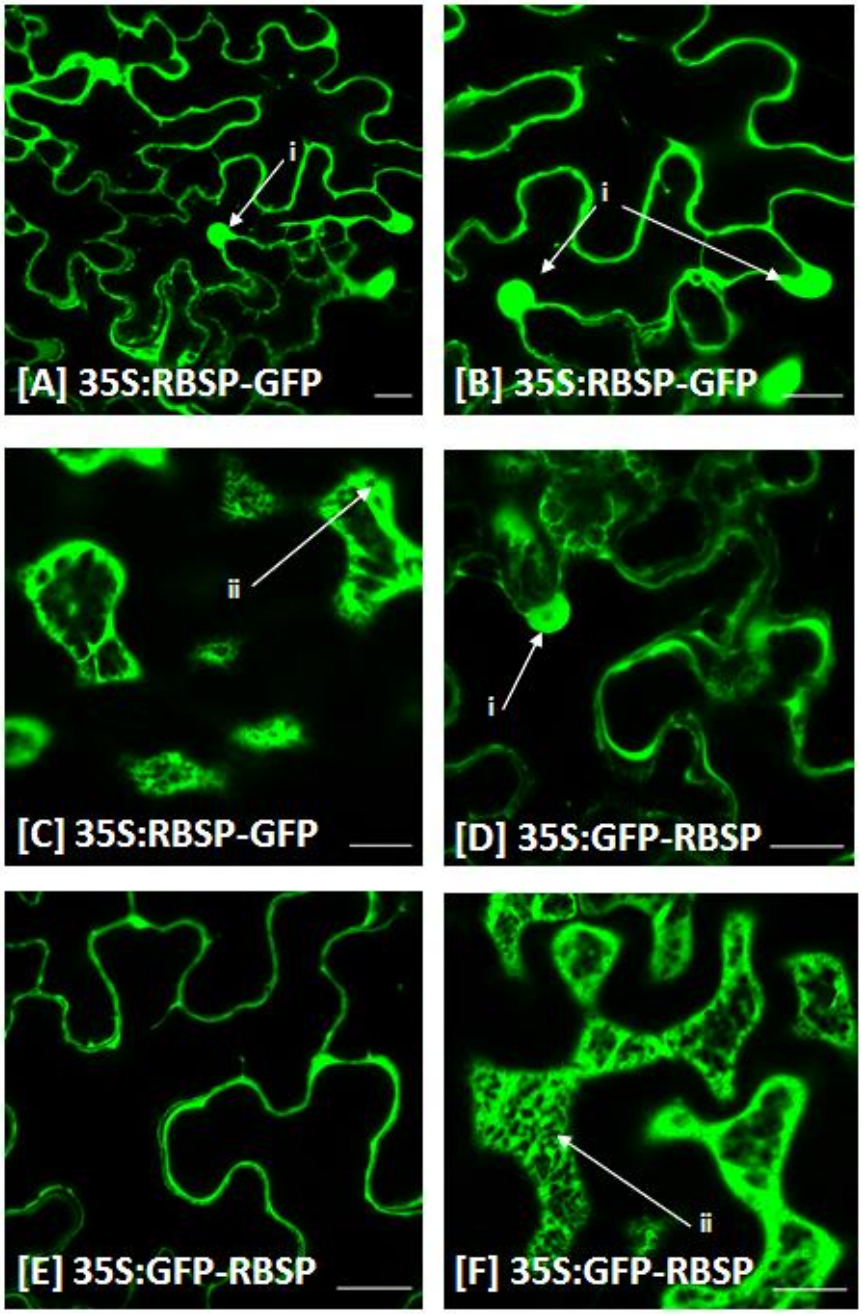

Figure 3.6 RBSP localises to the cytosol

RBSP was transiently expressed in *N. benthamiana* leaf cells and imaged after 3 days. (A) Overview of several 35S:RBSP-GFP (green) transformed cells showing a cytosolic localisation and signal in the nuclease (i). (B) Image 35S:RBSP-GFP (green) showing localisation in the nucleus (i) but no nuclear membrane signal, consistent with cytosolic localisation. (C) Cell cortex showing 35S:RBSP-GFP signal (green) with (ii) negative staining of organelles. (D) Overview of 35S:GFP-RBSP (green) transformed cells showing a cytosolic localisation and signal in the nucleus. (E) Overview of 35S:GFP-RBSP transformed cells showing the cytoplasm (green) around the vacuole. (F) Cell cortex showing 35S:GFP-RBSP signal (green) with (ii) negative staining of organelles. **Scale bars=20µm**

3.4 Discussion of subcellular localisations

3.4.1 HRT2 localises to the cytosol and may require a partner or complex to bring it to a membrane

Rubber biosynthesis is thought to take place on the surface of the rubber particle. In this chapter endomembranes in *N. Benthamiana* epidermal leaf cells were assumed to act as a proxy for rubber particles, however the cellular localisation of HRT2 was found to be cytosolic. At the time, this was the first localisation of a plant rubber related CPT, however since this, other rubber related CPTs in *L. sativa* have also had their cell localisations described as cytosolic (Qu *et al* 2015). The cytosolic localisation raises the question of how CPTs such as HRT2 would interact with the long, insoluble rubber polyisoprene within the rubber particle. Due to the limitations of HRT2s hydrophobic cleft and the nature of polyisoprene rubber, it seems unlikely that it could synthesise polyisoprene in the cytosol. It is therefore likely that another co-factor is needed to bring it into association with a membrane.

3.4.2 The closely related SRPP and REF both localise to the endoplasmic reticulum

Previously immunogold labelling has been utilised to detect the presence of SRPP and REF on fixed rubber particles confirming that, in *Hevea*, they localise to these organelles (Bahri and Hamzah 1996). However this is the first time that the cell localisations of *Hevea* SRPP or REF have been determined *in vivo*, albeit in a non-rubber producing model organism.

In much the same way that many lipid body proteins can be found on the endoplasmic reticulum and vice versa, it may be that rubber related proteins can be found on the endoplasmic reticulum in the absence of rubber particles.

The localisation of SRPP and REF to the endoplasmic reticulum in *N. benthamiana* may provide a further argument that rubber particles originate from this organelle. As rubber particles are thought to be topologically similar to lipid bodies it is perhaps unsurprising

that the two most common rubber particle proteins, REF and SRPP localise to the endoplasmic reticulum in non-rubber producing cells.

However, since the start of this project two research groups have described proteins of the SRPP family including lipid droplet associated proteins (LDAPs) in avocado, which would normally localise to lipid bodies, as localising to the cytosol in tissue that do not contain these organelles (Horn *et al* 2013, Kim *et al* 2016). Until rubber particle formation is observed *in vivo* it is very difficult to draw a definitive conclusion on their origin.

SRPP expression also results in the formation of substantial protein aggregates, which could be seen as small dots after 2 days and grew in size (data not shown), initially these gave the impression they could be lipid bodies or similar structures and attempts were made to stain the aggregates with the lipophilic Nile red stain. However Nile red did not stain the aggregates and the most likely explanation is that they are inclusion bodies, and an artefact of overexpression. Inclusion bodies are dense aggregates of protein, usually in a non-native conformation, and can occur as a result of overexpression. Certain proteins are more prone to aggregation especially in proteins, such as SRPP, that are hydrophobic (Berthelot *et al* 2014c). SRPPs may act to coat the rubber particle membrane surface (Berthelot *et al* 2014b) and latex SRPPs including those of *T. brevicorniculatum* as well as that of *Hevea* are supposed to present a negative charge facing the cytosol of the latex surrounding the rubber particles, which acts to stabilise rubber particles. This property of SRPP may leave it more vulnerable to a molecular crowding effect leading to aggregation, especially when overexpressed as was the case with the 35S promoter-driven constructs used here.

REF expression also led to the formation of unknown structure though these were markedly different than those of SRPP. They were small punctate structures that had the look of small vesicles; however after co-expression with a succession of marker proteins their identity remains unknown. Berthelot *et al* (2014a) reports that REF may insert itself into the membrane then break off forming micelles with the protein surrounded by a small fragment of the endoplasmic reticulum. This was tested by co-infiltrating with membrane marker calnexin, however calnexin was not found on the structures. If indeed REF does do this then this was not observed here. It is possible

therefore that, like its close relative SRPP, these structures are aggregates, the product of artificial overexpression under a 35S promoter.

3.4.3 Reticulon-receptor like protein HevNogo localises to the endoplasmic reticulum like its homologs in *T. brevicorniculatum* and *L. sativa*

HevNogo, like SRPP and REF localises to the endoplasmic reticulum. Nogo receptor-like proteins such as NgBR (Teng *et al* 2014) and *T. brevicorniculatum* TbRTA have previously been shown to localise to the endoplasmic reticulum, HevNogos localisation continues this trend. Given NgBRs association with reticulon proteins which are well characterised as being associated with the endoplasmic reticulum (Gia *et al* 2006) it was perhaps expected that HevNogo would localise here also. However until recently HevNogo had not been detected in latex nor is it known whether it would associate with a rubber particle.

T. brevicorniculatum CPTL, TbRTA has been shown to interact with dandelion CPT, co-expression of TbRTA and CPT, affects CPT localisation changing it from a cytosolic localisation to the endoplasmic reticulum (Epping *et al* 2015); as HRT2 was also detected as a cytosolic protein and HevNogo as localising to the endoplasmic reticulum. If it is the case that HevNogo does bring HRT2 to the endoplasmic reticulum then this could provide the mechanism for rubber biosynthesis. This will be discussed in the next section (**section 3.5**).

3.4.4 RBSP remains in the cytosol

RBSP, like HRT2 is cytosolic. RBSP is poorly studied: it may be that like certain SRPP homologs it will only localise to lipid bodies, but remain cytosolic elsewhere, and it is also possible that RBSP requires the action of a co-factor to bring it to a rubber particle. TOPCONS predictions for RBSP indicate that there are no transmembrane domains, so if it is to associate with a particle, then this is likely the case. The massive increase of IPP incorporation when RBSP is added to rubber particle assays indicates that it does have a role to play.

3.5 Cloning and characterisation of HevNogo

Human Nogo-B-receptor NgBR a CPTL enzyme, was first demonstrated to play a role in cholesterol trafficking through its interaction with NPC2, a protein involved in glycosylation (Park *et al* 2014) and the transport of water insoluble molecules including cholesterol. Mutations in NgBR are a cause of the genetic disorder Niemann-Pick type C disease (Harrison *et al* 2009). Since then NgBR was shown to play a role in in IPP polymerisation, especially in dolichol biosynthesis, interacting with CPT enzymes (Harrison *et al* 2011). Plant CPTLs in both *Arabidopsis* (Zhang *et al* 2008) and *T. brevicorniculatum* (Epping *et al* 2015) have been shown to have a similar role, however until now there has been no research investigating the role of CPTLs in rubber producing species, especially *Hevea*. Therefore I decided to attempt to identify a CPTL homolog in *Hevea* itself, the resulting homolog was named HevNogo.

HevNogo's cellular localisation and topology was determined for the first time. This was done by a combination of bioinformatics to study predicted protein regions and via mutation experiments where predicted transmembrane domains were deleted to determine their function. A list of constructs used in this section can be found in figure 3.7.

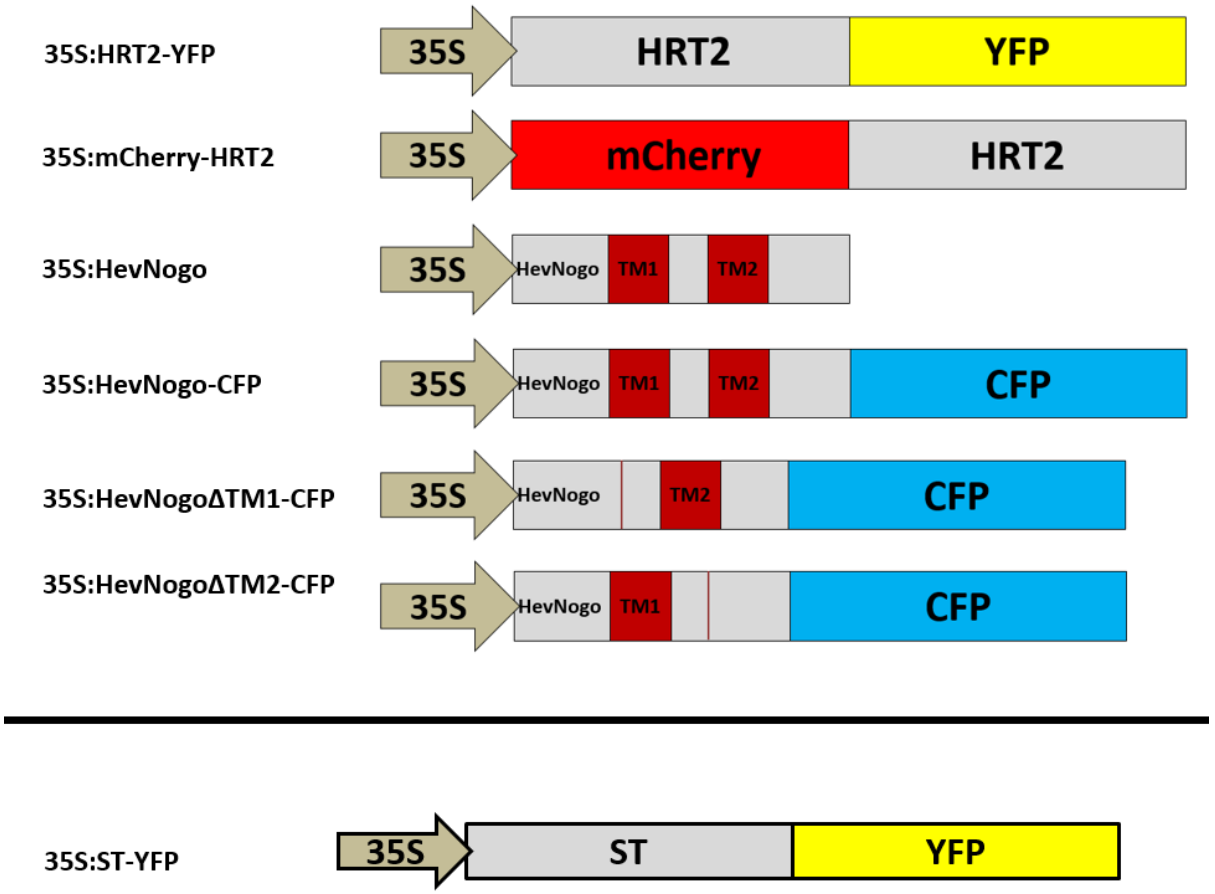

Figure 3.7 Constructs used for the characterisation of HevNogo

Above the line are constructs generated for this project which are fused with a fluorescent tag at either the N' or C' terminal. 35S:HevNogoΔTM1-CFP and 35S:HevNogoΔTM2-CFP are mutant created by the deletion of regions within 35S:HevNogo-CFP, these regions are indicated by the red bands TM1 and TM2. HevNogo was used in co-localisation studies in conjugation with HRT2.

Below the line is ST-YFP that was used as a marker for Golgi bodies and was previously generated (see **section 2.5.4** for references). All constructs are driven by a 35S promoter

3.5.1 Identifying and cloning HevNogo

CPTL sequences for *Arabidopsis* LEW1 (Zhang *et al* 2008) and *T. brevicorniculatum* TbRTA, were used initially as queries against the NCBI public database. There were no BLAST hits for a *Hevea* protein. The CPTL sequences were then used as a query for a pBLAST against TARRCs *Hevea* predicted protein database. A protein from the database with the ID tag 'HEVBR187338_AB_0629490' displayed a sequence identify of roughly 50% and was named temporarily HB50. The genome scaffold, >scaffold_161569.fa_seg, that contained the nucleotide sequence for HB50 was found using HB50 as a protein query against the nucleotide genome sequence.

The ORF of >scaffold_161569.fa_seg were annotated by using NBCI BLAST (Appendix figure A7) to compare the sequence against the public database. This revealed several close hits to predicted Nogo-B receptor like proteins and dedol-PP syntases from other plant species. It was also apparent from NCBI that HB50 gene was split into 3 ORFs, and that the 5' region of the gene was missing from the scaffold (Appendix figure A8).

Based upon the truncated version of HB50 in the *Hevea* scaffold sequence, primers were designed to amplify and sequence the gene from *Hevea* genomic DNA. This sequence of amplified gene was then used as the basis for further primer design, in order to sequence back into the unknown region, using genomic DNA as a template. As there were still missing sections of poor sequence coverage despite repeated sequencing attempts, GATC 'superior sequencing service for difficult templates' was utilised to sequence the entire region which contained the predicted 5' region of the gene, as determined by homology to other Nogo receptor like proteins. Primers were designed to amplify the entire sequence which now contained the complete gene. This was done from cDNA due to the presence of introns in the genomic DNA sequence. The gene was named HevNogo. HevNogo was initially cloned into a 35S promoter and pGreen vector without a tag, and then a CFP tag was added to both the N and C terminals of the predicted protein as described in **section 3.2**.

3.5.2 Predicted Topology of HevNogo compared to other CPTL proteins

To predict the protein topology of HevNogo, the TOPCONS prediction algorithm (Tsirigos *et al* 2015) was utilised. HevNogo was also compared to several, previously identified CPTL proteins (Figure 3.8). Whilst there were no consensus transmembrane regions predicted by TOPCONS, a combination of the prediction algorithm and comparison to other CPTLs was used to identify potential transmembrane regions 1 and 2 (TM1 and TM2) in the sequence of HevNogo.

There were strong predictions for two TM domains in the Plant CPTL proteins, LEW1 and *T. brevicorniculatum* TbRTA. Also analysed was the human NgBR which TOPCONS predicts as having a low confidence prediction for transmembrane domains with a similar result to HevNogo. NgBR however has experimentally been shown to have multiple transmembrane domains which are in a similar position to LEW1 and TbRTA (Harrison *et al* 2011). The predicted TM for HevNogo have a low confidence score and are only predicted by SPOCTOPUS. However they do align with the predicted regions TM regions in LEW1, TbRTA and NgBR. Therefore I proposed two transmembrane regions for HevNogo. Deletion analysis was performed, with subcellular localisation analysed by confocal microscopy.

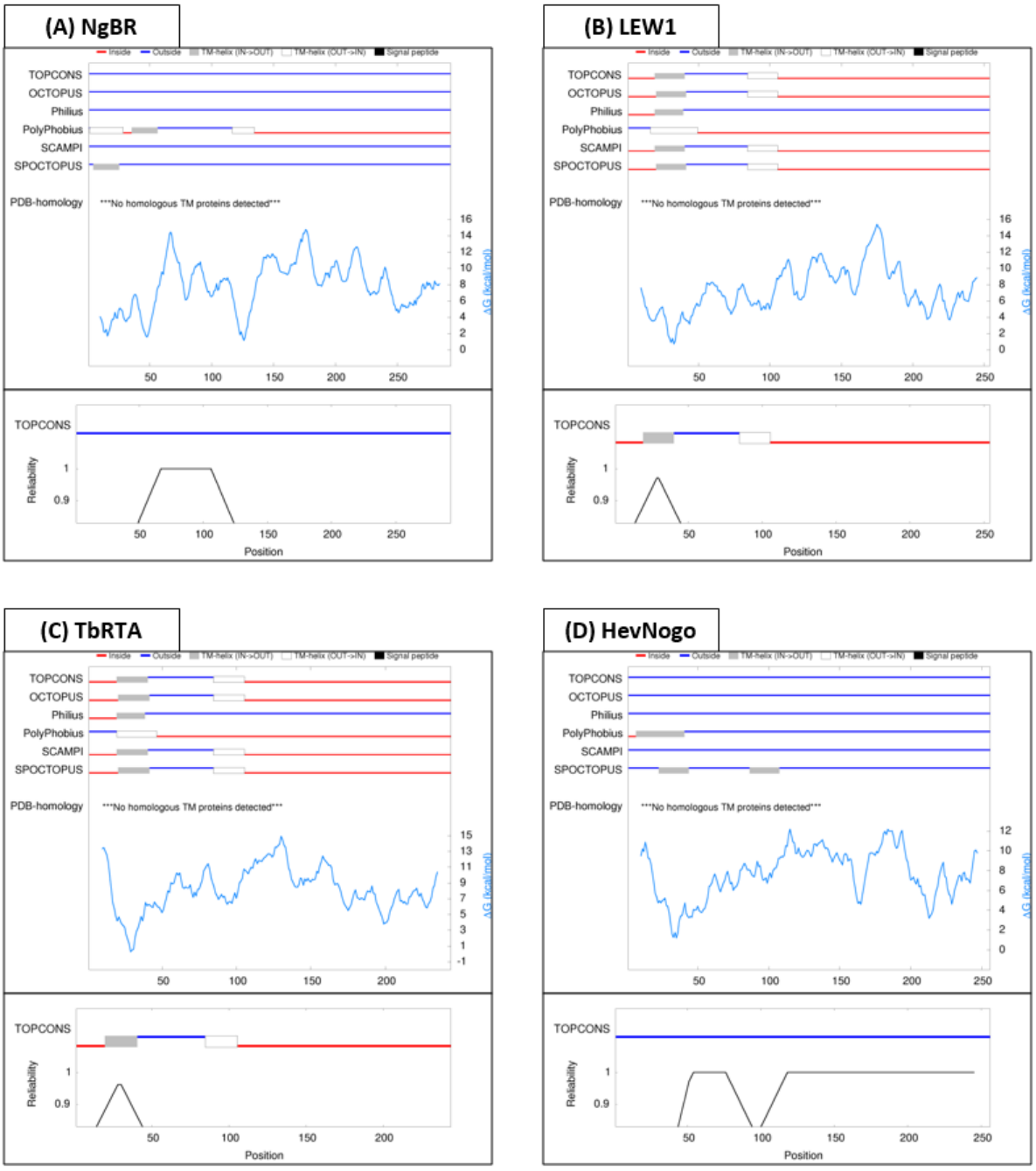

Figure 3.8 TOPCONS prediction of transmembrane regions in CPTL proteins
All four proteins have 2 potential transmembrane domains predicted although only *Arabidopsis* (B) and *T. brevicorniculatum* TbRTA (C) predictions are in agreement. NgBR (A) and HevNogo (D) have low confidence predictions from SPOCTOPUS for 2 transmembrane regions.

3.5.3 Deletion of HevNogo TM1 abolishes its localisation to the endoplasmic reticulum

A mutant version of HevNogo, HevNogoΔTM1 was created by deletion of amino acids from position 32-58 in accordance with the partial prediction from TOPCONS. This mutant was agroinfiltrated into *N. benthamiana* and imaged after 3 days (Figure 3.9). The TM1 deletion effected the localisation of HevNogo: whereas full length HevNogo localises to the endoplasmic reticulum, HevNogoΔTM1 localises to the cytoplasm, displaying the characteristic diffuse pattern, and presence in the nucleoplasm but not on the nuclear membrane.

3.5.4 Deletion of HevNogo predicted TM2 has no effect on its localisation

There was no consensus prediction for TM2 in HevNogo and this TM domain was only predicted by one of the prediction algorithms, SPOCTOPUS, (Figure 3.8). However, after comparison with other CPTLS which are predicated to contain a transmembrane region in the corresponding positions, it was decided to target this region for deletion as well. A mutant version of HevNogo; HevNogoΔTM2 was created by deletion of amino acids from positions 87-108. The mutant was agroinfiltrated into *N. benthamiana* and imaged after 3 days (Figure 3.9). Deletion of the TM2 region had no effect on the localisation of HevNogo: HevNogoΔTM2 localised to the endoplasmic reticulum displaying the characteristic network pattern and localisation to the nuclear membrane.

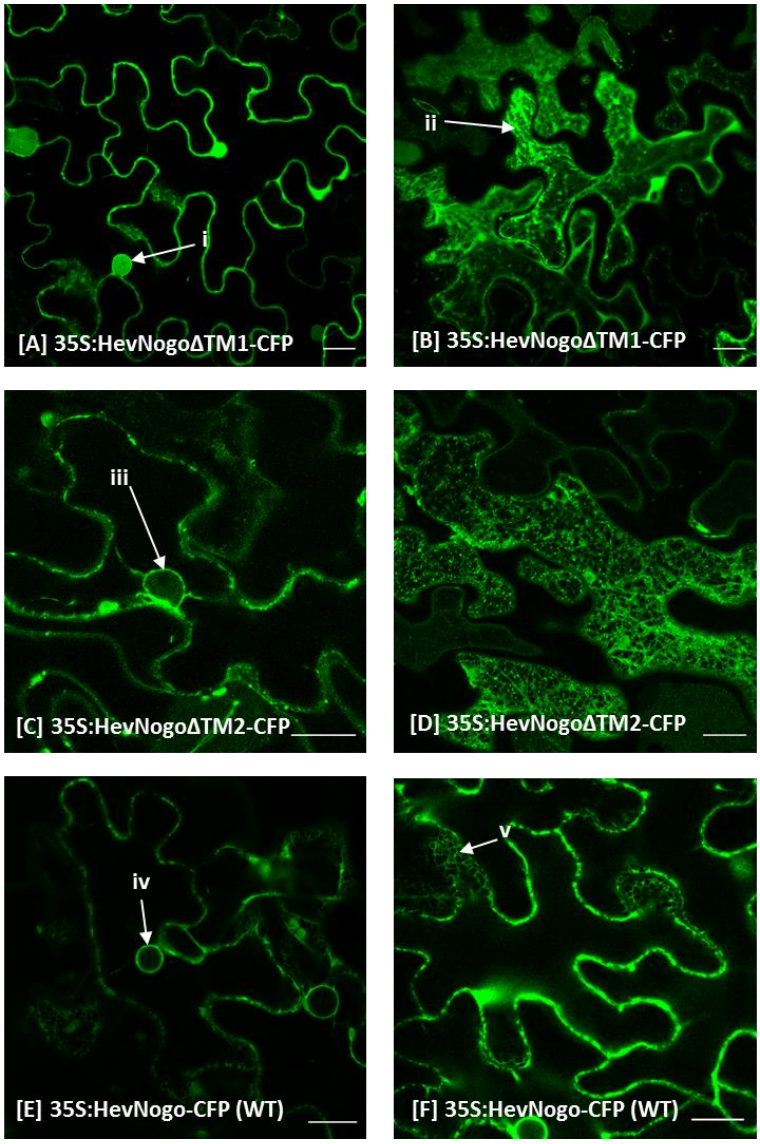

Figure 3.9 Deletion of HevNogo's predicted transmembrane region 1 changes the localization from endoplasmic reticulum to cytosol, whilst deletion of predicted transmembrane region 2 has no effect

HevNogoΔTM1 and HevNogoΔTM2 were transiently expressed in *N. benthamiana* leaf cells and imaged after 3 days.

(A) Cross-section of cells transformed with 35S:HevNogoΔTM1-CFP (green) showing signal in the nucleus (i) but not on the nuclear envelope consistent with cytosolic expression. (B) Cortex of cells transformed with 35S:HevNogoΔTM1-CFP (green) showing negative staining of organelles (ii). (C) Cross section of cells transformed with 35S:HevNogoΔTM2-CFP (green) showing localisation to the endoplasmic reticulum, signal is present on the nuclear membrane (iii) which is contiguous with the endoplasmic reticulum. (D) Cortex of cells transformed with 35S:HevNogoΔTM2-CFP (green) showing characteristic endoplasmic reticulum network pattern. (E and F) Wild Type (WT) 35S:HevNogo-CFP with nuclear membrane (iv) and fine endoplasmic reticulum network pattern (v).

3.5.5 HevNogo induces the relocalisation of HRT2 to the plasma membrane

In dandelions (Epping *et al* 2015) and lettuce (Qu *et al* 2015), CPTL proteins act to bring CPT proteins to the endoplasmic reticulum. In order to assess the effect, if any, HevNogo may have on the *Hevea* CPT protein HRT2, the newly generated, untagged 35S:HevNogo was transformed *A. tumefaciens* C58 and co-infiltrated into the leaf epidermal cells of *N. benthamiana* which were imaged after 3 days (Figure 3.10). HRT2 underwent a shift in cellular localisation, in the presence of HevNogo. The diffuse cytosolic pattern shifted to that of a continuous membrane and the signal in the nucleoplasm was lost entirely - although occasionally a faint signal could be detected around the nuclear envelope. The continuous membrane pattern encasing the cell was characteristic of a plasma membrane. To test this, HRT2/HevNogo transformed cells were stained with FM4-64 dye (Vida & Emr 1995) with the length of staining timed in order to selectively stain the plasma membrane (Figure 3.11). The position of the fluorescent protein on HRT2 did not seem to affect localisation (data not shown) in the presence of HevNogo.

Not only does HevNogo alter the cell localisation of HRT2, the localisation of HevNogo itself was affected when they are co-expressed. 35S:HevNogo-CFP was transformed into *A. tumefaciens* C58 and infiltrated into the leaf epidermal cells of *N. benthamiana* with the cell localisation described previously as endoplasmic reticulum. When 35S:HevNogo-CFP was co-infiltrated with 35S:mCherry-HRT2 (Figure 3.12a) both proteins localised to the plasma membrane in cells which expressed both constructs, whereas cells expressing 35S:HevNogo-CFP displayed HevNogo on the endoplasmic reticulum. The orientation of the fluorescent protein fusion on HevNogo did not affect localisation or the interaction with HRT2 (data not shown). At higher levels of infiltration and expression some remnants of protein could be detected on the endoplasmic reticulum, this was particularly true for HevNogo (Figure 3.12b).

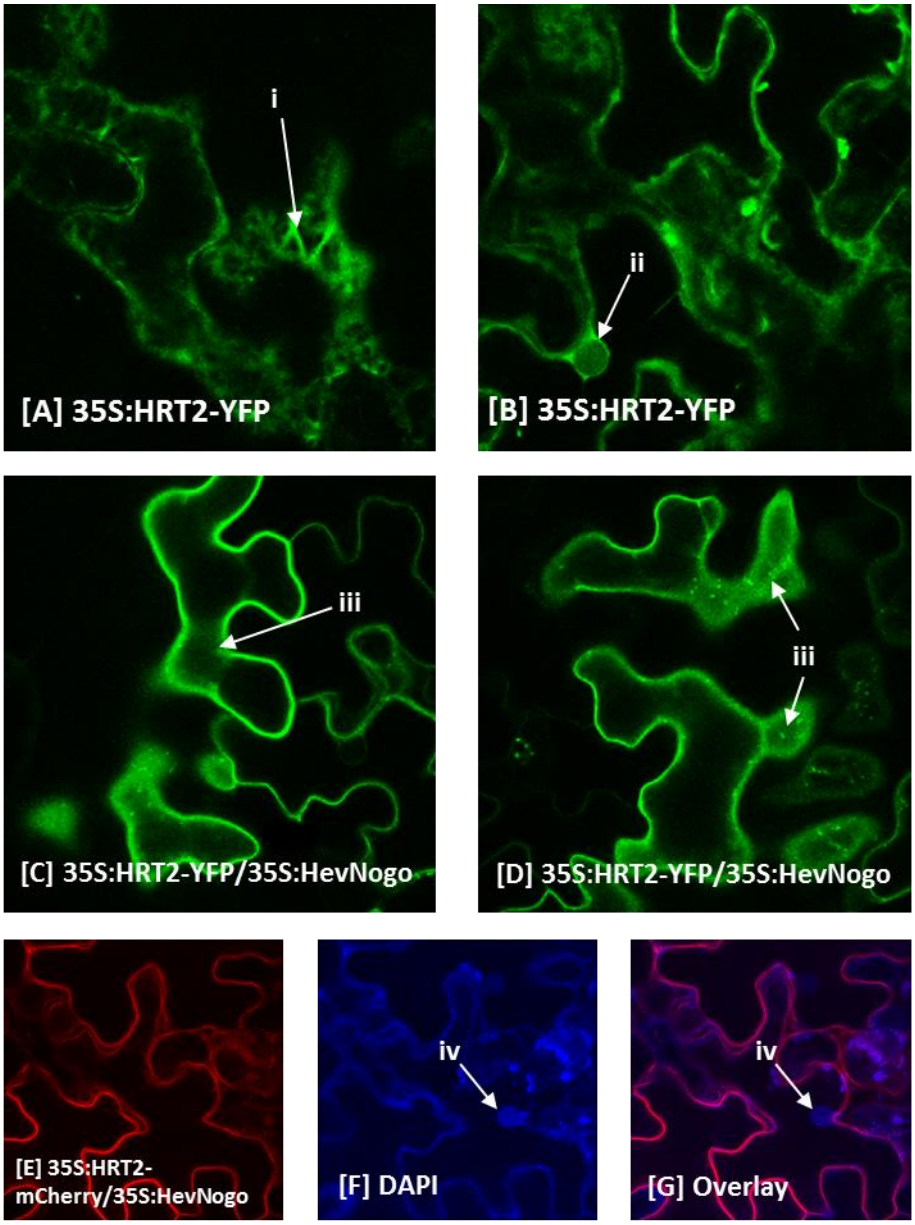

Figure 3.10 HevNogo coexpression affects HRT2 localisation

HRT2 and HevNogo were transiently expressed in *N. benthamiana* and imaged after 3 days.

(A). 35S:HRT2-YFP (green) transformed cell cortex showing diffuse cytosolic pattern with negative staining of organelles (i). (B) 35S:HRT2-YFP (green) transformed cells showing nucleoplasm (ii) signal consistent with cytosolic localisation. (C and D) 35S:HRT2-YFP (green) co-infiltrated with 35:HevNogo, the diffuse cytosolic pattern from image A has now changed to a solid membrane (iii).

(E, F and G) DAPI stain of HRT2/HevNogo transformed cell.

(E) 35S:mCherry-HRT2 (red) transformed cell. (F) DAPI stain (blue) highlighting the nucleus (iv). (G) Overlay of images images E and F, showing that there is no longer signal in the nucleus (iv) when HRT is expressed with HevNogo. In contrast to image B where the nucleoplasm (ii) is apparent when HRT is expressed alone.

Scale bars =20μm

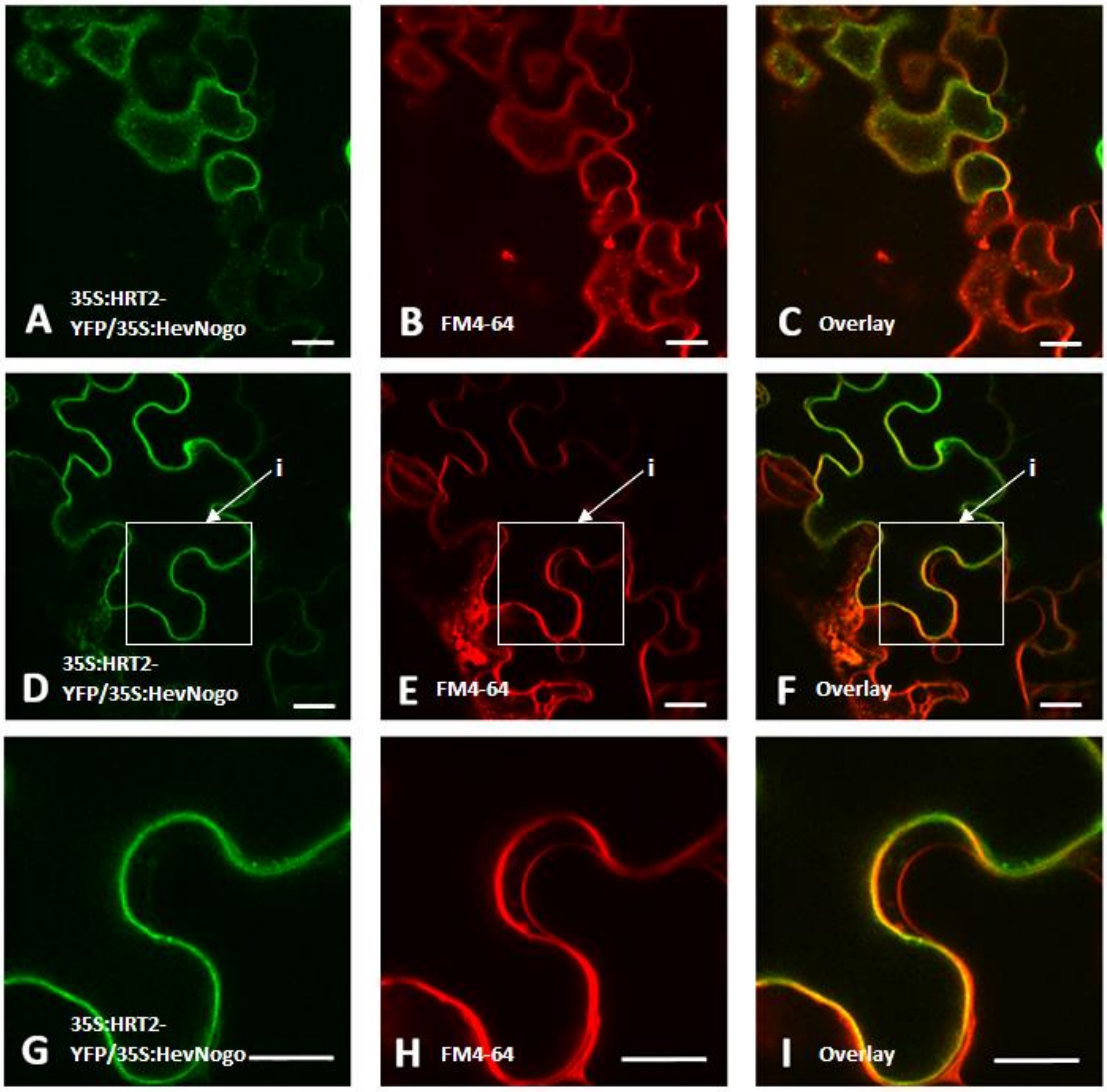

Figure 3.11 HevNogo changes HRT2 localisation to the plasma membrane

HRT2 and HevNogo were transiently expressed in *N. benthamiana* leaf cells and imaged/ stained with FM4-64 dye after 3 days.

(Top row) Cell cortex of cells transformed with 35S:HRT2-YFP, 35S:HevNogo and stained with FM4-64 dye. (A) YFP channel showing expression of 35S:HRT2-YFP. (B) FM4-64 channel, showing plasma membrane staining by FM4-64. (C) Overlay of images A and B showing co-localisation of HRT2 and FM4-64.

(Second row) Cell cross-section of cells transformed with 35S:HRT2-YFP, 35S:HevNogo and stained with FM4-64 dye. (D) YFP channel showing expression of 35S:HRT2-YFP. (E) FM4-64 channel, showing plasma membrane staining by FM4-64. (F) Overlay of images D and E showing co-localisation of HRT2 and FM4-64.

(Third row) Magnification of second row images (box i) with a close up of the cell membrane. (G) YFP channel showing expression of 35S:HRT2-YFP. (H) FM4-64 channel, showing plasma membrane staining by FM4-64. (I) Overlay of images G and H showing co-localisation of HRT2 and FM4-64.

Scale bars = 20µm

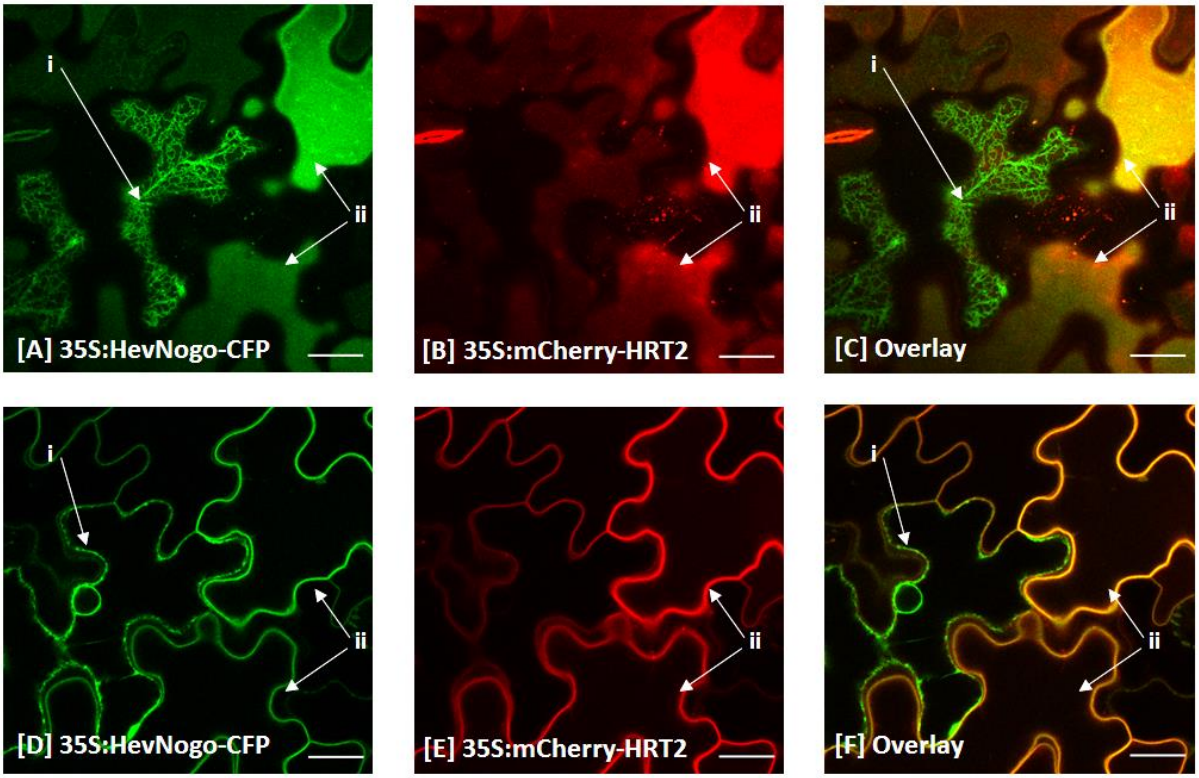

Figure 3.12a Co-expression of HRT2 and HevNogo results in both proteins travelling to the plasma membrane

HRT2 and HevNogo were expressed in *N. benthamiana* leaf cells and imaged after 3 days. The cell on the left hand side of the images (i) is expressing only HevNogo whilst the cells on the left hand side of the images are expressing both constructs.

(A, B and C) Cell cortex of cells expressing HRT2 and HevNogo. (A) CFP channel showing expression of 35S:HevNogo-CFP. Cell (i) shows HevNogo localization to the endoplasmic reticulum whilst cells (ii) show localization to the plasma membrane. (B) mCherry channel showing localization of 35S:mCherry-HRT2 to the plasma membrane. (C) Overlay of images A and B showing that HevNogo is present on the plasma membrane (ii) when expressed in the same cells as HRT2 but remains on the endoplasmic reticulum (i) when expressed alone.

(D, E and F) Cross-section of cells expressing HRT2 and HevNogo. (D) CFP channel showing expression of 35S:HevNogo-CFP. Cell (i) shows HevNogo localization to the endoplasmic reticulum with the nuclear membrane visible, whilst cells (ii) show localization to the plasma membrane. (E) mCherry channel showing localization of 35S:mCherry-HRT2 to the plasma membrane. (F) Overlay of images D and E showing that HevNogo is present on the plasma membrane (ii) when expressed in the same cells as HRT2, but remains on the endoplasmic reticulum (i) when expressed alone.
Scale bars = 20μm

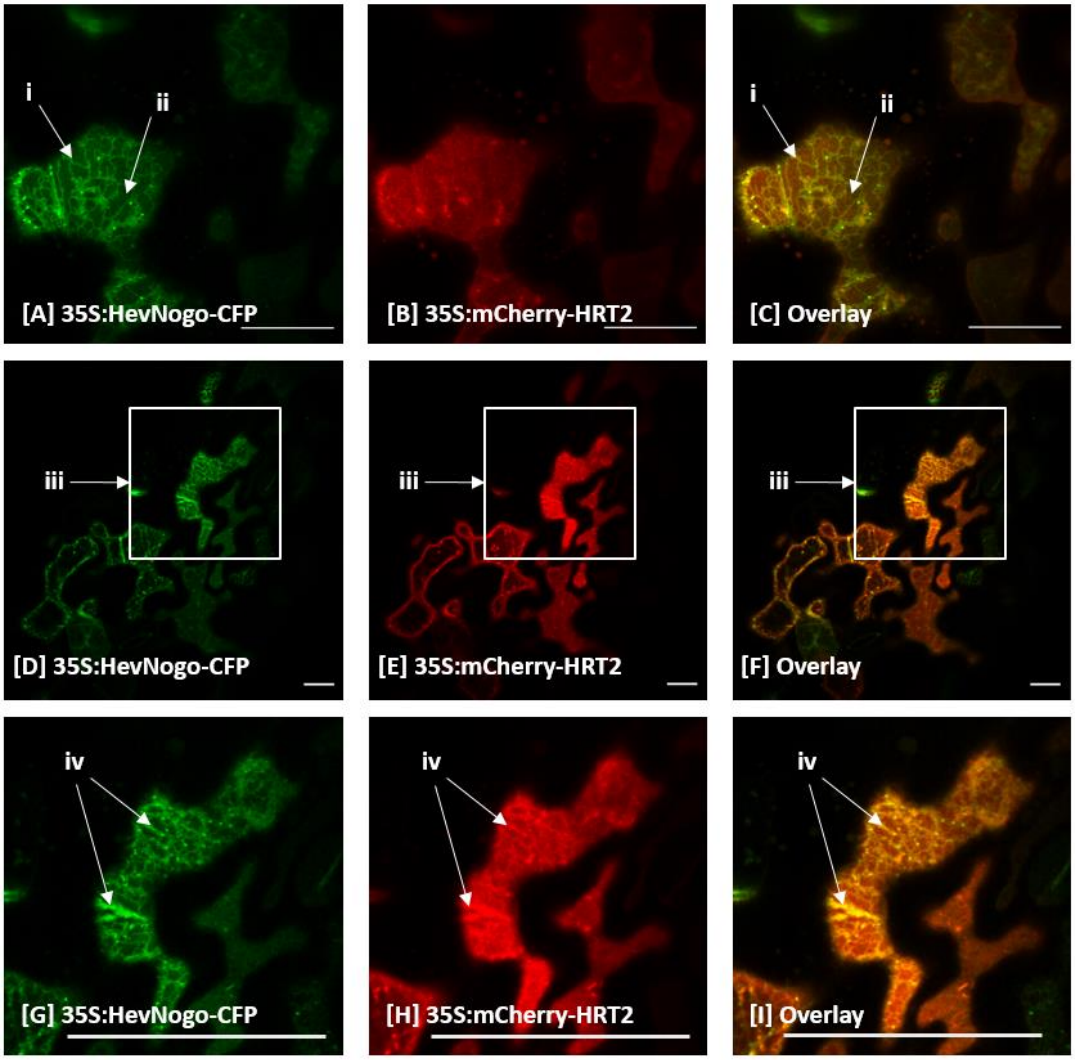

Figure 3.12b Overexpression of HRT2 and HevNogo results in both proteins travelling to the plasma membrane with some remnants observed at the endoplasmic reticulum

HRT2 and HevNogo transformed *A. tumeficiens* was infiltrated at an OD_{600} value of 1.5 and expressed in *N. benthamiana* leaf cells and imaged after 3 days.

(A, B and C) Cell cortex of cells overexpressing HevNogo and HRT2. (A) CFP channel 35S:HevNogo-CFP (green) showing both endoplasmic reticulum network pattern (i) and solid plasma membrane (ii). (B) mCherry channel showing 35S:mCherry-CPT which displays largely plasma membrane localization. (C) Overlay of images A and B.

(D, E and F) Cell cortex of cells overexpressing HevNogo and HRT2

(G, H and I) Magnification of second row images (box iii) showing HevNogo and HRT2 expression. (G) CFP channel 35S:HevNogo-CFP (green) showing both endoplasmic reticulum network pattern (iv) and some solid membrane. (H) mCherry channel showing 35S:mCherry-CPT which displays largely plasma membrane localization but also remnants of endoplasmic reticulum (iv). (I) Overlay of images G and H.

Scale bars = 20μm

3.5.6 HevNogo affects HRT2 localisation over time

To determine if HRT2 and HevNogo's affect on each other and to show that each protein had a real impact on the other independent of the plant or leaf tissue they were infiltrated, HRT2 and HevNogo were infiltrated sequentially into the same leaf sector then imaged over time. 35S:mCherry-HRT2 and 35S:HevNogo were transformed into *A. tumefaciens* C58 cells and were infiltrated into separate leaf sectors of *N. benthamiana*. The second construct was then infiltrated into the same sector 2 days later. It was possible therefore to image a single construct then study the effect of the second construct as it began to express. A leaf sector containing only the individual constructs was also infiltrated to act as a comparison after 5 days (Figure 3.13a/b)

Both proteins were shown to have an effect on the other as they began to express: HevNogo had the greater effect boosting HRT2 fluorescene and inducing its relocation to the plasma membrane, even at relatively low expression levels of HevNogo. HRT2 also affected HevNogo localisation though to a lesser degree with low levels of HRT2 not sufficient to send HevNogo to the plasma membrane, in cells where both constructs were expressing strongly both proteins localised to the plasma membrane.

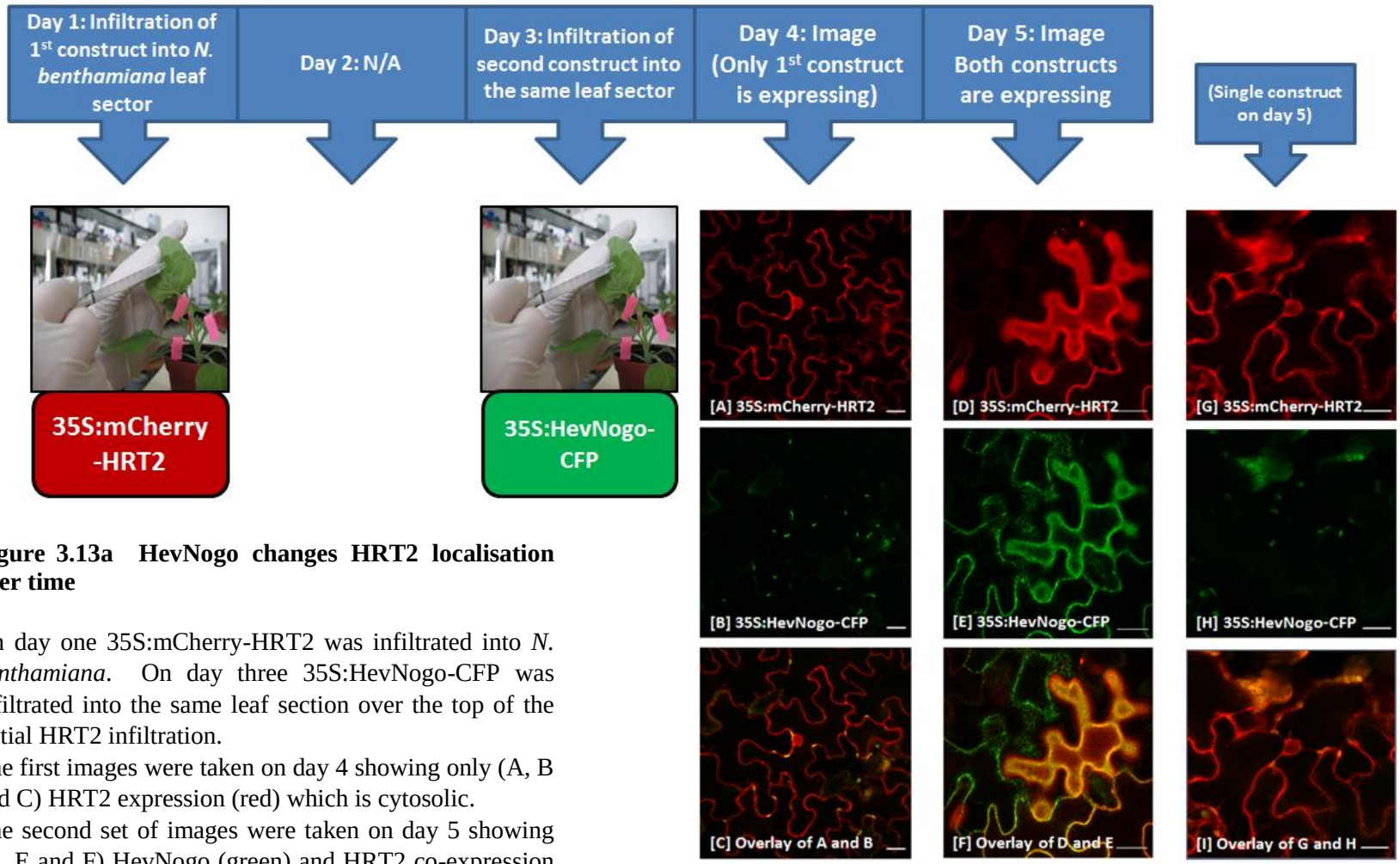

Figure 3.13a HevNogo changes HRT2 localisation over time

On day one 35S:mCherry-HRT2 was infiltrated into *N. benthamiana*. On day three 35S:HevNogo-CFP was infiltrated into the same leaf section over the top of the initial HRT2 infiltration.
The first images were taken on day 4 showing only (A, B and C) HRT2 expression (red) which is cytosolic.
The second set of images were taken on day 5 showing (D, E and F) HevNogo (green) and HRT2 co-expression with both proteins at the plasma membrane
Individual constructs were images on day 5 (G, H and I) showing that without HevNogo HRT2 (red) remains in the cytosol

Scale bars = 20µm

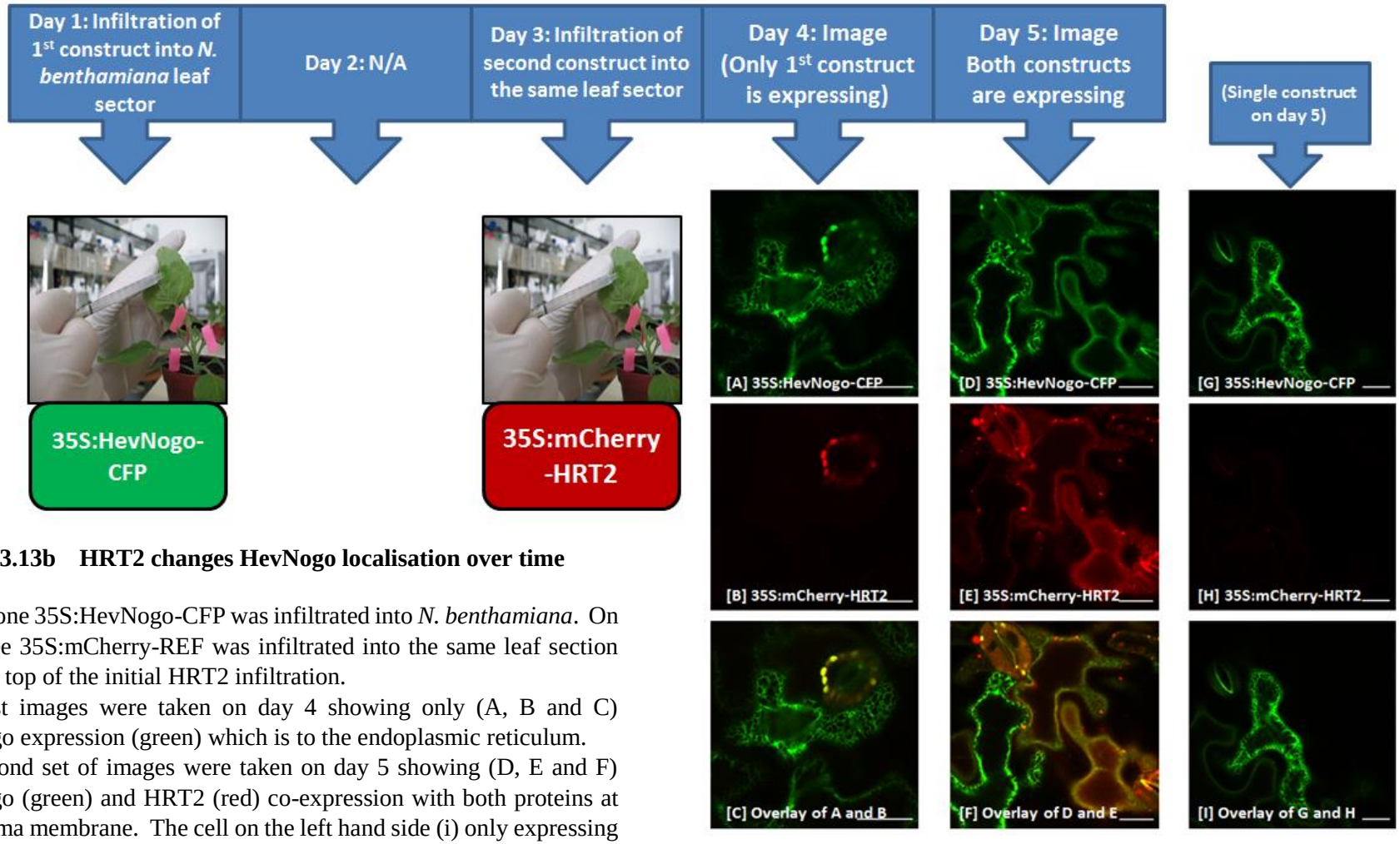

Figure 3.13b HRT2 changes HevNogo localisation over time

On day one 35S:HevNogo-CFP was infiltrated into *N. benthamiana*. On day three 35S:mCherry-REF was infiltrated into the same leaf section over the top of the initial HRT2 infiltration.

The first images were taken on day 4 showing only (A, B and C) HevNogo expression (green) which is to the endoplasmic reticulum.

The second set of images were taken on day 5 showing (D, E and F) HevNogo (green) and HRT2 (red) co-expression with both proteins at the plasma membrane. The cell on the left hand side (i) only expressing HevNogo remains at the endoplasmic reticulum, whilst the cell on the right hand side of the image (ii) expressing both is at the plasma membrane.

Individual constructs were images on day 5 (G, H and I) showing that without HRT2 HevNogo (green) remains at the endoplasmic reticulum

Scale bars = 20µm

3.5.7 BFA treatment of HevNogo/HRT2

HevNogo and HRT2 localisation to the plasma membrane was un-expected as CPT/CPTL co-expression in dandelion and lettuce results in an endoplasmic reticulum localisation (Epping *et al* 2015, Qu *et al* 2015). It may be possible that the complex containing both proteins is formed in the endoplasmic reticulum of the laticifer cells before being transferred to rubber particles. As our heterologous system lacks rubber particles, the complex may be secreted instead to the plasma membrane. Protein trafficking from the endoplasmic reticulum to the plasma membrane via the secretory pathway, or from the endoplasmic reticulum to a variety of destinations is often mediated by the Golgi. Brefeldin A was originally used as an antiviral drug that inhibits protein secretion at an early stage, resulting in the disappearance of Golgi bodies and protein accumulation in the endoplasmic reticulum (Fujiwara *et al* 1988). BFA works by inhibiting the ARF1 gene which is responsible for the recruitment of COPI proteins. The inhibition of COPI protein recruitment in turn inhibit the formation of transport vesicles that mediate Golgi/ endoplasmic reticulum transport. This results in the collapse of the Golgi which can fuse with the endoplasmic reticulum resulting in protein accumulation on the latter organelle (Nebenführ *et al* 2002).

35S:mCherry-HRT2 and 35S:HevNogo-CFP were each transformed into *A. tumefaciens*C58 cells and co-infiltrated into *N. benthamiana* leaf cells. For a positive control the Golgi marker construct ST-YFP was also infiltrated. After 3 days a section of leaf was exercised and imaged before BFA treatment. The section was then immersed into a BFA solution of 5 μg/ml and incubated for 1 hour at room temperature. The leaf sections were rinsed in dH_20 before being remounted on slides and images after BFA treatment. The HRT2/HevNogo complex was insensitive to BFA treatment and was present on the plasma membrane before and after immersion. ST-YFP in contrast which was present in Golgi bodies, accumulated on the endoplasmic reticulum in response to BFA treatment (Figure 3.14)

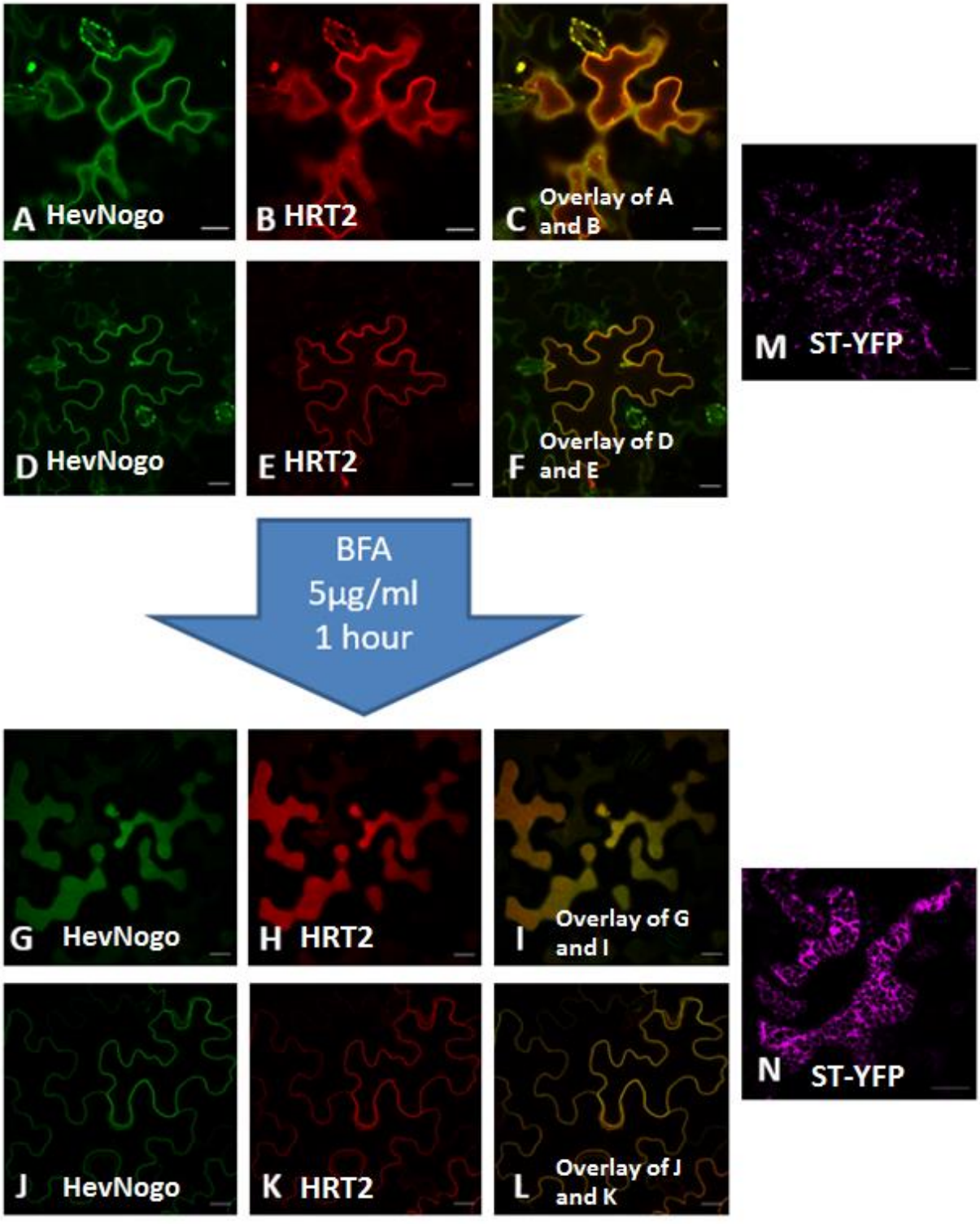
A HevNogo
B HRT2
C Overlay of A and B
M ST-YFP
D HevNogo
E HRT2
F Overlay of D and E
BFA
5µg/ml
1 hour
G HevNogo
H HRT2
I Overlay of G and I
N ST-YFP
J HevNogo
K HRT2
L Overlay of J and K

Figure 3.14 (previous page) HRT2/HevNogo trafficking to the plasma membrane is not sensitive to BFA treatment

HRT2 and HevNogo were expressed in *N. benthamiana* leaf cells, after 3 days sections were treated in 5µg/ml Brefeldin A solution for 1 hour, then imaged.

(A, B and C) Pre-BFA Treatment: Cell cortex of cell expressing (A) 35S:HevNogo-CFP (green) and (B) 35S:HRT2-YFP (red) with overlay image (C) demonstrating co-localisation on the plasma membrane.

(D, E and F) Pre-BFA treatment: Cross-section of cell expressing (D) 35S:HevNogo-CFP (green) and (E) 35S:HRT2-YFP (red) with overlay image (F) demonstrating co-localisation on the plasma membrane.

(G, H and I) Post-BFA Treatment: Cell cortex of cell expressing (G) 35S:HevNogo-CFP (green) and (H) 35S:HRT2-YFP (red) with overlay image (I) demonstrating co-localisation on the plasma membrane.

(J, K and L) Post-BFA treatment: Cross-section of cell expressing (J) 35S:HevNogo-CFP (green) and (K) 35S:HRT2-YFP (red) with overlay image (L) demonstrating co-localisation on the plasma membrane.

(M and N) ST-YFP (magenta) golgi marker. (M) ST-YFP (magenta) Pre-BFA treatment localises to golgi bodies. (N) ST-YFP (magenta) Post-BFA treatment localises to the endoplasmic reticulum.

3.5.8 Deletion of HevNogo TM1 prevents HRT2 and HevNogoΔTM1 from reaching the plasma membrane or endoplasmic reticulum

35S:HevNogoΔTM1 and 35S:mCherry-HRT2 were each transformed into *A. tumefaciens* C58 cells and co-infiltrated into *N. benthamiana* leaf epidermal cells, and imaged after 3 days. Both HRT2 and the mutant HevNogo TM1 deletion displayed a cytosolic localisation and were present in the nucleoplasm (Figure 3.15).

3.5.9 Deletion of HevNogo TM2 causes HRT2 and HevNogoΔTM2 to be retained at the endoplasmic reticulum

35S:HevNogoΔTM2 and 35S:mCherry-HRT2 were each transformed into *A. tumefaciens* C58 cells and co-infiltrated into *N. benthamiana* leaf epidermal cells, and imaged after 3 days. Both HRT2 and the mutant HevNogo TM2 delection were present on the endoplasmic reticulum with an additional, particularly strong signal on the nucleoplasm (Figure 3.16).

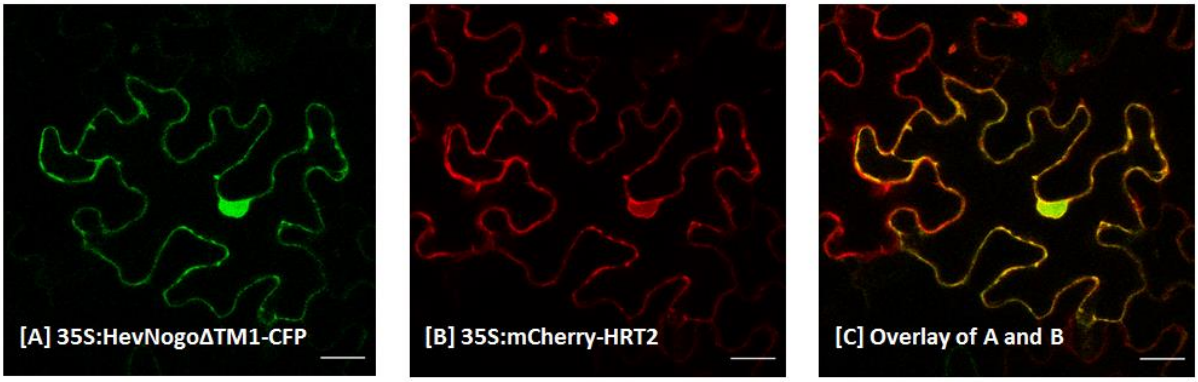

Figure 3.15 HevNogoΔTM1 does not affect the localisation of HRT2, with both proteins remaining in the cytosol

HRT2 and HevNogoΔTM1 were infiltrated in *N. benthamiana* leaf cells and imaged after 3 days (A, B and C) Cross -section of cells transformed with both HRT2 and HevNogoΔTM1. (A) CFP channel showing cytosolic expression of 35S:HevNogoΔTM1-CFP (green). (B) YFP channel showing cytosolic expression of 35S:HRT2-YFP (red). (C) Overlay of images A and B showing both constructs in the cytosol.

Scale bars =20µm

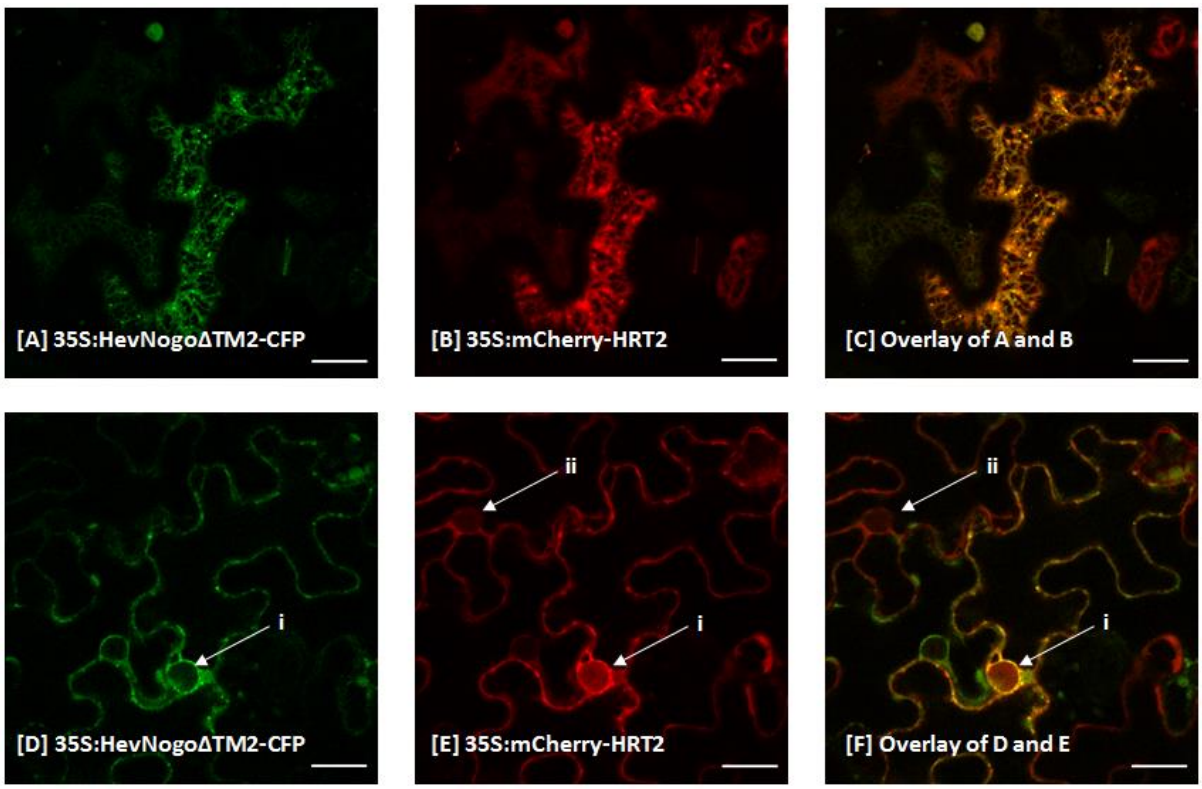

Figure 3.16 Co-expression of HevNogoΔTM2 with HRT2, relocates HRT2 to the endoplasmic reticulum

HRT2 and HevNogoΔTM2 were infiltrated in *N. benthamiana* leaf cells and imaged after 3 days (Top row) Cell cortex of cells transformed with both HRT2 and HevNogoΔTM2. (A) CFP channel showing a cell expressing 35S:HevNogoΔTM2-CFP (green) which displays characteristic endoplasmic reticulum pattern. (B) YFP channel showing cell expressing 35S:HRT2-YFP (red) which displays both characteristics of cytosolic and a finer endoplasmic reticulum pattern. (C) Overlay of images A and B showing co-localisation between HRT2 and HevNogoΔTM2.

(Second row) Cross section of cells transformed with both HRT2 and HevNogoΔTM2. (D) CFP channel showing CFP channel showing a cell expressing 35S:HevNogoΔTM2-CFP (green) with fluorescent signal on the nuclear membrane (i) which is contiguous with the endoplasmic reticulum. (E) YFP channel showing cells expressing 35S:HRT2-YFP (red) with nuclear membrane signal (i) in the cell also expressing 35S:HevNogoΔTM2-CFP, but no nuclear membrane signal in the top left cell (ii) which is just expressing 35S:HRT2-YFP. (F) Overlay of images D and E with co-localisation in cell (i).

Scale bars =20µm

3.6 HRT2 co-expression with SRPP

Rubber biosynthesis is thought to take place on the surface of the rubber particle, however the cell localisation of HRT2 was purely cytosolic, raising the question: if HRT2 is the key rubber transferase enzyme, then how it does interact with the long and insoluble rubber chains packaged within the rubber particle? It is possible that HRT2 is associated with co-factors located on the particle itself. Here 35S:HRT2-YFP was co-expressed with 35S:GFP-SRPP, 35S:SRPP-GFP was not included in this experiment as it did not display any localisation except for protein aggregates.

3.6.1 When co-infiltrated with SRPP, HRT2 displays endoplasmic reticulum localisation

35S:HRT2-YFP and 35S:GFP-SRPP were each transformed into *A. tumefaciens* and infiltrated into *N. benthamiana* and images after 3 days (Figure 3.17a/b) HRT2 seemed to co-localise with SRPP and whilst it retained some of its cytosolic characteristics, it also began associate more with the endoplasmic reticulum. This was particularly striking around the nuclear membrane: whereas previously no signal could be detected for HRT2 on the nuclear membrane, now it was very highly expressed.

HRT2 was also infiltrated with 35S:GFP-HDEL, to act as a control, especially to account for potential cross fluorescence between GFP and YFP tags. When HRT2 was co-expressed with SRPP there was strong signal around the nuclear envelope and co-localisation could be observed throughout the cell. HRT2 co-expression with GFP-HDEL showed that they did not co-localise. HDEL displays a strong nuclear membrane signal whereas HRT2 without SRPP is purely cytosolic, with signal coming only from the nucleoplasm but not the nuclear envelope. There was no difference between the two positions of the fluorescent protein within the fusion, 35S:HRT2-YFP and 35S:YFP-HRT2 (data not shown).

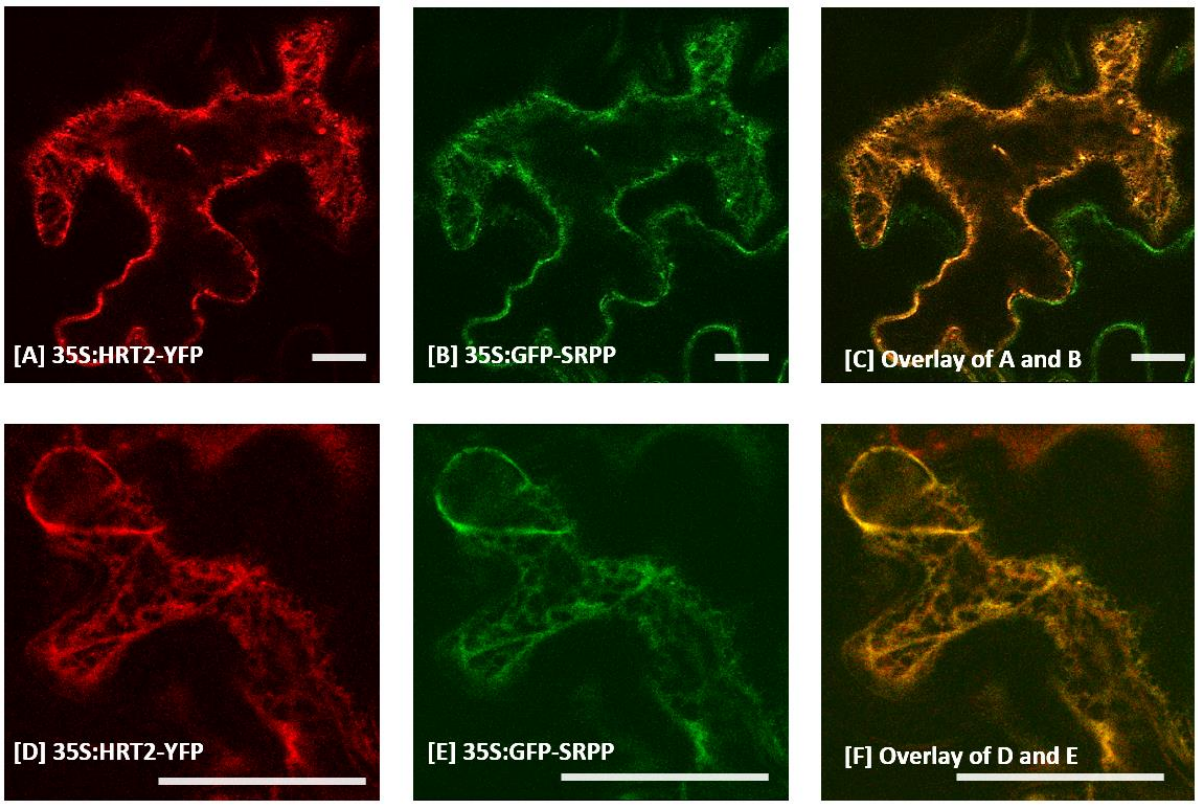

Figure 3.17a HRT2 and SRPP co-localise with a mixture of cytosolic and endoplasmic reticulum labelling

HRT2 and SRPP were transiently expressed in *N. benthamiana* leaf cells and imaged after 3 days. Image (A) of 35S:HRT2-YFP (red) transformed cell. (B) Overview of the 35S:GFP-SRPP (green) transformed cell and (C) overlay of images A and B showing co-localisation between HRT2 and SRPP with some finer endoplasmic reticulum detail.

Close up (D) of cell cortex of a 35S:HRT2-YFP transformed cell with (B) showing 35S:GFP-SRPP expression and overlay (F) of images D and E showing co-localisation and some fine endoplasmic reticulum pattern.

Scale bars =20µm

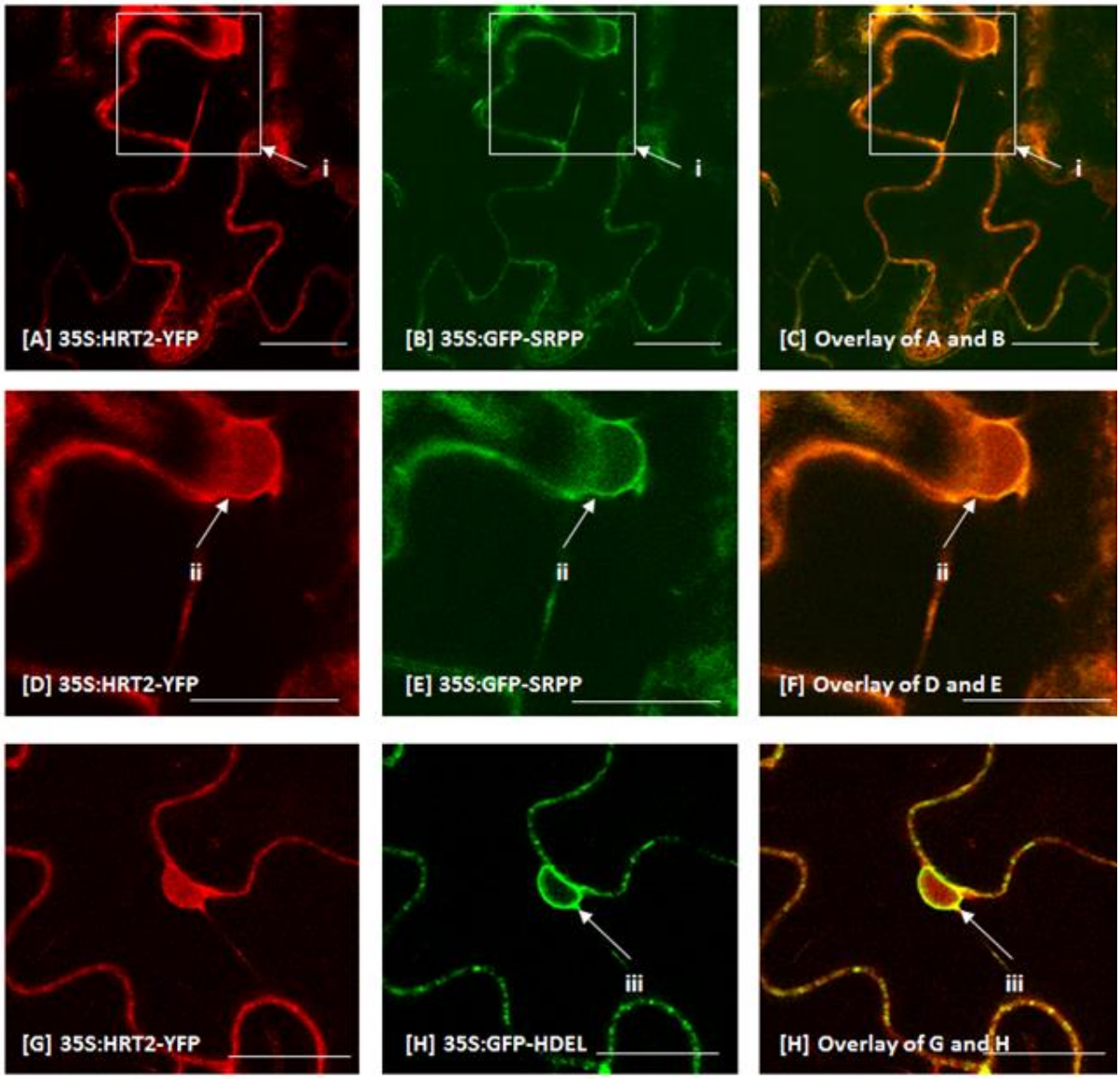

Figure 3.17b SRPP induces HRT2 localisation to the nuclear envelope
HRT2 and SRPP were transiently expressed in *N. benthamiana* leaf cells and imaged after 3 days. Overview (A) of 35S:HRT2-YFP (red) transformed cell. (B) Overview of the 35S:GFP-SRPP (green) transformed cell and (C) overlay of images A and B showing co-localisation between HRT2 and SRPP.
(D, E and F) Magnification of first row images (i) showing co-localisation between HRT2 (red) and SRPP (green) on the nuclear membrane.

(G) 35S:HRT2-YFP (red) transformed cell showing localisation to the nucleoplasm but not the nuclear membrane. (H) 35S:GFP-HDEL transformed cell showing strong signal (i) from the nuclear membrane. (H) Overlay of images G and H showing that HRT2 on itss own is distinctly not present on the nuclear membrane.

Scale bars =20µm

3.6.2 SRPP also affects HRT2 localisation over time

HRT2 then SRPP were infiltrated sequentially into the same leaf sector (Figure 3.18) and imaged over time. HRT2 was infiltrated into *N. benthamiana* followed by SRPP 2 days later. After 3 days, when only HRT2 was expressed, its localisation remained cytosolic with a diffuse pattern and no nuclear membrane signal. However on the 4th day, when SRPP begins to express, HRT2 shows increased labelling of the endoplasmic reticulum, particularly visible around the nuclear membrane, although it does still retain some cytosolic pattern.

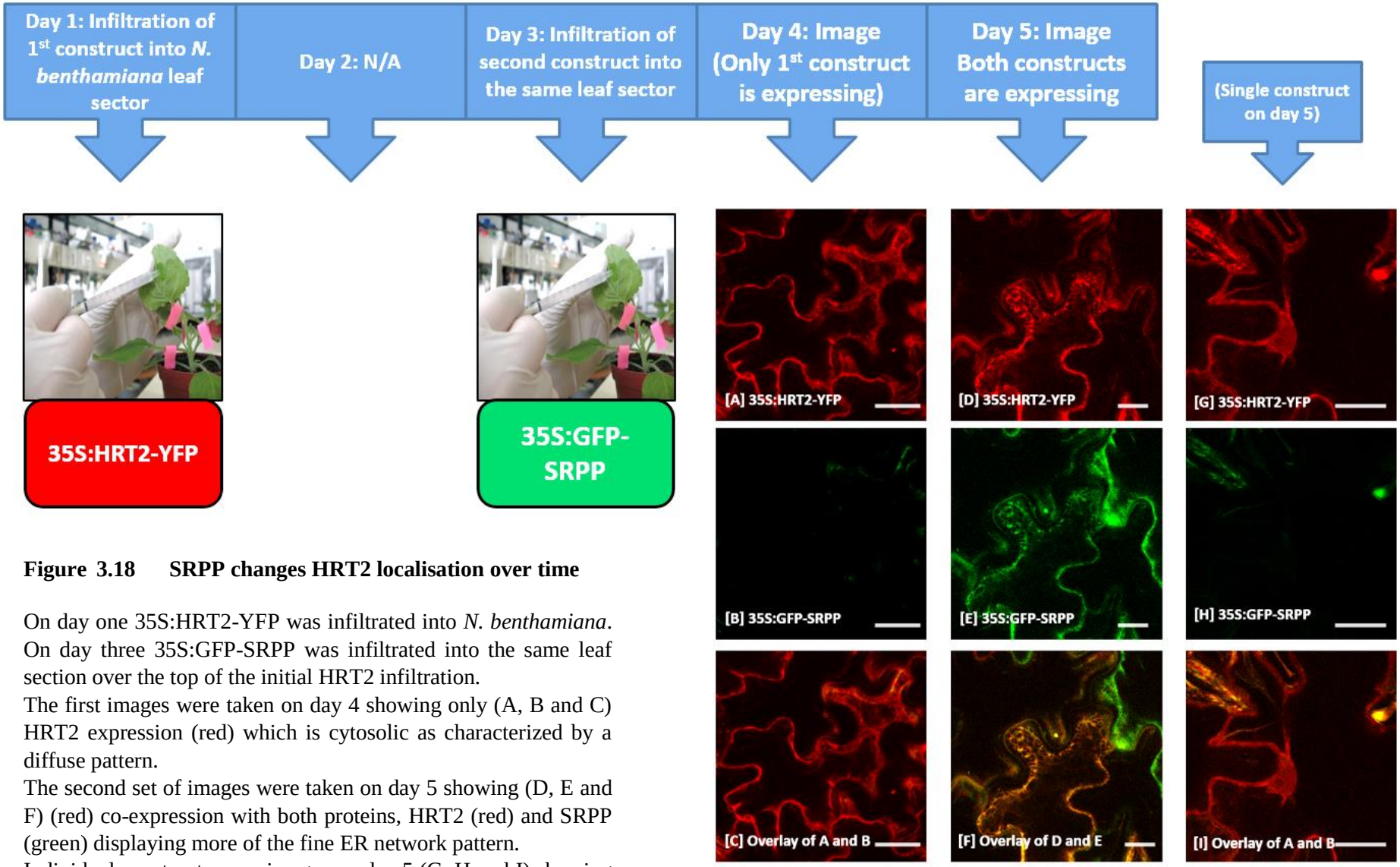

Figure 3.18 SRPP changes HRT2 localisation over time

On day one 35S:HRT2-YFP was infiltrated into *N. benthamiana*. On day three 35S:GFP-SRPP was infiltrated into the same leaf section over the top of the initial HRT2 infiltration.
The first images were taken on day 4 showing only (A, B and C) HRT2 expression (red) which is cytosolic as characterized by a diffuse pattern.
The second set of images were taken on day 5 showing (D, E and F) (red) co-expression with both proteins, HRT2 (red) and SRPP (green) displaying more of the fine ER network pattern.
Individual constructs were images on day 5 (G, H and I) showing that without SRPP (green) HRT2 remains at the purely cytosolic

Scale bars = 20µm

3.7 Analysis of binary protein-protein interactions by yeast-2-Hybrid assay

In order to screen each rubber related protein for potential interactions, in particular to test whether the HRT2-HevNogo and HRT2-SRPP co-localisations were actual interactions, yeast-2-hybrid screening was used. Any interactions would then be further investigated by co-immunoprecipitation.

3.7.1 Yeast-2-Hybrid assay

Yeast-2-hybrid works by taking advantage of the GAL4 transcription factor, which like many other eukaryotic transcription factors is modular in nature. Fields & Song (1989) discovered that GAL4 consists of two domains, an activation domain (AD), and a DNA binding domain (DB). In the presence of galactose binding to the activation domain, the DNA binding domain will bind to DNA, and initiate transcription of a reporter gene. The reporter gene can code for any number of proteins that could be used for selection including *LacZ*, and *HIS3*. *HIS3*, codes for the protein imidazoleglycerol-phosphate dehydratase, a key enzyme in histidine biosynthesis.

In order to create the desired constructs each gene of interest would have to be cloned into bait and prey vectors pDEST22 and pDEST32. This was done by designing primers to amplify each gene from their pGreen plasmid constructs previously generated in the study, with each sequence modified to contain Gateway entry sites. Gateway cloning was then carried out to clone each gene, into first an entry vector and then the destination prey and bait vectors. In order to maintain a higher confidence in any result, each gene was cloned into both bait and prey vectors with each combination tested both ways.

GAL4 is a modular protein and can be split into two halves, each containing one of the domains. pDEST22 contains the activation domain, with the target protein (X) forming an AD-X fusion, whilst pDEST32 contains the DNA binding domain with the second target protein (Y) containing forming a DB-Y fusion.

The two domains only need to be in close proximity to function, and do not have to bind directly. The interaction of the target proteins would bring the two domains close

enough for transcription of the reporter HIS3 gene, which would allow the yeast to grow in medium which lacked histidine.

In addition to containing one half of GAL4, each destination vector contained a selection gene of its own, TRP1 or LEU2 for pDEST22 and pDEST32 respectively which code for genes to synthesis tryptophan and leucine. This allowed for initial selection of transformed yeast *S. cerevisiae* on SD medium lacking these amino acids, and growth on media lacking in both amino acids would allow for the positive identification of successfully mated yeast.

Each plasmid containing the desired gene was transformed in haploid *S. cerevisiae* yeast strains, pDEST22 constructs were cloned into AH109 and pDEST32 was cloned into Y187. The yeast was mated and grown on selective media with interactions verified by the presence of growth on media lacking tryptophan, leucine and histidine. 3AT, an imidazole glycerol phosphate dehydrates was also added to reduce the possibility of any self-activation of HIS3.

As a positive control NF-YB2 and NF-YC2 were used and transformed into yeast along with the rubber related genes. NF-YB2 and NF-YC2 are two subunits of the transcription factor NF-Y which recognises the CCAAT box promoter and have been demonstrated to interact by yeast-2-hybrid as well as via a number of other methods (Calvenzani *et al* 2012).

3.7.2 No interactions could be verified by yeast-2-hybrid

Although each mating pair successfully grew on media lacking Leucine and Tryptophan, with yeast-2-hybrid, no interactions were found between any of the target genes (Figure 3.19) indicated by a lack of growth on both media Histidine. This was despite earlier confocal work indicating co-localisations between SRPP-HRT2 and HRT2-HevNogo. Interaction was detected however, between the positive NF-YB2 and NF-YC2 controls as indicated by the presence of growth on media lacking histidine. Each interaction was conducted in triplicate from 3 sets of transformed *S. cerevisiae* with no interactions seen in any plate.

Figure 3.19 (next page) **Yeast-2-Hybrid analysis**
There was no growth on both plates (1) SD –L/T/H or (2) SD –L/T/H+3AT except for the positive controls NF-YB2 and NF-YC2 which are circled in blue. There some degree of auto activation in column F (NF-YC2) which was seen on both plates (1) and (2).All colonies grew on plate (3) SD –L/T indicating that each yeast strain successfully mated.

Each gene was cloned into each destination vector and yeast strain and protein-protein interaction combinations are indicated by table (4)

Below the colonies which grew are scored according to the plate with red indicating no *S. cerevisiae* growth and green indicating growth of *S. cerevisiae*.

(1) –Leu/Trp/His (growth indicated protein-protein interaction)

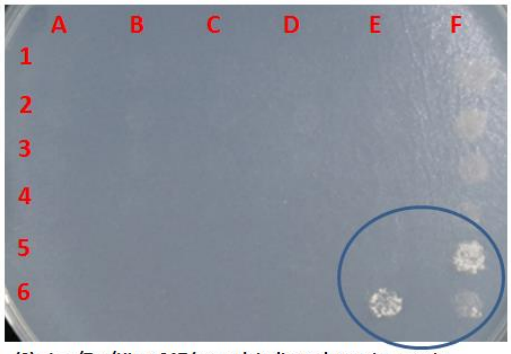

(2) –Leu/Trp/His + 3AT (growth indicated protein-protein interaction)

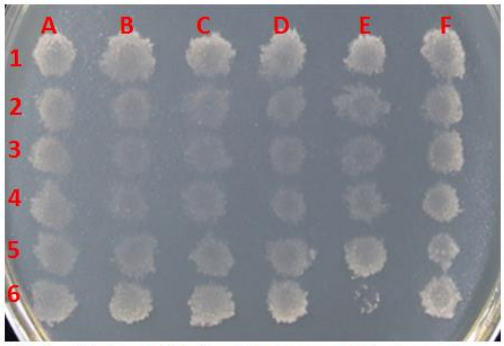

(3) –Leu/Trp (growth indicates the presence of both constructs

		pDEST22							
		A	B	C	D	E	F		
		HRT2	SRPP	REF	HevNogo	NF-B2	NF-YC2		
pDEST32	1 HRT2	1A	1B	1C	1D	1E	1F	HRT2 1	pDEST32
	2 SRPP	2A	2B	2C	2D	2E	2F	SRPP 2	
	3 REF	3A	3B	3C	3D	3E	3F	REF 3	
	4 HevNogo	4A	4B	4C	4D	4E	4F	HevNogo 4	
	5 NF-YB2	5A	5B	5C	5D	5E	5F	NF-YB2 5	
	6 NF-YC2	6A	6B	6C	6D	6E	6F	NF-YC2 6	
		HRT2	SRPP	REF	HevNogo	NF-B2	NF-YC2		
		A	B	C	D	E	F		
		pDEST22							

(4) Diagram representing each construct on the plates

[1] (-)Leu/Trp/His

		pDEST22							
		A	B	C	D	E	F		
		HRT2	SRPP	REF	HevNogo	NF-B2	NF-YC2		
pDEST32	1 HRT2	1A	1B	1C	1D	1E	1F	HRT2 1	pDEST32
	2 SRPP	2A	2B	2C	2D	2E	2F	SRPP 2	
	3 REF	3A	3B	3C	3D	3E	3F	REF 3	
	4 HevNogo	4A	4B	4C	4D	4E	4F	HevNogo 4	
	5 NF-YB2	5A	5B	5C	5D	5E	5F	NF-YB2 5	
	6 NF-YC2	6A	6B	6C	6D	6E	6F	NF-YC2 6	
		HRT2	SRPP	REF	HevNogo	NF-B2	NF-YC2		
		A	B	C	D	E	F		
		pDEST22							

[2] (-)Leu/Trp/His (+) 3AT

		pDEST22							
		A	B	C	D	E	F		
		HRT2	SRPP	REF	HevNogo	NF-B2	NF-YC2		
pDEST32	1 HRT2	1A	1B	1C	1D	1E	1F	HRT2 1	pDEST32
	2 SRPP	2A	2B	2C	2D	2E	2F	SRPP 2	
	3 REF	3A	3B	3C	3D	3E	3F	REF 3	
	4 HevNogo	4A	4B	4C	4D	4E	4F	HevNogo 4	
	5 NF-YB2	5A	5B	5C	5D	5E	5F	NF-YB2 5	
	6 NF-YC2	6A	6B	6C	6D	6E	6F	NF-YC2 6	
		HRT2	SRPP	REF	HevNogo	NF-B2	NF-YC2		
		A	B	C	D	E	F		
		pDEST22							

[3] (-)Leu/Trp

		pDEST22							
		A	B	C	D	E	F		
		HRT2	SRPP	REF	HevNogo	NF-B2	NF-YC2		
pDEST32	1 HRT2	1A	1B	1C	1D	1E	1F	HRT2 1	pDEST32
	2 SRPP	2A	2B	2C	2D	2E	2F	SRPP 2	
	3 REF	3A	3B	3C	3D	3E	3F	REF 3	
	4 HevNogo	4A	4B	4C	4D	4E	4F	HevNogo 4	
	5 NF-YB2	5A	5B	5C	5D	5E	5F	NF-YB2 5	
	6 NF-YC2	6A	6B	6C	6D	6E	6F	NF-YC2 6	
		HRT2	SRPP	REF	HevNogo	NF-B2	NF-YC2		
		A	B	C	D	E	F		
		pDEST22							

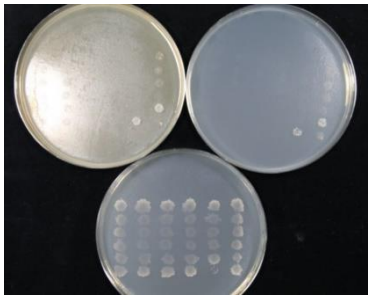

3.7.3 Yeast-2-Hybrid discussion

The lack of protein-protein interactions could be due to the fact that the proteins do not directly interact or it could be due to the limitations of the Yeast-2-Hybrid system. Yeast-2-Hybrid does have limitations although it was run as an exploratory screen. The absence of growth does not necessarily indicate that there are no interactions. This is especially true when taken in conjunction with confocal images. False positive and false negative results occur at a high rate for a number of reasons: *S. cerevisiae* can lack the ability to confer higher eukaryotic post-translational modifications, or does not contain appropriate chaperone proteins that would be present in plants; for proteins to be assayed they must be fused with the GAL4 domains. This fusion could affect proper folding or interaction between target proteins; the yeast-2-hybrid interaction takes place in the nucleus of the cell: interactions from proteins that do not localise to the nucleus would therefore be very hard to detect (Brückner *et al* 2009). No interactions were detected from the two cytosolic proteins HRT2 and RBSP. SRPP and REF are endoplasmic reticulum proteins as is HevNogo, although HevNogo's localisation was not ascertained at the time, and SRPP displayed some remnants of cytosolic localisation and is predicted to coat the membrane rather than be integral to it.

Homologs of HevNogo, TbRTA and NgBR have had interactions determined via yeast-2-hybrid (Harrison *et al* 2009, Epping *et al* 2015) despite their membrane localisations, so it was felt justified to run the assay. No interactions were detected from the two cytosolic proteins HRT2 and RBSP.

The yeast-2-hybrid assay was conducted as purely a screen. Despite the negative results, at least 2 sets of proteins co-localised from confocal data, especially HRT2 and HevNogo. It would have been possible to delete the known transmembrane region, TM1, from HevNogo to study the interaction between the cytosolic HRT2 and the cytosolic HevNogoΔTM1 mutant, which would have presumably localised to the nucleus in *S. cerevisiae*. However this would still be a low confidence result and the deletion of transmembrane domains could affect protein folding. Split ubiquitin assays could be a future test to determine interactions of membrane bound proteins.

Transient interactions or indirect interactions would not be picked up by Yeast-2-Hyrbid. Therefore interactions were tested with a higher confidence method, co-immunoprecipitation which does allow for testing in-direct interactions.

3.8 Protein-protein interactions by reverse co-immunoprecipitation

To test some of the co-localisations observed by confocal microscopy and co-expression of rubber related proteins, co-immunoprecipitation assays were used.

Interactions were tested between rubber particle proteins fused to GFP and its relatives CFP, EGFP and YFP, versus those with RFP –based fluorescent protein fusions which included RFP and mCherry. Constructs transformed into either *Agrobacterium* C58 or GV3101 strains were co-infiltrated into *N. benthamiana* leaf epidermal cells and tissue was harvested after 3 days.

The leaf tissue was lysed and an anti- GFP or RFP specific nanobody, bound to agarose beads, was used to bind to, and precipitate, the bait. The beads were centrifuged to separate them from the supernatant. If the bait protein formed a complex with a second partner, then the second partner would also be pulled down into the bead pellet. This could be detected by an RFP or GFP antibody specific to the second protein, using standard western blot (Figure 3.20). To increase confidence in any pull-downs the assay was performed in both ways, i.e. using each of the putative interacting proteins in turn as the bait.

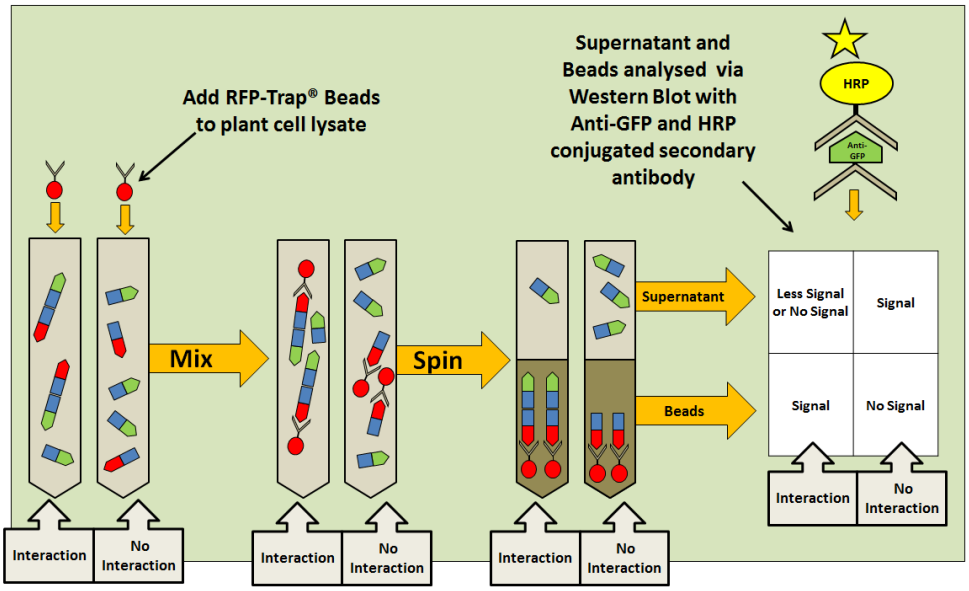

Figure 3.20 Co- immunoprecipitation

Plant extract is mixed with RFP-Trap® Beads, which are used as bait to pull RFP-tagged protein and any interactors down. The pellet (bead) fraction and supernatant are then analysed with an antibody specific to a potential binding partner, in this case anti-GFP. If the proteins interact then signal will be detected in the pellet. If the proteins do not interact then the partner will not be pulled down into the pellet fraction and will only be detectable in the supernatant. This example shows the use of RFP-Trap® and detection with anti-GFP. The reverse was also used in the experiment and proteins were pulled down with GFP-Trap® Beads and detected with anti-RFP.

3.8.1 HRT2 interacts with HevNogo, but HRT2-SRPP interaction was not observed

mCherry-HRT2 was co-infiltrated with GFP-SRPP, HevNogo-CFP and RBSP-GFP. Also co-infiltration with GFP-HDEL was used as a control. mCherry-HRT2 was successfully detected with anti-RFP in the bead pellet of the HRT2-HevNogo GFP-Trap® pulldown. HevNogo-CFP was also detected with anti-GFP in the bead fraction for the HRT-HevNogo pulldown using RFP-Trap® as bait (Figure 3.21a). Neither GFP-SRPP nor mCherry-HRT2 could be detected in the bead fractions for the HRT2-SRPP pulldown. No co-immunoprecipitation was detected between HRT2 and RBSP or HRT2 and GFP-HDEL.

3.8.2 REF displayed a weak interaction with SRPP

REF-mCherry was co-infiltrated with HRT2-YFP, GFP-SRPP and RBSP-GFP. Also co-infiltration with GFP-HDEL was used as a control. A small amount of REF-mCherry was detected via anti-RFP in the bead pellet of the REF-SRPP GFP-Trap® pulldown. A small amount of GFP-SRPP was also detected via anti-GFP in the reverse orientation using RFP-Trap® as bait (Figure 3.12b)

None of the proteins were pulled down by the opposite nanobody on their own and each protein could be detected in bead fraction after pull down with its own nanobody (Figure 2.21c and 2.21d).

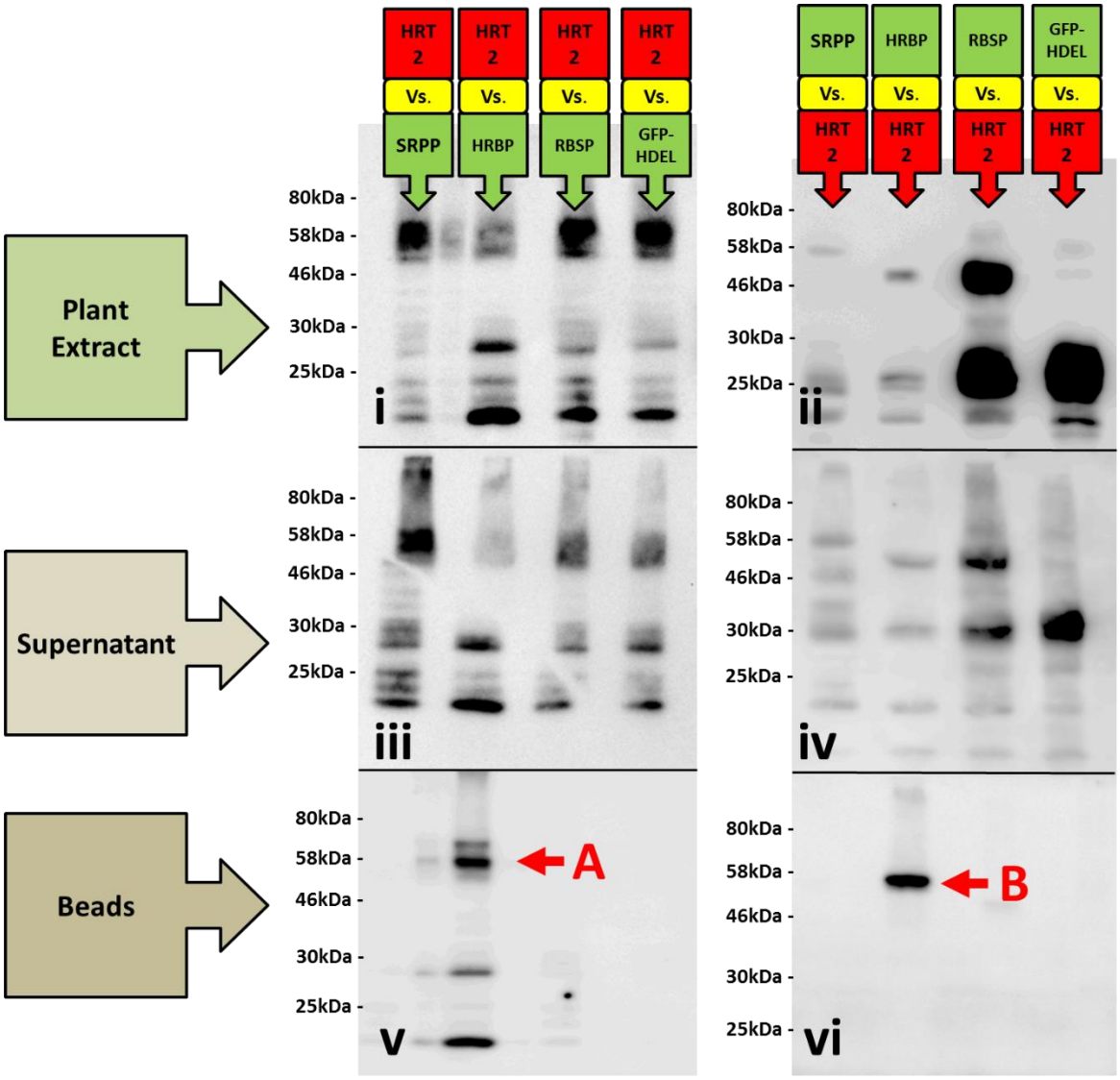

Figure 3.21a HevNogo interacts with HRT2: Co-immunoprecipitation of mCherry-HRT2 against GFP tagged proteins

(First Column) Pulldown by GFP-Trap, detection by anti-RFP. mCherry-HRT2 was detected by anti-RFP in all lanes, in both the plant extract (i) and supernatant fractions (iii). mCherry-HRT2 interacted with HevNogo-CFP and was therefore pulled down by HevNogo and was detected in the bead fraction by anti-RFP (A).

(Second Column) Pulldown by RFP-Trap, detection by anti-GFP. GFP derived fusion proteins, GFP-SPP, HevNogo-CFP, RBSP-GFP and GFP-HDEL were detected by anti-GFP in both the plant extract (ii) and supernatant (iv) fractions. Only HevNogo-CFP was detected in the bead fraction (B) demonstrating its interaction with HRT2.

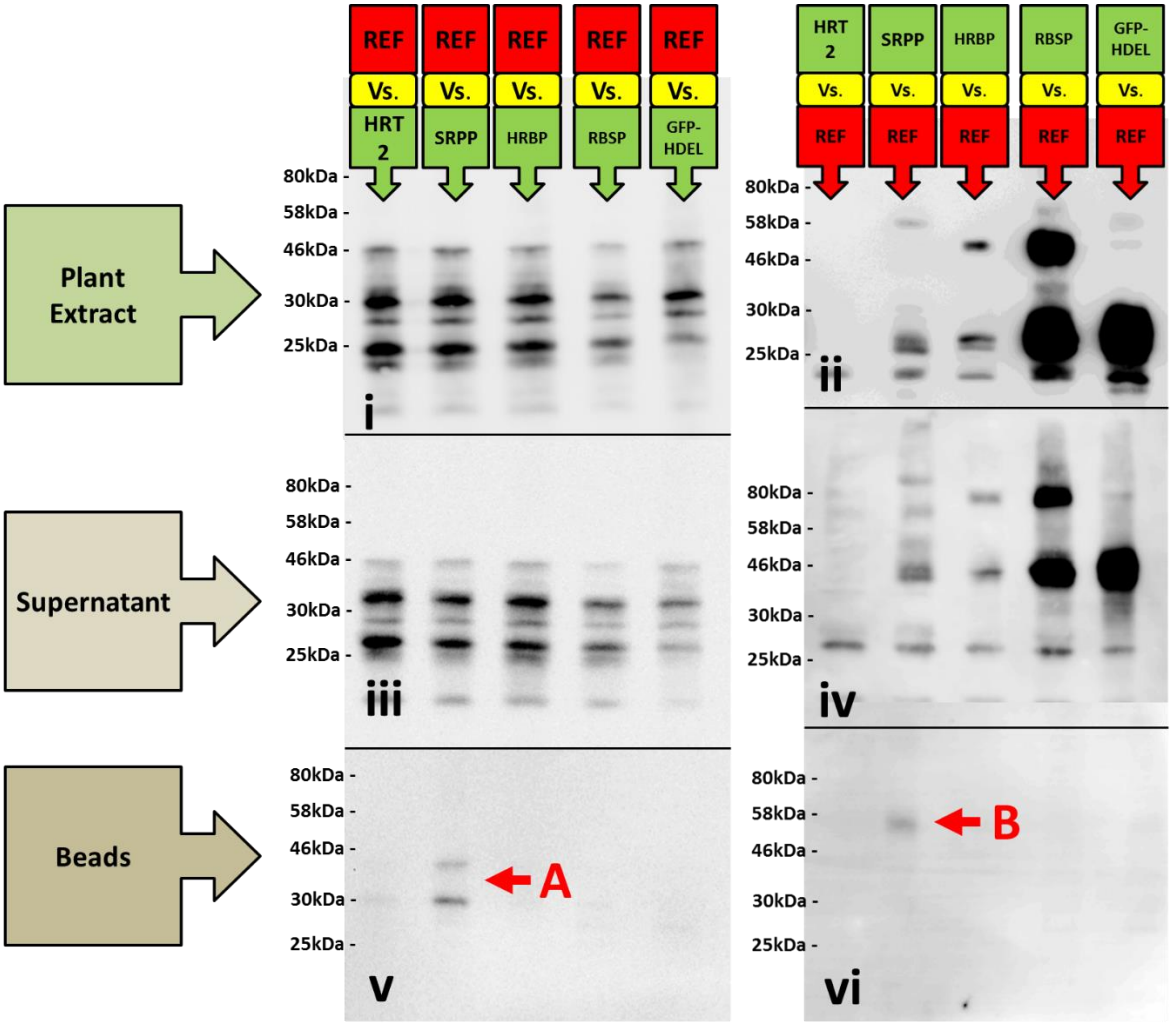

Figure 3.21b REF has a weak interaction with SRPP: Co-immunoprecipitation of REF-mCherry against GFP tagged proteins

(First Column) Pulldown by GFP-Trap, detection by anti-RFP. REF-mCherry was detected by anti-rfp in all lanes, in both the plant extract (i) and supernatant fractions (iii). REF-mCherry interacted with GFP-SRPP and was therefore pulled down by HevNogo and was detected as a weak band in the bead fraction by anti-RFP (A).

(Second Column) Pulldown by RFP-Trap, detection by anti-GFP. GFP-derived fusion proteins, HRT2-YFP, GFP-SPP, HevNogo-CFP, RBSP-GFP and GFP-HDEL were detected by anti-GFP in both the plant extract (ii) and supernatant (iv) fractions although HRT2-YFP levels were low. Only GFP-SRPP was detected in the bead fraction (B) as a weak band, indicating it has a weak interaction with REF.

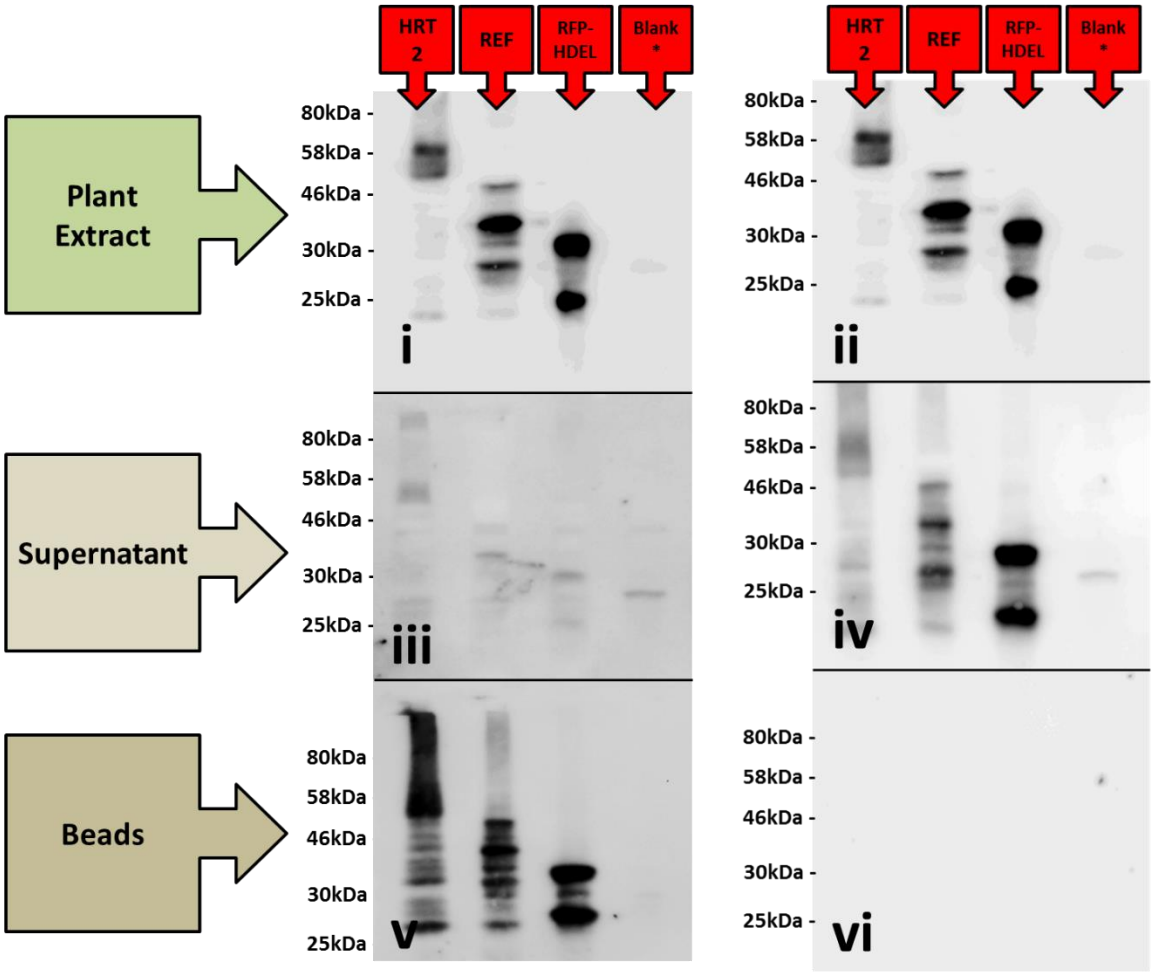

Figure 3.21c Single RFP-tagged protein controls for co-immunoprecipitation
(First Column) Pulldown by GFP-Trap, detection by anti-RFP. (Second Column) Pulldown by RFP-Trap, detection by anti-GFP. RFP tagged proteins singles: mCherry-HRT2, REF-mCherry, RFP-HDEL and blank* are detected in the plant extract (i/ii) and supernatant. There is significantly less protein in the RFP-Trap supernatant (ii) than GFP-Trap® supernatant (iii) as the protein has been pulled down and is detected in the bead fraction for RFP-Trap® (iv) No protein could be detected in the GFP-Trap® bead fraction (v) as GFP-Trap® does not pull down RFP tagged proteins.

*Blank = Leaf sector infiltrated with infiltration media only

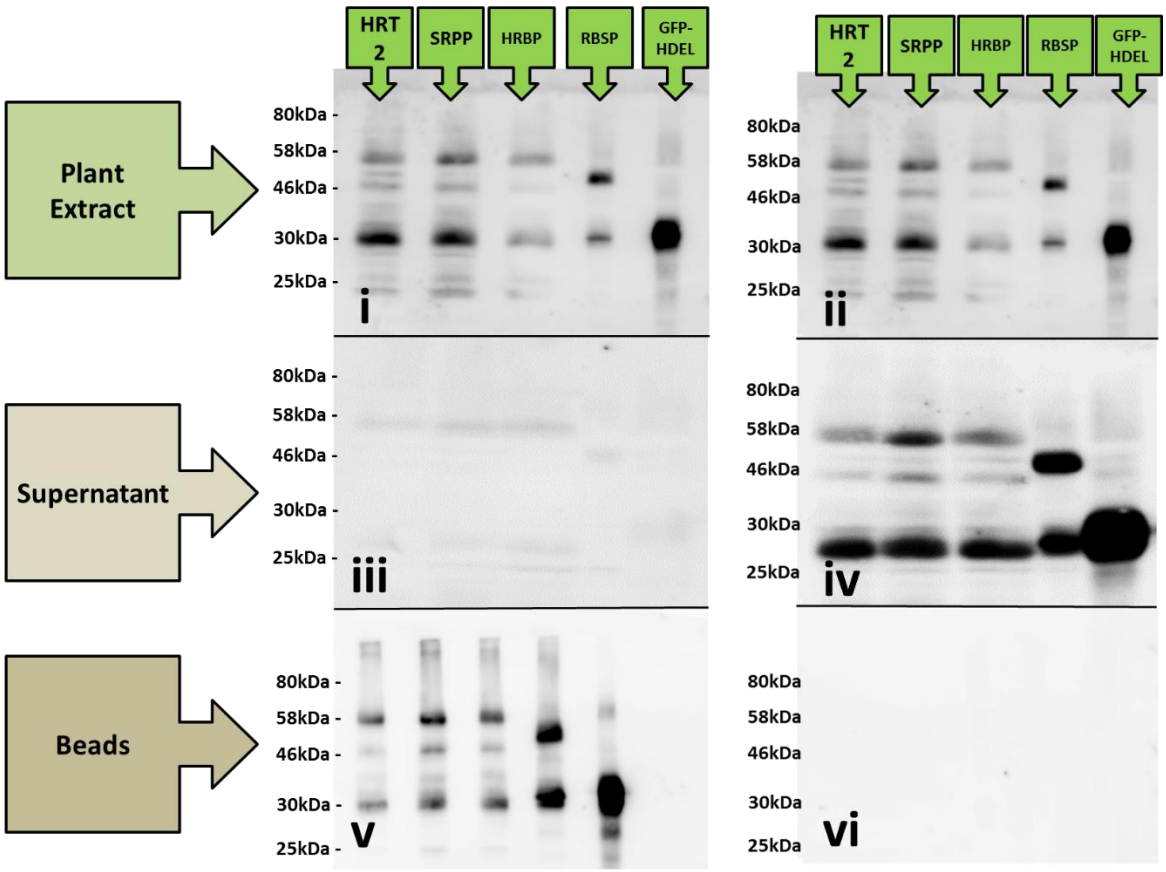

Figure 3.21d Single GFP-tagged protein controls for co-immunoprecipitation
(First Column) Pulldown by GFP-Trap, detection by anti-RFP. (Second Column) Pulldown by RFP-Trap, detection by anti-GFP. GFP tagged proteins singles: HRT2-YFP, GFP-SRPP, HevNogo-CFP, RBSP-GFP and GFP-HDEL are detected in the plant extract (i/ii) and supernatant by anti-GFP. There is significantly less protein in the GFP-Trap supernatant (iii) than RFP-Trap® supernatant (iv) as the protein has been pulled down and is detected in the bead fraction for GFP-Trap (v) No protein could be detected in the RFP-Trap® bead fraction (vi) as RFP-Trap® does not pull down GFP tagged proteins.

3.8.3 Discussion of protein interaction

From the confocal data (chapter 3, sections 3.5 and 3.6), two protein-protein interactions were proposed. HRT2 interacting with HevNogo, and HRT2 interacting with SRPP. Yeast-2-Hybrid results were negative for all interactors, though this may have been due to the intrinsic limitations of the system. One of these interactions, between HRT2 and HevNogo, could be observed via co-immunoprecipitation, but HRT2 and SRPP was not. However a weak interaction was detected between SRPP and REF.

The HRT2-HevNogo interaction was a strong interaction with a significant amount of protein pulled down in each assay. This is in accordance with confocal data and suggests that these proteins form a strong complex.

3.8 Transient expression in *L. sativa*: problems and future outlook

In the latter stages of this project HevNogo and RBSP were successfully expressed in *L. sativa* leaf epidermal cells via *Agrobacterium*-mediated transient expression. Whilst the work was not completed, due to time constraints, it will be mentioned briefly here as it offers a platform for future research.

Rubber related proteins transformed into *Agrobacterium* C58 cells were infiltrated into the leaves of *L. sativa* at various OD_{600} values and imaged after 3-6 days, the constructs were simultaneous infiltrated into *N. benthamiana* leaf cells to confirm their viability. However infiltration with low OD_{600} values of cell culture, between 0.01 and 0.1, resulted in no detectable expression. Anything higher than 0.1 resulted in visible necrosis of the infiltrated leaf tissue within 2 days, and as a result, no protein expression. Constructs were also co-infiltrated with p19 protein, a suppressor of gene silencing (Voinnet *et al* 2003) however this had no effect on expression levels.

However high levels of expression were detected with both the GFP-HDEL and YFP-Calnexin ER marker constructs transformed into *Agrobacterium* GV3101 cells. Also

high levels of expression were detected with RBSP-EGFP and an mRFP1-HevNogo construct, also in GV3101 cells (Figure 3.22). Although other constructs and interactions were not tested, this work provides the basis for future work investigating these proteins.

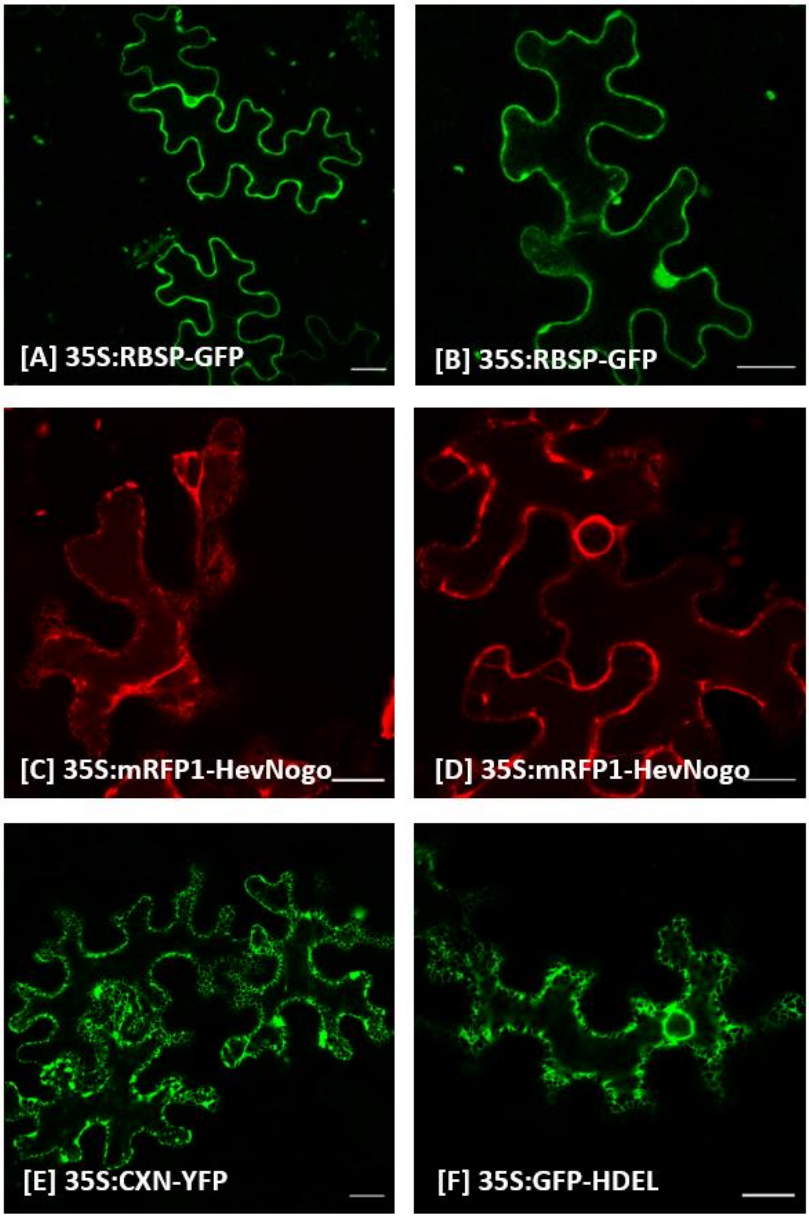

Figure 3.22 Transient expression in *L. sativa* leaf epidermal cells
[A and B] Overview of leaf epidermal cells transformed with RBSP (green) showing cytosolic localisation with a diffuse pattern and signal inside the nucleoplasm.

[C and D] Overview of cells leaf epidermal cells transformed with HevNogo (red) displaying an endoplasmic reticulum localisation with fine network pattern visible in (C) and the nuclear membrane in (D)

[E and F] Overview of leaf epidermal cells transformed with (E) Calnexin (green) and (F) GFP-HDEL (green) with signal from the endoplasmic reticulum

Chapter 4: Recombinant rubber particle protein purification

4.1 Introduction

The aim of this part of the project is to synthesise and purify recombinant rubber biosynthesis associated proteins. Purified proteins were to be used in IPP incorporation assays and also into rubber particle association assays. The proteins chosen for synthesis were HRT2, SRPP, REF and HevNogo. Whilst SRPP and REF were produced and purified in sufficient quantities, HRT2 and HevNogo were not. This was despite many attempts at troubleshooting and optimisation of expression. As HRT2 in particular was key to any assay, this section of the research was not successful, however some lessons can be learned and further purification efforts can be made in any future research.

Previously, infiltration and confocal work in *N. benthamiana* leaves demonstrated the cell localisations of rubber-associated proteins and also that there was a possible interaction between HRT2 and SRPP. SRPP seemed to bring HRT2 to the endoplasmic reticulum. The nature of the system used was a limitation, so rubber particle association assays were proposed as a possible method to study these proteins on rubber particles themselves. Berthelot *et al* (2014a) were able to use recombinant SRPP and REF and study their interactions on model membranes via PM-IRRAS analysis, so there was a precedent for using recombinant protein in this type of experiment.

4.2 Cloning and protein expression system

Sequences for the rubber related proteins were amplified from the appropriate constructs generated in the previous chapter (section 3.2). HRT2YFP was amplified from 35S:HRT2-YFP, GFPSRPP was amplified from 35S:GFP-SRPP, and REF-mCherry was amplified from 35S:REF-mCherry.

The sequences were modified to contain appropriate restriction sites at the C and N terminus. These were used to clone into a pTXB1 *E. coli* expression vector (NEB^{TM} IMPACT^{TM}), downstream of a T7 promoter and *lac* operon, and upstream of a self-cleavable intein tag, and chitin binding domain (CBD). The CBD is an affinity tag for chitin and allows the synthesised fusion protein product to bind to chitin beads prior to

cleavage and purification. The rubber related genes were cloned both with their fluorescent fusion tags in the case of HRT2-YFP, GFP-SRPP and REF-mCherry, and also single, non-XFP - tagged proteins in the case of HRT2 and HevNogo. Amyc c tag was added at the C termini of the last two proteins to allow for detection and verification of the purified protein via western blot (Figure 4.1).

The pTXB1 protein expression system is IPTG inducible. IPTG is a synthetic mimic of allolactose which, when added to the growth media at an appropriate stage, will allow transcription of the target gene.

Protein splicing involves the removal of a specific protein segment, which is known as the intein (INTervening protEIN). First the intein contained within the precursor protein is cleaved at its N terminus. Normally the process would continue and the intein would also be cleaved at its C' terminus then the two flanking sequences (exteins) would be joined together by a new peptide bond (Wang *et al* 2008).

Only the first step is exploited in this purification system, which cleaves the target protein from the N terminus of the intein, leaving the intein attached to the CDB on the chitin beads within the purification column. In the PTXB1 vector, modification at the C terminus of the intein tag prevents the C' terminal cleavage meaning that, in theory, only the target protein is eluted off the column (Xu *et al* 1996).

Once the target protein-CBD fusion binds to the chitin beads on the column, thiol induced cleavage of the intein region removes the target protein from the CBD with cleavage occurring exactly at the C' terminus of the target protein, allowing subsequent elution and purification.

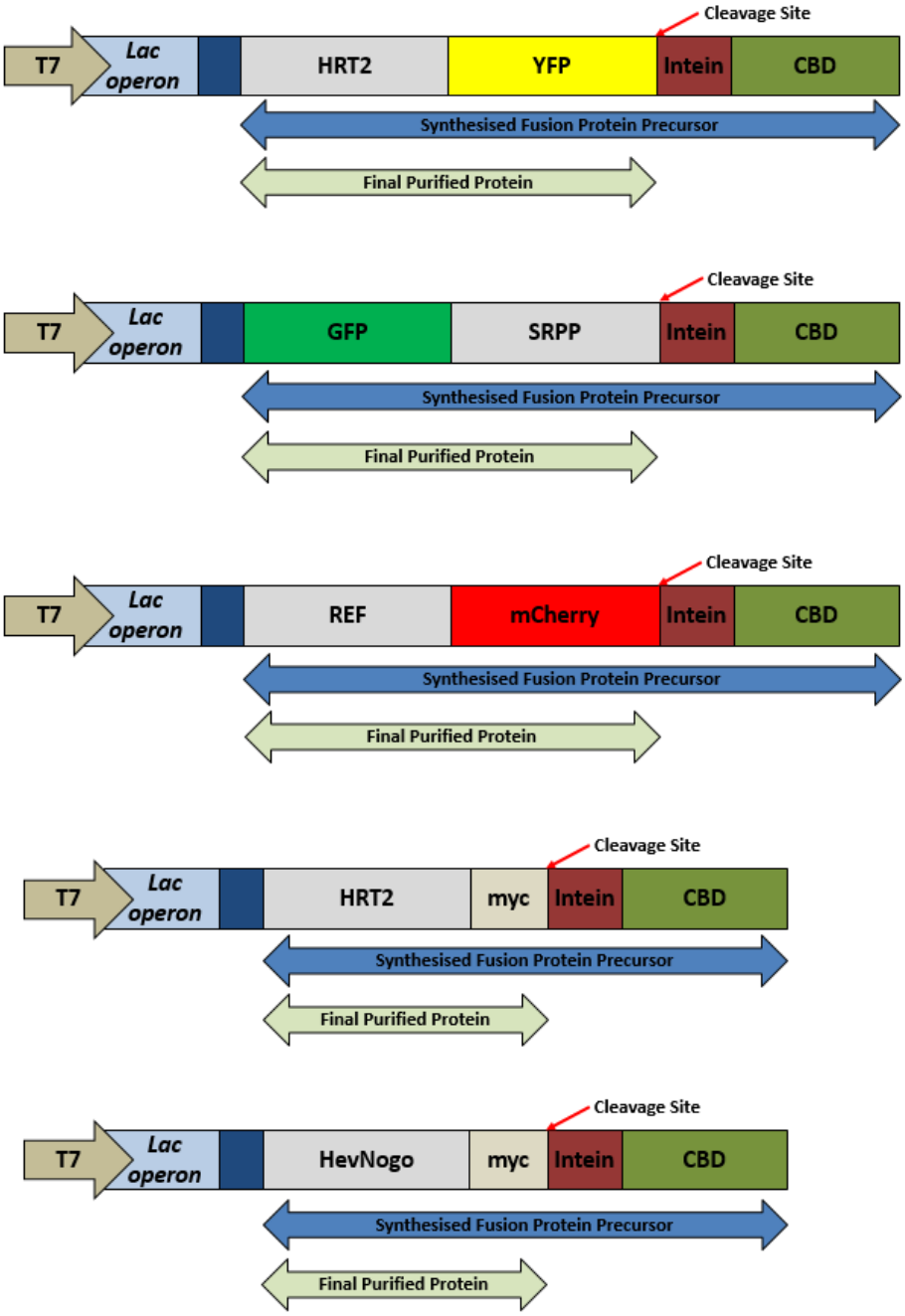

Figure 4.1 Constructs used for purification of recombinant rubber associated protein
All constructs were generated during this project and cloned in frame with a thiol-induced cleavable intein tag and chitin binding domain (CBD). The initial protein precursor and final post cleavage product are indicated with arrows below each construct.

4.3 Purification of HRT2-YFP, GFP-SRPP and REF-mCherry for rubber particle association assays

The idea was to produce recombinant fluorescent protein fusions of HRT2, SRPP and REF, and attempt to localise them to rubber particles. In particular the question that would have been asked is, would GFP-SRPP bring HRT2-YFP to rubber particles in the same way that it appeared to relocate it to the ER in *N. benthamiana*? The majority of this work took place, and was abandoned prior to the Epping *et al* (2015) paper on TbRTA, and the subsequent cloning and characterisation of HevNogo. As a result HevNogo is not included here. GFP-SRPP and REF-mCherry were able to be purified in large amounts, although HRT2-YFP was not, as this limited the value of any assays the decision was taken to finish the work on rubber particle association assays.

4.3.1 IPTG induction and solubilisation of rubber associated proteins

PTXB1 vectors containing the rubber associated protein constructs T7:HRT2-YFP-CBD, T7:GFP-SRPP-CBD and T7:REF-mCherry-CBD, were transformed into competent 'T7 Express' *E. coli* ER2566 cells. These were inoculated and grown according the methods section 2.3 and 2.6 (Figure 4.2). IPTG was used to induce protein expression which was then analysed using SDS-PAGE and coomassie staining (Figure 4.3a). GFP-SRPP-CBD and REF-mCherry-CBD were produced and were visible on a coomassie stain before confirmation by Western Blotting (Figure 4.3b). However significantly less HRT2-YFP-CBD was produced and this required further optimisation and Western Blotting with the use of commercial antibodies against the CBD tag to detect any recombinant protein (Figure 4.3c). Each of the cell cultures were lysed and centrifuged to separate soluble and insoluble fractions, and only soluble protein was suitable to load onto the purification column. HRT-YFP-CBD was soluble and required no further optimisation on this point although levels of protein remained very low. GFP-SRPP-CBD and REF-mCherry-CBD however were present only in the insoluble fraction as inclusion bodies. Different lysis buffers and incubation conditions were unsuccessful in generating soluble protein so a protocol for solubilisation of protein aggregates was adapted from the NEB Impact Kit Manual. 7M guanidine solution and

then subsequent dialysis against decreasing concentrations of urea was used to break apart and refold these aggregates into soluble protein (Figure 4.4).

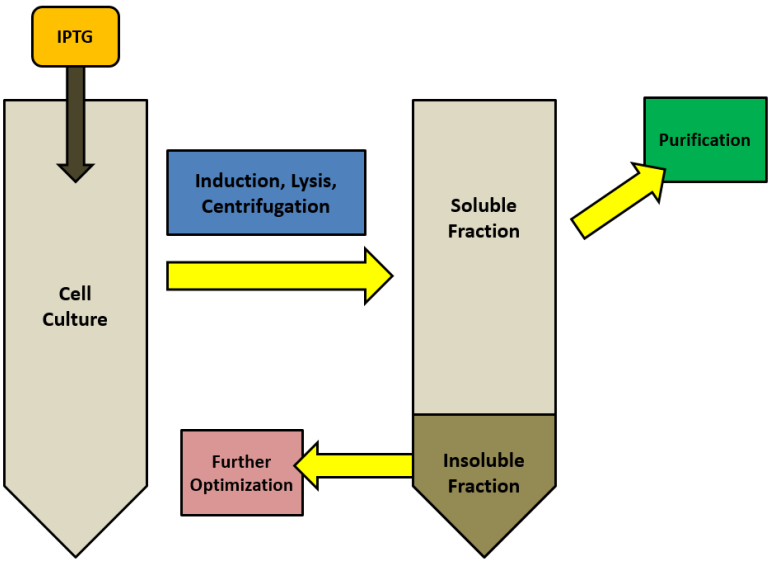

Figure 4.2 IPTG induction and separation in soluble and insoluble fractions
IPTG is added to the cell culture to induce protein synthesis. The cells are lysed to release protein before centrifuge to separate into soluble and insoluble fractions. Soluble protein can be loaded onto the AKTA for purification whereas insoluble protein must undergo further optimisation or refolding to be made soluble.

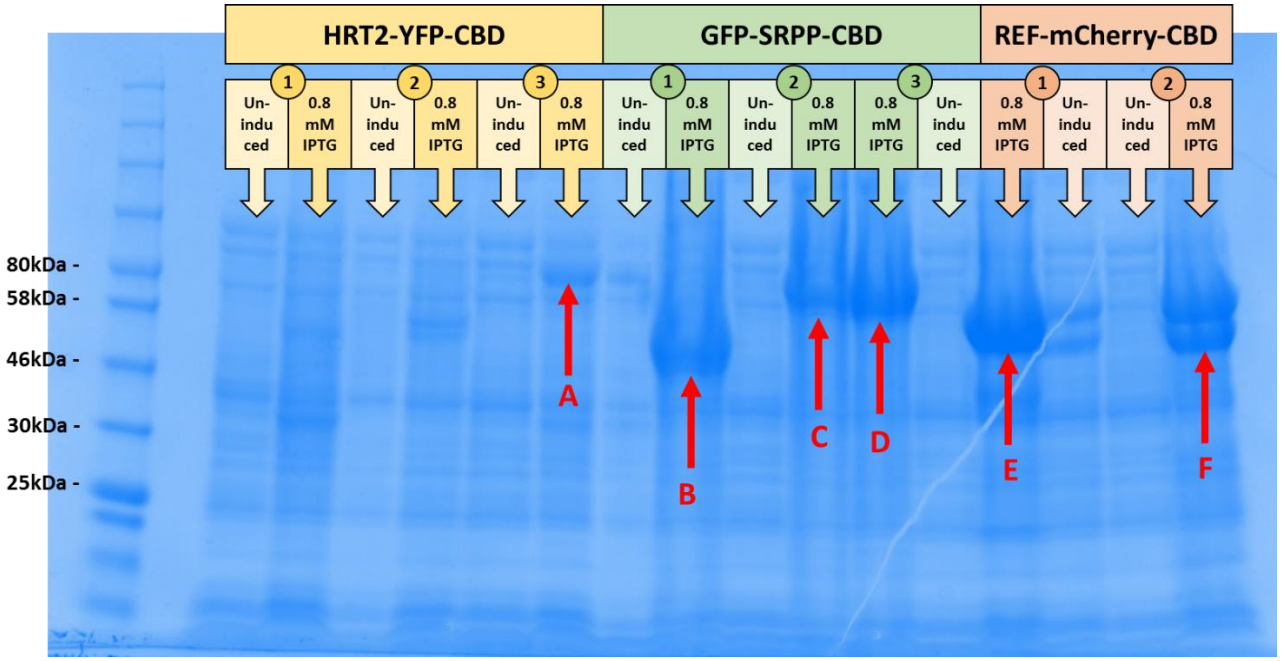

Figure 4.3a IPTG induction of HRT2-YFP-CBD, GFP-SRPP-CBD and REF-mCherry-CBD
Cultures were grown at 37°C until an OD^{600} value of ~0.5, before the addition of 0.8mM IPTG

Samples of induced culture (0.8mM IPTG, 37°C for 2 hours) were taken and analysed via SDS-PAGE and coomassie staining. Un-induced samples before the addition of IPTG were also taken as a control. Three colonies were analysed for HRT2, SRPP and two colonies analysed for REF.

[A] Possible band for HRT2-YFP-CBD (3) though this was not confirmed by western blot and was not repeated. [B] Strong band for GFP-SRPP-CBD though lower than expected, most likely caused by cleaved product. [C and D] Strong bands at the correct size for GFP-SRPP-CBD later verified by western blot. [E and F] Strong bands for REF-mCherry-CBD later verified by western blot, though band F shows size of cleavage. Cultures from bands C and E were taken forward for purification.

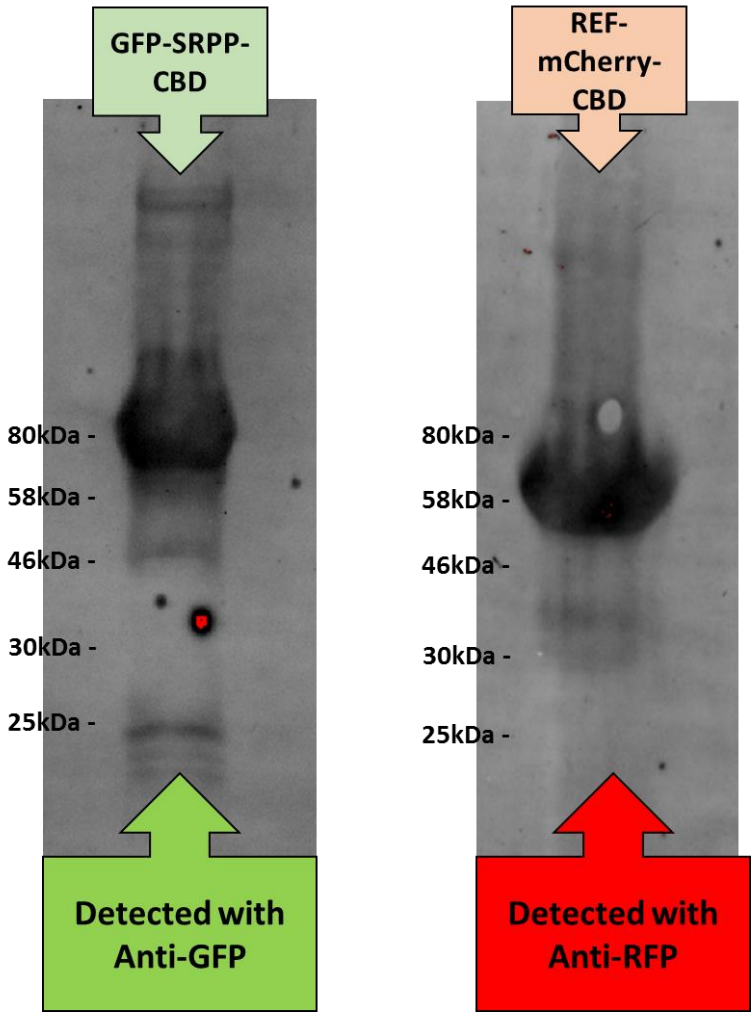

Figure 4.3b Western blot of GFPSRPP-CBD and REFmCherry-CBD IPTG inductions

Sample of inoculated culture after IPTG induction, was taken and analysed by SDS-PAGE and Western Blot. GFPSRPP-CBD was detected using anti-GFP and REF-mCherry was detected using anti-RFP

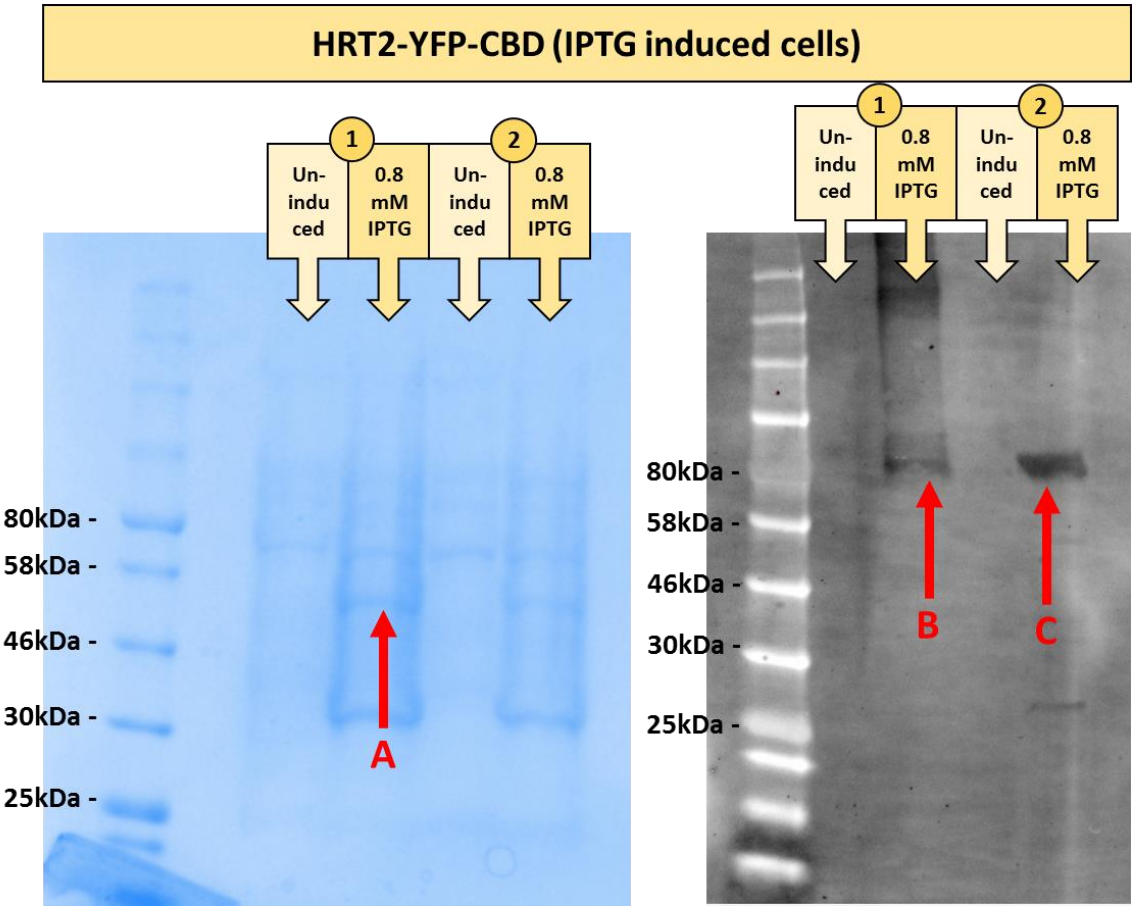

Figure 4.3c IPTG induction of HRT2-YFP-CBD, with Western Blot to detect protein
Cultures were grown at 37°C until an OD^{600} value of ~0.5, before the addition of 0.8mM IPTG. Samples were analysed via SDS-PAGE with coomassie stain and western blot using anti-CBD antibody. Samples were taken after induction (0.8mM IPTG, 37°C for 3 hours) and un-induced samples were taken as a control.

[A] Lower bands detected from coomassie stain but no corresponding bands from a western blot, this may be cleaved product. [B and C] HRT2-YFP-CBD detected using anti-CBD at around 90kDA, expected band size was 87kDA

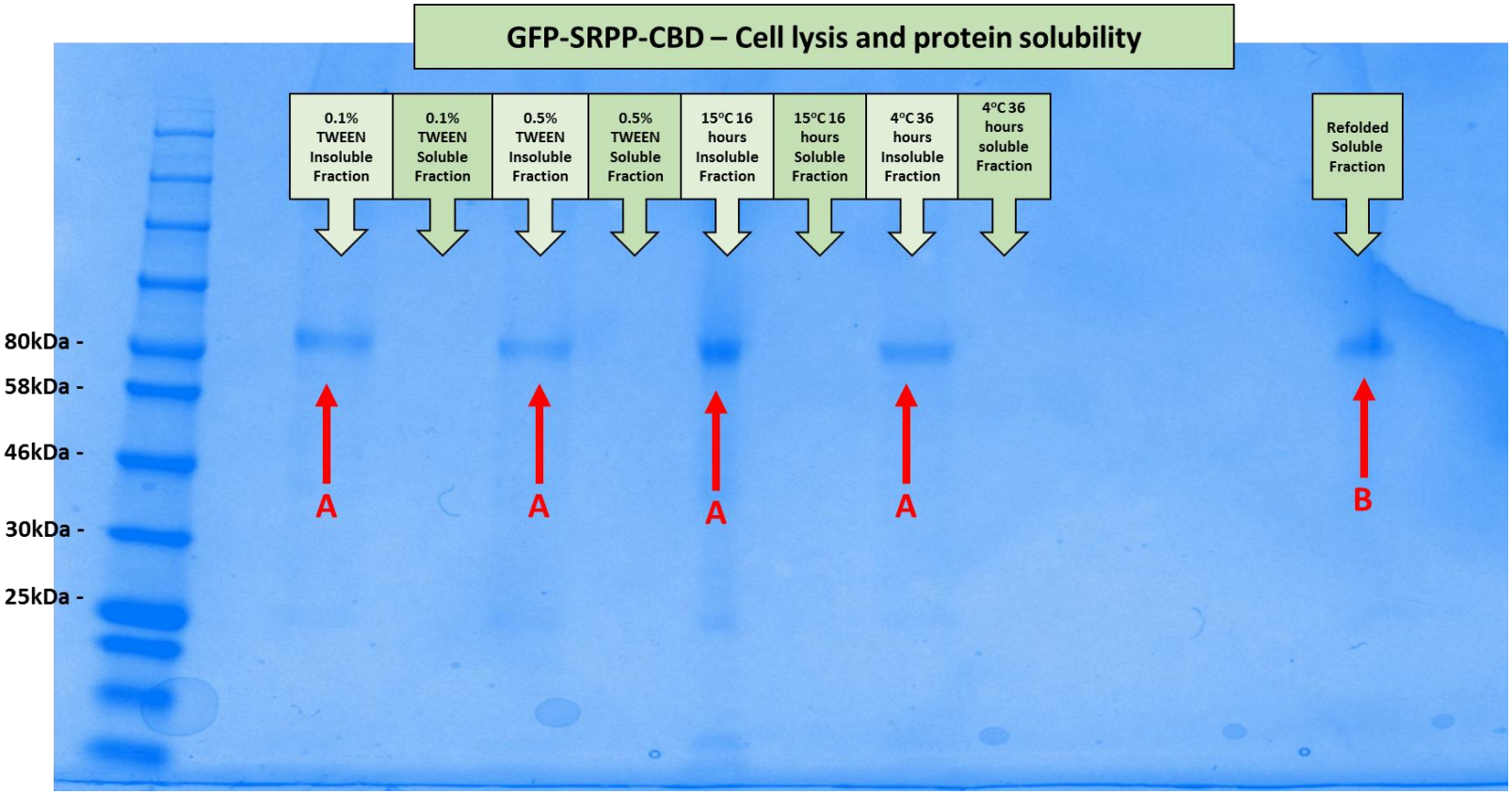

Figure 4.4a Cell lysis and solubilising GFP-SRPP-CBD: A selection of techniques and protein refolding
Coomassie stain of insoluble and insoluble fractions of GFP-SRPP-CBD protein from different lysis buffer and growth conditions. Bands [A] are only present in the insoluble fraction so the protein was refolded and made soluble as can be seen in band [B].

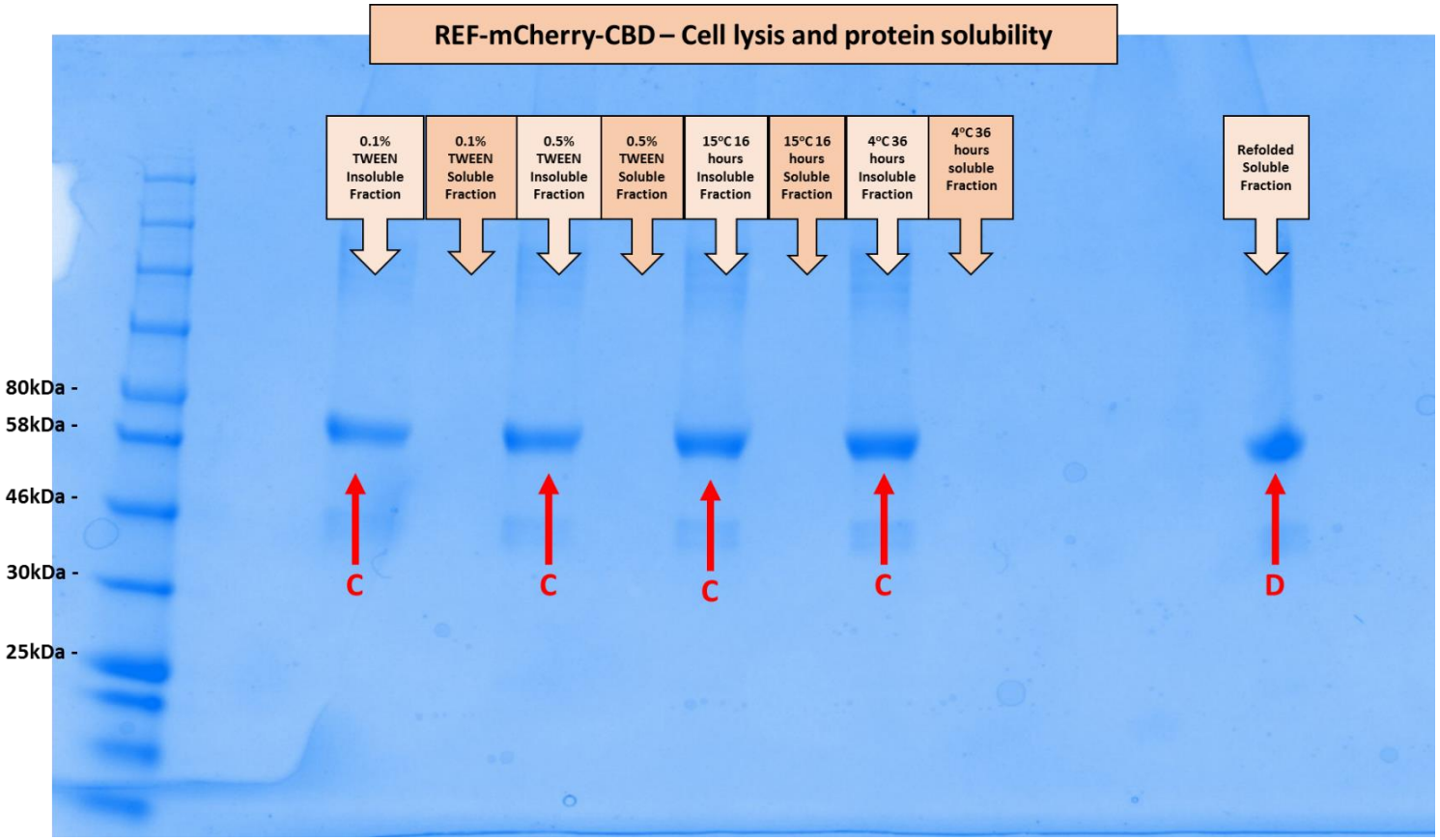

Figure 4.4b Cell lysis and solubilising REF-mCherry-CBD: A selection of techniques and protein refolding
Coomassie stain of insoluble and insoluble fractions of REF-mCherry-CBD protein from different lysis buffer and growth conditions. Bands [C] are only present in the insoluble fraction so the protein was refolded and made soluble as can be seen in band [D].

4.3.2 Thiol mediated cleavage and elution of rubber associated protein

Soluble fractions of HRT2-YFP-CBD, GFP-SRPP-CBD and REF-mCherry-CBD were each loaded onto a purification column packed with chitin beads as detailed in methods section 2.6. The CBD was bound to the chitin beads and the remaining unbound non-targeted *E. coli* protein was washed through the column into waste collection. 50mM DTT was added to induce cleavage separating the target rubber associate protein from the CBD tag (Figure 4.5). HRT2-YFP, GFP-SRPP and REF-mCherry recombinant proteins were then eluted from the column, collected, dialysed and concentrated for further use.

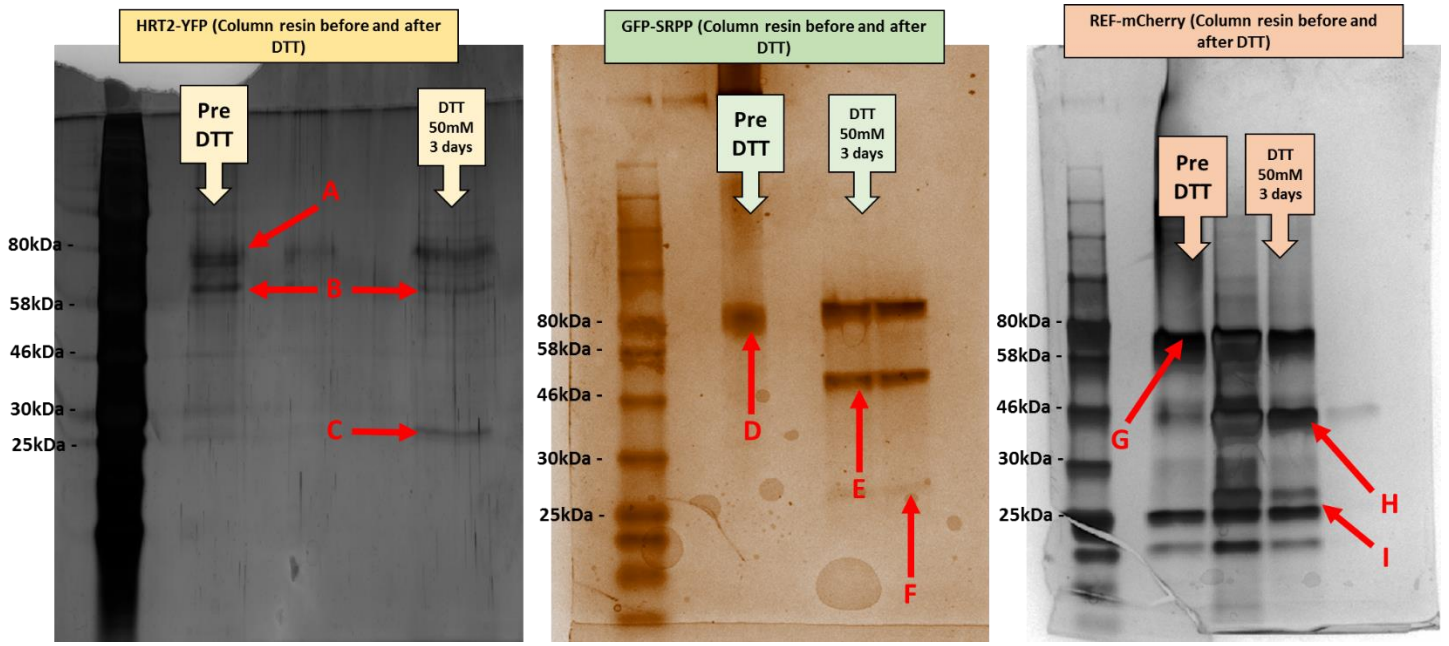

Figure 4.5 Silver stains of recombinant protein pre and post DDT cleavage

Soluble protein was loaded onto a chitin column. A sample of protein/ chitin beads was taken before the addition of DTT and boiled in SDS-buffer to release the protein. 50 mM of DTT was added to the column with cleavage taking place over three days. A second sample was taken after three days to check for cleavage of the target protein before elution.

[A] Precursor HRT2-YFP-CBD. [B] Cleaved HRT2-YFP though this was present pre and post DTT and may be a contaminant. [C] Cleaved CBD tag.

[D] Precursor GFP-SRPP-CBD. [E] Cleaved GFP-SRPP. [F] Cleaved CBD tag.

4.3.3 Protein yields

GFP-SRPP and REF-mCherry were purified, concentrated and re-suspended in TBS (pH7.5) a nanodrop was used to measure absorbance at 280nm with concentrations measured at approximately 9 mg/ml (SRPP) and 14 mg/ml (REF). The eluted protein was able to be visualised using a stereoscope (Figure 4.6), HRT2-YFP was barely detectable on a silver stain or western blot and the YFP could not be visualised, it was also undetectable using either a nanodrop or Bradford assay. Various methods of optimization were undertaken including different induction temperatures, cell strains and choice of antibiotics. However the expression levels of HRT2-YFP did not improve.

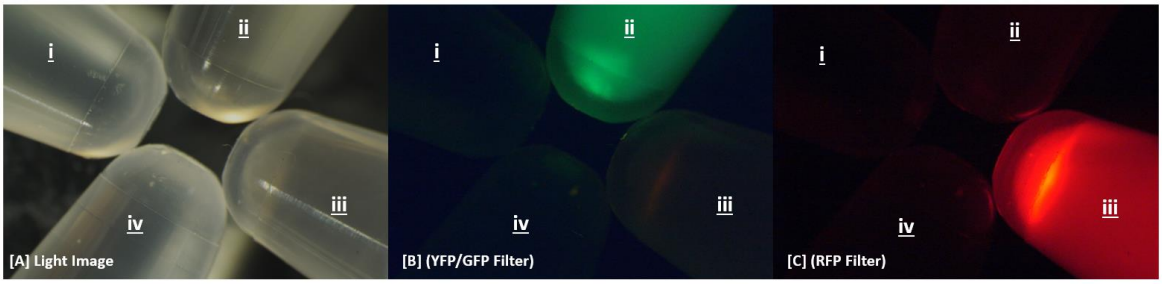

Figure 4.6 Fluorescence of purified protein under a stereoscope

Concentrated recombinant protein samples in 1.5 ml Eppendorf tubes were visualised under a stereoscope with light image [A] using a standard light, and fluorescence [B and C] detected using a mercury lamp with appropriate filter.

[i] HRT2-YFP displayed no fluorescence. [ii] GFP-SRPP fluoresced strongly under a YFP/GFP filter and [iii] REFmCherry fluoresced under an RFP filter. [iv] Blank control of TBS.

4.4 Purification of HRT2myc and HevNogomyc for phosphorylase assays

The rubber particle association assays were not pursued but the experience gained was used to attempt to clone HRT2-myc and HevNogo-myc. This was for phosphorylase assays to measure IPP incorporation. However, as before, and despite optimisation and troubleshooting attempts HRT2-myc could not be produced in significant amounts. It may be that a different expression system is required for efficient purification of HRT2. A new problem with self-splicing arose in the purification of HevNogo-myc a way around this by mutating the intein tag itself was attempted. However this led to very low yields of protein that could be obtained.

4.4.1 A mutation in the intein tag helps prevent in-vivo cleavage of HevNogo-myc-CBD, but inhibits effective cleavage in-column

HevNogo-myc-CBD was transformed into a variety of *E. coli* protein expression cell strains (Figure 4.7a). C43 and C41strains with a Rosetta helper plasmid showed promising bands which were further analysed via western blot (Figure 4.7b). The bands however had significantly lower electrophoretic mobility than expected and were around the same size as the cleaved protein. *In vivo* cleavage between the target protein and the intein/CBD tag can result in loss of yield and can be a common drawback using the intein system (Cui *et al* 2006).

The first residue of an intein sequence is a cysteine. Cui *et al* (2006) reports that *in vivo* cleavage can be a result of the free sulfhydryl group of this cysteine attacking the upstream peptide bond, between the target protein and intein tag. This can occur independently of the addition of thiol. Cui *et al* (2006) proposed a modification to the intein tag found in PTXB1 in which the third residue, a threonine, is substituted for a cysteine (T3C mutation) which will also contain a free sulfhydryl group. This results in the free sulfhydryl group of T3C forming a disulphide bond with the free sulfhydryl group of the first cysteine residue. As the first sulfhydryl group is no longer free it cannot cause in-vivo cleavage. The addition of DTT should reduce this disulphide bond thereby allowing on column cleavage to occur as normal.

A substitution in the intein tag of HevNogo-myc-CBD was made, creating HevNogo-myc-CBD(T3C). This was expressed in the same C43 *E. coli* cells, with protein expression induced by IPTG. Although the protein size as detected by western blot was at expected level for full length protein, the addition of DTT did not result in cleavage as expected (Figure 4.7b). Even after increasing the concentration of DTT to 100mM with a 10 day incubation, only a small fraction of purified HevNogo was able to be eluted from the column (Figure 4.8).

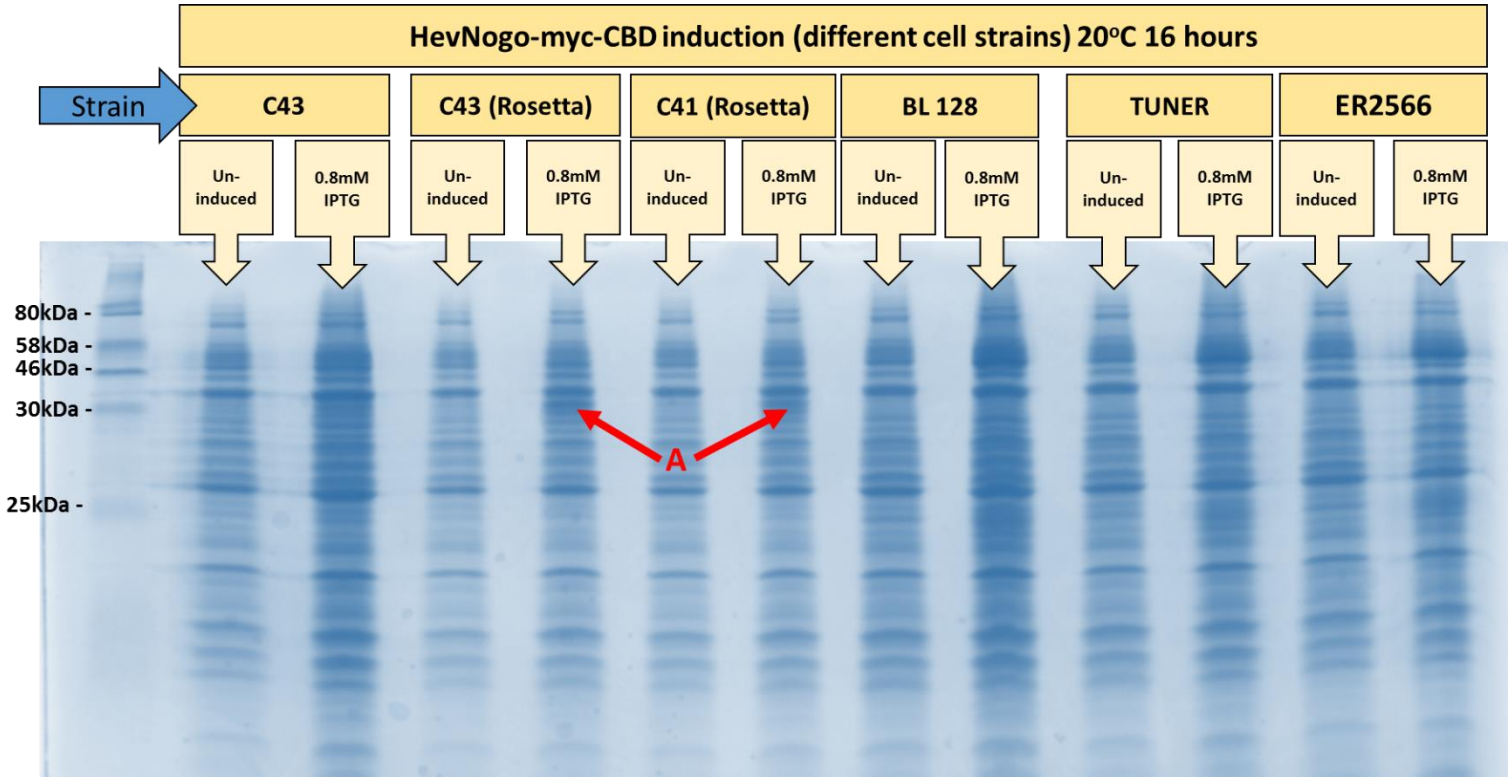

Figure 4.7a IPTG induction of HevNogo-myc-CBD with different *E. coli* host strains

Cells were grown at 37°C until an OD_{600} value of 0.5 with a sample was taken before induction. 0.8 mM IPTG was added, with protein induction carried out at 20°C overnight. There was no significant difference between non-induced and induced samples although a thicker band (A) could be observed in C43 (Rosetta) and C41 (Rosetta) *E. coli* cell strains

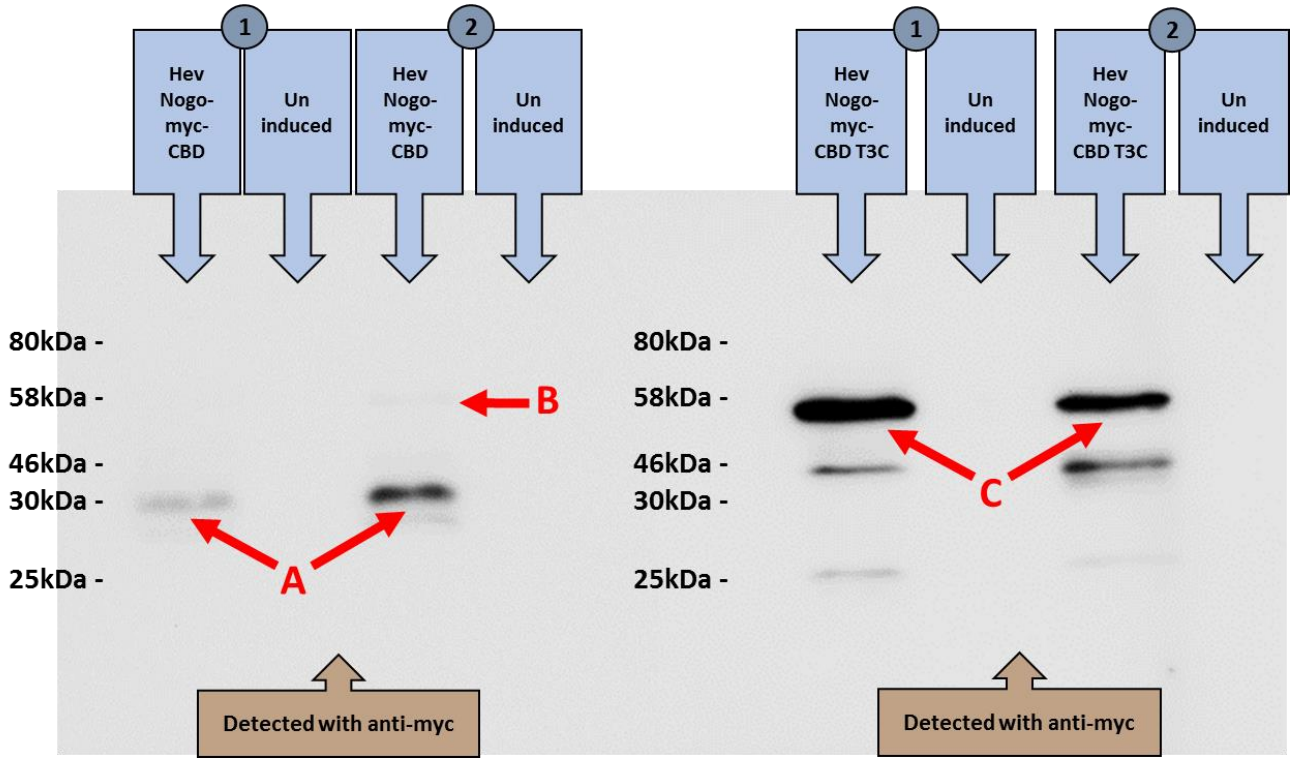

Figure 4.7b Comparison of HevNogo-myc-CBD with HevNogo-myc-CBD(T3C)
Sample of induced *E. coli* transformed with either HevNogo-myc-CBD or HevNogo-myc-CBD(T3C) were analysed using Western blot with anti-myc and anti-mouse-HRP primary and secondary antibodies. The bands for Wild Type HevNogo-myc-CBD (A) were significantly lower than expected, a very faint band at the expected height can just be made out (B). In HevNogo-myc-CBD(T3C) the intein tag was mutated to prevent *in vivo* cleavage. The bands were at the expected size (C) of ~60 kDA.

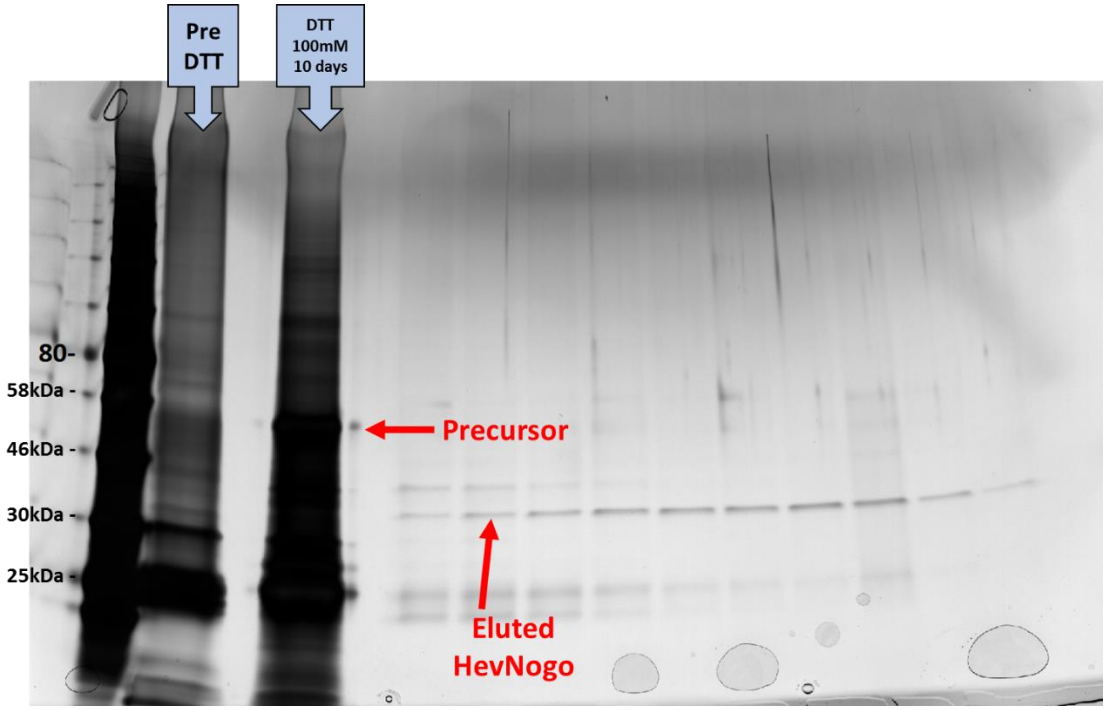

Figure 4.8 Only a small amount of HevNogo-myc was eluted from the chitin binding column
Soluble HevNogo protein was loaded onto a chitin column. A sample of protein/ chitin beads was taken before the addition of DTT and boiled in SDS-buffer to release the protein. 100 mM of DTT was added to the column with cleavage taking place over ten days. A second sample was taken after ten days to check for cleavage of the target protein before elution.

Eluted protein was collected as 10 fractions and 20µl of sample was taken from each to be analysed by SDS-PAGE and silver stain. Only a small band at the expected size was visible as indicated by the arrow 'Eluted HevNogo' and this required massive overstaining of the rest of the gel.

4.4.2 Pyrophosphate assay

HRT2 could not be purified although a small amount of HevNogo was eluted from the column and concentrated to 80μg/ml in final volume of 20μl. Recombinant *Arabidopsis* CPTL, LEW1 is able to catalyse the synthesis of dolichols when added to IPP incorporation experiments (Zhang *et al* 2008). However in the case *T. brevicorniculatum* CPTL, TbRTA whilst knockdown prevents rubber biosynthesis, it has no effect on dolichol accumulation. (Epping *et al* 2015).

To test whether HevNogo could demonstrate CPT activity on its own. HevNogo recombinant protein purification was used in a pyrophosphate assay. A by-product of IPP incorporation in polyisoprene synthesis, including natural rubber is inorganic pyrophosphate (Figure 1.2).

The pyrophosphate assay can be split into two parts although both were carried out in the same tube and at the same time. The first part of the assay relies on the premise that any IPP polymerisation creates a by-product of inorganic pyrophosphate (see Figure 1.2, chapter 1). This is then converted to two molecules of inorganic phosphate by the actions of the enzyme inorganic pyrophosphatase. The second part of the assay involved the conversion of inorganic phosphate and 2-amino-6-mercapto-7-methylpurine ribonucleoside (MESG) to ribose-1-phosphate and 2-amino-6-mercapto-7-methyl-purine (Figure 4.9). This reaction was catalysed by the enzyme purine nucleoside phosphorylase (PNP). The conversion of MESG to its products was able to be measured by a spectral shift as 2-amino-6-mercapto-7-methyl-purine has an absorbance of 360nm compared to 300nm for MESG. Thus the rate of IPP incorporation and subsequent pyrophosphate release was able to be measured in-directly using a UV spectrophotometer (Upson *et al* 1996).

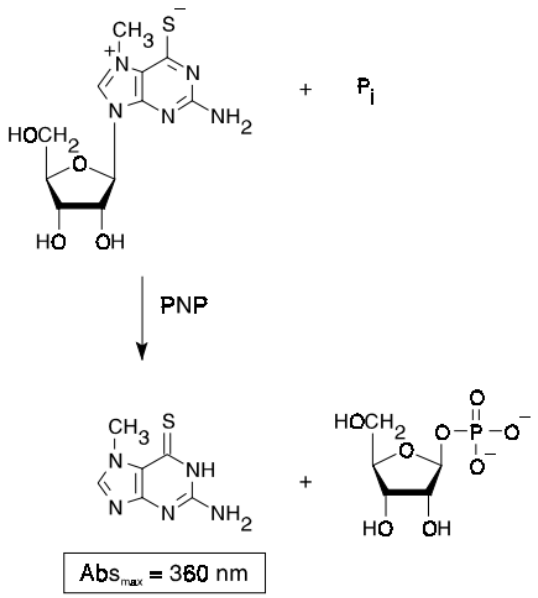

Figure 4.9 MESG conversion by PNP
MESG and inorganic phosphate are converted to ribose-1-phosphate and 2-amino-6-mercapto-7-methyl-purine by the enzyme PNP

This image is taken directly from the EnzChek® Pyrophosphate Assay Kit Manual which can be found at https://tools.thermofisher.com/content/sfs/manuals/mp06645.pdf.

4.4.3 HevNogo is not sufficient to catalyse IPP polymerisation

Recombinant HevNogo protein was added to the pyrophosphate assay mix. Using FPP and IPP as substrates. Absorbance was measured at 360nm against a blank control of assay mix without recombinant protein (Figure 4.10). A baseline was previously established by testing the absorbance change of IPP and FPP (Appendix Figure A.9) and using this as a zero.

No change in absorbance was detected after the addition of HevNogo protein. This indicates that pyrophosphate was not being produced and no IPP polymerisation was occurring. 2 µl of 0.1M sodium-pyrophosphate was added at the end of the assay as a positive control, resulting in an increase of absorbance at 360nm indicating that the assay mix was able to detect pyrophosphates if they were present.

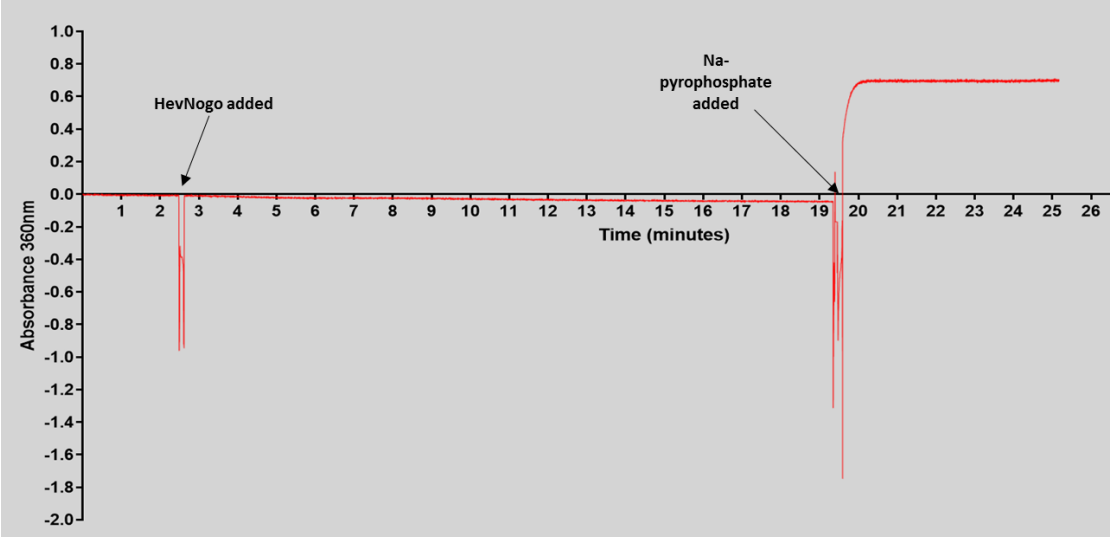

Figure 4.10 HevNogo Pyrophosphatase assay

2µl of recombinant HevNogo (140µl/ml) was added to the reaction mix at 2.5 minutes with absorbance at 360nm measured. No change could be detected after the addition of HevNogo. The reaction mixture was tested by the addition of Na-pyrophosphate after 19.5 minutes resulting in a significant increase in absorbance

4.5 Recombinant protein discussion

Although SRPP and REF were able to be produced and purified in large amounts, HRT and HevNogo were not. A small amount of HevNogo was purified which was used in a pyrophosphate assay. Recombinant HevNogo was unable to catalyse the polymerisation of IPP. There could be many reasons for that HevNogo alone could not catalyse IPP polymerisation, and the protein induction and assay conditions will need optimising for future study.

The first reason is that whilst there was enough HevNogo purified to create a viable assay, 100µg of protein was sufficient to test LEW1 in *Arabidopsis* (Zhang *et al* 2008), not enough was produced to optimise the assay efficiently. HevNogo activity may be dependent on pH or temperature, or any number of conditions. Determining the correct conditions through further optimisation would require larger volumes of recombinant protein. This will require further optimisation of the purification process, and perhaps the use of a different purification system.

The second is that HevNogo itself is not sufficient to catalyse IPP polymerisation. Although *Arabidopsis* LEW1 has been shown to catalyse the formation of dolichols in an IPP incorporation assay (Zhang *et al* 2008). TbRTA from *T.brevicorniculatum* and CPTL from *L. sativa* have not (Epping *et al* 2015, Qu *et al* 2015). In fact *L. sativa* CPTL1 alone was unable to incorporate ^{14}C-IPP in a series of assays, whereas in conjunction with its CPT partner ^{14}C-IPP incorporation was observed. It is possible that in rubber species, CPTL proteins, although necessary for natural rubber production are not the enzymatic component of the complex, but instead scaffolding proteins. The fact that HevNogo and other CPTL proteins can interact with CPTs binding them to a membrane, seen both in this study (Chapter 3) and in previous literature supports this.

Further optimisation is required for further studies involving recombinant protein purification. It will be necessary to improve on the protein induction conditions. Of particular importance is the purification of HRT2 as this is likely the central component of any rubber transferase complex.

Chapter 5: Discussion and Conclusions

5.1 Characterising rubber associated proteins

A rubber biosynthetic protein or complex is likely to contain a CPT enzyme. From existing research (Asawatreretanakul *et al* 2003) the prime candidate was the *Hevea* CPT enzyme HRT2. The original hypothesis of this report is that any rubber biosynthetic enzyme would be membrane bound, or membrane-associated, and in the absence of rubber particles it would be most likely associated with the endoplasmic reticulum. This could either occur by individual proteins inserting/associating with the ER membrane, or through the action of helper proteins.

During this project potential rubber-associated proteins were cloned and characterised. This was to be the first step in determining the nature of the rubber biosynthetic complex. HRT2, SRPP, REF, HevNogo and RBSP cellular localisations were determined for the first time. SRPP, REF and HevNogo localised to the endoplasmic reticulum, consistent with the hypothesis that rubber particle proteins would be located on the endoplasmic reticulum in non-native tissue. HRT2 was initially shown to be a cytosolic protein. This localisation is difficult to reconcile with the presumed key role of this protein as the core of the rubber transferase complex. However, subsequent protein-protein interaction work, particularly with the CPTL protein HevNogo, revealed that it was possible for HRT2 to associate with a membrane through heterotypic interactions. This could provide a scaffold for rubber biosynthesis on rubber particles, although the composition of the entire complex remains incomplete, both in *Hevea* and other latex-producing model species. Although attempts to produce recombinant proteins were not successful, the cell localisation and interaction work may be an important initial step in Hevea rubber particle biogenesis research.

5.2 Identification of a Hevea CPTL protein, HevNogo

Recently CPTL proteins were identified in *T. brevicorniculatum* and *L. sativa*. Through a combination of yeast-2-hybrid assays and confocal microscopy in both *N. benthamiana* and yeast, CPTLs were discovered to interact with CPT proteins to form a

complex on the endoplasmic reticulum in *N. benthamiana*, and on lipid bodies in yeast (Epping *et al* 2015, Qu *et al* 2015).

CPTLs belongs to a class of proteins, including NgBR, which have been shown to be involved in the synthesis of dolichols, a long chain polyisoprene molecule. This function seems to be conserved across the few higher eukaryotic species in which they have been characterised, including Arabidopsis, and humans (Harrison *et al* 2011, Zhang *et al* 2008). Qu *et al* (2015) also demonstrated that *L. sativa* CPTL silencing led to reduced, but not suppressed, natural rubber synthesis in lettuce. In addition to this TbRTA silencing in *T. brevicorniculatum* results in a reduced rubber content. However dolichol production is not suppressed indicating that the function of this protein has diverged from NgBR (Epping *et al* 2015). Given their apparently conserved function, there is a strong chance that these proteins fulfil a role in natural rubber biosynthesis in all species, including Hevea.

The CPLT/CPT complexes in T. brevicorniculatum and *L. sativa* fit the hypothesis that any rubber biosynthetic complex would be membrane bound, and it was likely that a corresponding complex was present in Hevea.

In this report a CPTL protein named HevNogo was cloned and characterised and was localised to the endoplasmic reticulum in *N. benthamiana*. As it is a membrane protein, HevNogo partly fulfils the requirement of any rubber biosynthetic factor: that it be membrane bound. Although it was not determined within this project whether HevNogo could associate with rubber particles, the ability of other CPTL proteins to associate with yeast lipid bodies (Qu *et al* 2015), would indicate that this type of protein is likely to be capable of doing so.

Part of characterising HevNogo was determining some of its protein topology, in particular the existence of transmembrane regions. Two potential regions TM1 and TM2 were deleted to create HevNogoΔTM1 and HevNogoΔTM2 mutants. The subcellular localisation of these mutants was analysed: whilst HevNogoΔTM2 remained on the endoplasmic reticulum, HevNogoΔTM1 lost its membrane localisation and was present in the cytosol.

It was possible that human CPTL NgBR contained an N-terminal signal peptide, however this has been experimentally shown to be not the case (Harrison *et al* 2009). For HevNogo the same is probably true for two reasons; (1) the deletion of TM1 alone is sufficient to cause a cytosolic localisation, and (2), cleavage of a signal peptide at the start of the N terminus would prevent detection by confocal microscopy of the CFP-HevNogo construct. This was not the case.

Deletion of TM1 was sufficient to prevent ER localisation, whereas deletion of TM2 had no apparent effect. It therefore appeared that HevNogo had only one transmembrane region and that HevNogo is a type I membrane protein (Figure 5.1). Analysis of the amino acid sequence around TM1 revealed sequential positively charged lysine and argenine residues flanking the C-terminal end of TM1. Positively charged residues are well characterised as affecting the orientation of proteins within a membrane (Lerch-Bader *et al* 2008, Von Heijne, 1986). The 'positive-inside' rule states that "positively charged residues tend to be enriched near the cytosolic end of transmembrane helices" (Lerch-Bader *et al* 2008). It is therefore proposed than the N terminus of HevNogo lies within the lumen of the endoplasmic reticulum, whereas the C terminus, consisting of the majority of HevNogo, is within the cytoplasm. This topology is consistent with HevNogo acting as a potential scaffold for the assembly of the rubber transferase complex on the cytosolic side of the ER membrane

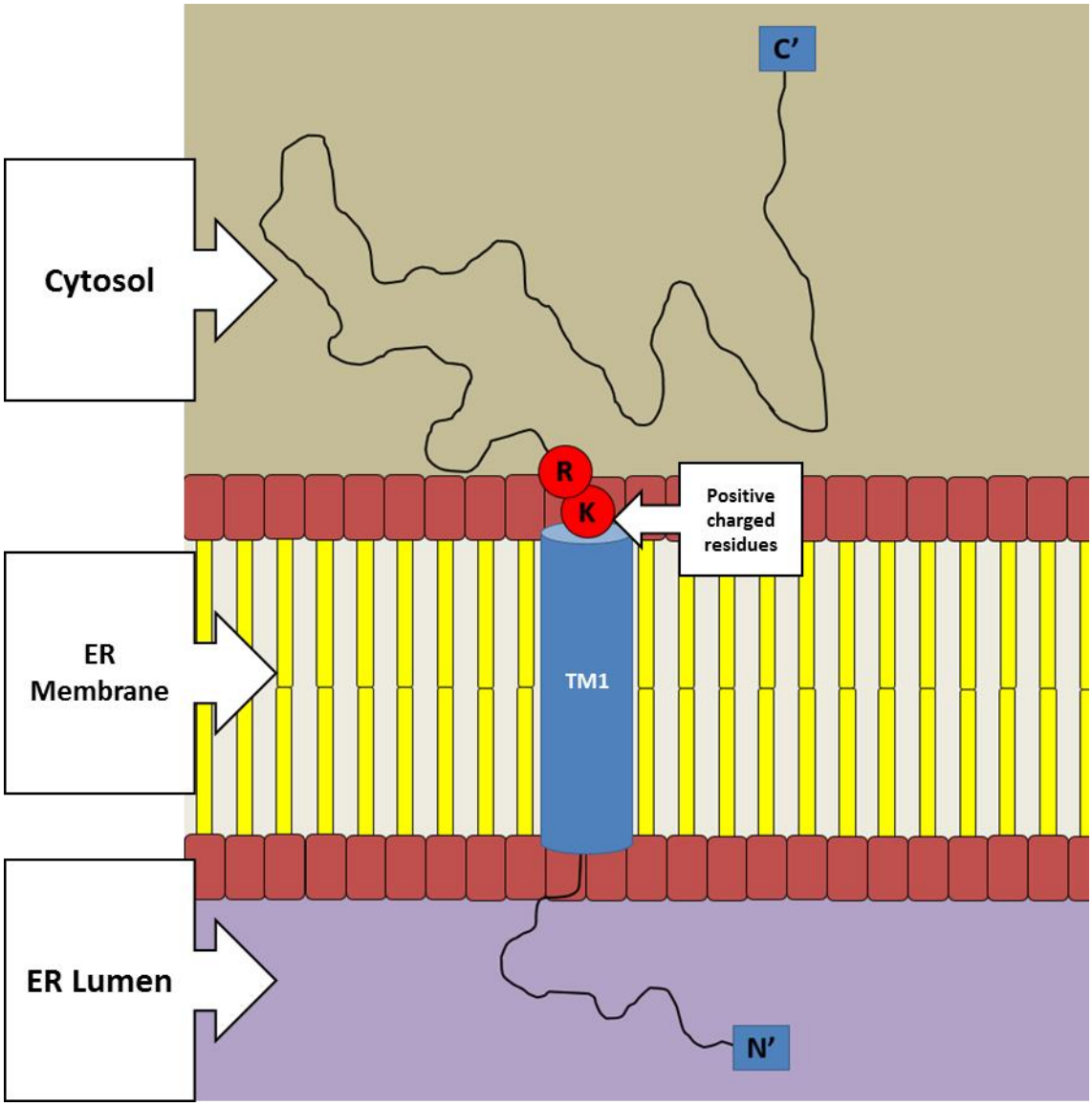

Figure 5.1 Proposed model of HevNogo topology
A single transmembrane domain (TM1) anchors HevNogo to the endoplasmic reticulum membrane. Orientation is determined by 2 positively charged residues, a lysine and arginine, on the C' end of TM1. The C' terminus faces the cytosol, whilst the N' terminus resides in the lumen of the endoplasmic reticulum.

5.3 HevNogo interacts with HRT2, however the complex is not retained at the endoplasmic reticulum

T. brevicorniculatum TbRTA and *L.sativa* CPTLs bring CPT to the endoplasmic reticulum in their respective species, therefore a similar role for *Hevea* HevNogo was proposed. The effect of HevNogo on HRT2 was investigated by co-expression of the two constructs.

TOPCONS predictions indicated that HRT2 lacked a transmembrane domain, and cell localisation in *N. benthamiana* confirmed this by revealing that it is a cytosolic protein. Based upon the results in this thesis, it can be proposed that HevNogo is an integral membrane protein, which acts to tether HRT2 to a membrane peripherally. HRT2's new localisation on the surface of the membrane could provide a mechanism for the biosynthesis of insoluble rubber polyisoprene, from soluble IPP substrate on rubber particles.

However, surprisingly, whilst HRT2 and HevNogo co-localised and were shown to interact by co-immunoprecipitation, they were not retained at the endoplasmic reticulum, and instead the complex travelled to the plasma membrane. In addition neither SRPP nor REF were sufficient to keep the complex on the endoplasmic reticulum. The significance of this finding is not clear at present, however it is likely that the endoplasmic reticulum remains the main site for the interaction of these proteins.

At high expression levels, fluorescence of both HevNogo and HRT2 could still be seen on the endoplasmic reticulum, indicating that the initial interaction did happen on this organelle. A possibility is that the complex may be formed on the endoplasmic reticulum in laticifers cells, but then moved to rubber particles in latex. It is also possible that HRT2 binding to HevNogo affected a particular domain or caused misfolding, resulting in the complex exiting the ER.

There was no evidence of Golgi transport. The fact that subsequent trafficking to the plasma membrane was insensitive to Brefeldin A treatment hints at the possibility that the complex is not travelling through the Golgi complex.

This unusual result of HRT2/HevNogo localising to the plasma membrane, may be down to the nature of the experimental system. *N. benthamiana* was useful in providing an initial subcellular map of rubber related proteins. However the system does not produce rubber particles, or indeed lipid bodies, therefore rubber protein interactions occur in a significantly different cellular milieu. It is possible that in the homologous system a different result would be observed and this should be the focus for any further study. However it should be noted that in the research into lettuce and dandelion CPT/CPTL proteins by Epping *et al* (2015) and Qu *et al* (2015), expression in *N. benthamiana* was sufficient to keep the CPTL/CPT complex at the endoplasmic reticulum in *T. brevicorniculatum* and *L. sativa*. It may be that the rubber transferase complex is more complicated in *Hevea* than other species, and that further unknown partners are required to keep HRT2 on the endoplasmic reticulum. *Hevea* contains more protein types on the rubber particle than any other species (Cornish 2000). Whether there are further unknown partners is however speculation at this stage.

To investigate whether HevNogo could affect HRT2 independently of its endoplasmic reticulum location, HevNogo deletion mutant ΔTM1 was co-expressed with HRT2. HRT2 was also co-expressed with ΔTM2. HevNogoΔTM1 co-expression with HRT2 resulted in both proteins remaining in the cytosol.

However the complex ends up at the plasma membrane, the process starts at the endoplasmic reticulum. This process remains unknown: it could be some sort of post-translational modification induced by one of the interacting proteins, or that the interaction induces misfolded resulting in the complex not being retained at the endoplasmic reticulum.

Even harder to explain is that HevNogoTMΔ2 co-expression with HRT2 also prevented trafficking to the plasma membrane, and resulted in a similar phenotype to HRT2-SRPP co-expression. HevNogoΔTM2 remained on the ER and HRT2, whilst displaying some cytosolic signal, also showed increasing endoplasmic reticulum labelling, particularly around the nuclear envelope.

TM2 therefore is perhaps not important for binding of HRT2 but could contain a signal that is usually masked when HevNogo is expressed alone. In the presence of HRT2 a conformational change could result in this sequence becoming exposed resulting in transport to the plasma membrane. Likewise deletion of TM2 may results in alteration of HevNogo structure, hiding an otherwise available signal.

5.4 The rubber biosynthetic complex is likely to contain additional partners

The interactions found may represent only a small proportion of any rubber biosynthetic complex (Figure 5.2). Whilst HevNogo/HRT2 was shown to interact, the potential interaction between HRT2 and SRPP could not be verified. In addition, the HRT2/SRPP interaction was unable to prevent HRT2/HevNogo from trafficking to the plasma membrane. It is possible that the HRT2-SRPP interaction is weak or transient in nature or that the interaction is sensitive to detergents in the lysis buffer. It is also possible that the cytosolic orientation of GFP-SRPP on the ER gave the illusion of co-localisation, however this would not account for the clear nuclear envelope signal detected when HRT2 was co-expressed with SRPP. Fixation with chemical cross-linkers before co-immunoprecipitation may be a future option to validate transient interactions and confirm or deny the HRT2-SRPP interaction.

Future work should focus on building upon these initial interaction: it should be possible to investigate some of these interactions through a series of pulldowns perhaps from *Hevea* itself with specifically designed antibodies.

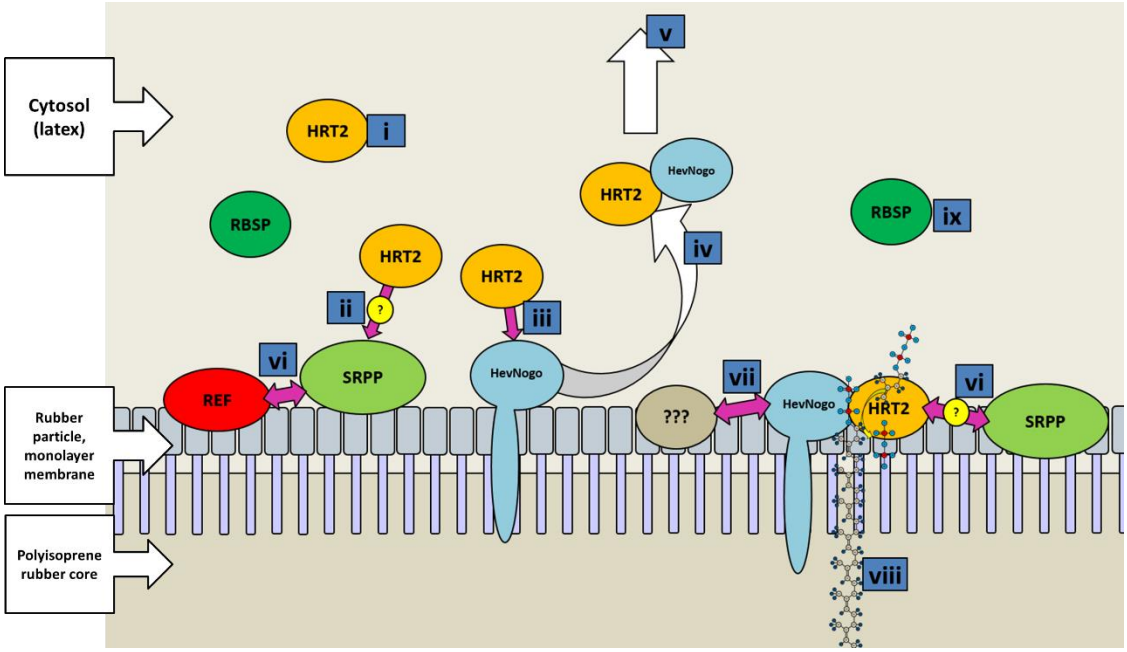

Figure 5.2 Proposed model of rubber transferase complex

[i] HRT2 is a cytosolic protein and therefore would be unable to polymerize polyisoprene rubber on the surface of rubber particles. [ii] Confocal data hints at a potential interaction between HRT2 and SRPP but this was unable to be verified by subsequent experiments. [iii] HRT2 did interact with the CPTL protein HevNogo, however the complex was not retained at the membrane surface [iv] and instead travelled [v] to the plasma membrane. This interaction was verified by subsequent experiments. Neither REF nor the potential interaction between HRT and SRPP [vi] was sufficient to retain the HRT2/HevNogo complex at the membrane surface. It is possible that additional components [vii] are required to retain a complete rubber transferase complex at the surface of rubber particles in order to polymerise natural rubber [viii]. RBSP displayed a cytosolic signal [ix]. It may be that it is uninvolved in the complex or that it required additional interactions to bring it to the rubber particle surface.

5.5 Opportunities for further research

In May and June of 2016 two new *Hevea* genome sequences were published (Lau *et al* 2016, Tang *et al* 2016). These were much more complete than anything seen before. The genomes revealed a whole host of new potential rubber biosynthetic proteins unavailable at the start of this project. The genome drafts showed particular expansions of gene families involved in IPP synthesis; polyisoprene APP initiator enzymes such as GPPS and FPPS; and rubber elongation and rubber particle related proteins such as CPT, and SRPP. Here new genome drafts will be discussed in relation to the results already obtained; the genome drafts may provide the basis for future work investigating rubber biosynthesis in *Hevea*.

The first genome published in May, (Tang *et al* 2016) revealed an expansion of SRPP protein with known members all of a similar size to the SRPP from this report which will now be known as SRPP2. 18 separate REF/SRPP proteins were discovered, and by comparing RNA transcript reads from different tissues the report was able to establish that different members of the SRPP protein family were differentially expressed according to tissue. Some members displayed no expression in latex and others were expressed at a very high level. Reads per kilobase of transcripts per million mapped reads (RPKM) were measured to quantify the level of gene expression.

While SRPP2 is preferentially expressed in latex, with 680.28 RPKM compared to around 200 RPKM in other tissue, it by no means had the highest expression levels. Mapping the sequence SRPP1 was found to contain 13284.72 RPKM in latex, compared to around 100-400 RPKM in other tissue. Although SRPP2 had a preferential expression in latex this was still lower than REF3 at 9644.16 RPKM and REF7 at 76665.58 and therefore may be a minor player in any rubber biosynthetic complex, although it could potentially have a role in HRT2 interaction based on the confocal data in this thesis.

By far the most highly expressed protein in latex was REF, which we investigated in this project. Hereafter it should be known as REF1. Despite the nomenclature of the paper in naming many REF proteins, they could be more accurately be called SRPP as they are of a similar length and homology to SRPP. REF1 is the only truncated version of SRPP that exists and has not been found in other rubber producing species. In *Hevea* it

is the most highly expressed protein, present in 38998.66 RPKM around three times the level as the next highest which was SRPP1. This hints at an important role for REF and this is likely to be involved in stabilisation of the rubber particle.

From the confocal data and through experience with recombinant protein production it was found that SRPP2 is very prone to aggregation. This is in contradiction to the findings of Berthelot *et al* (2014b), where REF was shown to aggregate but SRPP was not. The discrepancy between our SRPP and SRPP1, which was used in Berthelot *et al*'s (2014b) assay, may explain this. In the TARRC *Hevea* genome sequence, only SRPP2 was found, which is why it was cloned and used in the study.

11 different CPT enzymes were found in *Hevea*, of which only 3 were expressed to any degree in latex. One of these was HRT2 expressed at 153 RPKM, much lower than some of the SRPP family. However this may be expected for what is likely an enzyme, rather than a structural component. Particularly surprising was the fact that the most highly expressed protein was HRT1 at 545 RPKM. Asawatreratanakul *et al* (2002) managed to purify HRT1 but found it displayed no prenyl-transferase activity, with or without rubber particles. This was in stark contrast to HRT2. However in light of our findings regarding HevNogo it may be that HRT1 requires a CPTL protein or similar partner not known at the time of Asawatreratanakul's assay. Also Asawatreratanakul did not test HRT1 in the presence of HRT2 and it may be that they act in tandem as part of a larger complex. Again this is an appropriate topic for future work and the field is now expanding at a fast rate. A third hitherto unknown CPT was expressed at a high rate in latex and may also provide material for further research.

Interestingly, the Tang *et al* (2016) genome did not manage to identify HevNogo or any other CPTL proteins, either in the rubber genome or public databases based upon the *T. brevicorniculatum* TbRTA protein. This is mentioned in the paper itself, and they propose that *Hevea* must have a different rubber transferase complex composition. This is contradicted by the findings in this report where HevNogo was identified and its interaction with HRT2 was observed.

However the second paper by Lau *et al* (2016) did manage to locate HevNogo in their *Hevea* genome analysis. In their expression analysis they reveal that HevNogo now referred to as *Hevea* CPTL is highly, and preferentially, expressed in latex, an encouraging result indicating there is a good chance that HevNogo has a role to play in *Hevea* rubber synthesis.

The two *Hevea* genomes open up the field and provide a range of targets; in particular there may be a new interest in HRT1. HRT1 was detected in the TARRC *Hevea* genome, and an attempt to amplify and clone HRT1 was made both within and previously to this project. Despite designing primers lying outside of the coding region to distinguish it from HRT2 this was not successful, and any gene regions amplified by using HRT2 primers, which would be identical to HRT1, only yielded HRT2. In light of the cloning and characterising SRPP2, it is crucial now to examine SRPP1 as well as other SRPP/REF proteins more highly expressed in latex, and examine the interactions between them and any potential CPT/CPTL complex.

5.6 Heterologous expression systems

The majority of the experiments and characterisation work carried out within this report was performed in the leaves of *N. benthamiana*. This was justified, as the aim of the project was to gather new information and provide an important first step in characterising rubber related proteins, and some of their interactions. As there was very limited information at the start of the project, transient expression in *N. benthamiana* was an efficient and well characterised technique for doing just that

However the next step will to try and generate a system more homologous to rubber particle proteins. Currently genetic manipulation in *Hevea* itself is not a viable strategy of its long life cycle and the difficulty of conducting any transient expression or infiltration experiments in the tough leaves of *Hevea*. But a possibility would be to express and characterise these proteins in another latex-producing organism such as *L. sativa*.

5.7 Concluding remarks

The publication of the two genome drafts means that the next logical step is a continuation of this work to clone and characterise the newly available genes. Interactions between them will be verified in the search for the rubber biosynthetic complex. The HRT2/HevNogo complex is likely to be a vital component of this and should be investigated further in a more suitable system.

There are major questions that remain to be answered: is HRT2/HevNogo sufficient for rubber biosynthesis? What is the role of the SRPP protein family, are they structural components necessary for rubber particle stability or binding of a biosynthetic complex, enzymatic components, or both? Why does *Hevea* produce much more latex than other species? CPT/CPTL proteins are present in *T. brevicorniculatum* and *L. sativa* and they associate with the endoplasmic reticulum. Is the rubber particle biogenesis process different or more complex in *Hevea*, and is the unexpected trafficking of HRT2/HevNogo to the plasma membrane indicative of this? It will be important to try and examine HRT2/HevNogo in actual laticifers cells, and to determine if they can be found on rubber particles as they are the site of natural rubber biosynthesis in *Hevea*.

Natural rubber is currently one of the most importance natural resources known to man. The research conducted in this project, particularly the discovery of the interaction between HRT2 and HevNogo represents an important step in determining just how natural rubber is synthesised on rubber particles in the laticifers cells of *Hevea*.

References

Abraham PD, Wycherley PR & Pakianatan SW (1968). 'Stimulation of latex flow in *Hevea brasiliensis* of 4-amino-3,5,6-trichloropicolonic acid and 2-chloroethane-phosphonic acid' *J. of Rubber Research*, 20: 291-305

Adair Jr WL, Cafmeyer N, Keller RK (1984). 'Solubilization and characterization of the long chain prenyltransferase involved in dolichyl phosphate biosynthesis' *J Biol Chem*, 259: 4441–4446

Akhtar TA, Matsuba Y, Schauvinhold I, Yu G, Lees HA, Klein SE, Pichersky E (2013). 'The tomato *cis*-prenyltransferase gene family.' *Plant Journal*, 73: 640-652

Archer BL & Audley EGC (1963). 'The biosynthesis of rubber: Incorporation of mevalonate and isopentenyl pyrophosphate into rubber by *Hevea brasiliensis*-latex fractions.' *J. Biochem* 89, 565

Asawatreratanakul K, Zhang YW, Wititsuwannakul D, Wititsuwannakul R, Takahashi S, Rattanapittayaporn A, Koyama T (2003). 'Molecular cloning, expression and characterization of cDNA encoding cis-prenyltransferases from Hevea brasiliensis a key factor participating in natural rubber biosynthesis.' *Eur. J. Biochem*. 270: 4671-4680

Bahri AR & Hamzah S (1996). 'Immunocytochemical localisation of rubber membrane protein in *Hevea* latex' *J. of Natural Rubber Research*, 11(2): 88-95

Berthelot K, Lecomte S, Esteves Y, Zhendre V, Henry S, Thévenot J, Dufourc EJ, Alves ID, Peruch F (2014a). 'Rubber particle proteins HbREF and HbSRPP, show different interactions with model membranes.' *Biochemica et Biophysica Acta*, 1838: 287-299

Berthelot K, Lecomte S, Esteves Y, Coulary-Salin B, Peruch F (2014b). 'Homologous *Hevea brasiliensis* REF (Hevb1) and SRPP (Hevb3) present different auto-assembling.' *Biochemica et Biophysica Acta*, 1844(2): 473-485

Berthelot K, Lecomte S, Esteves Y, Peruch F (2014c). '*Hevea brasiliensis* REF (Hevb1) and SRPP (Hevb3): An overview on rubber particle proteins. *Biochimie*, 106: 1-9 doi: 10.1016/j.biochi.2014.07.002. Epub 2014 Jul 11.

Brach T, Soyk S, Muller C, Hinz G, Hell R, Brandizzi F, Meyer AJ (2009). 'Non-invasive topology analysis of membrane proteins in the secretory pathway.' *The Plant Journal*, 57: 534-541

Brasàemle DL, Dolios G, Shapiro L, Wang R (2004). 'Proteomic analysis of proteins associated with lipid droplets of basal and lipolytically stimulated 3T3-L1 adipocytes.' *J Biol Chem*, 279(45): 46835-46842

Campbell RE, Tour O, Palmer AE, Steinbach PA, Baird GS, Zacharias DA, Tsien RY (2002). 'A monomeric red fluorescent protein.' *PNAS*, 99(12): 7877-7882

Chiang CK, Xie W, McMahan C, Puskas JE (2011). 'Unravelling the mystery of natural rubber biosynthesis. Part1: Investigation of the composition and growth of in vitro natural rubber using high resolution size exclusion chromatography.' *Rubber Chemistry and Technology*, 84(2): 166-177

Chow KS, Lim M, Han KH (2006). 'An assessment of stimulation of *Hevea brasiliensis* rubber biosynthesis by eIF-5A protein-enriched bacterial lystates' *J. of Rubber Research*, 9(4): 251-259

Chow KS, Wan KL, Mat-Isa MN, Bahari A, Tan SH, Harikrishna K, Yeang HY (2007). 'Insights into rubber biosynthesis from transcriptomes analysis of *Hevea brasiliensis* latex.' *Journal of Experimental Botany*, 58(10):2429-2440

Chow KS, Mat-Isa MN, Bahari A, Ghazali AK, Alias H, Zainuddin ZM, Hoh CC, Wan KL (2012). 'Metabolic routes affecting rubber biosynthesis in *Hevea brasiliensis* latex', *Journal of Experimental Botany* 63(5): 1863-1871.

Cornish K (2000). 'Similarities and differences in rubber biochemistry among plant species' *Phytochemistry*. 57: 1123-1134

Collins-Silva J, Nural AT, Skaggs A, Scott D, Hathwaik U, Woolsey R, Schegg K, McMahan C, Whalen M, Cornish K, Shintani D (2012). 'Altered levels of *Taraxacum kok-saghyz* (Russian dandelion) small rubber particle protein, TkSRPP3, result in qualitative and quantitative changes in rubber metabolism.' *Phytochemistry* 79: 46-56

Cui C, Zhai W, Chen J, Wang J, Li Q (2006). 'Elimination of in vivo cleavage between target protein and intein in the intein-mediated protein purification systems.' *Protein Expr Purif*, 50(1): 74-81

Dai L, Kang G, Li Y, Nie Z, Duan C, Zeng R (2013). 'In-depth proteome analysis of the rubber particle if *Hevea brasiliensis* (para rubber tree).' *Plant Mol Biol* 82:155-168

Dennis MS & Light DR (1989). 'Rubber Elongation Factor from *Hevea brasiliensis*'. *J. of Biological Chemistry*, 264(31): 18608-18617

Duckett JG & Ligrone (1995). 'The formation of catenate foliar gemmae and the origin of oil bodies in the Liverwort *Odeontoschisma denudatum* (Mart.) Dum. (Jungermanniales): a light and electron microscope study', *Annals of Botany*, 76: 405-419

Dussourd DE & Eisner T (1987). 'Vein-cutting behavior: insect counterploy to the latex defense of plants', *Science* 237: 898–900.

Epping J, van Deenen N, Niephaus E, Stolze A, Fricke J, Huber C, Eisenreich W, Tywman RM, Prufer D, Gronover CS (2015). 'A rubber transferase activator is necessary for natural rubber biosynthesis in dandelion' *Nature Plants*, 15049: http://dx.doi.org/10.1038/NPLANTS.2015.48

EnzChek® Pyrophosphate Assay Kit (E-6645). MP06645,

Farrell BD, Dussourd DE & Mitter C (1991). 'Escalation of plant defense: do latex and resin canals spur plant diversification', *American Naturalist* 138: 881–900.

Fujihashi M, Zhang YW, Higuchi Y, Li XY, Koyama T, Miki K (2001). 'Crystal structure of *cis*-prenyl chain elongating enzyme, undecaprenyl diphosphate synthase,' *PNAS* 98(8): 4337-4342

Fujiwara T, Oda K, Yokota S, Takatsuki A, Ikehara Y (1988). 'Brefeldin A causes dissaembly of the golgi complex and accumulation of secretory proteins in the endoplasmic reticulum.' *Journal of Biological Chemistry*, 263: 18545-18552

Greenspan P, Mayer EP, Fowler ST (1985). 'Nile red: a selective fluorescent stain for intracellular lipid droplets.' *Journal of Cell Biology*, 100(3): 965-973

Harrison KD, Mia RQ, Fernandez-Hernando C, Suarez Y, Davalos A, Sessa WC (2009). 'Nogo-B receptor stabilizes Niemann-Pick Type C2 protein and regulates intracellular cholesterol trafficking.' *Cell Metabolism*, 10(3): 208-218

Harrison KD, Park EJ, Gao N, Kuo A, Rush JS, Waechter CJ, Lehrman MA, Sessa WC (2011). 'Nogo-B receptor is necessary for cellular dolichol biosynthesis and protein *N*-glycosylation', *The EMBO Journal*, 30: 2490-2500

Hellens RP, Edwards EA, Leyland NR, Bean S, Mullineaux PM (2000). 'pGreen: a versatile and flexible binary Ti vector for Agrobacterium-mediated plant transformation', *Plant Molecular Biology*, 42: 819-832.

Herman EM (2008). 'Endoplasmic reticulum bodies: solving the insoluble.' *Curr Opin Plant Biol*, 11(6): 672-679

Hillebrand A, Post JJ, Wurbs D, Wahler D, Lenders M, Krzyzanek V, Prufer D, Gronover CS (2012). 'Down-regulation of small rubber particle protein expression affects integrity of rubber particles and rubber content in *Taraxacum brevicorniculatum*.' *PlosONE*, 7(7): e41874

Horn J, James CN, Gidda SK, Kilaru SK, Dyer JM, Mullen RT, Ohlrogge JB, Chapman KD (2013). 'Identification of a new class of lipid droplet-associated proteins in plants.' *Plant Physiology*, 162: 1926-1936

Irons SL, Evans DE, Brandizzi F (2003). 'The first 238 amino acids of the human lamin B receptor are targeted to the nuclear envelope in plants.' *Journal of Experimental Botany*, 54: 943-950

InvitrogenTM (2005). 'ProQuestTM Two-Hybrid System: A sensistive method for detecting protein-protein interactions.'

Invitrogen™ (2012). 'Gateway® pDONR™ Vectors. 25-0531

Kato J, Fujisaki S, Nakajima K, Nishimura Y, Sato M, Nakano A (1999). 'The Escherichia coli homologue of yeast RER2, a key enzyme of dolichol synthesis, is essential for carrier lipid formation in bacterial cell wall synthesis.' *J. Bacteriol*, 181(9): 2733-2738

Kim EY, Park KY, Seo YS, Kim WT (2016). 'Arabidopsis small rubber protein homolog SRPs play dual roles as positive factors for tissue Growth and Development and in Drought Stress Responses,' *Plant Physiology Preview*, DOI:10.1104/pp.16.00165

Ko TP, Chen YK, Robinson H, Tsai PC, Gao YG, Chen APC, Wang AHJ, Liang PH (2001). 'Mechanism of product chain length determination and the role of a flexible loop in *Escherichia coli* undecaprenyl pyrophosphate synthase catalysis' *J. of Biological Chemistry*, 276 (60): 47474-47482

Kotzer AM, Brandizzi F, Neumann U, Paris N, Moore I, Hawes C (2004). '*At*RabF2b (Ara7) acts on the vacuolar trafficking pathway in tobacco leaf epidermal cells,' *Journal of Cell Science*, 117(26): 6377-89

Kharel Y, Zhang YW, Fujihashi M, Miki K, Koyama T (2001). 'Identification of significant residues for homoallylic substrate binding of *Micrococcus luteus* B-P 26 undecaprenyl diphosphate synthase,' *J. Biol. Chem.* 276:28459-28464

Lau NS, Makita Y, Kawashima M, Taylor TD, Kondo S, Othman AS, Sun-Chien AC, Matsui M (2016). 'The rubber tree genome shows expansion of gene family associated with rubber biosynthesis.' *Scientific Reports*, 6(28594): DOI: 10.1038/srep28594

Lerch-Bader M, Lundin C, Kim, H, Nilsson I, von Heijne G (2008). 'Contribution of positively charged flanking residues to the insertion of transmembrane helices into the endoplasmic reticulum.' *PNAS*, 105(11): 4127-4132

Miao RQ, Gao Y, Harrison KD, Prendergast J, Acevado LM, Yu J, Hu F, Strittmatter SM, Sessa WC(2006). 'Identification of a receptor necessary for Nogo-B

stimulated chemotaxis and morphogenesis of endothelial cells.' *PNAS*, 103(29): 10997-11002

Monosov EZ, Wenzel TJ, Luers GH, Heyman JA, Subramani S (1996). 'Labelling of peroxisomes with green fluorescent protein in living *P. pastoris* cells.' *J Histochem Cytochem*, 44(6): 581-589

Nakamura S, Mano S, Tanaka Y, Ohnishi M, Nakamori C, Araki M, Niwa T, Nishimura M, Kaminaka H, Nakagawa T, Sato Y, Ishiguro S (2010). 'Gateway binary vectors with the bialaphos resistance gene, *bar*, as a selection marker for plant transformation.' *Biosci Biotechnol Biochem*, 74(6): 1315-1319

Napier JA, Stobart AK, Shewry PR (1996). 'The structure and biogenesis of plant oil bodies: the role of the ER membrane and the oleosin class of proteins.' *Plant Mol Biol* 31: 945-956

NEB™ 'IMPACT™ Kit: Instruction Manual' NEB#E6901S

Nebenführ A, Ritzenthaler C, Robinson DG (2002). 'Brefeldin A: Deciphering an enigmatic inhibitor of secretion.' *Plant Physiology*, 130: 1102-1108

Park EJ, Grabinska KA, Guan Z, Stranecky V, Hartmannova H, Hodanova K, Baresova V, Sovova J, Jozsef L, Ondruskova N, Hansikova H, Honzik T, Zeman J, Hulkova H, Wen R, Kmoch S, Sessa WC (2014). 'Mutation of Nogo-B Receptor, a subunit of *cis*-prenyltransferase causes a congenital disorder of glycosylation.' *Cell Metabolism*, 20: 448-457

Priya P, Perumal V, Thulaseedharan A (2007). 'Differential expression pattern of rubber elongation factor (REF) mRNA transcripts from high and low yielding clones of rubber tree (*Hevea brasiliensis* Muell. Arg.).' *Plant Cell Reports*, 26:1833-1838

Post J, van Deenen N, Fricke J, Kowalski N, Wurbs D, Schaller H, Eisenreich W, Huber C, Tywman RM, Prufer D, Gronover CS (2012). 'Laticifer-specific *cis*-prenyltransferase silencing affects the rubber triterpene and inulin content of *Taraxacum brevicorniculatum*.' *Plant Physiology*, 158: 1406-1417

Oh SK, Kang H, Shin DH, Yang J, Chow KS, Yeang HY, Wagner B, Breiteneder H, Han KH (1999). 'Isolation, characterization, and functional analysis of a novel cDNA clone encoding a small rubber particle protein from Hevea brasiliensis.' *J. of Biological Chemistry*, 274(24): 17132-17138

Oh SK, Han KH, Ryu SB, Kang H (2000). 'Molecular cloning, expression, and functional analysis of a *cis*-prenyltransferase from *Arabidopsis thaliana*.' *J. of Biological Chemistry*, 278(24): 18482-18488

Qu Y, Chakrabarty R, Tran HT, Kwon EJG, Kwon M, Nguyen TD, Ro DK (2015). 'A lettuce (*Lactuca sativa*) homolog of human Nogo-B Receptor interacts with *cis*-prenyltransferase and is necessary for natural rubber biosynthesis.' *J. of Biological Chemistry*, 290(4): 1898-1914

Saint-Jore CM, Evins J, Batoko H, Brandizzi F, Moore I, Hawes C (2002). 'Redistribution of membrane proteins between the Golgi apparatus and endoplasmic reticulum in plants is reversible and not dependent on cytoskeletal networks,' *Plant Journal*, 29(5): 661-678

Sato M, Sato K, Nishikawa S, Hirata A, Kato J, Nakano A (1999). 'The yeast RER2 gene, identified by endoplasmic reticulum protein localization mutations, encodes cis-prenyltransferase, a key enzyme in dolichol synthesis.' *Mol Cell Biol*, 19(1): 471-483

Sando T, Hayashi T, Takeda T, Akiyama Y, Nakazawa Y, Fukusaki E, Kobayashi A (2009). 'Histochemical study of detailed laticifer structure and rubber biosynthesis-related protein localization in *Hevea brasiliensis* using spectral confocal laser and scanning microscopy.' *Planta*, 230:215-225

Sansatsadeekul J, Sakdapipanich J, Rojruthai P (2011). 'Characterization of associated proteins and phospholipids in natural rubber latex.' *Journal of Bioscience and Bioengineering*, 111(6): 628-634

Schmidt T, Hillebrand A, Wurbs D, Prufer D (2010a). 'Molecular cloning and characterization of rubber biosynthetic genes from *Taraxacum koksaghyz*.' *Plant Mol Biol Reports*, 28:277-284

Schmidt T, Lenders M, Hillebrand A, van Deenen N, Munt O, Reichelt R, Eisenreich W, Fischer R, Prufer D, Gronover CS (2010b). 'Characterization of rubber particles and rubber chain elongation in *Taraxacum koksaghyz*' *BMC Biochemistry*, DOI: 10.1186/1471-2091-11-11

Shimada TL & Hara-Nishimura I (2010). 'Oil-body-membrane proteins and their physiological functions in plants.' *Biol Pharm Bull*, 33(3): 360-363

Shimizu N, Koyama T, Ogura K (1998). 'Molecular cloning, expression and purification of Undecaprenyl diphosphate synthase.' *Journal of Biological Chemistry*. 275(31): 19475-19481

Singh AP, Wi SG, Chung GC, Kim YS, Kang H (2003). 'The micromorphology and protein characterization of rubber particles in *Ficus carica*, *Ficus benghalensis* and *Hevea brasiliensis*' *J. of Experimental Botany*, 54(384): 985-992

Sparkes IA, Runions J, Kearns A, Hawes C (2006). 'Rapid, transient expression of fluorescent protein fusion proteins in tobacco plants and generation of stably transformed plants.' *Nature Protocols*, 1(4): 2019-2015

Suire C, Bouvier F, Backhaus RA, Begu D, Bonneu, Camara B (2000). 'Cellular localisation of isoprenoid biosynthetic enzymes in *Marchantia polymorpha*. Uncovering a new role of oil bodies', *Plant Physiology*, 124(3): 971-978

Tang C, Yang M, Fang Y, Luo Y, Gao S, Xiao X, An Z, Zhou B, Zhang B, Tan X, Yeang HY, Qin Y, Yang J, Lin Q, Mei H, Montoro P, Long X, Qi J, Hua Y, He Z, Sun M, Li W, Zeng X, Cheng H, Liu Y, Yang J, Tian W, Zhuang N, Zeng R, Li D, He P, Li Z, Zou Z, Li S, Li C, Wang J, Wei D, Lai CQ, Yu J, Hu S, Huang H (2016). 'The rubber tree genome reveals new insights into rubber production and species adaptation.' *Nature Plants*, 2(16073): doi:10.1038/nplants.2016.73

Tarachiwin L, Sakdapipanich J, Ute K, Kitayama T, Bamba T, Fukusaki E, Kobayashi A, Tanaka Y (2005a). 'Structural Characterization of r-Terminal Group of Natural Rubber. 1. Decomposition of Branch-Points by Lipase and Phosphatase Treatments' *Biomacromolecules*, 6: 1851-1857

Tarachiwin L, Sakdapipanich J, Ute K, Kitayama T, Tanaka Y (2005b). 'Structural Characterization of r-Terminal Group of Natural Rubber. 2. Decomposition of Branch-Points by Phospholipase and Chemical Treatments'. *Biomacromolecules*, 6: 1858-1863

Teng RJ, Rana U, Afolayan AJ, Zhai B, Miao QR, Konduri GG (2014). 'Nogo-B Receptor modulates angiogenesis response of pulmonary artery endothelial cells through eNOS coupling.' *American Journal of Respiratory Cell and Molecular Biology*, 51(1): 169-177

Tsirigos KD, Peters C, Shu N, Kall L, Elofsson A (2015). 'The TOPCONS web server for combined membrane protein topology and signal peptide prediction.' *Nucleic Acids Research*, 43(Webserver Issue): W401-W407

Upson RH, Haugland RP, Malekzadeh MN, Haugland RP (1996). 'A spectrophotometric method to measure enzymatic activity in reactions that generate inorganic pyrophosphate.' *Analytical Biochemistry*, 243(1): 41-45

Van der Schoot, Paul LK, Paul SB, Rinne PLH (2011). 'Plant lipid bodies and cell-cell signalling: A new role for an old organelle' *Plant Signal Behaviour*, 6(11): 1732-1738

Vida TA & Emr SD (1995). 'A new vital stain for visualizing vacuolar membrane dynamics and endocytosis in yeast.' *Journal of Cell Biology*, 128(5): 779-92

Voeltz GK, Prinz WA, Shibata Y, Rist JM, Rapoport TA (2006). 'A class of membrane proteins shaping the tubular endoplasmic reticulum.' *Cell*, 124(3): 573-586

Voinnet O, Rivas S, Mestre P, Baulcombe D (2003). 'An enhanced transient expression system in plants based on suppression of gene silencing by the p19 protein of tomato bushy stunt virus.' *The Plant Journal*, 33: 949-956

Von Heijne (1986). 'The distribution of positively charged residues in bacterial inner membrane proteins correlates with the trans-membrane topology.' *The EMBO Journal*, 5(11): 3021-3027

Wang L, Jang JH, Kim KH, Lee EK (2009). 'Expression of intein-tagged fusion protein and its applications in downstream processing.' *J. Chem. Technol. Biotechnol*, 85: 11-18

Winter D, Vinegar B, Nahal H, Ammar R, Wilson GV, Provart NJ (2007). 'An "electronic fluorescent pictograph" browser for exploring and analysing large-scale biological data sets' *Plos One*, http://dx.doi.org/10.1371/journal.pone.0000718

Xiang Q, Xia K, Dai L, Kang G, Li Y, Nie Z, Duan C, Zeng R (2012). 'Proteome analysis of the large and the small rubber particles of *Hevea brasiliensis* using 2D-DIGE' *Plant Physiol. Biochem*. 60: 207-213

Xu MQ & Perler FB (1996). 'The mechanism of protein splicing and its modulation by mutation.' *EMBO Journal*, 15: 5146-5153

Yeang HY, Cheong KF, Sunderasan E, Hamzah S, Chew NP, Hamid S, Hamilton RG, Cardosa MJ (1996). 'The 14.6 kd rubber elongation factor (Hev b 1) and 24 kd (Hev b 3) rubber particle proteins are recognized by IgE from patients with spina bifida and latex allergy.' *J Allergy Clin Immunol*, 98(3):628-39

Yusof F, Chow KS, Ward W, Walker JM (2000). 'A Stimulator protein of rubber biosynthesis from *Hevea brasiliensis* latex' *J. of Rubber Research*, 3(4): 232-247

Zalucki MP, Brower LP & Alonso A (2001). 'Detrimental effects of latex and cardiac glycosides on survival and growth of first-instar monarch butterfly larvae *Danaus plexippus* feeding on the sandhill milkweed *Asclepias humistrata*', *Ecological Entomology* 26: 212–224.

Zhang H, Ohyama K, Boudet J, Chen Z, Yang J, Zhang M, Muranaka T, Maurel C, Zhu JK, Gong Z (2008). 'Dolichol biosynthesis and its effects on the unfolded protein response and abiotic stress resistance in *Arabidopsis*' *Plant Cell*, 20: 1879-1898

Zhu J & Zhang Z (2009). 'Ethylene stimulation of latex production in *Hevea brasiliensis*' *Plant Signal Behaviour*, 4(11): 1072-1074

Appendices

A.1 Primers

Table A1: List of oligonucleotides used for cloning and sequencing

Construct	Primer	Sequence 5' - 3'
35S:HRT2-YFP	*XbaI* FWD	CTATAGCTAGACCTAAAATCATGACC
	HRT2…YFP RVS	CTCCTCGCCCTTGCTGCCCATTTTTAAGTATTCCTTATGTTTC
	HRT2…YFP FWD	GAAACATAAGGAATACTTAAAAATGGGCAGCAAGGGCGAGGAG
	SacI RVS	CTATAGCTAGACCTAAAATCATGACC
35S:YFP-HRT2	*XbaI* FWD	CAGATATCTAGAATGGGCAGCAAGGGCGAGGAGC
	YFP…HRT2 RVS	CTCACCGTTGTATAATTCCATGATCACCTTGTACAGCTCGTC
	YFP…HRT2 FWD	GACGAGCTGTACAAGGTGATCATGGAATTATACAACGGTGAG
	SacI RVS	CAGATATCTAGAATGGGCAGCAAGGGCGAGGAGC
35S:HRT2-mCherry	*XbaI* FWD	CTATAGCTAGACCTAAAATCATGACC
	HRT2…mCherry RVS	GTCCTCCTCGCCCTTGCTCACCATCTCCTCGCCCTTGCTGCCCAT
	HRT2…mCherry FWD	GAAACATAAGGAATACTTAAAAATGGTGAGCAAGGGCGAGGAGGAC
	SacI RVS	CAGATATCTAGAATGGGCAGCAAGGGCGAGGAGC
35S:mCherry-HRT2	*XbaI* FWD	CAGATATCTAGAATGGTGAGCAAGGGCGAGGAGGAC
	mCherry…HRT2 RVS	CTCACCGTTGTATAATTCCATCTTGTACAGCTCGTCCATGCCGC

	mCherry…HRT2 FWD	GCGGCATGGACGAGCTGTACAAGATGGAATTATACAACGGTGAG
	SacI RVS	CAGATAGGATCCTTACTTGTACAGCTCGTCCATGCCG
35S:SRPP-GFP	*XbaI* FWD	CAGATATCTAGAATGGCCGAAGGCGA
	SRPP...GFP RVS	CTCCTCGCCCTTGCTCACCATGCTGGAAACAAGTGGCATG
	SRPP...GFP FWD	CAATCCATGCCACTTGTTTCCAGCATGGTGAGCAAGGGCGAGGAGCTGTTC
	SacI RVS	CAGATAGAGCTCTTACTTGTACAGCTCGTCCATGC
35S:GFP-SRPP	*XbaI* FWD	CAGATATCTAGAATGGTGAGCAAGGGCGAGGAGCTG
	GFP…SRPP RVS	CGTTTCCTTCGCCTTCGGCCATCTTGTACAGCTCGTCCATGCCGAG
	GFP…SRPP FWD	CTCGGCATGGACGAGCTGTACAAGATGGCCGAAGGCGAAGGAAACG
	SacI RVS	CAGATAGAGCTCTCAGCTGGAAACAA
35S:REF-mCherry	*XbaI* FWD	CAGATATCTAGAATGGCTGAAGACGAAGACAACCAAC
	REF…mCherry RVS	GTCCTCCTCGCCCTTGCTCACCATATTCTCTCCATAAAACACCTTAG
	REF…mCherry FWD	CTAAGGTGTTTTATGGAGAGAATATGGTGAGCAAGGGCGAGGAGGAC
	BamHI RVS	CAGATAGGATCCTTACTTGTACAGCTCGTCCATGCCG
35S:mCherry-REF	*XbaI* FWD	CAGATATCTAGAATGGTGAGCAAGGGCGAGGAGGAC
	mCherry…REF RVS	GGTTGTCTTCGTCTTCAGCCATCTTGTACAGCTCGTCCATGCCGC
	mCherry…REF FWD	GCGGCATGGACGAGCTGTACAAGATGGCTGAAGACGAAGACAACC
	BamHI RVS	CAGATAGGATCCTCAATTCTCTCCATAAAACACCTTAG
35S:HevNogo-CFP	*XbaI* FWD	CAGATATCTAGAATGGATTTGAAACCTGGAG

	HevNogo…CFP RVS	CTCCTCGCCCTTGCTCACCATCTAACCATAATTTTGCTGCAC
	HevNogo…CFP FWD	GTGCAGCAAAATTATGGTTAGATGGTGAGCAAGGGCGAGGAG
	SacI RVS	CAGATAGAGCTCCTAACCATAATTTTGCTGCAC
35S:CFP-HevNogo	*XbaI FWD*	CAGATATCTAGAATGGTGAGCAAGGGCGAG
	CFP…HevNogo RVS	CTCCAGGTTTCAAATCCATCTTGTACAGCTCGTCCATGCCG
	CFP…HevNogo FWD	CGGCATGGACGAGCTGTACAAGATGGATTTGAAACCTGGAG
	SacI RVS	CAGATAGAGCTCTTACTTGTACAGCTCGTCC
35S:HevNogoΔTM1-CFP	ΔTM1 FWD	AAACGCTATGGAGCCCTC
	ΔTM1 RVS	ATGTAGAGTACGCCACAG
35S:HevNogoΔTM2-CFP	ΔTM2 RVS	GGAGTTCTCAAGACAAACAAG
	ΔTM2 FWD	AACTTTAGAAATTTGGTAAGCTTC
T7:HRT2-YFP-CBD	*NheI* FWD	CAGATAGCTAGCATGGAATTATACAACGGTGAGAG
	XhoI RVS	CAGATACTCGAGTTAGATCACCTTGTACAGCTCGTC
T7:GFP-SRPP-CBD	*NheI* FWD	CAGATAGCTAGCATGGAATTATACAACGGTGAGAG
	EcoRI RVS	CAGATAGCTAGCATGGAATTATACAACGGTGAGAG
T7:REF-mCherry-CBD	*NheI* FWD	CAGATAGCTAGCATGGCTGAAGACGAAGACAACCAAC
	EcoRI RVS	CAGATAGAATTCTTACTTGTACAGCTCGTCCATGCCG
T7:HRT2-myc-CBD	*NheI* FWD	CAGATAGCTAGCATGGAATTATACAACGGTGAGAG
	XhoI RVS	CAGATAGCTAGCATGGAATTATACAACGGTGAGAG
	myc (1) RVS	GATGAGTTTTTGTTCTTTTAAGTATTCCTTATG

T7:HevNogo-myc-CBD	*NheI* FWD	CAGATAGCTAGCATGGATTTGAAAC
	XhoI RVS	CAGATACTCGAGCTGTACCATAATTTTGCTG
	myc (1) RVS	GATGAGTTTTTGTTCTGTACCATAATTTTGCTGC
PTXB1 myc and *SapI* addition	ptMYCSap1RVS(1)(*)	CAGATAGCTCTTCCGCACAGATC
	ptMYCSap1RVS(2)(*)	CACAGATCCTCTTCTGAGATGAGTTTTTGTTC
PTXB1 T3C Mutation	FWD	TGCGGAGATGCACTAGTTG
	RVS	GATGCACAGATCCTCTTC
HRT2 Gateway Entry	attb1 FWD	AAAAAAGCAGGCTTCATGGAATTATACAACGGTGAGAG
	attb2 RVS	CAAGAAAGCTGGGTCTTTTAAGTATTCCTTATGTTTC
	attb2 RVS (no stop codon)	CAAGAAAGCTGGGTCTCATTTTAAGTATTCCTTATGTTTC
SRPP Gateway Entry	attb1 FWD	AAAAAAGCAGGCTTCATGGCCGAAGGCG
	attb2 RVS	CAAGAAAGCTGGGTCTCAGCTGGAAACAAG
	attb2 RVS (no stop codon)	CAAGAAAGCTGGGTCGCTGGAAACAAG
REF Gateway Entry	attb1 FWD	AAAAAAGCAGGCTTCATGGCTGAAGACGAAGACAACCAAC
	attb2 RVS	CAAGAAAGCTGGGTCTTACTTGTACAGCTCGTCCATGCCG
	attb2 RVS (no stop codon)	CAAGAAAGCTGGGTCCTTGTACAGCTCGTCCATGCCG
	attb1 FWD	AAAAAAGCAGGCTTCATGGATTTGAAACCTG

HevNogo Gateway Entry	attb2 RVS	CAAGAAAGCTGGGTCTCATGTACCATAATTTTG
	attb2 RVS (no stop codon)	CAAGAAAGCTGGGTCTGTACCATAATTTTG
RBSP Gateway Entry	attb1 FWD	AAAAAAGCAGGCTTCATGTCGGACGAGGAACAC
	attb2 RVS	CAAGAAAGCTGGGTCTTAATTTTTAGGACCAATGTCC
	attb2 RVS (no stop codon)	CAAGAAAGCTGGGTCATTTTTAGGACCAATGTCC
Gateway att (secondary) primers	FWD	GGGGACAAGTTTGTACAAAAAAGCAGGCT
	RVS	GGGGACCACTTTGTACAAGAAAGCTGGGT
35S '*EcoRV*' Primers	35S (Phos) FWD	[5'Phos]ATCGATCTGGATTTTAGTACTGG
	35S (Phos) RVS	[5'Phos]ATCGTACCCCTACTCCAAAAATG
Sequencing Primers	35S FWD	GATATCGTACCCCTACTCCAAAAATG
	35S RVS	CTATAGCTAGACCTAAAATCATGACC
	T7 Universal FWD	TAATACGACTCACTATAGGG
	M13 FWD	GTAAAACGACGGCCAGT
	M13 RVS	AACAGCTATGACCATG
	NogoFWD	CAATGGAGGAGTAATAAAAGGATATACAG
	NogoRVS	CATAAATGTTTCACACCCATATCTTC

A.2 Vector maps

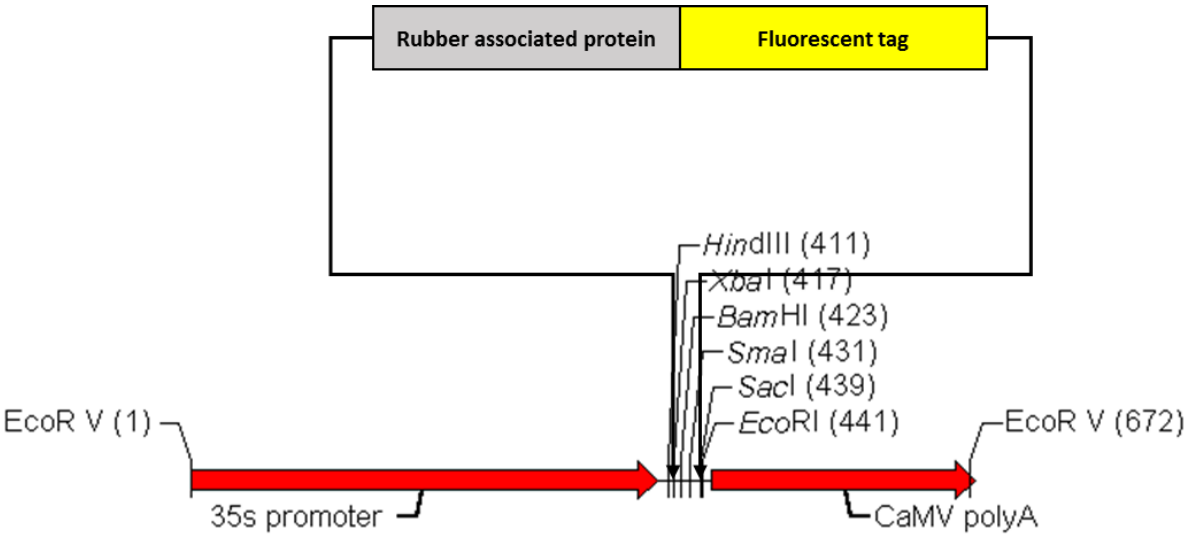

Figure A2 35SCamV Cassette
A 2852bp vector containing ampicillin resistance. Contains a number of cloning sites cloning sites downstream of a 35S promoter and upstream of a terminator. Used for initial cloning of rubber associated products and for sub-cloning into pGreen vector. Rubber associate protein constructs were generally cloned into Xba1 and Sac1 sites. Image taken from www.pGreen.ac.uk

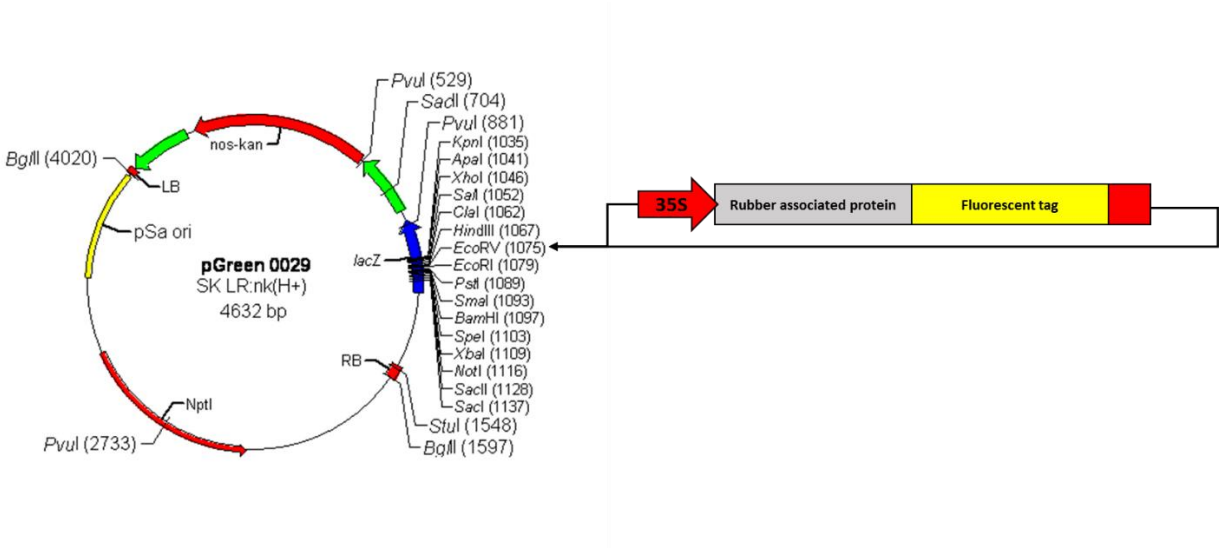

Figure A3 pGreenII-0029
A 4632bp plant binary transformation vector with kanamycin resistance and a pSA replication origin. Contains a number of cloning sites. EcoRV was used to clone the 35S: rubber associated construct. The vector was transformed into *A. tumefaciens* and used to transform *N. benthamiana* leaf epidermal cells. Image taken from www.pGreen.ac.uk

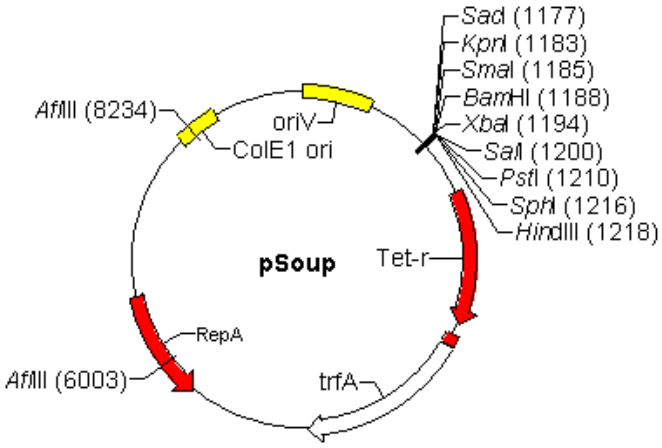

Figure A3 pSoup
A 9274bp plasmid containing tetracycline resistance. A helper plasmid for pGreen which contains the gene coding for pSA replicase which acts upon the pSA replication origin of pGreen. pGreen can only replicate in the presence of pSoup. Image from www.pGreen.ac.uk

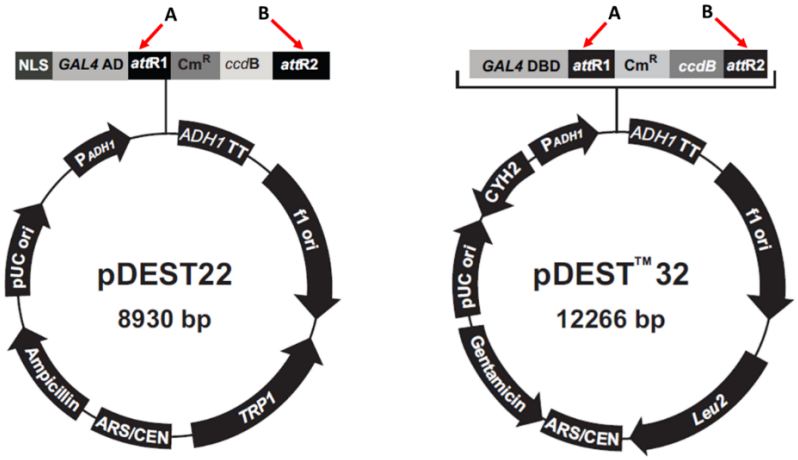

Figure A4 pDEST 22 and pDEST32

pDEST 22: A 8930bp yeast expression vector containing ampicillin resistance and TRP1 gene for tryptophan synthesis. The gene of interest is cloned via the use of gateway technology, from an entry vector, at gateway recombination sites attR1 (A) and attR2 (B). This is downstream of a GAL4-AD. Image taken from Invitrogen 'ProQuest™ Two-Hybrid System' manual

pDEST 32: a 12266bp yeast expression vector containing gentamicin resistance and Leu2 gene for leucine synthesis. The gene of interest is cloned via the use of gateway technology, from an entry vector, at gateway recombination sites attR1 (A) and attR2 (B). This is downstream of GAL4-BD. Image taken from Invitrogen 'ProQuest™ Two-Hybrid System' manual

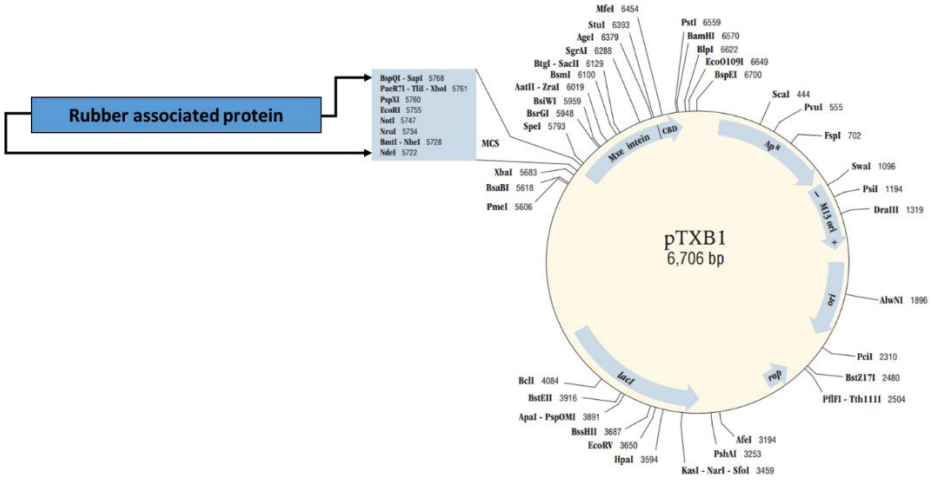

Figure A5 pTXB1

A 6706bp *E. coli* expression vector containing ampicillin resistance. Contains multiple cloning sites and the rubber associated gene of interest was inserted downstream of T7 promoter and. The Sap1 site was used to clone the 3' end of the insert in frame with and adjacent to the downstream intein tag and CBD. Image from the NEB™ IMPACT™ Kit: Instruction manual.

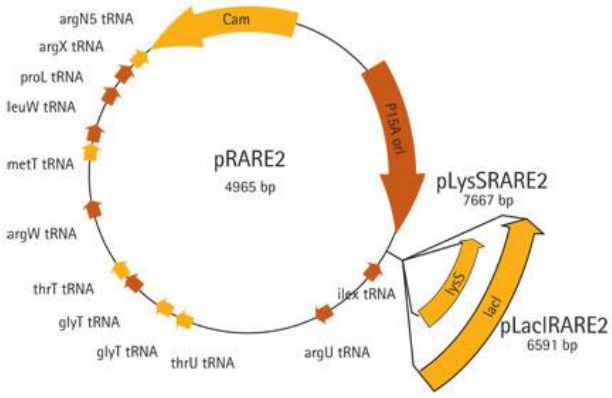

Figure A6 pRARE contained within C43 and C41 Rosetta™ *E. coli* cells

A 4965bp helper plasmid for protein expression containing chloramphenicol resistance. Contains tRNA genes for codons that are rare in *E. coli*.

A.3 HevNogo Cloning

>scaffold_161569.fa_seq
GTTATCATTTTCTTCAATTTCTGTGGCGTACTCTACATCTTCTTGTCAGCTTATGGTACCTTCAAGTTAGTAT
GGTCCAAATGATCGAAGGCTTTCTAATCTCTAGTGGACTTGTGAAACGCTATGGAGCCCTCGATATTGACAAG
GTCCGGTACCTTGCCATTGTGGTAGATAGTGAAGAAGCTTACCAAATTTCTAAAGTTATTCAGCTTTTGAAAT
GGGTGGAAGATATGGGTGTGAAACATTTATGCCTCTATGATTCAAAAGGTAAGTATGAGGATACTCAGTGAAA
CTGAGCAGTTGAGGACATTCTTTCACTATTTATTGATTTTACCGTTGCTCGTAAACATATGGAGATTACATTA
AACTCTTTCAATTTAAAATAGTGTGTTTTTGAACTTCTTTTTTCTTATAGGAGTTCTCAAGACAAACAAGAAA
ACCATCATGGAGAGTTTGAACAATGCTATGCCATTTGAGGTATTATTTTCTATTTATATGATATTTTTTCTTT
TATTTATCAGTTTCCCGACATTCATGGATAGAATTTATGTTTACGTGGTGAGGCTGCTTGGCTCACATGTGAT
TTTGATTAGGCTGCCCTTTTAGGAACTTGCGTAACTGGTCTTACCATCTGGTTTTATAGGAAGCAGTTGAAAA
AGATGTTTTACTGGACCAGAAACAGATGACTGTGGAATTTGCTTCCACTCCGATGGAAAGGAAGCAATAACCA
GGGCAGCTAACGTACTCTTTATGAAGTATTTGAAGTATGCTAAAACTGGTGTAGGAAAGGAAGAACCATGCTT
TACAGAAGATCAAATGGATGAGGCACTAAAAGCTATAGGTTTGTCTTACTTCTTGGATATATGCTGAATGGTT
TAGGAGATTGATCTCTTTTCAAAATTTGATTTTATACTTAATTGGGAATTGATGTTCTTATGCAATCATCAGG
TTACAAAGGGCCGGAACCTGACTTGCTATTAATTTATGGACCTGTTAGATGCCATCTAGGTTTCTCACCGTGG
AGACTTCGATATACTGAGATGGTGTAAGTGTTCTGATTCAATAGGTTGATCAAGTTAGTGGCATTAATTTTGT
CAGTTATTCCATTTGGCTGTTAAAGCTGGGGTATCATAGCTATTTCAAATTATACTGCCAGTTCAAGGTGAAG
GAAATGTTTCCACATGAAGCCAAATACTTCATGGTTCATACTTCATACTTCTTTGGTGGATGGTACATCTGAC
ATTGCACCCATCAATCATTCTTGTTCTCCTTCTCTTCAACAGTCAACAGCATTCAACTTAATTGATAGTATGA
AGTCTTAATTTATAATATGAAATCAGCTATTAATTTTAGATTTTATTTTGTTTCTCTTTTTGATAGGAGAACT
CAACAATGATTAAAATGTTAATATCTGCCATTTTTCTGTTTGTGGTTGTTGTAAGTTGGAGGGGCATGTAAAA
ATATTAACTAAGTTCTGGATGATGTTCTTTGGAAAGTTTAATGTGTTATTAACATATCATCTTAGTTGTGAAA
TTGACAGGGTTTGAAACTCGACAATTTGTNNNNNNNNNNNNNNNNNNNNNNNNNNNNNNNNNNNNNNNNNN
NNNNNNNNNNNNNNNNNNNNNNNNNNNNNNNNNNNNNNNNNNNNNNNNNNNNNNNNNNNNNNNNNNNNNN
NNNNNNNNNNNNNNNNNNNNNNNNNNNNNNNNNNNNTTTTACTTTGGGTGTGCATGTTGTGTCGATTGGTTTGG
GGAGGGAGAGAGAGAGAGAGAGAATATGGAGTGTGACCAGCAAAGATTTAGATAGCTTATTTTTTTGCAAGAT
TAAGTTTTTTTTTTTTTTTTTACTGCATTCAATTTCCTGCTTTTAGATATTGATTTCGGAATAAACTTTTTAAT
TGAACGTCTTCATTCTCAATATTTTAGCATTGTGGGATCTTCCTCATCTACCTTGCTTGGATGTTCTGCAACT
TCACTATTATGTCATTTCAAAGCTTTGCATTTTTTGGTCTAAATTGTGTTCTATTTTGTGTTACAGGCATATG
GGACCCTTGAGGTACATGAACCTCGGTTCACTAAAAAAGGCCATTCACAGGTTCACAACAGTGCAGCAAAATT
ATGGT

>scaffold_161569.fa_seq

ORF					Homology		Identity		
ORF	Frame	Size (amino acids)	Start(n)	Stop(n)	Match	Organism	%	Amino Acids	Accession No.
1	(+)2	74	1838	2121	PREDICTED: nogo-B receptor isoform X2	Nicotiana sylvestris	71%	20/28	XP_009763832.1
					PREDICTED: nogo-B receptor isoform X2	Brassica rapa	71%	20/28	XP_009148511.1
2	(-)3	74	1509	1733	no match	n/a	n/a	n/a	n/a
3	(+)3	72	72	290	PREDICTED: dehydrodolichyl diphosphate syntase complex subunit NUS1 isoform X4	Jatropha curcas	70%	46/66	XP_012069755
					(ALSO ISOFORMS X1-X3)	Jatropha curcas	n/a	n/a	n/a
					PREDICTED: nogo-B receptor-like	Eucalyptus grandis	63%	39/62	KCW70589.1
4	(+)1	53			hypothetical protein ADIS_2422	Cyclobacteriaceae bacterium AK24	38%	15/39	EON77112.1
5	(-3)	49	96	245	no match	n/a	n/a	n/a	n/a
6	(+)3	46	1182	1322	no match	n/a	n/a	n/a	n/a
7	(+)1	39	751	870	hypothetical protein POPTR_0004s16020g	Populus trichocarpa	54%	21/39	XP_006384501.1
					Nogo-B receptor	Gossypium arboreum	53%	20/38	KHG20634.1
8	(+)3	37	936	1049	PREDICTED: nogo-B receptor-like isoform X2 [Solanum tuberosum]	Solanum tuberosum	70%	26/37	XP_006367462.1
					PREDICTED: nogo-B receptor-like isoform X1 [Solanum tuberosum]	Solanum tuberosum	70%	26/37	XP_006367461.1
					PREDICTED: dehydrodolichyl diphosphate syntase complex subunit NUS1 isoform X2	Solanum lycopersicum	70%	26/37	XP_004241992.1
9	(+1)	36	256	366	no match	n/a	n/a	n/a	n/a
10	(-)3	34	1350	1454	no match	n/a	n/a	n/a	n/a

Figure A7 Nucleotide sequence of scaffold_161569.fa_seq and ORF annotation
Scaffold is from the TARRC *Hevea* genome database, and was annotated using NCB1 ORF Finder and BLAST using ORF as queries.

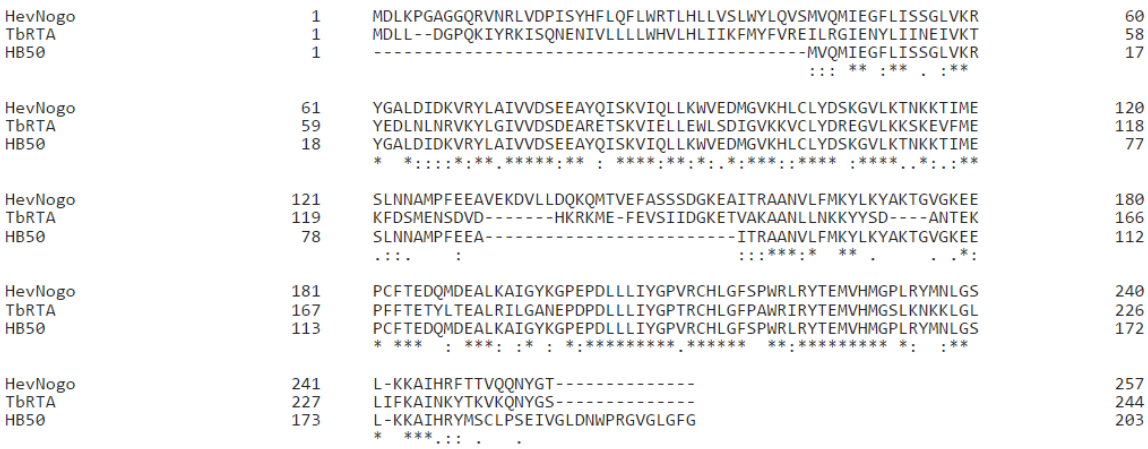

Figure A8 Alignment of TbRTA, HB50 and complete HevNogo Sequence
HB50 was identified from the TARRC protein database. Based on sequence alignment with other CPTL proteins it was thought to be missing the N' terminus. Further sequencing of the genome reveals the 'missing' terminus which was a similar length to TbRTA.

A4 Pyrophosphatase assays

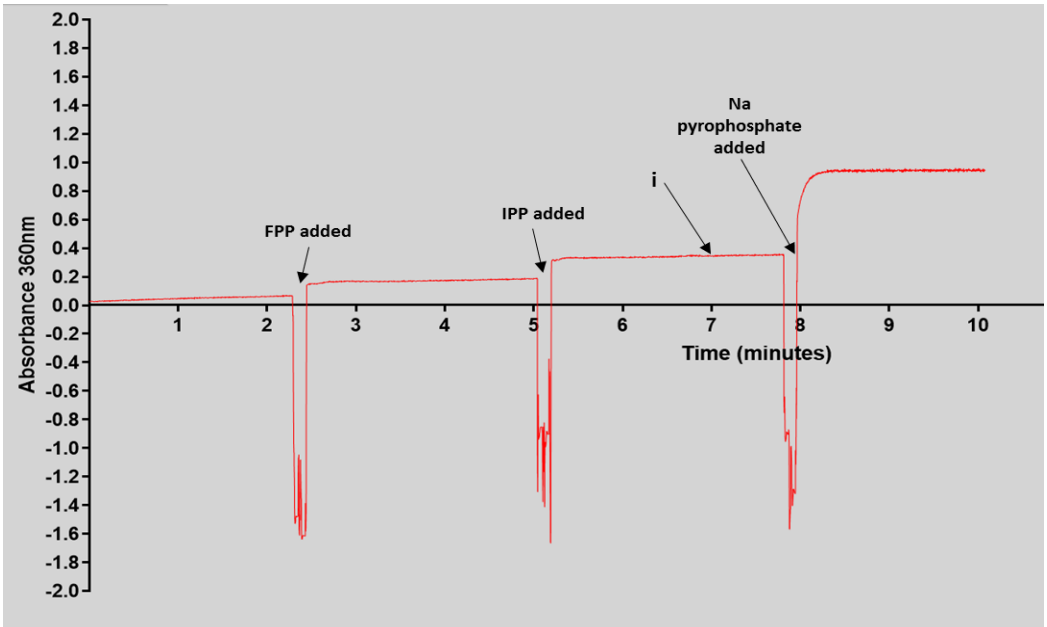

Figure A9 FPP and IPP contain free phosphates that must be controlled for in the final assay

The initial reaction mix was added to a quartz cuvette. After ~2 minutes FPP was added and after ~5 minutes IPP was added. An increase in absorbance was observed a result of free phosphates in IPP and FPP being converted by PNP. The new baseline (i) was used for any subsequent experiments. To check that the components in the mix was not being used up by the phosphates in IPP and FPP substrates Na pyrophosphate was added as a positive control resulting in a large increase in absorbance.

Plant Mol Biol
DOI 10.1007/s11103-016-0462-y

The *Hevea brasiliensis* XIP aquaporin subfamily: genomic, structural and functional characterizations with relevance to intensive latex harvesting

David Lopez[1] · Maroua Ben Amira[1] · Daniel Brown[2,7] · Beatriz Muries[3] · Nicole Brunel-Michac[1] · Sylvain Bourgerie[4] · Benoit Porcheron[5] · Remi Lemoine[5] · Hervé Chrestin[6] · Ewan Mollison[7] · Alessandra Di Cola[7] · Lorenzo Frigerio[2] · Jean-Louis Julien[1] · Aurélie Gousset-Dupont[1] · Boris Fumanal[1] · Philippe Label[1] · Valérie Pujade-Renaud[1,8] · Daniel Auguin[4] · Jean-Stéphane Venisse[1,9]

Received: 14 October 2015 / Accepted: 25 February 2016

Abstract X-Intrinsic Proteins (XIP) were recently identified in a narrow range of plants as a full clade within the aquaporins. These channels reportedly facilitate the transport of a wide range of hydrophobic solutes. The functional roles of XIP *in planta* remain poorly identified. In this study, we found three XIP genes (*HbXIP1;1*, *HbXIP2;1* and *HbXIP3;1*) in the *Hevea brasiliensis* genome. Comprehensive bioinformatics, biochemical and structural analyses were used to acquire a better understanding of this AQP subfamily. Phylogenetic analysis revealed that *Hb*XIPs clustered into two major groups, each distributed in a specific lineage of the order Malpighiales. Tissue-specific expression profiles showed that only *HbXIP2;1* was expressed in all the vegetative tissues tested (leaves, stem, bark, xylem and latex), suggesting that *HbXIP2;1* could take part in a wide range of cellular processes. This is particularly relevant to the rubber-producing laticiferous system, where this isoform was found to be up-regulated during tapping and ethylene treatments. Furthermore, the XIP transcriptional pattern is significantly correlated to latex production level. Structural comparison with *So*PIP2;1 from *Spinacia oleracea* species provides new insights into the possible role of structural checkpoints by which *Hb*XIP2;1 ensures glycerol transfer across the membrane. From these results, we discuss the physiological involvement of glycerol and *HbXIP2;1* in water homeostasis and carbon stream of challenged laticifers. The characterization of *HbXIP2;1* during rubber tree tapping lends new insights into molecular and physiological response processes of laticifer metabolism in the context of latex exploitation.

Keywords XIP aquaporin · *Hevea brasiliensis* · Latex · Evolution · Glycerol · Cell homeostasis

Electronic supplementary material The online version of this article (doi:10.1007/s11103-016-0462-y) contains supplementary material, which is available to authorized users.

✉ Daniel Auguin
auguin@univ-orleans.fr

✉ Jean-Stéphane Venisse
j-stephane.venisse@univ-bpclermont.fr

[1] Clermont Université, Université Blaise Pascal, INRA, UMR 547 PIAF, BP 10448, 63000 Clermont-Ferrand, France

[2] School of Life Sciences, University of Warwick, Coventry CV4 7AL, UK

[3] Institut des Sciences de la Vie, Université catholique de Louvain, 1348 Louvain-la-Neuve, Belgium

[4] Laboratoire de Biologie des Ligneux et des Grandes Cultures, Université d'Orléans, UPRES EA 1207, INRA-USC1328, 45067 Orléans, France

[5] Ecologie, Biologie des Interactions, Equipe SEVE, UMR 7267 CNRS/Université de Poitiers, Bâtiment B31, TSA 51106, 86073 Poitiers Cedex 9, France

[6] Institut de Recherche pour le Développement, UR060/CEFE-CNRS, 1029 route de Mende, 34032 Montpellier, France

[7] Biotechnology Unit, Tun Abdul Razak Research Centre, Brickendonbury, Hertford, UK

[8] CIRAD, UMR AGAP, 63000 Clermont-Ferrand, France

[9] Campus Universitaire des Cézeaux, 8 Avenue Blaise Pascal, TSA 60026, CS 60026, 63178 Aubiere Cedex, France

Published online: 11 April 2016

Introduction

Of all the rubber-producing plants of substantial economic value, *Hevea brasiliensis* remains the world's sole commercial source of natural rubber thanks to its high yields and ease of harvest. Natural rubber, which consists mainly of *cis*-1,4-polyisoprene biopolymer, is highly valued due to its unrivalled biochemical and physical properties (Cornish 2001). Rubber biosynthesis occurs in latex, the milky cytoplasm of laticifers, highly specialized anastomosed cells forming a distinct network in the phloem tissues of the rubber tree (Hagel et al. 2008). Latex is harvested by a process known as tapping, which consists of regularly incising the trunk bark to cut through the laticifer network. This allows latex to flow out through the wound to be collected and later processed into natural rubber. Tapping is repeated regularly, so an important limiting factor of natural rubber yield is latex regeneration. Regeneration relies on both complex rubber biosynthesis pathways in laticifers, and on water and various organic sources such as sucrose and nitrogen supplied to these cells by the surrounding parenchyma (Tungngoen et al. 2009). The biological mechanisms underlying the latex biosynthesis pathways and the artificial outflow of latex from injured trunks (both qualitatively and quantitatively) are not yet fully understood. However, the global economic importance of natural rubber justifies thorough investigation of these physiological processes.

Ethylene pretreatments (using the ethylene releaser Ethrel®) are commonly used to ease latex flow and stimulate the regeneration metabolism, allowing higher yields of latex production (Coupé and Chrestin 1989; Zhu and Zhang 2009). However, both ethylene pretreatments and repeated tapping are liable to affect ionic and water homeostasis, causing the depletion of organic resources, and potentially undermining the integrity of the exploited trees (d'Auzac et al. 1997). Molecular homeostasis is the process by which cells regulate vital parameters, i.e. turgor, fluid balance, pH and energy levels. As part of the water homeostasis process, the concentrations of various solutes (or osmolytes/electrolytes) are co-regulated. Osmolytes help to ensure the maintenance and recovery of vital homeostasis conditions (Parida and Das 2005). In particular, specific osmolytes such as sugars and sugar alcohols (cyclic or acyclic) may be diverted from the overall carbon metabolism to participate in these homeostatic adjustments (Hare et al. 1998). Sucrose loading of laticifers is an extremely important process, as it supplies the acetate pool, which provides the energy for the cell to function properly, and which is crucial for *H. brasiliensis* as it initiates the biosynthesis of isoprene chains and thereby rubber biosynthesis (Dusotoit-Coucaud et al. 2009; Chow et al. 2007, 2012). Some latex carbohydrates are thought to act as protective osmolytes but this has not yet been demonstrated (Dusotoit-Coucaud et al. 2010b). Glycerol, identified as an essential osmolyte for yeast, bacteria and animals, may be one candidate. Information on its protective role in plants remains scant (George et al. 2011; Hasegawa et al. 2000; Eastmond 2004), although some dedicated channels (aquaglyceroporins or aquaporins) have been well documented (Zardoya et al. 2002). There is no information on the presence and putative osmotic regulating role of glycerol in latex-producing plants. It is thus of interest to characterize the molecular players in water and organic solute transport, notably glycerol, which is involved in global cell homeostasis maintenance, and aquaglyceroporins (or aquaporins, AQP) which are likely candidates for adjusting hydric and electrolyte status, since both water and glycerol are transported by these channels.

Aquaporins are integral membrane proteins of the Major Intrinsic Protein (MIP) multigene family. They are specialized channel proteins that allow rapid selective transport of water and diverse small neutral solutes across the lipid bilayer (Li et al. 2013; Chaumont and Tyerman 2014). They are ubiquitous in all living systems, consistent with their fundamental role of homeostasis. In plants, AQPs are remarkably diverse. Their classification, based on their sequence comparison and sub-cellular localization, is well established. Typically, AQP are clustered into seven subfamilies (Anderberg et al. 2012). One of these recently characterized subfamilies is designated X-Intrinsic Protein (XIP) (Danielson and Johanson 2008). The presence of XIP appears to be shared by a narrow range of living organisms including protozoa, fungi, and some non-vascular and vascular *Viridiplantae* (Danielson and Johanson 2008; Gupta and Sankararamakrishnan 2009; Lopez et al. 2012). Although XIPs show sequence differences from other MIPs, overall their structure remains highly conserved. Like MIPs, they are composed of six transmembrane helices (TMH1-6) connected by five loops (LA-E), and two membrane-embedded short half-helices facing each other named hemipore-1 (TMH1-3, LA-C) and -2 (TMH4-6, LD-E). These hemipores are buried inside the membrane and virtually constitute a seventh helix added to the above 6 TMH bundle. Each contains the conserved MIP asparagine-proline-alanine (NPA) signature sequence. These motifs are embedded in the lipid bilayer and form a narrow hydrophilic path (Murata et al. 2000). Each hemipore is contiguous with N- and C-terminal ends facing the cytoplasmic side of the membrane. As usually observed in most plant AQPs, these helix–helix interface regions show small weakly polar amino acid residues (Wallace and Roberts 2004). A second feature in common with MIPs is the aromatic/

arginine (ar/R) constriction region composed of four amino acid residues (R1-R4) found in TMH2 (R1), TMH5 (R2), and loop E (R3 and R4), which forms a selectivity filter contributing to a size exclusion barrier and a hydrogen bond acceptor and donor continuum needed for the efficient transport of substrates (Murata et al. 2000). At present, the few biological functions clearly assigned to XIP remain hypothetical (Bienert et al. 2011; Lopez et al. 2012; Park et al. 2010; Giovanetti et al. 2012; Zhang et al. 2013; Reuscher et al. 2013; Venkatesh et al. 2013; Yue et al. 2014; de Paula Santos Martins et al. 2015). However, the fact that tobacco *Nt*XIP1;1 appears to be located at the plasma membrane of epidermal and parenchyma cells (Bienert et al. 2011), together with its putative function of allowing the diffusion of certain polar solutes across the membrane suggests that XIP may represent significant cellular checkpoints (like other MIP) for controlling cellular permeability and osmolarity.

Research programs studying the characterization of metabolic pathways responsible for latex biosynthesis, outflow and regeneration, especially in the case of ethylene-stimulated latex production, are rapidly expanding (Chow et al. 2007; Tang et al. 2013; Chao et al. 2015; Wei et al. 2015; An et al. 2015). One of the major topics is ethylene-stimulated latex production and the study of various trans-membrane transporter families. In the latter field, it was shown that the expression of AQP *HbPIP2 s* and *HbTIP1;1* (Tungngoen et al. 2009, 2011; An et al. 2015) and of the sucrose transporters *HbSUT1B* (=*HbSUT3*) and *HbPLT2* (Dusotoit-Coucaud et al. 2010a, b; Tang et al. 2010) were stimulated in the latex following ethylene treatments correlating with yield increase. Since ethylene tends to induce a concomitant dilution of latex, the hydric homeostasis of the laticifers in and near the tapping cut is severely challenged.

The aim of this study was first to investigate the composition of the whole XIP subfamily in *H. brasiliensis* in terms of protein structure, subcellular localization and functional properties, the latter by testing the ability of some of its members to enable water and glycerol to diffuse. In the context of rubber tree production, we focused on the stress-induced XIP isoform, *HbXIP2;1*. We then characterized its contribution to the molecular response during ethylene stimulation and tapping of *H. brasiliensis*, to assess its potential role in the regulation of glycerol and water homeostasis in the physiological context of intensive latex production. Lastly, we discuss our findings with a special focus on glycerol and its potential role as a general stress osmo-protectant and organic source of carbon, and then on the physiological significance of aquaporin permeability to glycerol, which remains poorly understood *in planta*.

Materials and methods

Plant material

Plant material used for monitoring the modulated XIP expression in challenged trees came from field experiments carried out at the Bongo/SAPH plantation (Ivory Coast) (Dusotoit-Coucaud et al. 2010b). Latex and bark samples were collected from trunks of 2 independent mature PB217 rubber trees (10 years old), industrially harvested for 2 years. Trees had been regularly tapped (three times per week) without Ethrel® stimulation for 3 months and left untapped for 1 week before Ethrel® treatment and the first sample collection. The latex samples were collected as described by Pujade-Renaud et al. (1994). Plant material used for monitoring the constitutive XIP expression in various vegetative organs came from 3 independent untapped PB217 rubber trees (6 years old) grown in a controlled-environment greenhouse (Blaise Pascal University, Clermont-Ferrand, France) under a 16 h light/8 h dark photoperiod, at 18/22 °C (night/day), with a relative humidity set at 80 ± 10 %.

Genomic DNA extraction, amplification PCR and cloning

XIP genomic sequences from *H. brasiliensis* (PB217) were cloned by PCR with degenerate primers and RACE methods, according to manufacturer's protocols (Invitrogen, Carlsbad, USA). Genomic DNA was extracted from 0.25 g of leaves using the CTAB method (Doyle and Doyle 1987). The 500 bp up- and downstream proximal non-coding regions from the start and stop codons for each *HbXIP* gene were targeted using the primer sets detailed in Supplementary Tab S2. Primers were designed from XIP sequences identified from the *H. brasiliensis* unpublished genome sequence information (TARRC). PCR was performed using 0.5U of platinum *Taq* DNA polymerase (Invitrogen, Saint Aubin, France), and amplicons were cloned into the *p*GEM®-T Easy vector (Promega, Madisson, WI, USA), and sequenced on both strands.

RNA extraction and quantitative RT-PCR

Total RNA from latex and bark sampled from plantation trees were obtained by Dusotoit-Coucaud et al. (2010a). Real-time PCR was performed using a MyiQ instrument (Bio-Rad) with MESA GREEN qPCR MasterMix Plus (Eurogentec) containing 2 µl of 20-fold diluted cDNA. Calculations of the differential accumulation of genes in response to stress (standardized with unstressed samples at t_0) were carried out with the $2^{-\Delta\Delta Ct}$ equation according to

Pfaffl's procedure (2001). Constitutive assessment of gene expression between vegetative organs was plotted on a percentage scale. In our experimental conditions, the arbitrary value of 100 corresponds to a C_t value of 19, the highest gene expression level in *H. brasiliensis*; the arbitrary value of 0 is related to C_t corresponds to a C_t value of 37, a non-accumulation of transcript. PCR efficiency was 100 ± 3 % for all primer pairs. Primer specificity and amplification efficiency were verified for each gene by both melting curve analysis (after 40 cycles) and TAE/2 % agarose gel electrophoresis. Normalization of the target gene expression was achieved using three housekeeping genes (*HbAct*, *HbCYP* and *HbUBQ)* chosen from a panel of widely used housekeeping genes (Li et al. 2011) using the software application BestKeeper v1 (Pfaffl et al. 2004). These genes were chosen from different protein families in order to reduce the risk of co-regulations. All the primers used for this study were designed with the Primer3plus application (Untergasser et al. 2007) and detailed in Supplementary Tab S2. qPCR analyses were carried out in triplicate from each biological samples. For statistical analysis, aquaporin steady-state gene expression levels were computed by one-way analysis of variance (ANOVA) followed by a Tukey's honest significant difference (HSD) post hoc test ($p < 0.001$).

In silico bioinformatics analysis

The *Hevea* XIP subfamily was explored in silico using described heterologous XIP sequences (Lopez et al. 2012) as initial queries. tBLASTn (Altschul et al. 1997) was used against several genome resources: the non-redundant generalist databases National Center for Biotechnology information (NCBI) and the *Hevea* genomic databank generated from *H. brasiliensis* clone RRIM 928 provided by the TARRC (Tun Abdul Razak Research Centre, Hertford, United Kingdom, http://www.tarrc.co.uk). *Viridiplantae* XIP sequences were retrieved from NCBI and Phytozome portals from different plant species: two basal embryophyte phyla with the lycophyte *Selaginella moellendorffii* and the avascular bryophyte *Physcomitrella patens*, a basal eudicot phylum with the Ranunculales *Aquilegia cærula*, and several core eudicot phyla with a selection of rosid and asterid species. Special attention was paid to the rosid phylum (with APG III as repository; Chase and Reveal 2009), for which a maximum number of Malpighiales XIP sequences were collected (Supplementary Tab S1). Percentages of amino acid similarity and identity were calculated using the BLAST algorithm. The unrooted phylogenetic tree was constructed with 61 protein sequences using the maximum likelihood method implemented in the PhyML program v3.0 (Guindon and Gascuel 2003). The maximum likelihood analyses were performed with the Jones–Taylor–Thornton evolutionary model using 1000 bootstrap replicates to assess the reliability for degree of support for each internal branch on the phylogenetic trees. Trees were viewed and edited with TreeDyn (Chevenet et al. 2006), and bootstrap values <60 % were discarded. The data for the three XIP sequences mentioned for this work can be found in the GenBank data library under the accession numbers KT071670 (*Hb*XIP1;1), KT071669 (*Hb*XIP2;1) and KT071668 (*Hb*XIP3;1). All accession numbers for sequence dataset reported herein are listed in Supplementary Tab S1.

XIP structure modeling

*Hb*XIP2;1 models were obtained using a standalone version of the I-TASSER (Iterative Threading ASSEmbly Refinement) program suite (V3) (Zhang 2008; Roy et al. 2010; Yang et al. 2015). Tetramer modeling consisted of a superimposition of four monomers on a tetramer template structure (pdb code 2b5f) followed (to remove any possible intermolecular bump) by a single minimization stage diverting the CHARMM-GUI online input generator program from its original aim (Jo et al. 2008; Brooks et al. 2009). Alternate conformations for loop D that suited tetramer formation by clearing off the required interface were previously found using modeller 9.13 (Webb and Sali 2014) as embedded in UCSF Chimera macrocommand 'refine loops' (Yang et al. 2012). The MOLE 2.0 program (Sehnal et al. 2013) was used to delineate, and characterize in terms of physico-chemical properties the channels along the aquaporin structures. The glycerol molecule was placed according to the I-TASSER binding site prediction. APBS (Adaptive Poisson-Boltzmann Solver) (Baker et al. 2001) was used with the PARSE forcefield (Tang et al. 2007) on PDB2PQR generated files (Dolinsky et al. 2007) out of the submitted coordinates to calculate the electrostatic potentials. PyMOL (DeLano 2004) was used to analyze and illustrate the molecular structures and models.

Yeast expression for monitoring of water and glycerol transport assays

Transcripts of *HbXIP2;1* and *PtPIP2;8* as positive control of water transporter (*P. trichocarpa*, Potri.005G109300) were cloned in *p*YX212 (specific PCR primers detailed Supplementary Tab S2). For water measurement assays, transfected yeast strains were grown on synthetic minimal medium (uracil-deficient SC medium) supplemented with glucose, at 30 °C overnight. For the yeast labeling and fluorescent experiments, transfected yeast cells were previously loaded for 30 min at room temperature with 5(6)-carboxyfluorescein diacetate *N*-succinimidylester (CFSE; Sigma, France) (40 µM in buffer A: Tris–HCl 50 mM pH

8.0, 0.5 M NaCl). A simplified technique was used to monitor cell volume changes induced by osmotic shocks, as described by Soveral et al. (2007). Experiments were performed on a POLARstar Omega fluorimeter (BMG Labtech, France). In each assays 50 µL of labeled cells was mixed with an equal volume of hypo- (buffer A) or iso-osmotic (buffer A without NaCl) solutions. Four runs were done. Following optimization, the increased fluorescence intensities of the intact cells were recorded at 0.2 s. Results were expressed as a percentage increase compared with measured fluorescence at t_0 (i.e. before osmotic shock) and set at 100 %. For the glycerol transport assays, the yeast strain JT4014 (*fps1::leu2* in JT100) kindly provided by Dr. J. Thevelein (Katholieke Universiteit Leuven, Belgium) was used. The ability of yeast strain to grow under osmotic stress (1 M sorbitol) was assessed on solid synthetic minimal medium supplied with 1 M sorbitol. After inoculation, plates were incubated for 5 days at 30 °C. Cell growth comparison, for the same dilution factor, revealed growth rate gain or loss. Radiolabeled glycerol uptake assays were performed by a modified method of Anderca et al. (2004). Yeast cells transfected with either empty (*p*YX212) or integrating *HbXIP2;1* gene (*p*YX212-*HbXIP2;1*) were cultivated in synthetic minimal medium. At t_0, 100 µL of cells in MES buffer was diluted with 100 µL of MES buffer containing 2 mM [^{14}C]-glycerol (0.14 µCi). Assays were repeated three times. Results are expressed as difference in radioactivity measured between 10 min and 20 min of incubation.

Confocal microscopy

The cDNA encoding *HbXIP2;1* was fused to the 3′ end of the cDNA of YFP (lacking its stop codon) by fusion PCR, resulting in a YFP-*HbXIP2;1* translational fusion. The fusion was inserted into the Xba*I*–Sac*I* sites downstream of the CaMV 35S promoter of vector *p*GREEN0029 (Hellens et al. 2000) using the primers listed in Supplementary Tab S2. The construct was introduced into *Agrobacterium tumefaciens* C58 and used for agroinfiltration of leaf epidermal cells as described previously (Sparkes et al. 2006). After 3 day of incubation, leaf segments were incubated with 8 µM FM4-64 for 10 min, and the abaxial epidermal cells visualized by confocal microscopy with a Leica TCS SP5 microscope (Leica, Germany). YFP was excited at 514 nm and detected in the range 525–550 nm, FM4-64 was excited at 514 nm and detected in the range 616–645-nm.

In situ hybridization

Fresh stems were harvested, cut and immediately fixed in FAA (3,7 % (v/v) formaldehyde, 50 % (v/v ethanol, 5 % (v/v) acetic acid) at 4 °C overnight. Fixed samples were dehydrated and progressively embedded in paraffin (Paraplast, Sigma-Aldrich, St Louis, MO, USA) (Brunel et al. 2002). Transversal section 10 µm thick were cut with a rotary microtome (HM 340E, Microm International GmbH, Walldorf), mounted on Polysine slides (O. Kindler GmbH, Freiburg, Germany) and dried at 42 °C for 1 day for in situ mRNA localization according to Dusotoit-Coucaud et al. (2010a). Gene-specific RNA probes were designed to be located in the variable 3′UTR region of *HbXIP2;1* transcripts with an average size of 229 ribonucleotides (primers detailed in Supplementary Tab S2). DNA coding the probes were cloned in *p*GEM® T-Easy vector (Promega). Sense and antisense digoxigenin (DIG)-labeled RNA probes were synthesized as described in Brunel et al. (2002). Stem sections were incubated overnight at 50 °C with 1.5 ng µl^{-1} of either sense or antisense probes and leaf sections with 3 ng µl^{-1}. Digoxigenin-labeled probe was detected using anti-digoxygenin alkaline phosphatase conjugate (Sigma-Aldrich), followed by colorimetric detection of phosphatase activity using an AP conjugate substrate kit (Bio-rad Hercules, CA, USA). After suitable color development, the reaction was stopped by rinsing with water, and sections were dried and mounted in Eukitt (Euromedex, Mündelsheim, France). Observations were performed with an Axioplan 2 microscope (Zeiss, Jena, Germany). Data were recorded on a digital camera (AxioCam HR, Zeiss) using Axiovision digital imaging software.

Results and discussion

To date, among the few sequenced genomes of *H. brasiliensis* (Müll. Arg.), only one draft genome sequence has been published (Rahman et al. 2013). The sequence information used in this study was obtained from a second draft genome generated by the Malaysian Rubber Board (unpublished results). A first sequence dataset from this draft genome showed it to contain genes encoding the four orthodox subfamilies of aquaporins (PIP, TIP, NIP and SIP; unpublished results). A previous study of MIP from this species focusing on PIP and TIP subfamilies (Tungngoen et al. 2009) demonstrated their capacity to allow water diffusion across biological membranes, with mRNA expression patterns correlating with those of sucrose transporters. It was hypothesized that these proteins were key players in modulating the efficiency of latex outflow in mature rubber trees challenged by tapping and hormone treatment. Among these proteins, MIP may aid water circulation between latex cells and liber/xylem tissues inherent to a coordinated liber tissue turgor and an active sucrose mobilization (Dusotoit-Coucaud et al. 2010a, b;

Tungngoen et al. 2011). Here we show that *H. brasiliensis* possesses at least three MIP members belonging to the *X*-Intrinsic Proteins subfamily. Only one member appears to be transcribed, together with other PIP or sucrose transporters, with expression profiles correlating with the latex outflow from exploited rubber trees. This plant species and the particular physiological context lent by its growing and exploitation conditions thus offer an interesting and original viewpoint for further exploration of this XIP subfamily.

Isolation and bioinformatics analysis of three *Hevea brasiliensis* XIP members

HbXIP genes and protein analysis

A first full-length cDNA encoding an *XIP* gene was preliminarily isolated from *H. brasiliensis* leaf tissues, and named *HbXIP2;1* (KT071669), based on phylogenetic data (as explained below) and BLAST comparison with identified XIP from poplar. An analysis of the XIP subfamily across rosids plant species to show that several isoforms are usually present (Gupta and Sankararamakrishnan 2009; Lopez et al. 2012). However, searches in various expression datasets revealed that very few XIP members are expressed, in contrast to other MIP subfamilies in which most members are expressed, confirming an earlier evolutionary hypothesis of possible loss of expression/function for some XIP (Lopez et al. 2012; Venkatesh et al. 2015).

Two other partial *HbXIP* isoforms named *HbXIP1;1* (KT071670) and *HbXIP3;1* (KT071668) were cloned from *Hevea* genomic DNA using degenerate primers designed from highly conserved regions of XIP orthologs from *Malpighiales* (Supplementary Tab S1). *HbXIP1;1* and *HbXIP3;1* full-length sequences were completed from the *Hevea* genomic databank made available by the TARRC Institute. The proposed nomenclature for *Hb*XIP sequences has been established based on the phylogenetic analyses (Fig. 1a) as previously proposed by Lopez et al. (2012) and in full accordance with the conventional MIP nomenclature (Johansson et al. 2001).

HbXIP(1-2-3);1 genes encode polypeptides of 289, 305 and 308 amino acids residues respectively (Fig. 1b; Supplementary Fig. S1). Predicted peptide sizes and molecular masses (Supplementary Fig. S2) are consistent with most reports on aquaporins, which generally range from 270 to 360 AA and 26 to 35 kD (Gomes et al. 2009). *HbXIP* share a similar exon–intron structure with their plant cognates from the same phylogenetic clade: *HbXIP1;1* presents two exons, and *HbXIP(2-3);1* three exons (Fig. 1b). All introns are systematically positioned upstream of the first transmembrane helix (TMH1), and exhibit the classic canonical dinucleotides GT and AG for donor and acceptor splice sites. This exon/intron organization is shared by plants belonging to the same phylogenetic clade, as observed for each MIP subfamily (Johansson et al. 2001). Exons are conserved within each XIP sub-group (60–80 % similarity, Supplementary Fig. S2) in regard to introns that exhibit strong variability in lengths and nucleotide sequences (±45 % similarity). Overall, the genomic architecture of the XIP subfamily appears to be conserved among most *Viridiplantae*, and could be considered *de facto* as a plant lineage specific profile.

HbXIP phylogenetic analysis

The unrooted tree confirmed that XIP clearly diverge from other MIP subfamilies (represented here by *Hb*PIP1;1 and *Hb*PIP2;1, as outliers) (Fig. 1a). All the XIP members fall into three independent monophyletic master clusters. Cluster I groups orthologous members from moss and spikemoss, which are basal to all other XIP. Clusters II and III group all XIP from the Tracheobionta taxon. Cluster II includes sequences from the Rosanae taxon exclusively, and Cluster III encompasses sequences from the Rosanae and Asteridae taxons. These four branches present strong bootstrap supports of 100, 94, 89 and 97 %, respectively. The *Hb*XIPs are integrated into polyphyletic groups belonging to Clusters II (for *Hb*XIP1;1) and III (for *Hb*XIP2;1 and *Hb*XIP3;1). Interestingly, *Hb*XIP2;1 and *Hb*XIP3;1 are clustered together in a distinct clade exclusive to the Rosanae phylum with a significant bootstrap support of 72 %. In Cluster III, XIP from asterid plant species form a specific clade (bootstrap support of 94 %). Finally, all identified *Hb*XIPs share the shortest distance with the milky-sapped tropical shrub *Manihot esculenta*, another latex-producing *Euphorbiaceae* species. This is consistent with the eudicotyledonous placement of *Hevea* in the order Euphorbiales based on chloroplast gene phylogeny (Tangphatsornruang et al. 2011). The clade that includes *Hb*XIP2;1 includes XIP sequences from *Euphorbiaceae* only, such as *M. esculenta*, *Ricinus communis*, *Jatropha curcas*, *Plukenetia volubilis* and *Euphorbia esula*. Also, *Hb*XIPs fall into distinct monophyletic clades within paraphyletic master clusters (II and III). This indicates that XIP from these clades are closely related, consistent with previous work (Lopez et al. 2012; Venkatesh et al. 2015).

The XIP are considered as a singular MIP sub-family. Sequence analysis confirms that XIP display an original plant taxa-organized pattern of evolution while maintaining species-specific structural features such as the exon–intron splicing junctions. All this suggests that XIP sequences are closely inter-related, and points to possible evolution from a common ancestor.

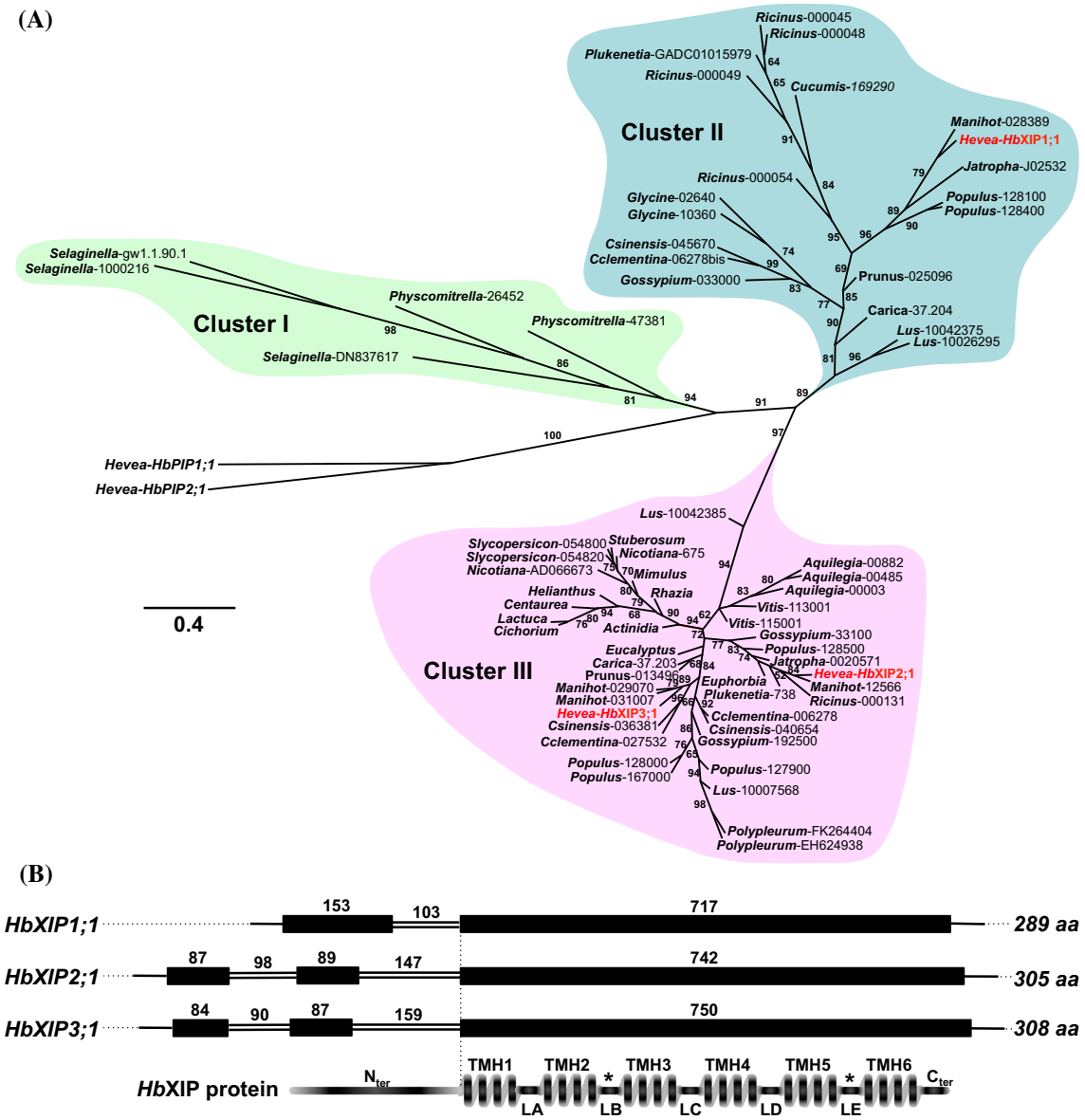

Fig. 1 Valuer's *Hb*XIP subfamilly. **a** Unrooted phylogeny of XIP protein sequences from *H. brasiliensis* and selected *Viridiplantae*. Numbers at the nodes represent percent of bootstrap values (above 60 %) based on 1000 reassembling. The distance scale denotes the evolutionary distance expressed in number of amino acid substitutions per site. The three *Hevea* XIPs sequences are highlighted in *red*. The colored clusters mark the three major XIP phylogenic subdivisions of *Viridiplantae*. Species and accession numbers are listed in Supplementary Tab S1. *Hb*PIP1 and *Hb*PIP2 sequences from *H. brasiliensis* were introduced as outliers. **b** Schematic representation of the three *HbXIP* genes including exons (*solid line*), introns (*double line*), number of nucleic acids for each segment, and corresponding amino acid number. *Hb*XIP protein structure is detailed with the six putative trans-membrane helices (TMH), the five inter-helice loop regions (LA–LE) and the terminal segments (N_{ter} and C_{ter}). AQP signature NPAs are included within loop B (*LBα_{NPA1}) and loop E (*LEα_{NPA2}). Details of the *Hb*XIP genes and protein sequences are available in Supplementary Fig. S1 and S2

Conserved functional roles of XIP in the MIP superfamily suggested by a comparative analysis, modeling by homology, and in vivo functional tests

In contrast to PIP sequences, little is known to date about XIP function, and particularly about the effective regulation sites in their primary sequence directly involved in their transport activities. In addition, XIP from different plant species are reported to show some contrasting transport functionalities (Bienert et al. 2011; Lopez et al. 2012). Clearly, *Hevea* XIP fit the conventional topology of the MIP superfamily (Supplementary Fig. S3A). However, when XIP amino acid sequences are compared with *So*PIP2;1 from *Spinacia oleracea*, Törnroth-Horsefield

et al. 2006), new distinctive structural features that could affect the structure and/or the diffusion function of MIP emerge (Fig. 2; Supplementary Fig. S3BC). They were sustained through a realistic view of their three-dimensional organization. This work mainly addresses the characterization of the *Hb*XIP2;1 isoform, since this is the only *Hb*XIP transcribed in our biological conditions.

General shape of XIP cavity

The structural analysis of MIP has so far helped to determine or understand key features of their solute transport capacity, supported by what is already established for other members. Beyond their conserved 3D shape in the superfamily, three structural signatures located within or near the cavity, namely NPA signatures, the aromatic/Arg filter and Froger's signature, have been commonly used to associate the channel with a particular transport.

*Hb*XIP comprises six membrane-spanning α-helical regions (TMH1 to TMH6), separated by five hydrophilic loops (LA–LE) (Fig. 1b). The N- and C-terminal ends of the protein face the cytoplasmic side of the membrane. The subcellular localization of YFP-*Hb*XIP2;1 fusion in tobacco leaf epidermal cells by agroinfiltration lends direct support to this membrane prediction (Fig. 3). A substantial signal is located at the plasma membrane, and this result confirms the *Nt*XIP1;1 location already reported by Bienert et al. (2011). However, in our experiments, we observed an additional fluorescence at the nucleus and the endoplasmic reticulum (i.e. endomembrane system). Whether this signal is not an artefact, this unexpected endomembrane system fluorescence identified for *Hb*XIP2;1 is interesting, and suggests a possible recruiting system based on intracellular membrane trafficking to modulate the cell permeability to particular osmolytes, in this case between cytosol and a part of the morphoplasm. Such a localization pattern deserves more thorough exploration. Of the five hydrophilic loops, LB and LE present the highest level of similarity between XIP counterparts (Fig. 2, Supplementary Fig. S3A). Structural analysis shows the presence of two hemipores that face each other inside the membrane, forming an iconic hourglass-like shape (Fig. 2, Supplementary Fig. S4). These two inner protrusions pointing into the core of the protein structure, also named the "aquaporin fold" (Murata et al. 2000), are part of the archetypal MIP structure. They contain the two conserved NPA (Asn-Pro-Ala) signatures, which are located at the center of the monomer pore and intervene in the channel interior constriction as part of a solute and/or water selectivity filter (Chaumont et al. 2005). The first NPA exhibits the less conserved sequence <N/S-P-L/I/V/A>, and the second motif harbors the conserved residues <N-P-A>. A fine reading of a complete XIP alignment shows that the NPA motifs are integrated within a larger conserved region: <P-ψ-S/T-G-G-H/F-ψ-N/S-P-ψ/T> for the first NPA motif, and <G-ψ-G/S-ψ-N/S-P-A/S-R–C-ψ>for the second one (where ψ is typically a hydrophobic residue) (Lopez et al. 2012). These regions constitute remarkable hallmarks that quickly discriminate XIP members from among other MIP counterparts.

The aromatic/Arg (or ar/R) filter is composed of four residues. Given their position in the pore constriction region (Fig. 2, Supplementary Fig. S3A), and their predictive intrinsic physicochemical behaviors, they have been considered as co-defining the substrate selectivity (Sui et al. 2001; Forrest and Bhave 2008). The *Hb*XIP ar/R tetrad signature harbors specific plant XIP profiles including TMH2(F81I/F81V)-TMH5(H210I/H210T)-LBα_{NPA1}(T105T/T105S)-LEα_{NPA2}(R225) residues.

In general, each MIP subfamily exhibits specific variations in the amino acid composition of NPA motifs and ar/R filter (Anderberg et al. 2011; Hove and Bhave 2011), some of which could provide spatial compensations in terms of both occupancy and physicochemical properties. Such amino acid substitutions within the pore should thus be considered as key features accounting for major evolutionary changes in the protein's functional fate. Plant XIPs exhibit some specific features within the predicted pore regions, suggesting a discrimination between two sister groups, Clusters II and III, where different residues can be found at specific positions: TMH2 (F *vs.* I/V) and

Fig. 2 I-TASSER model comparison of *Hb*XIP2;1 **(b, d, f)** with the high resolution structure of *Spinacia oleracea So*PIP2;1 **(a, c, e)** in the opened state. **a**, **b** The tetramers are shown with one of the four subunits highlighted in a *bright color* (*magenta* for *So*PIP2;1 and *green* for *Hb*XIP2;1). A grid, calculated with MOLE 2.0, covers the course of the transported molecules within the pore. By analogy with the structure of *So*PIP2;1, for which the position of a cystine at the extracellular space is shown, a plausible intermolecular disulfide bridge is proposed involving the N-terminal extremity of TM5, since it is compatible in terms of distance according to the model. The electrostatics calculated with APBS (using the PARSE forcefield) for both channels (**c**, **d**) are displayed at the surfaces of the pores. The positions involved in the constitution of the pores are drawn and labeled with a balls-and-sticks representation. A charge gradient appears to be orientated from acid (*red*) to basic (*blue*) following a vertical direction from into out in both cases. The changes in polarity index and the pore dimensions are drawn in a diagram built (**e**, **f**) on MOLE 2.0 raw data (the letter *o* in *red* next to the amino acid name indicates the major contribution of the backbone carbonyl group). The *indices* indicate a more polar vestibule of the inner side for *Hb*XIP2;1 than for *So*PIP2;1 over the first third of the course, but afterwards the orders of magnitude are comparable with only few subtle differences. The pore diameters along the channel are very close in both cases. **g** Trace representation of the superimposition performed by Mustang of *Hb*XIP2;1 with the high resolution structure of *So*PIP2;1. Residues at similar positions surrounding the pore are revealed in wireframe. Figure 2 is offered in high-definition format in the Supplementary Fig. 10

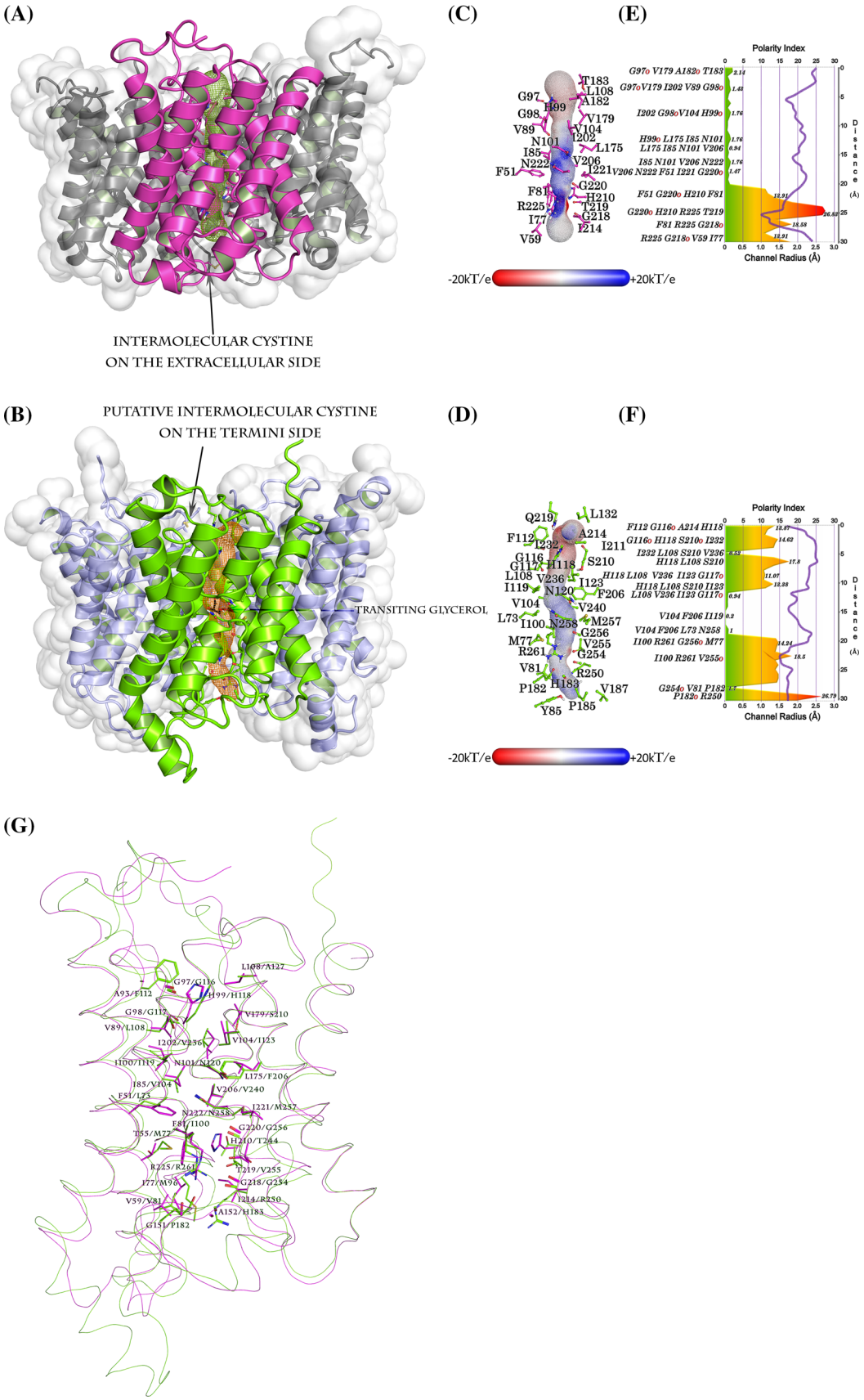
(A)
INTERMOLECULAR CYSTINE
ON THE EXTRACELLULAR SIDE
(B)
PUTATIVE INTERMOLECULAR CYSTINE
ON THE TERMINI SIDE
TRANSITING GLYCEROL
(C)
(D)
(E)
(F)
Polarity Index
Channel Radius (Å)
Distance (Å)
-20kT/e
+20kT/e
(G)

TMH5 (H *vs.* T/I). Taken together, the duet histidine (TMH5) and arginine (LEα_{NPA2} position) are typical of water-specific PIP2 structure (as observed for *Hb*PIPs), both providing donor hydrogen bonds for water molecules. The backbone also contributes to the hydrogen bond acceptor network along the channel in correspondence with several positions of the highly conserved embedded loops (SGG motif on LBα_{NPA1} or G/P on LC).

Like other plants XIPs, the surrounding residues lining the lumen of the cavity at its entrance display a slightly less polar profile near the ar/R filter compared with other *Hevea* or plant MIPs (Fig. 2c–f). According to some authors, this moderately hydrophobic feature could favor the transport of polar uncharged molecules such as glycerol, urea, and metalloids, but not permeability to water (Bienert et al. 2011; Lopez et al. 2012). We also note that XIP ar/R resembles some *Hevea* NIP and TIP (data not shown). Both are able to transport these bulky molecules, but interestingly have been shown to have weak or no permeability to water (Dynowski et al. 2008; Bienert et al. 2011; Lopez et al. 2012). Accordingly, there is an ongoing debate concerning probable functional redundancy between these sub-families that occurred during plant evolution, especially since XIP seem to have disappeared from several plant genomes such as coniferophyts, monocotyledons, and various dicotyledons such as *Arabidopsis* (Gupta and Sankararamakrishnan 2009; Bienert et al. 2011; Anderberg et al. 2012; Venkatesh et al. 2013). This assumption incurs the risk of it becoming a commonly used truism to definitely explain the discontinuous presence of XIP in the plant kingdom. More recently, Abascal et al. (2014) advanced a potential deep orthology between XIP, HIP, TIP and AQP8, and that speciation events would have expunged some MIP subfamilies between reign and/or organisms. Clarifying the physiological benefits that XIP confer to organisms will help to answer this paradoxical question.

Finally, five other residues (P1-P5 positions also called Froger's signature) are usually predicted to play a functional role in MIP activity. The diversity at these positions between MIP subfamilies has been correlated to substrate selectivity, discriminating orthodox "water channel" aquaporins (AQPs) from "glycerol transporter" aquaglyceroporins (GLPs) (Froger et al. 1998; Lagree et al. 1999). For XIP, Froger's signature contains a number of hydrophobic amino acids with P1(V160/M)-P2(C262)-P3(A266/S)-P4(F280)-P5(W281) residues (positions numbered according to *Hb*XIP2;1), suggesting a transport of bulky hydrophobic molecules (Gupta and Sankararamakrishnan 2009). However, we parse this motif for *Hb*XIP2;1 cautiously (Supplementary Fig. S5). The remote location of the above residues from the cavity suggests that (even for P2, the only nearby constriction site) they may not play this role, but instead a mechanical one, probably through involvement in the placement of the alpha helix bundle.

Physicochemical environment of the XIP cavity

Notwithstanding the involvement of these structural checkpoints regarding the potential XIP channel specificity as a whole, they may play their full role when combined with other factors such as physicochemical conditions or dedicated regulatory effectors. 3D structure prediction is the easiest reliable alternative to experimental structure resolution, especially when membrane proteins are concerned (Du et al. 2015). Fortunately, high-resolution structures of AQPs are available and can be used as templates for a homology study approach (Yang et al. 2015). *Hb*XIP2;1 structure was therefore modeled with I-TASSER software using *So*PIP2;1 as reference. The scores provided by the program indicate that the modeled coordinates are satisfactory: notably, the C-score (estimating the quality of the prediction) is 0.88, suggesting a good level of confidence in the prediction (the normal range of C-scores being between −5 and 2). A further analysis driven with MolProbity (Chen et al. 2010) indicates that the model lies within the acceptable range in terms of geometry for an aquaporin. Compared with the 3.90 Å resolution structure of *So*PIP2;1 (pdb:2b5f) the proportion of dihedral angles to be within the favored Ramachandran limits is slightly higher (86.56 *vs.* 72.65 % for chain A of 2b5f) and the proportion of residues to be outside those limits (or Ramachandran outliers) is smaller (3.95 *vs.* 9.4 % for chain A of 2b5f). To sum up, 96.1 % (244/254) of all residues are in the allowed regions for the model, whereas this is the case for only 90.6 % (212/234) of all the residues of the structure. Concerning the rotamer evaluation, values of the same order are reached for both cases (82.59 % for the *Hb*XIP2;1 model *vs.* 77,84 % for chain A of 2b5f are within the favored limits). Superimposition shows that the *Hb*XIP2;1 modeled channel resembles that of *So*PIP2;1 with only a few differences in amino acid composition (Fig. 2g, Supplementary Fig. S3B). This suggests that the evolutionary distance between plant PIPs and XIPs is short, but this serves yet again to prove the existence of a potential deep orthology connection between a specific protein subfamily (i.e. XIP) and its superfamily (i.e. MIP) (Abascal et al. 2014).

PIP and XIP differences mostly comprise changes at four positions around the pore bottleneck: L175/F206, F51/L73, F81/I100 and H210/T244. The mutations of the first two positions tend to compensate for each other, but taken together, the last two are mostly responsible for both a larger diameter and a lower polarity index at the constriction zone for *Hb*XIP2;1 (Fig. 2e, f). The last remarkable change with a possible incidence on transport

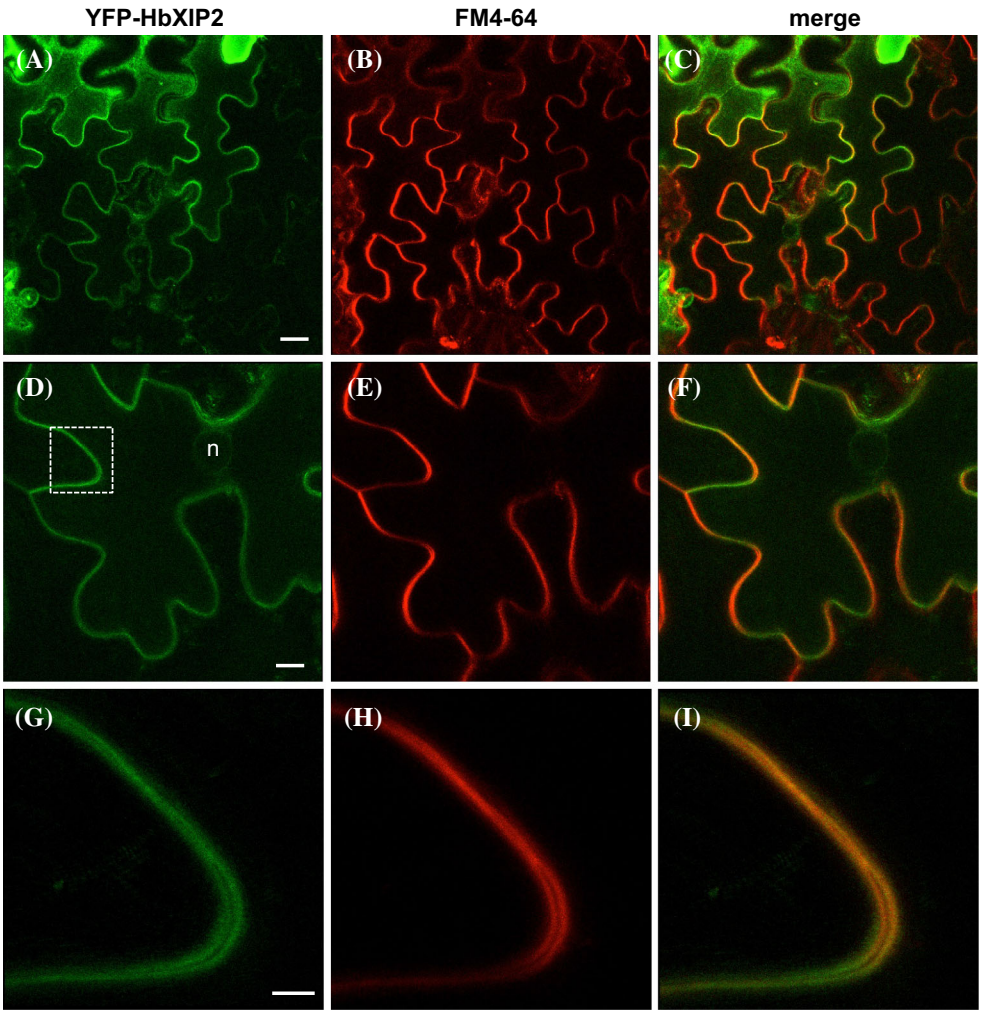

Fig. 3 Subcellular localization of *Hb*XIP2;1. Tobacco epidermal leaves were infiltrated with agrobacteria carrying the 35S::YFP-*HbXIP2;1* expression construct. After a 3-day incubation, leaf segments were incubated with plasmalemma probes FM4-64 for 10 min and the abaxial epidermal cells visualized by confocal microscopy. *Scale bars*, 20 µm (**a–c**), 10 µm (**d–f**), 5 µm (**g–i**). Panels **g–i** are a magnification of the area delimited by the square in **d.** *n* nucleus

specificity is located at the outer side of the pore with the replacement of an isoleucine (I214 in *So*PIP2;1) by an arginine (R250 in *Hb*XIP2;1). Globally, the positive charge borne by the guanidinium group of this residue is nonetheless present in *So*PIP2;1 in the ammonium group of one lysine (K237) located at the external surface of the protein, though not at the immediate perimeter of the cavity.

Aquaporins are capable of tetramerization, suggesting a possible cooperativity by allostery between the subunits with a predictable effect on transport efficiency. With the *So*PIP2;1 structure, X-ray crystallography has demonstrated the presence of a cystine bridging two subunits (Törnroth-Horsefield et al. 2006; Bienert et al. 2012). The authors have investigated the role of this particular bridge and concluded that it lends the complex greater stability. In other words, the organism's fitness to a changing environment might result in a tightening of the composition of the tetramer during the AQP oligomer synthesis in the endoplasmic reticulum. By analogy and because of the high degree of conservation of the C214 present in 23 % of the 70 XIP sequences analyzed (data not shown), the option of an intermolecular cystine (a disulfide bridge linking two cysteine residues) cannot be excluded, but this time in the cytoplasm. According to our model, C214 is easily accessible for disulfide bonding during the dimer association as it faces (and can be close enough to) its reciprocal homologue of the other subunit. This bonding may have an incidence on the movement of two adjacent loops D suspected here of playing a major role in the gating of the pore. This should be confirmed in the future by mutagenesis.

Other putative XIP intra-regulatory elements

In addition to the residues discussed above, a few conserved residues in orthodox AQPs offer promising prospects as co-players involved in solute and ion permeability. To date *Hb*XIP displays at least four features in common with characterized AQPs (Supplementary Fig. S3A): (1) the amino-terminal end di-acidic signal (D/E)-X-(E/D), here predominantly DEE (<Asp-Glu-Glu>) for *Hb*XIP2;1 and *Hb*XIP3;1 respectively, is shared by most plant XIPs belonging to the Cluster II. This motif, frequently found in transmembrane proteins, including AQP, has been assigned a putative function in the export from the endoplasmic reticulum (Nishimura and Balch 1996; Zelazny et al. 2007, 2009). However, besides functioning as a cargo recognition site ER export signals (Barlowe 2003; Sato and Nakano 2007) together with a polylysine motif it could also constitute, in our hypothesis, the docking sites of a partner protein required for modulating the activity of the channel. Docked partners could also further provide an efficient way to control specifically which molecules are to be exported in a coupled protein system. (2) The "Ser115″ located within the first cytoplasmic loop B of the spinach *So*PIP2;1 was characterized in a phosphorylated state, suggesting a role in modulating the water channel activity (Johansson et al. 1998; Nyblom et al. 2009). This residue (either serine or threonine) is also found at the same position in some XIPs, including S134 in *Hb*XIP2;1. The plausible phosphorylation of elements exposed to the cytoplasm is in full agreement with this hypothesis (further detailed in the following section) of a modulator of the opened or closed state (i.e. a kinase). LD bears an arginine (R187) at a mid-position that could find the required counterion to quench its positive charge, thereby sterically closing the inner mouthpiece of the AQP. (3) The "AEF" motif located in TMH1 appears to be highly conserved but its function has not yet been identified (Zardoya and Villalba 2001; Perez Di Giorgio et al. 2014). We believe that it could be considered a structural invariant motif (Chothia 1975) indispensable for proper folding. The glutamate at the second third of TMH1 (in the middle of the "AEF" motif) can be confidently compared to the conserved glutamate at the first third of TMH4 (topological homologue) as both probably help to neutralize the resulting positive charges of the $LB\alpha_{NPA1}$ and $LB\alpha_{NPA2}$ helices protruding inside the hydrophobic core of the AQP. (4) XIP presumably occur as tetramers embedded in the membrane like other known aquaporins. This supports the idea of an allosteric cooperativity between the subunits that could provide another level of osmolarity control for cells (Fig. 2). Mammalian AQP0 has been suggested to function in this way in the eye lens (Reichow and Gonen 2008; Reichow et al. 2013).

In contrast to PIP, the process of identifying some regulation sites appears quite delicate: (1) the histidine H193 located in the PIP loop D and involved in the cytosolic pH-dependent gating is absent in most XIP (including *Hb*XIP2;1) (Tournaire-Roux et al. 2003; Fischer and Kaldenhoff 2008; Frick et al. 2013). For several XIP members (but not for *Hb*XIP2;1), a histidine can be detected upstream of this loop, and its involvement in pH-dependent regulation events needs further analysis. (2) The sites accepting methylation events such as the first Lys and Glu residues located in the N-terminal tail of *At*PIP2;1 do not seem to have emerged spontaneously. However, some residues could offer interesting directions, and need to be biochemically explored (Santoni et al. 2006), (3) Lastly, the motifs potentially targeted by serine or threonine phosphorylation that are located at either ends of some PIP2 s do not appear in XIP (Johansson et al. 1998; Prak et al. 2008), thus suggesting alternative activity regulations.

Validation of the XIP function as channels, and critical examination

All these structural predictions become meaningful particularly when they are in line with functional and biochemical cues. This is especially true since XIP from plants belonging to different clades (Asteranae/Rosanae) are found to exhibit different transport functionalities (Bienert et al. 2011; Lopez et al. 2012). First of all, we show that *Hb*XIP2;1 appears to be localized mainly in the plasma membrane (Fig. 3), suggesting that such a subcellular localization might imply a role for *Hb*XIPs in solute exchange between the cytoplasmic and the extracellular spaces. To assess a potential transporter function, *Hb*XIP2;1 coding cDNA was expressed in *Saccharomyces cerevisiae*, where the ectopic expression of a XIP protein leads to growth cessation (Anderca et al. 2004). Water transport was monitored with *Hb*XIP2;1 transfected intact yeast (strain W303-1A) which was treated with the non-fluorescent precursor CFSE and challenged in a hypotonic solution. A change in fluorescence signal due to cell swelling (water influx) was recorded and compared with strains transfected with the empty *p*YX212 vector as a negative control, or carrying *PtPIP2;8* (*p*YX212-*PtPIP2;8*) as positive control with a functional water channel role (Secchi et al. 2009). As shown in Fig. 4a, a very small increase in cell size and fluorescence signals were measured for *p*YX212-*HbXIP2;1* assay, compared with *p*YX212-*PtPIP2;8* which presented a high water channel activity. The weak signals for *p*YX212-*HbXIP2;1* may reflect background permeability probably due to the yeast membrane itself, as reported previously by Meyrial et al. (2001). Thus we conclude, consistent with what follows, that *Hb*XIP2;1 did not enhance significant osmotic

water permeability and thus cannot be considered as a water channel.

With water transport ruled out, we assessed a possible glycerol transport capability while keeping in view that the sequence between *Hb*XIP2;1 and *Nt*XIP1;1 (an efficient glycerol permease, Bienert et al. 2011) strongly differs (identity of 65 %) (Supplementary Fig S3). A functional assay for glycerol was carried out on the constitutive yeast mutant Δ*fps1* (strain JT4014) lacking the endogenous glycerol transporter FPS1, which complemented by a constitutive expression of an efficient glycerol transporter, exhibits a growth default consecutive to osmotic shock by the use of high concentrations of 1 M sorbitol (Luyten et al. 1995). Qualitative data from intact cell growth assay (Fig. 4b) and semi-quantitative data related to the [^{14}C]-glycerol uptake (Fig. 4c) clearly show that *HbXIP2*-transfected yeast cells take up glycerol significantly faster than mock-transfected cells. This indicates that *Hb*XIP2 acts as a channel protein that facilitates glycerol diffusion, at least in yeast. This result echoes the physiological effect of *At*NIP1 and *At*NIP2 overexpressed in an *FPS1*-defective yeast strain (Weig and Jakob 2000) or *Chlamydomonas reinhardtii Cr*MIP1 (Anderca et al. 2004) as glycerol channels. Taken together, *Hb*XIP2;1 functional data are in line with the transport capabilities of *Nt*XIP1;1 (Bienert et al. 2011). A further crucial aspect highlighted here is that XIP, although they exhibit a strict phylogenetic allocation in a plant lineage fashion (Fig. 1), can deliver contrasting transport abilities at the intra-clade level. *Pt*XIP2;1 and *Hb*XIP2;1, two comparatively closed sequences (79 % identity) found in plant species belonging to the order Malpighiales exhibit differential water transport (Lopez et al. 2012), while two sequences comparatively more divergent sequences (Rosidae *Hb*XIP2;1 *vs.* Asteridae *Nt*XIP1;1, 65 % identity) exhibit common glycerol transport ability. Finally, it suggests that the XIP sub-family is functionally more complex than expected, and that phylogenetic correlations are still often not sufficient to conclude on a specific function between homologs.

Here we consider *Hb*XIP2;1 as a glyceroporin. On the other hand, on the basis of these kinds of observations, this channel is usually considered as the only actor of transport selectivity. Nonetheless, when we compare the central channels for amino acid composition and relative structure between a PIP archetype like *So*PIP2;1 and an XIP model like *Hb*XIP2;1, the difference remains subtle (Fig. 2g, Supplementary Fig. S3B). Even if this finding is based on a modeled structure, the relatively high similarity shared by AQP in general and the quite satisfactory superimposition of the lateral chains of key amino acids (comparing the model with a high resolution structure of AQP) (Supplementary Fig. 3) intervening in particular in the lumen of the pore is still a measure of the reliability of the *Hb*XIP2;1 model. The subtle difference observed may thus suggest that the specificity of the transport does not reside solely in the channel properties. In such a hypothesis, the specificity could more likely arise from other structural elements of the aquaporin interacting with a dedicated partner responsible for the transport selectivity or effectiveness. Water is small and polar, and the two compared channels are both polar and apolar—with a slight difference around the vestibule of the inner side—but with an acid–base gradient

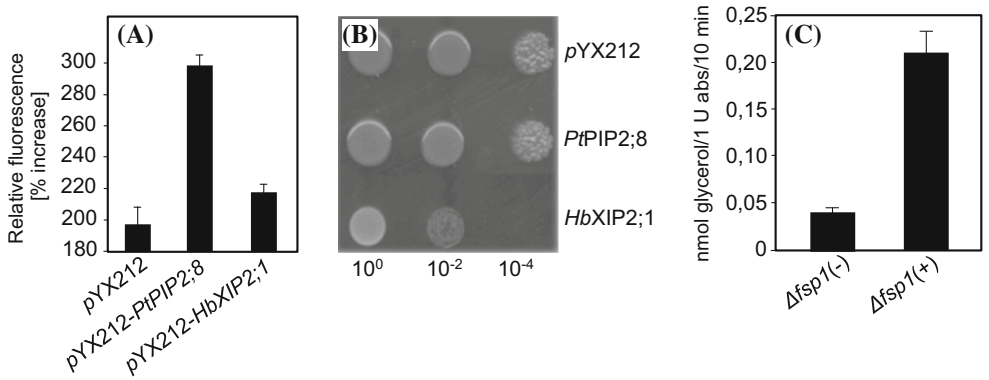

Fig. 4 Osmotic water and glycerol transport assay. **a** Analysis of water transport of *HbXIP2;1* aquaporin expressed in yeast. Relative fluorescence signal obtained after 0.2 s following osmotic shock, for yeast strains expressing *Hb*XIP2;1 and *Pt*PIP2;8 (positive control) are compared with the negative control of cells transformed with empty vector. Cells were loaded with CFSE and subjected to hypo-osmotic shock. The signal obtained corresponded to an average of four individual measures. Data are mean ± SEM (n = 3). **b** Functional complementation of *Dfps1* yeast strain transformed with the centromeric *p*YX212 vector expressing *HbXIP2;1* or *Pt*PIP2;8. Cells were grown on agar plates with synthetic minimal medium (lacking uracil) containing 1 M sorbitol. The initial suspension at 1 unit of A_{600nm}/ml was diluted 1/10 four times. Empty, *Δfps1* transformed with the empty *pYX212* vector; *Pt*PIP2;8, *Δfps1* transformed with *pYX212-PtPIP2;8* cDNA; *Hb*XIP2;1, *Δfps1* transformed with *pYX212-HbXIP2;1* cDNA. **c** Analysis of glycerol transport of *HbXIP2;1* aquaporin by radioactive substrate uptake. Yeast strains (JT4014-*Δfps1*) transformed with *p*YX212-*HbXIP2;1* (+) or the empty vector (*p*YX212: (−)) were assayed for uptake of ^{14}C-glycerol. Data are mean ± SEM (n = 3)

oriented in the same orientation (Fig. 2c–f). In our case, and given the heterologous biological context, *Hb*XIP2;1 lacking effectiveness in water transport could then be ascribed to the absence of a specific regulator dedicated to controlling the aquaporin gating. If we assume that the functioning of an aquaporin can be roughly summarized as the adoption of two limit states or two limit conformations (favored thermodynamically), an opened and a closed form, then the activity of a regulator (*inter alia* the cycling of kinases and phosphatases to change the phosphorylated state of residue participating in a lock with a basic residue, or the influence of a conditional partner on the first helical turn at the amino-terminal of TMH1 displacing a negative charges borne by a largely conserved acid residue) would consist in directing the change of conformation from one to the other. In such systems, the regulator should no longer be neglected and studying the activity of an aquaporin should require identifying that putative essential partners or chaperons. On the way to understanding the mechanism, this latter identification could first be bypassed by using the targeted mutation of key residues involved in the upholding of the gate on a closed state, whose expected consequence would be to clear the way in the central channel for any molecule compatible in terms of size and charge. Even so, to gain a full picture of the sequence of events in the regulation in situ, identification of the regulators is mandatory.

The underlying mechanism (which to our knowledge has not yet been found for the XIP subfamily) implies the movement of mobile portions borne by the aquaporin itself. For instance, in our model of *Hb*XIP2;1 and as previously put forward (Tournaire-Roux et al. 2003), loop D could act as a lid covering up inner mouthpiece. A largely conserved positive residue (K221) rightly placed in the middle of loop D sustains a possible lock secured by pairing with a more static negative charge facing that structural element. This would block free circulation of water as observed in our experimental study. In addition to our hypothesis, both open and closed states were previously observed at atomic resolution for spinach *So*PIP2;1. The closed form results essentially from the presence of a cation (cadmium, probably calcium in situ), which, by neutralizing the negative charges of two carboxylates, stabilizes the first helical turn of TMH1 and indirectly loop D. In such a form, loop D adopts a twisted antiparallel β-hairpin shape, and the aspartate 191 of the RDS motif bridges the displaced lysine of the N-terminal end (direct consequence of TMH1 first helical turn stabilization) leading to the occlusion of the tunnel (Törnroth-Horsefield et al. 2006). This closed conformation supports the authors hypothesis of a hydrophobic gating controlled by the protonation state of a conserved residue, a histidine in the middle of loop D. Beyond its natural pH sensor activity consisting of switching from a charged to a neutral state and vice versa, histidine 193 can interact with a negatively charged residue at the beginning of TMH1 depending on local pH conditions. This can result in placing loop D before the pore and blocking any molecular circulation through it, or instead, moving it away to allow a flow through. Here again, these authors thoroughly tested the implications of histidine 193 and loop D in different conditions and with complementary approaches, leaving less room for doubt about the major role of that loop for that particular aquaporin, *So*PIP2;1. In this light, the absence of an observed water transport for *Hb*XIP2;1 is thus to be taken cautiously and remains to be demonstrated in a native context. In a situation where a closed state is expected, and within the limits of the heterologous system employed to test a transport capability (in others words where dedicated regulators could be missing), it is legitimate to wonder about the observed transport in the case of glycerol. First we note that we are only able to monitor and provoke an "out-to-in" glycerol transport because of experimental limitations. We consider that it is probably directly correlated with the proneness of osmolytes such as glycerol to alter locally by their presence the surrounding solvation enough to favor the opened conformation, which frees the way for glycerol itself and associated water if necessary; while in the absence of glycerol, water fills the entire channel without causing structural distortions to the protein, so that when it is closed, it remains closed. Also in our test, the introduction of 1 mM glycerol in the external medium favors an entering flow, the outer side (or vestibule) of *Hb*XIP2;1 being opened. Once it has entered, because of its size (with a diameter around 3.6 Å in the smallest dimension, while the pore is around 3.0 Å in the narrowest zone) and its relatively extended interaction with the channel, it might induce a conformational change producing allosteric repercussions on the lid position. Certainly, as seen by others in molecular dynamics simulations on aquaglyceroporins, transiting glycerol has no alternative other than to line-up in a single line with water (smaller and interacting with isolated glycerol by establishing H-bonds in a "fluid" of water) in between (Chen 2013). The biological relevance of such a process where an extra osmolyte (higher concentration) may enter the cell by an initially closed aquaporin (to impede water coming out, for instance) could be to ensure prompt equalization of the above osmolyte at both sides of the membrane barrier and inhibit water leak by the same aquaporin at the same time.

On the basis of these structural and functional considerations, elucidation of the physiological role of XIP in plants through in-depth functional studies with XIP variants in key residues will answer these important, still open questions.

Physiological framework for potential *Hb*XIP2;1 involvement

Factual molecular information

For decades pretreatment with the ethylene releaser Ethrel® underneath the tapping cut has been used to stimulate latex production (d'Auzac and Ribaillier 1969). The rubber clone PB217 used in this study is well known for its high yield potential: although it shows a low yield in the absence of ethylene treatment, it can reach high and sustainable production under hormonal stimulation, owing to a strong metabolic activity and a high sugar loading capacity (Fig. 5; Obouayeba et al. 1996; Lacote et al. 2010). The laticifer network in the phloem tissue does not have symplastic connections with the surrounding cells (De Fay et al. 1989). Because of the semi-permeability of the plasma membrane, a controlled transport of water was thought to be involved in the dilution of latex on tapping that is crucial for its fluidity and consequently for the rubber production yield. Previous studies demonstrated that the up-regulation of aquaporins in response to tapping and ethylene treatments might underpin water exchanges between xylem, phloem and laticifer tissues, and thus latex dilution (Tungngoen et al. 2009, 2011; An et al. 2015). Concomitantly, the up-regulation of sucrose and monosaccharide transporter genes in response to the ethylene treatment is thought to increase sugar upload in the laticifers, thus stimulating the rubber biosynthesis pathway and globally latex regeneration while increasing the osmotic force necessary for driving water fluxes (Dusotoit-coucaud et al. 2009, 2010a, b; Tang et al. 2010; Tungngoen et al. 2011).

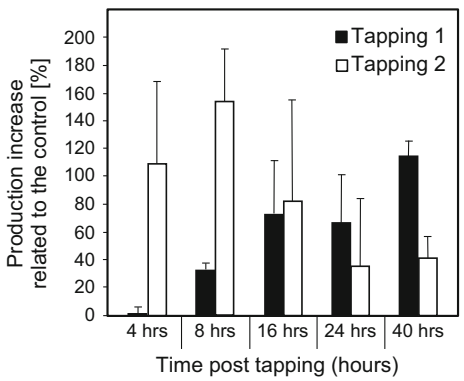

Fig. 5 Latex yield of exploited PB217 clones after ethylene treatment and two consecutive taps. Batches of three homogenous mature trees, regularly tapped for 2 years but left to rest for 3 months, were pretreated with 2 % of the ethylene releaser Ethrel® 4, 8, 16, 24 and 40 h before the first tap (TAP1). After 3 days without treatment, a second tap was performed on the same trees (TAP2). Latex production is expressed in percentage of increased production in relation to unstimulated tree production. The formula used was: Production increase (%) = ((Production of stimulated tree−Production of unstimulated tree)/Production of stimulated tree) × 100. *Bars* represent the biological standard deviation

In the present work, study of XIP members was concurrently conducted with PIP and PLT counterparts, suggesting that XIP may play a role in this scenario. Among the three *Hevea* XIP genes for which expression was monitored by real-time RT-PCR, only *HbXIP2;1* appeared to be expressed. Whatever the physiological conditions and organs, no signal was detected for *HbXIP1;1* and *HbXIP3;1*. *Hb*XIP2;1 transcripts were found in all the vegetative organs examined (Fig. 6a, Supplementary Fig. S6), with an abundant constitutive accumulation in young and mature leaves (dropping drastically in senescent leaves), buds, young developing stem, bark and latex. The accumulation of *HbXIP2;1* transcripts in bark and laticifers was also confirmed by in situ hybridization (Fig. 7, Supplementary Figs. S7 and S8). In addition, XIP seem widely distributed within these organs, corroborating most MIP data showing their ubiquitous behavior between and inside various vegetative organs. Extending our analysis to other MIP genes, we found that the relative proportion of each MIP isoform was largely constant throughout the different tissues, in agreement with previous observations in other ligneous species (Lopez et al. 2012; Yue et al. 2014). Exceptionally, the relative proportion of *HbXIP2;1* transcripts compared with the other MIPs was smaller in roots and xylem. We note that constitutive steady-state levels of *HbXIP2;1* in these organs were very similar to those observed for the most expressed *HbPIP* or *HbPLT* genes (Fig. 6b, Supplementary Fig. S6), including in bark and laticifers. The co-regulation of these transporters suggests a common biological involvement. Thus like most AQP, XIP are ubiquitously and constitutively expressed in vegetative plant tissues, suggesting multiple roles of this subfamily for the plant overall (Bienert et al. 2011); however, in view of the physiological context referred to above, only bark and laticifers will be further discussed.

In a context of exploited rubber trees undergoing simultaneous ethylene treatment and successive tapping, *HbXIP2;1* gene expression was up-regulated with a maximum increase 24 and 8 h after ethylene treatment respectively in latex and bark. This profile was conserved on the second tapping, with even higher expression levels. *HbXIP2;1* expression profile was similar to that of *HbPIP1;1, HbPIP1;3*, *HbPIP2.2* and *HbPIP2;4* in latex, and the four *HbPIP2 s* in bark, which were also up-regulated. Conversely, *HbPIP1;2* was down-regulated in latex, as were *HbPIP2;1* and *HbPIP2;3* in bark (Fig. 8a, b, Supplementary Fig. S9). More interestingly, *HbXIP2;1* expression correlated remarkably well with the kinetics of latex yield of the trees with which the expression analyses

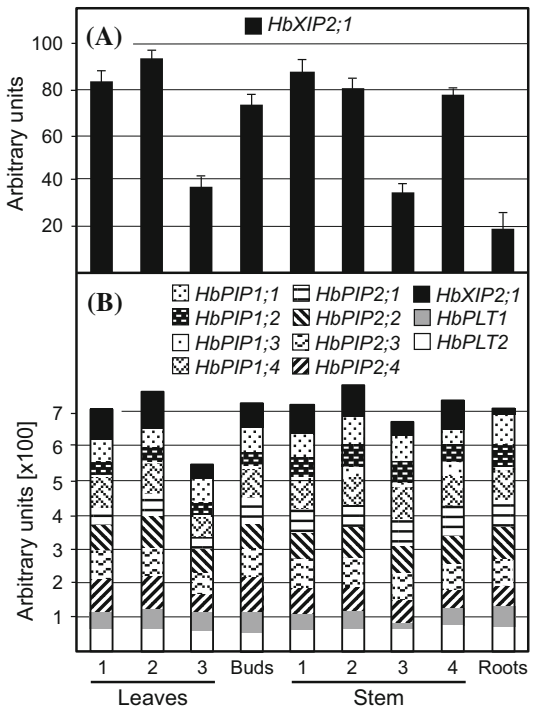

Fig. 6 Constitutive transcript accumulation of *HbXIP2;1*, *HbPIPs* and *HbPLTs* gene in various vegetative organs from *H. brasiliensis* (clone PB217). Transcript accumulation of *HbXIP2;1* gene was monitored alone (**a**), and in relative proportion compared with *HbPIPs* and *HbPLTs* genes (**b**). Leaf samples 1, 2, and 3 are young, adult and senescent leaves, respectively. Stem samples 1, 2, 3 and 4 are growing apical parts of stem, bark, xylem and latex, respectively. Expression was monitored using real-time quantitative RT-PCR analyses and normalized with the expression of three housekeeping genes (*HbACT, HbCYP* and *Hb18S rRNA).* Arbitrary unit calculation is detailed in Materials and Methods. Expression rates for each isoform of *HbPIP1s*, *HbPIP2s* and *HbPLTs* are detailed in Supplementary Fig. S6. Data correspond to means of three technical repeats from three independent biological experiments, and *bars* represent the biological standard deviation

were carried out (Fig. 5). In addition, screening the 5′-flanking region of *HbXIP2;1* revealed an AGC box (or AGCCGCC box, SOOO232) (nucleotide position −1425, Supplementary Fig. S1), which is a functional *cis*-ethylene responsive promoter element (Fujimoto et al. 2000). The fact that *HbXIP*2;1 and several other transporter genes act in a concerted and regulated manner suggests that *HbXIP*2;1, as a potential glycerol transporter could take an active part in the regulation of ethylene-induced fluidity modulation of the latex, as previously documented for *Hb*PIP and *HbPLT*. Water circulation in the inner bark and latex cells may be potentiated by the concomitant up-regulation of both *HbPIP* genes, resulting in a direct increase in water fluxes, and transporter genes such as *HbXIPs* and *HbPLTs,* indirectly increasing the osmotic force by accumulation of polyols and other osmolytes.

An in situ glycerol facilitator? An unravelled question for HbXIP2;1

The upregulated expression of *Hb*XIP2;1 coincides with rubber synthesis, yet *Hb*XIP2;1 appears to facilitate the transport of glycerol in the heterologous system of yeast. Comparison is not proof, but although these molecular analyses were carried out in distinct biological systems or previously reported for other transporters and their potential solutes in similar physiological situations in *H brasiliensis*, we speculate on a plausible connection between these biological events. The ability to transport glycerol and several organic solutes has been experimentally demonstrated for numerous aquaporins in plant systems ever since the 1990s, but the role, accumulation or partitioning for glycerol specifically as a hub-metabolite fluxed from or between compartments in plants has not yet been investigated. Our study and the capacity to validate many of our hypothesis is restricted by the facts that (1) although the AQP subfamily are physiologically relevant glycerol transporter, the solute is to our knowledge technically impossible to trace and assay, and (2) *H. brasiliensis* is a non-model plant for which metabolic analysis on laticifers and/or functional validation by genetic transformation remain highly complex. Still, there remain important questions about the potential roles that glycerol passing through *Hb*XIP2;1 might play. Two avenues warrant discussion and exploration: glycerol could be an osmo-protective substance for maintaining cellular integrity, and/or a source of carbon and energy required for rubber biosynthesis.

Is glyceroporin XIP of central importance for laticifer osmoregulation?

The duration of latex outflow during tapping, and the capacity of latex regeneration after tapping are key parameters of rubber production yield. From a biological standpoint, both depend on the hydric fluxes across the liber and laticifer networks. Ethylene treatment acts on both parameters, allowing latex dilution and stimulation of sugar loading. Stressful repeated tapping with hormonal stimulation may dangerously disrupt the hydric homeostasis of the challenged cells, for example by generating reactive oxygen species, leading in extreme cases to the physiological disorder known as “tapping panel dryness” (Sookmark et al. 2002). In most living organisms, a number of different osmolytes are produced or imported by the cells with the objective of improving stress resistance (Chen and Murata 2002). Glycerol is one such osmolyte (Hasegawa et al. 2000), but despite wide occurrence in living organisms, its accumulation in plant cells remains generally very low (Gerber et al. 1988). However, we postulate that a controlled accumulation of glycerol can

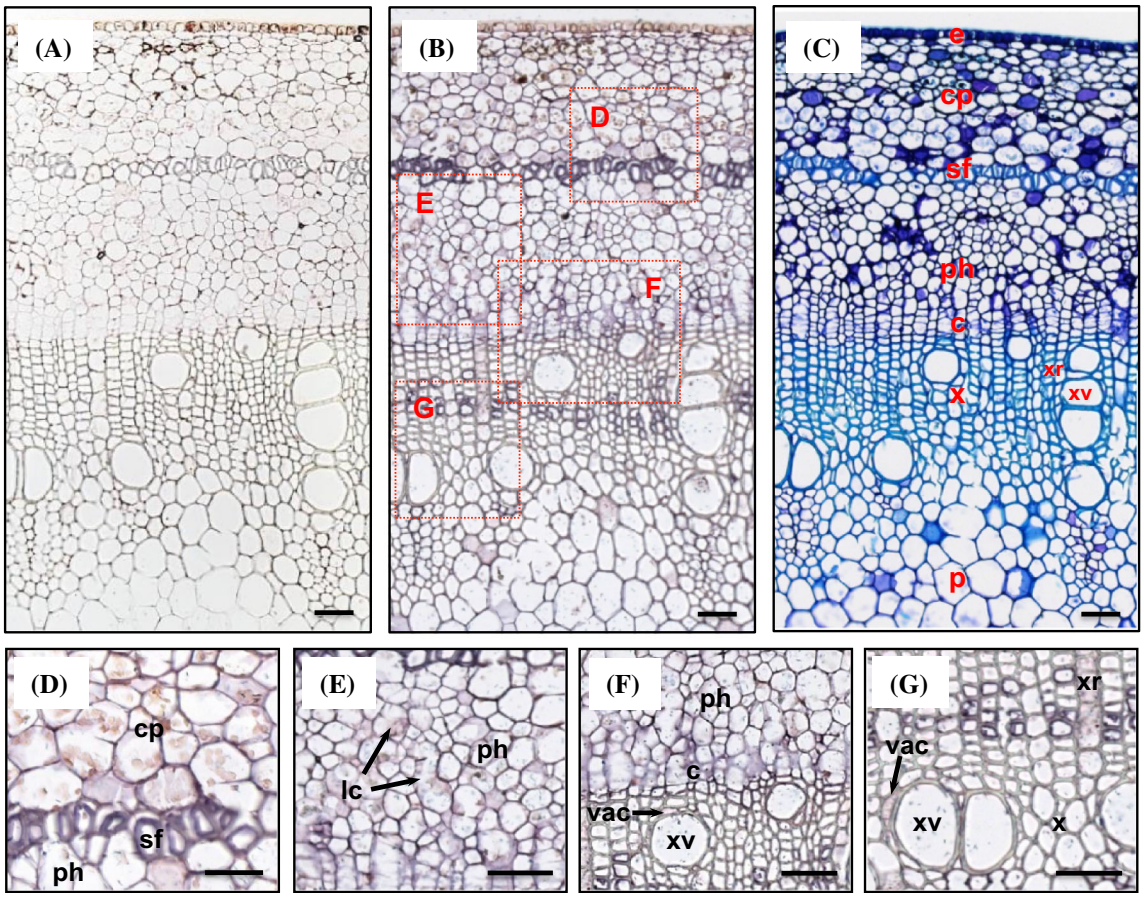

Fig. 7 In situ localization of *HbXIP2;1* mRNA in stems. Transversal sections 10 µm thick from paraffin-embedded *H. brasiliensis* young stem hybridized with specific sense probes (negative control) (**a**), with antisense probes (positive hybridization) (**b, d–f, g**), and with a toluidine *blue staining* (**c**) to identify the cellular structure. Positive hybridization signals are visualized by *violet staining* using a DIG-labeled RNA immunodetection system as described in "Materials and Methods". *c* cambium, *cp* cortical parenchyma, *e* epidermis, *lc* laticifer cell, *sf* sclerenchyma fiber, *p* pith, *ph* phloem, *vac* vessel associated cell, *x* xylem, *xv* xylem vessel, *xr* xylem ray. Alkaline phosphatase staining controls without probe and a fine description of stem cellular structures are detailed in Supplementary Fig. S7. Original photographs in which selected consensus zones were connected together for creating the artificial pictures A, B and C are given in Supplementary Fig. S8. *Scale bar* indicates 50 µm

operate in damaged tissues to maintain the water balance. Together with other sugars, glycerol could act as a "laticiferous osmo-protectant": it could help prevent the disaggregation of membranes, proteins and multimeric complexes induced by the osmotic stress (Pahlman et al. 2001; Hohmann 2002). In rubber trees, the glyceroporin *Hb*XIP2;1, by mediating glycerol transport across plasma membranes in the inner bark and latex cells, may contribute to the osmoprotection of these cells in compensation for the exploitation-induced oxidative stress that jeopardizes membrane integrity (d'Auzac et al. 1997).

Does glyceroporin XIP modulate glycerol import as an energy source for stimulated laticiferous metabolism?

Sucrose is the precursor of rubber synthesis in the laticifers (Tupy 1985). Concomitant increases of sucrose loading, glycolysis and glycerolipid biosynthesis have been demonstrated during an upregulated laticiferous metabolism (Dusotoit-Coucaud et al. 2009, 2010a, b; Tang et al. 2013; Wei et al. 2015). In a cell energy scenario and concurrently to possible re-routing of glycerol and other carbohydrates in producing intermediate substrates for the biosynthesis of rubber precursors, glycerol might also be one of the sucrose routes for glycerol-3-phosphate (G3P) production. Cytosolic influxes of glycerol are known to supply the bioprocesses of carbohydrate fermentation and oxidative phosphorylation. This oxidative pathway includes glycolysis (after glycerol conversion to glyceraldehyde-3-phosphate (GA3P)) and the G3P shuttle after glycerol conversion to G3P. Both are interconnected biochemical pathways where the G3P shuttle regenerates NAD^+ from NADH, a by-product of glycolysis that contributes to regenerate the ATP pool through the mitochondrial oxidative phosphorylation pathway (Shen et al.

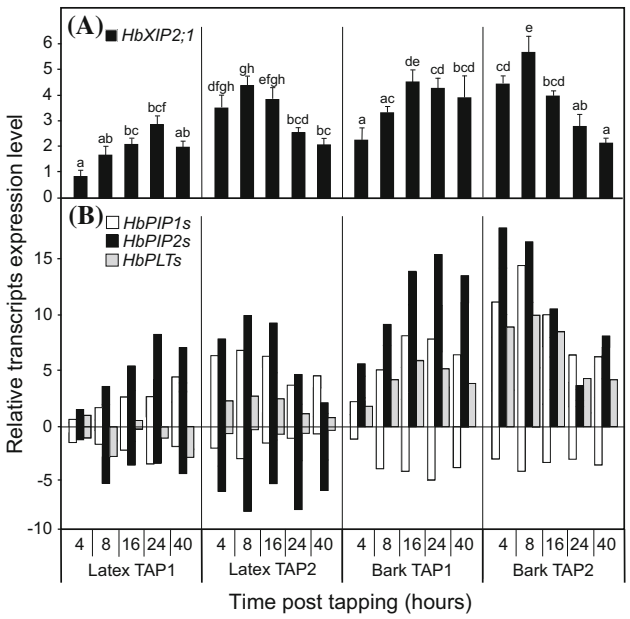

Fig. 8 *HbXIP2;1*, *HbPIPs* and *HbPLTs* gene expressions in tapped rubber tree. Effect of tapping and ethylene treatment on *HbXIP2;1* gene expression **(a)** compared with *HbPIP1s*, *HbPIP2s* and *HbPLTs* isoformes **(b)** in latex and bark of exploited *H. brasiliensis* trees (clone PB217). Samples were collected on two successive tapping days (TAP1 and TAP2), from trees treated with ethylene respectively 4, 8, 16, 24 and 40 h before the first tapping. Expression was monitored using real-time quantitative RT-PCR analyses and normalized by the expression of three housekeeping genes (*HbACT, HbCYP* and *Hb18S rRNA).* Relative expression rate was obtained by the $E^{-\Delta\Delta Ct}$ method with the untreated samples as controls. Expression rates for each isoform of *HbPIP1s*, *HbPIP2s* and *HbPLTs* are detailed in Supplementary Fig S9. Data correspond to means of three technical repeats from two independent biological experiments, and bars represent the biological standard deviation. XIP data were statistically evaluated using Student's *t* test ($p < 0.001$)

2006). The glycerol metabolic pathway is also crucial for phospholipid biosynthesis with its derivative G3P and dihydroxyacetone phosphate as precursors (Vance 2001). The involvement of primary metabolism in stressed plants is generally underestimated, and yet some studies show that enhanced plant resistance involves a glycerol-triggered enhancement of the G3P pool (Eastmond 2004; Chanda et al. 2008). Interestingly, XIP are sparsely or not expressed in differentiating xylem of poplar and tobacco (Gupta and Sankararamakrishnan 2009; Bienert et al. 2011; Lopez et al. 2012). This is in line with *HbXIP2;1* exhibiting a very low transcriptional expression in mature xylem. Bienert et al. state that *Nt*XIP1;1 will not ensure solute exchanges within the vascular tissues. This assumption is not in question, but rather it emphasizes interesting features linked to the activity of the laticiferous system in which XIP are strongly expressed, and could play pivotal roles in allowing imports of glycerol and potentially of more hydrophobic solutes. In this regard, we do not exclude the possibility that these solutes also integrate the rubber biosynthesis pathway. Whether XIP could play this role needs to be investigated directly in plants, a very promising path for future works.

Concluding remarks about XIP and outlook

Although the laticiferous system is structurally unconnected to the parenchyma of surrounding tissues, fluxes do occur through specific regulation between these tissues. It is of interest to understand the fine controls of fluid balance that exist between these specialized tissues and the coordinated regulation of gene families involved in the rubber biosynthesis pathway in latex harvesting contexts. Among the three XIP genes present in *H. brasiliensis* genome, only *HbXIP2;1* was expressed in our physiological conditions. In particular, *HbXIP2;1* is expressed in laticifers cells and modulation in challenged rubber trees remarkably correlates with the kinetics of latex yield. Given the interesting features of *Hb*XIP2;1 (glycerol channelling, plasma membrane location and tissue distribution), it is legitimate to speculate on its role in the molecular dialogues between the two non-connected cell systems, i.e. the highly specialized laticiferous and the vascular networks. AQP are key players for cell osmoregulation. However, AQP structure and functions remain to be explored, such as specificity of transport and pore gating, given that the pore diameter and charge gradient inference seem to be structurally conserved between *Hb*XIP2;1 and *So*PIP2;1. Comparative modeling results have highlighted probable structural checkpoints by which *Hb*XIP2;1 could regulate substrate diffusion, such as loop D which could play the role of a lid to gate the pore, or an inter-chain disulfide bond that could be part of an allosterical trick to favor cooperativity between the subunits of a tetrameric *Hb*XIP2;1 during the activity process. Some of our observations described here may guide future research. Glycerol remains an emblematic substrate for all the non-exclusive water-channeling MIP. The predictive protein structure and the functional validation in heterologous system show *Hb*XIP2;1 as a glyceroporin, possibly with diverse hypothetic biological functions. There is considerable evidence that several channels are permeable to glycerol. However, no physiological function of glycerol-permeable aquaporins *in planta* had been experienced using knockout or loss-of-functions mutants in model plant such as Arabidopsis, rice or maize. To make the link between the abilities of *Hb*XIP2;1 to transport glycerol and to be involved in a transmembrane glycerol transport will require further experimental confirmations. The same would apply to other solutes that XIP is able to transport. Such findings would be crucial for the plant aquaporin research field and for the

whole plant physiology community. While no physiological evidence is given to fully demonstrate XIP-mediated glycerol transport into laticifers, our data provides a first step in studying processes involving XIP during latex harvesting. The physiological roles of XIP and/or glycerol mobilizations in laticifers, and more broadly *in planta*, remain to be clearly demonstrated. If XIP are plasma membrane-localized and participate in glycerol fluxes between cells, how much glycerol could be transiently accumulated in the apoplastic space and then be remobilized as a carbon source? Could glycerol act as a modulator of the osmotic driving forces that adjust the integrity of cells, and therefore for laticifers, regulate the latex metabolism and its gradual outflow? All these questions are hard to answer owing to the lack of appropriate biochemical methodologies to monitor infinitesimal changes in the extra/intracellular accumulation of this small solute. Functional *in planta* analysis should further refine our understanding of the relationship between glycerol metabolism, cell osmo-protection and the functional role of XIP, or other glyceroporins, in latex-producing plants.

Acknowledgments We are in Professor François Chaumont's debt for reading carefully the manuscript and for his constructive remarks that helped us to improve it with relevant arguments. We thank Sylvaine Blateyron for her excellent technical support. This research was supported by the earmarked funds from the PIAF and LBLGC Research Systems. The funders -whatever this may mean- had no role in study design, data collection and analysis, decision to publish, or preparation of the manuscript. We would also like to thank the anonymous reviewers for their constructive comments and encouragement on the article. The authors declare no competing financial interests.

Author Contributions David Lopez co-designed and participated to most of the experiments and wrote the first draft of the article; Jean-Stéphane Venisse, Beatriz Muries and Maroua Ben Amira carried out the gene expression experiments and bioinformatics analysis; Nicole Brunel-Michac carried out and interpreted the in situ hybridization experiments; Daniel Auguin performed the *Hb*XIP2;1 3D structure modeling and the structural analysis; Sylvain Bourgerie performed water permeability assessment in yeast and the functional complementation of *Dfps1* yeast strain; Benoit Porcheron and Rémy Lemoine preformed glycerol permeability; Daniel Brown and Lorenzo Frigerio directed and performed YFP-*HbXIP2;1* construction, agro-infiltration of tobacco and confocal microscopy analysis, and appropriate interpretation; Ewan Mollison and Alessandra Di Cola retrieved full-length *HbXIP* sequences in *H. brasiliensis* genome; Hervé Chrestin provided the latex yield data; Jean-Stéphane Venisse and Boris Fumanal performed and interpreted the phylogenetic analysis; Aurélie Gousset-Dupont, Philippe Label, Valérie Pujade-Renaud and Jean-Louis Julien have ensured a critical examination of the manuscript; Valérie Pujade-Renaud provided plant materials needed for this work; Jean-Stéphane Venisse led the program, co-designed the experiments, obtained the funding, and coordinated and compiled authors' contributions to the final version of the article; Daniel Auguin and Jean-Stéphane Venisse wrote the final draft of the article and edited it; All the authors participated in the analysis of data, and collectively approved whole of the result interpretation and related hypothesis.

Compliance with ethical standards

Conflict of interest The authors declare that they have no conflict of interest.

References

Abascal F, Irisarri I, Zardoya R (2014) Diversity and evolution of membrane intrinsic protein. Biochim Biophys Acta 1840:1468–1481

Altschul SF, Madden TL, Schaffer AA, Zhang J, Zhang Z, Miller W, Lipman DJ (1997) Gapped BLAST and PSI-BLAST: a new generation of protein database search programs. Nucleic Acids Res 25:3389–3402

An F, Zou Z, Cai X, Wang J, Rookes J, Lin W, Cahill D, Kong L (2015) Regulation of HbPIP2;3, a latex-abundant water transporter, is associated with latex dilution and yield in the rubber tree (*Hevea brasiliensis* Muell. Arg.). PLoS one 10:e0125595

Anderberg HI, Danielson JAH, Johanson U (2011) Algal MIPs, high diversity and conserved motifs. BMC Evol Biol 11:110

Anderberg HI, Kjellbom P, Johanson U (2012) Annotation of *Selaginella moellendorffii* major intrinsic proteins and the evolution of the protein family in terrestrial plants. Front Plant Sci 3:33

Anderca MI, Suga S, Furuichi T, Shimogawara K, Maeshima M, Muto S (2004) Functional identification of the glycerol transport activity of *Chlamydomonas reinhardtii* CrMIP1. Plant Cell Physiol 45:1313–1319

Baker NA, Sept D, Joseph S, Holst MJ, McCammon JA (2001) Electrostatics of nanosystems: application to microtubules and the ribosome. Proc Natl Acad Sci USA 98:10037–10041

Barlowe C (2003) Signals for COPII-dependent export from the ER: What's the ticket out? Trends Cell Biol 13:295–300

Bienert GP, Bienert MD, Jahn TP, Boutry M, Chaumont F (2011) *Solanaceae* XIPs are plasma membrane aquaporins that facilitate the transport of many uncharged substrates. Plant J 66:306–317

Bienert GP, Cavez D, Besserer A, Berny MC, Gilis D, Rooman M, Chaumont F (2012) A conserved cysteine residue is involved in disulfide bond formation between plant plasma membrane aquaporin monomers. Biochem J 445:101–111

Brooks BR, Brooks CL, Mackerell AD, Nilsson L, Petrella RJ, Roux B, Won Y, Archontis G, Bartels C, Boresch S, Caflisch A, Caves L, Cui Q, Dinner AR, Feig M, Fischer S, Gao J, Hodoscek M, Im W, Kuczera K, Lazaridis T, Ma J, Ovchinnikov V, Paci E, Pastor RW, Post CB, Pu JZ, Schaefer M, Tidor B, Venable RM, Woodcock HL, Wu X, Yang W, York DM, Karplus M (2009) CHARMM: the biomolecular simulation program. J Comput Chem 30:1545–1614

Brunel N, Leduc N, Poupard P, Simoneau P, Mauget JC, Viemont JD (2002) KNAP2, a class I KN1-like gene is a negative marker of bud growth potential in apple tress (*Malus domestica* L. Borkh.). J Exp Bot 53:2143–2149

Chanda B, Venugopal SC, Kulshrestha S, Navarre D, Downie B, Vaillancourt L, Kachroo A, Kachroo P (2008) Glycerol-3-phosphate levels are associated with basal resistance to the hemibiotrophic fungus *Colletotrichum higginsianum* in Arabidopsis. Plant Physiol 147:2017–2029

Chao J, Chen Y, Wu S, Tian WM (2015) Comparative transcriptome analysis of latex from rubber tree clone CATAS8-79 and PR107 reveals new cues for the regulation of latex regeneration and duration of latex flow. BMC Plant Biol 15:104

Chase MW, Reveal JL (2009) A phylogenetic classification of the land plants to accompany APG III. Bot J Linn Soc 161:122–127

Chaumont F, Tyerman SD (2014) Aquaporins: highly regulated channels controlling plant water relations. Plant Physiol 164:1600–1618

Chaumont F, Moshelion M, Daniels MJ (2005) Regulation of plant aquaporin activity. Biol Cell 97:749–764

Chen LY (2013) Glycerol modulates water permeation through *Escherichia coli* aquaglyceroporin GlpF. Biochim Biophys Acta 1828:1786–1793

Chen TH, Murata N (2002) Enhancement of tolerance of abiotic stress by metabolic engineering of betaines and other compatible solutes. Curr Opin Plant Biol 5:250–257

Chen VB, Arendall WB, Head JJ, Immornino RM, Kapral GL, Murray LW, Richardson JS, Richardson DC (2010) MolProbity: all-atom structure validation for macromolecular crystallography. Acta Crystallogr D Biol Crystallogr 66:12–21

Chevenet F, Brun C, Banuls AL, Jacq B, Chisten R (2006) TreeDyn: towards dynamic graphics and annotations for analyses of trees. BMC Bioinformatics 7:439

Chothia C (1975) Structural invariants in protein folding. Nature 254:304–308

Chow KS, Wan KL, Isa MN, Bahari A, Tan SH, Harikrishna K, Yeang HY (2007) Insights into rubber biosynthesis from transcriptome analysis of *Hevea brasiliensis* latex. J Exp Bot 58:2429–2440

Chow KS, Isa MN, Bahari A, Ghazali AK, Alias H, Zainuddin Z, Hoh CC, Wan KL (2012) Metabolic routes affecting rubber biosynthesis in *Hevea brasiliensis* latex. J Exp Bot 63:1863–1871

Cornish K (2001) Similarities and differences in rubber biochemistry among plant species. Phytochemistry 57:1123–1134

Coupé M, Chrestin H (1989) Physico-chemical and bio-chemical mechanisms of the hormonal (ethylene) stimulation: early biochemical events induced in *Hevea* latex by hormonal bark stimulation. In: d'Auzac J, Jacob JL, Chrestin H (eds) Physiology of rubber tree latex. CRC Press Inc., Boca Raton, pp 295–319

D'Auzac J, Ribaillier D (1969) Ethylene: a new stimulant of latex yield for *Hevea brasiliensis*. CR Acad Sci D Sci Nat 268:3046–3049

D'Auzac J, Jacob JL, Prévôt JC, Clément A, Gallois R (1997) The regulation of cis-polyisoprene production (natural rubber) from *Hevea brasiliensis*. In: Pandalai SG (ed) Recent research developments in plant physiology. Research Singpost, Trivandrum, pp 273–332

Danielson JAH, Johanson U (2008) Unexpected complexity of the aquaporin gene family in the moss *Physcomitrella patens*. BMC Plant Biol 8:45

De Fay E, Sanier C, Hebant C (1989) Distribution of plasmodesmata in the phloem of *Hevea brasiliensis* in relation to laticifer loading. Protoplasma 149:155–162

DeLano WL (2004) PyMOL User's Guide. DeLano Scientific, San Carlos, p 2004

Di Giorgio JP, Soto G, Alleva K, Jozefkowicz C, Amodeo G, Muschietti JP, Ayub ND (2014) Prediction of aquaporin function by integrating evolutionary and functional analyses. J Membr Biol 247:107–125

Dolinsky TJ, Czodrowski P, Li H, Nielsen JE, Jensen JH, Klebe G, Baker NA (2007) PDB2PQR: expanding and upgrading automated preparation of biomolecular structures for molecular simulations. Nucleic Acids Res 35:W522–W525

Doyle JJ, Doyle JL (1987) A rapid DNA isolation procedure for small quantities of fresh leaf tissue. Phytochem Bull 19:11–15

Du H, Brender JR, Zhang J, Zhang Y (2015) Protein structure prediction provides comparable performance to crystallographic structures in docking-based virtual screening. Methods 71:77–84

Dusotoit-Coucaud A, Brunel N, Kongsawadworakul P, Viboonjun U, Lacointe A, Julien JL, Chrestin H, Sakr S (2009) Sucrose importation into laticifers of *Hevea brasiliensis*, in relation to ethylene stimulation of latex production. Ann Bot 104:635–647

Dusotoit-Coucaud A, Kongsawadworakul P, Maurousset L, Viboonjun U, Brunel N, Pujade-Renaud V, Chrestin H, Sakr S (2010a) Ethylene stimulation of latex yield depends on the expression of a sucrose transporter (HbSUT1B) in rubber tree (*Hevea brasiliensis*). Tree Physiol 30:1586–1598

Dusotoit-Coucaud A, Porcheron B, Brunel N, Kongsawadworakul P, Franchel J, Viboonjun U, Chretin H, Lemoine R, Sakr S (2010b) Cloning and characterization of a new polyol transporter (HbPLT2) in *Hevea brasiliensis*. Plant Cell Physiol 51:1878–1888

Dynowski M, Mayer M, Moran O, Ludewig U (2008) Molecular determinants of ammonia and urea conductance in plant aquaporin homologs. FEBS Lett 582:2458–2462

Eastmond PJ (2004) Glycerol-insensitive *Arabidopsis* mutants: gli1 seedlings lack glycerol kinase, accumulate glycerol and are more resistant to abiotic stress. Plant J 37:617–625

Fischer M, Kaldenhoff R (2008) On the pH regulation of plant aquaporin. J Biol Chem 283:33889–33892

Forrest KL, Bhave M (2008) The PIP and TIP aquaporins in wheat form a large and diverse family with unique gene structures and functionally important features. Funct Integr Genomics 8:115–133

Frick A, Järvå M, Törnroth-Horsefield S (2013) Structural basis for pH gating of plant aquaporins. FEBS Lett 587:989–993

Froger A, Tallur B, Thomas D, Delamarche C (1998) Prediction of functional residues in water channels and related proteins. Protein Sci 7:1458–1468

Fujimoto SY, Ohta M, Usui A, Shinshi H, Ohme-Takagi M (2000) Arabidopsis ethylene-responsive element binding factors act as transcriptional activators or repressors of GCC box-mediated gene expression. Plant Cell 12:393–404

George N, Somero GN, Yancey PH (2011) Osmolytes and cell-volume regulation: physiological and evolutionary principles. Handbook of Physiology. Cell Physiol. doi:10.1002/cphy.cp140110

Gerber D, Byerrum RU, Gee RW, Tolbert NE (1988) Glycerol concentrations in crop plants. Plant Sciences 56:31–38

Giovanetti M, Balestrini R, Volpe V, Guether M, Straub D, Costa A, Ludewig U, Bonfante P (2012) Two putative aquaporin genes are differentially expressed during arbuscular mycorrhizal symbiosis in *Lotus japonicus*. BMC Plant Biol 12:186

Gomes D, Agasse A, Thiebaud P, Delrot S, Geros H, Chaumont F (2009) Aquaporins are multifunctional water and solute transporters highly divergent in living organisms. Biochim Biophys Acta 6:1213–1228

Guindon S, Gascuel O (2003) A simple, fast, and accurate algorithm to estimate large phylogenies by maximum likelihood. Syst Biol 52:696–704

Gupta AB, Sankararamakrishnan R (2009) Genome-wide analysis of major intrinsic proteins in the tree plant *Populus trichocarpa*: characterization of XIP subfamily of aquaporins from evolutionary perspective. BMC Plant Biol 20:134

Hagel JM, Yeung EC, Facchini PJ (2008) Got milk? The secret life of laticifers. Trends Plant Sci 13:1360–1385

Hare PD, Cress WA, Van Staen J (1998) Dissecting the roles of osmolyte accumulation during stress. Plant Cell Environ 21:535–553

Hasegawa PM, Bressan RA, Zhu JK, Bohnert HJ (2000) Plant cellular and molecular responses to high salinity. Annu Rev Plant Physiol Plant Mol Biol 51:463–499

Hellens RP, Edwards EA, Leyland NR, Bean S, Mullineaux PM (2000) pGreen: a versatile and flexible binary Ti vector for Agrobacterium-mediated plant transformation. Plant Mol Biol 42:819–832

Hohmann S (2002) Osmotic stress signaling and osmoadaptation in yeasts. Microbiol Mol Biol Rev 66:300–372

Hove RM, Bhave M (2011) Plant aquaporins with non-aqua functions: deciphering the signature sequences. Plant Mol Biol 75:413–430

Jo S, Kim T, Iyer VG, Im W (2008) CHARMM-GUI: a web-based graphical user interface for CHARMM. J Comput Chem 29:1859–1865

Johansson I, Karlsson M, Shukla VK, Chrispeels MJ, Larsson C, Kjellbom P (1998) Water transport activity of the plasma membrane aquaporin PM28A is regulated by phosphorylation. Plant Cell 10:451–459

Johansson U, Karlsson M, Johansson I, Gustavsson S, Slovall S, Fraysse L, Weig AR, Kjellbom P (2001) The complete set of genes encoding major intrinsic proteins in Arabidopsis provides a framework for a new nomenclature for major intrinsic proteins in plants. Plant Physiol 126:1358–1369

Lacote R, Gabla O, Obouayeba S, Eschbach JM, Rivano F, Dian K, Gohet E (2010) Long-term effect of ethylene stimulation on the yield of rubber trees is linked to latex cell biochemistry. Field Crops Res 115:94–98

Lagree V, Froger A, Deschamps S, Hubert JF, Delamarche C, Bonnec G, Thomas D, Gouranton J, Pellerin I (1999) Switch from an aquaporin to a glycerol channel by two amino acids substitution. J Biol Chem 274:6817–6819

Li H, Yunxia Qin Y, Xiao X, Tang C (2011) Screening of valid reference genes for real-time RT-PCR data normalization in *Hevea brasiliensis* and expression validation of a sucrose transporter gene HbSUT3. Plant Sci 181:132–139

Li G, Santoni V, Maurel C (2013) Plant Aquaporins: roles in Plant Physiology. Biochim Biophys Acta 1840:1574–1582

Lopez D, Bronner G, Brunel N, Auguin D, Bourgerie S, Brignolas F, Carpin S, Tournaire-Roux C, Maurel C, Fumanal B, Martin F, Sakr S, Label P, Julien JL, Gousset-Dupont A, Venisse JS (2012) Insights into Populus XIP aquaporins: evolutionary expansion, protein functionality, and environmental regulation. J Exp Bot 63:2217–2230

Luyten K, Albertyn J, Skibbe WF, Prior BA, Ramos J, Thevelein JM, Hohmann S (1995) Fps1, a yeast member of the MIP family of channel proteins, is a facilitator for glycerol uptake and efflux and is inactive under osmotic stress. EMBO J 14:1360–1371

Martins CPS, Pedrosa AM, Du D, Gonçalves LP, Yu Q, Gmitter FG Jr, Costa MGC (2015) Genome-wide characterization and expression analysis of major intrinsic proteins during abiotic and biotic stresses in sweet orange (*Citrus sinensis* L. Osb.). PLoS one 10:e0138786

Meyrial V, Laize V, Gobin R, Ripoche P, Hohmann S, Tacnet F (2001) Existence of a tightly regulated water channel in *Saccharomyces cerevisiae*. Eur J Biochem 268:334–343

Murata K, Mitsuoka K, Hirai T, Walz T, Agre P, Heymann JB, Engel A, Fujiyoshi Y (2000) Structural determinants of water permeation through aquaporin1. Nature 407:599–605

Nishimura N, Balch WE (1996) A Di-acidic signal required for selective export from the endoplasmic reticulum. Science 277:556–558

Nyblom M, Frick A, Wang Y, Ekvall M, Hallgren K, Hedfalk K, Neutze R, Tajkhorshid E, Tornroth-Horsefield S (2009) Structural and functional analysis of SoPIP2;1 mutants adds insight into plant aquaporin gating. J Mol Biol 387:653–668

Obouayeba S, Boa D, Jacob JL (1996) Performance of the PB217 Hevea clone in Cote d'Ivoire. Plant Rech Dev 3:346–354

Pahlman AK, Granath K, Ansell R, Hohmann S, Adler L (2001) The yeast glycerol-3-phosphatases Gpp1p and Gpp2p are required for glycerol biosynthesis and differentially involved in the cellular responses to osmotic, anaerobic, and oxidative stress. J Biol Chem 276:3555–3563

Parida AK, Das AB (2005) Salt tolerance and salinity effects on plants: a review. Ecotoxicol Environ Saf 60:324–349

Park W, Scheffler BE, Bauer PJ, Campbell BT (2010) Identification of the family of aquaporin genes and their expression in upland cotton (*Gossypium hirsutum* L.). BMC Plant Biol 10:142

Pfaffl MW (2001) A new mathematical model for relative quantification in real-time RT-PCR. Nucleic Acids Res 29:2003–2007

Pfaffl MW, Tichopad A, Prgomet C, Neuvians TP (2004) Determination of stable housekeeping genes, differentially regulated target genes and sample integrity: bestKeeper–excel-based tool using pair-wise correlations. Biotechnol Lett 26:509–515

Prak S, Hem S, Boudet J, Viennois G, Sommerer N, Rossignol M, Maurel C, Santoni V (2008) Multiple phosphorylations in the C-terminal tail of plant membrane aquaporins: role in subcellular trafficking of *At*PIP2;1 in response to salt stress. Mol Proteomic 7:1019–1030

Pujade-Renaud V, Clement A, Perrot-Rechenmann C, Prevot JC, Chrestin H, Jacob JL, Guern J (1994) Ethylene-induced increase in glutamine synthetase activity and mRNA levels in *Hevea brasiliensis* latex cells. Plant Physiol 105:127–132

Rahman AYA, Usharraj AO, Misra BB, Thottathil GP, Jayasekaran K, Feng Y et al (2013) Draft genome sequence of the rubber tree *Hevea brasiliensis*. BMC Genom 14:75

Reichow SL, Gonen T (2008) Noncanonical binding of calmodulin to aquaporin-0: implications for channel regulation. Structure 16:1389–1398

Reichow SL, Clemens DM, Freites JA, Nemeth-Cahalan KL, Heyden M, Tobias DJ, Hall JE, Gonen T (2013) Allosteric mechanism of water-channel gating by Ca^{2+}-calmodulin. Nat Struct Mol Biol 20:1085–1092

Reuscher S, Akiyama M, Mori C, Aoki K, Shibata D, Shiratake K (2013) Genome-wide identification and expression analysis of aquaporins in tomato. PLoS one 8:e79052

Roy A, Kucukural A, Zhang Y (2010) I-TASSER: a unified platform for automated protein structure and function prediction. Nat Protoc 5:725–738

Santoni V, Verdoucq L, Sommerer N, Vinh J, Pflieger D, Maurel C (2006) Methylation of aquaporins in plant membrane. Biochem J 400:189–197

Sato K, Nakano A (2007) Mechanisms of COPII vesicle formation and protein sorting. FEBS Lett 581:2076–2082

Secchi F, Maciver B, Zeidel ML, Zwieniecki MA (2009) Functional analysis of putative genes encoding the PIP2 water channel subfamily *Populus trichocarpa*. Tree Physiol 29:1467–1477

Sehnal D, Svobodova Varekova R, Berka K, Pravda L, Navratilova V, Banas P, Ionescu CM, Otyepka M, Koca J (2013) MOLE 2.0: advanced approach for analysis of biomacromolecular channels. J Cheminform 5:39

Shen W, Wei Y, Dauk M, Tan Y, Taylor D, Selvaraj G, Zou J (2006) Involvement of glycerol-3-phosphate dehydrogenase ion modulating the NADH/NAD^+ ratio provides evidence of a mitochondrial glycerol-3-phosphate shuttle in *Arabisopsis*. Plant Cell 18:422–441

Sookmark U, Pujade-Renaud V, Chrestin H, Lacote R, Naiyanetr C, Seguin M, Romruensukharom P, Narangajavana J (2002) Characterization of polypeptides accumulated in the latex cytosol of rubber trees affected by the tapping panel dryness syndrome. Plant Cell Physiol 43:1323–1333

Soveral G, Madeira A, Loureiro-Dias MC, Moura TF (2007) Water transport in intact yeast cells as assessed by fluorescence self-quenching. Appl Environ Microbiol 73:2341–2343

Sparkes IA, Runions J, Kearns A, Hawes C (2006) Rapid, transient expression of fluorescent fusion proteins in tobacco plants and generation of stably transformed plants. Nat Protoc 1:2019–2025

Sui H, Hana BG, Lee JK, Wallan P, Jap B (2001) structural basis of water-specific transport through the AQP1water channel. Nature 414:872–878

Tang CL, Alexov E, Pyle AM, Honig B (2007) Calculation of pKas in RNA: on the structural origins and functional roles of protonated nucleotides. J Mol Biol 366:1475–1496

Tang C, Huang D, Yang J, Liu S, Sakr S, Li H, Zhou Y, Quin Y (2010) The sucrose transporter HbSUT3 plays an active role in sucrose loading to laticifer and rubber productivity in exploited trees of *Hevea brasiliensis* (para rubber tree). Plant Cell Environ 33:1708–1720

Tang C, Xiao X, Li H, Fan Y, Yang J, Qi J, Li H (2013) Comparative analysis of latex transcriptome reveals putative molecular mechanisms underlying super productivity of *Hevea brasiliensis*. PLoS one 8:e75307

Tangphatsornruang S, Uthaipaisanwong P, Sangsrakru D, Chanprasert J, Yoocha T, Jomchai N, Tragoonrung S (2011) Characterization of the complete chloroplast genome of *Hevea brasiliensis* reveals genome rearrangement, RNA editing sites and phylogenetic relationships. Gene 475:104–112

Törnroth-Horsefield S, Wang Y, Hedfalk K, Johanson U, Karlsson M, Tajkhorshid E, Neutze R, Kjellbom P (2006) Structural mechanism of plant aquaporin gating. Nature 439:688–694

Tournaire-Roux C, Sutka M, Javot H, Gout E, Gerbeau P, Luu DT, Bligny R, Maurel C (2003) Cytosolic pH regulates root water transport during anoxic stress through gating of aquaporins. Nature 425:393–397

Tungngoen K, Kongsawadworakul P, Viboonjun U, Katsuhara M, Brunel N, Sakr S, Narangajavana J, Chrestin H (2009) Involvement of HbPIP2;1 and HbTIP1;1 aquaporins in ethylene stimulation of latex yield through regulation of water exchanges between inner liber and latex cells in *Hevea brasiliensis*. Plant Physiol 151:843–856

Tungngoen K, Viboonjun U, Kongsawadworakul P, Katsuhara M, Julien JL, Sakr S, Chrestin H, Narangajavana J (2011) Hormonal treatment of the bark of rubber trees (*Hevea brasiliensis*) increases latex yield through latex dilution in relation with the differential expression of two aquaporin genes. J Plant Physiol 168:253–262

Tupy J (1985) Some aspects of sucrose transport and utilization in latex producing bark of *Hevea brasiliensis* (Müll. Arg.). Biol Plant 27:51–64

Untergasser A, Nijveen H, Rao X, Bisseling T, Geurts R, Leunissen JA (2007) Primer3Plus, an enhanced web interface to Primer3. Nucleic Acids Res 35:W71–W74

Vance DE (2001) Phospholipid biosynthesis in eukaryotes. In: Vance DE, Vance JE (eds) Biochemistry of lipids, lipoproteins and membranes (4th edn), vol 8. Elsevier, Amstardam, pp 205–232

Venkatesh J, Yu JW, Park SW (2013) Genome-wide analysis and expression profiling of the *Solanum tuberosum* aquaporins. Plant Physiol Biochem 73:392–404

Venkatesh J, Yu JW, Gastonb D, Park SW (2015) Molecular evolution and functional divergence of X-intrinsic protein genes in plants. Mol Genet Genomics 290:443–460

Wallace IC, Roberts DM (2004) Homology modeling of representative subfamilies of Arabidopsis major intrinsic proteins. Classification based on the aromatic/arginine selectivity filter. Plant Physiol 135:1059–1068

Webb B, Sali A (2014) Protein structure modeling with MODELLER. Methods Mol Biol 1137:1–15

Wei F, Luo S, Zheng Q, Qiu J, Yang W, Wu M, Xiao X (2015) Transcriptome sequencing and comparative analysis reveal long-term flowing mechanisms in *Hevea brasiliensis* latex. Gene 10:153–162

Weig AR, Jakob C (2000) Functional identification of the glycerol permease activity of *Arabidopsis thaliana* NLM1 and NLM2 proteins by heterologous expression in *Saccharomyces cerevisiae*. FEBS Lett 481:293–298

Yang Z, Lasker K, Schneidman-Duhovny D, Webb B, Huang CC, Pettersen EF, Goddard TD, Meng EC, Sali A, Ferrin TE (2012) UCSF Chimera, MODELLER, and IMP: an integrated modeling system. J Struct Biol 179:269–278

Yang J, Yan R, Roy A, Xu D, Poisson J, Zhang Y (2015) The I-TASSER Suite: protein structure and function prediction. Nat Methods 12:7–8

Yue C, Cao H, Wang L, Zhou Y, Hao X, Zeng J, Wang X, Yang Y (2014) Molecular cloning and expression analysis of tea plant aquaporin (AQP) gene family. Plant Physiol Biochem 83:65–76

Zardoya R, Villalba S (2001) A phylogenetic framework for the aquaporin family in eukaryotes. J Mol Evol 52:391–404

Zardoya R, Ding X, Kitagawa Y, Chrispeels MJ (2002) Origin of plant glycerol transporters by horizontal gene transfer and functional recruitment. Proc Natl Acad Sci USA 12:14893–14896

Zelazny E, Borts JW, Muylaert M, Batoko H, Hemminga MA, Chaumont F (2007) FRET imaging in living maize cells reveals that plasma membrane aquaporins interact to regulate their subcellular localization. Proc Natl Acad Sci USA 104:12359–12364

Zelazny E, Miecielica U, Borst JW, Hemminga MA, Chaumont F (2009) An N-terminal diacidic motif is required for the trafficking of maize aquaporins *Zm*PIP2;4 and *Zm*PIP2;5 to the plasma membrane. Plant J 57:346–355

Zhang Y (2008) I-TASSER server for protein 3D structure prediction. BMC Bioinformatics 9:40

Zhang DY, Ali Z, Wang CB, Xu L, Yi JX, Xu ZL, Liu XQ, He XL, Huang YH, Khan IA, Trethowan RM, Ma HX (2013) Genome-wide sequence characterization and expression analysis of major intrinsic proteins in Soybean (*Glycine max* L.). PLoS one 8:e56312

Zhu J, Zhang Z (2009) Ethylene stimulation of latex production in *Hevea brasiliensis*. Plant Signal Behavior 4:1072–1074